
The Role of Parental Obesity in Lung Development and Alveolar Macrophage Priming

Ernesto Elorduy Vergara



München 2020

Aus dem
Comprehensive Pneumology Center (CPC)
Institut für Lungenbiologie (iLBD)
des Helmholtz Zentrums München
Vorstand: Dr. Ali Önder Yildirim

The Role of Parental Obesity in Lung Development and Alveolar Macrophage Priming

Dissertation
zum Erwerb des Doktorgrades der Naturwissenschaften
an der Medizinischen Fakultät der
Ludwig-Maximilians-Universität München

vorgelegt von
Ernesto Elorduy Vergara

aus
Puebla, Mexiko

2020

Mit Genehmigung der Medizinischen Fakultät
der Ludwig-Maximilians-Universität München

Betreuerin: apl. Prof. Dr. rer. nat. Silke Meiners

Zweitgutachter: Univ. Prof. Dr. phil. nat. Carolin Daniel

Dekan: Prof. Dr. med. dent. Reinhard Hickel

Tag der mündlichen Prüfung: 28.06.2021

Ich widme diese Arbeit meiner Frau und Familie

Acknowledgements

I would like to thank my family and colleagues for their support during the completion of this work. Especially, I would like to express my gratitude to my wife, who accompanied me throughout this time and endured with me the challenges that came along with this process. I want to thank Prof. Dr. Silke Meiners for her supervision and help. Also the members of the Stöger Lab, particularly Dr. Tobias Stöger, Nunja Habel-Ungewitter, Anna Fuchs, David Kutschke and Raphaël Prungnaud for their assistance during brainstorming sessions and their support in the lab. I would also like to thank colleagues at the German Mouse Clinic (GMC) for the possibility of cooperation and opportunity to work at GMC facilities. Thank you Dr. Jan Rozman for the expertise in the work with metabolic-related mouse models. Many thanks to Dr. Antonio Aguilar-Pimentel for the scientific discussions held and the help in measuring plasma cytokines. Many thanks to Ann-Elisabeth Schwarz and all animal care takers that assisted my work at the GMC.

Contents

Summary	iv
Zusammenfassung	vi
Abbreviations	viii
1 Introduction	1
1.1 Developmental origins of health and disease	1
1.2 The lung	2
1.3 Tissue macrophages	4
1.4 Alveolar macrophages	7
1.5 Obesity	15
1.6 Obesity and the respiratory system	19
2 Hypothesis and aims	23
2.1 Background	23
2.2 Objectives	24
2.3 Experimental setting	25
3 Materials and methods	28
3.1 Animal experiments	28
3.2 Flow cytometry	34
3.3 Histology	38
3.4 Enzyme-linked immunosorbent assay	41
3.5 Analysis of alveolar macrophages	42
3.6 RNA isolation and reverse transcription	43
3.7 Real-time polymerase chain reaction	44
3.8 Statistical analysis	46
4 Results	53
4.1 HFD induces obesity, systemic inflammation and hyperglycaemia	53
4.2 HFD distorts the course of lung inflammation and alveolar macrophage's phagocytosis	56
4.3 Parental obesity reduces foetal viability and delays weight gain after birth	62
4.4 No effect of parental obesity on placental inflammatory gene expression . .	63
4.5 Parental obesity has no effect on offspring's circulating cytokine levels . . .	65
4.6 Parental obesity delays final alveolarization in lungs of female offspring . .	68
4.7 Parental obesity transiently alters the gene expression and leukocyte population composition in the offspring's lung	71
4.8 No effect of parental obesity on endotoxin-induced acute lung inflammation	77
4.9 No evidence of long-term pro-inflammatory alveolar macrophage priming by parental obesity	84

5 Discussion	87
5.1 Mouse model of high-fat diet-induced obesity	88
5.2 LPS challenge of the parental generation	93
5.3 Intergenerational effects of diet-induced parental obesity	100
5.4 LPS challenge of the offspring generation	114
6 Outlook	118
Appendix	120
References	125
Eidesstattliche Versicherung	155

Summary

Studies on tissue macrophage ontogeny have led to a paradigm shift around alveolar macrophages (AMs), demonstrating their ability to self-renew in a closed fashion, without replenishment by circulating monocytes. AMs develop from foetal monocytes that seed the lung before birth. These tissue macrophages reside at the air-tissue interface, where they coordinate the response to environmental stimuli. AMs not only act as the first line of defence, but also orchestrate both the initiation and resolution of lung inflammation. Additionally they perform pivotal trophic functions that support lung development and maintenance of tissue homeostasis. These manifold functions are possible thanks to the extraordinary plasticity of AMs.

Multiple studies have shown that obese individuals present increased risk for different medical conditions, including pulmonary diseases like asthma, lung fibrosis and higher mortality rates from influenza. This complex disease affects not only the current generation, but possesses far-reaching, transgenerational repercussions. For instance, mouse models of maternal diet-induced obesity suggest an impaired lung development in offspring.

Developmental immunotoxicity studies have pointed to a specially high sensitivity of macrophages to alterations by early life environmental insults and foetal programming. Paternal obesity can lead to epigenetic reshaping of the gametes and so alter foetal development and impair pregnancy efficiency. Most importantly, obesity-induced systemic inflammation can extend to the uterus and impact gene transcription in the foetal lung. As this can induce a pro-inflammatory environment in the developing lung, this thesis addresses the hypothesis, that the period of AM development can present a window of vulnerability for programming effects by parental diet-induced obesity. Specifically, the possible impact of pro-inflammatory priming effects of parental obesity on AM maturation and its expected long-lasting adverse consequences for the offspring's lung were studied.

For this thesis, a mouse model of diet-induced obesity was established on C57BL/6J animals. Male and female mice were fed with either high-fat diet (HFD, 60 kJ% fat) or low-fat control diet (LFD, 11 kJ% fat) for 12 weeks and mated at the age of 15 weeks within diet groups. During this time, their body composition was monitored weekly by time-domain nuclear magnetic resonance. HFD effectively led to increases in body weight, body fat and body lean mass in a sexual dimorphic fashion. Changes in body composition were accompanied by hyperglycaemia and a systemic inflammation, characterised by increased circulating levels of CXCL1 and IL6. Direct effects of obesity on the lung inflammatory dynamics were analysed during an endotoxin-induced acute lung inflammation. This challenge was chosen as a proxy for a pro-inflammatory environmental stimulus on the lung. Only HF males presented differences in the course of inflammation, displaying not only lower numbers of AMs at steady state, but also a delayed initiation and resolution of inflammation. Even though

polarization studies on AMs exhibited no differences between diet groups, HF diet lead to impaired phagocytosis. These results confirmed that HFD effectively induces obesity, hyperglycaemia and systemic inflammation, which can lead to alterations in lung inflammatory dynamics in mice.

Although HFD caused direct effects in parent animals, it did not lead to a pro-inflammatory placental gene expression, affect foetal body weights nor did it compromise the structural development of the foetal lung. A reduced foetal viability was however observed, leading to a relative risk of 5.6 in HF foetuses of being resorbed before birth.

Offspring animals were further analysed two (P15) and ten weeks (P70) after birth. In order to recognize intergenerational effects of parental obesity, offspring animals were exclusively fed with LFD after weaning. Out of the three time points selected, the strongest effects of parental diet were observed at P15 in a sexual dimorphic manner. P15 HF female offspring displayed decreased body weights ($p = 3.16E-3$) and reduced internal alveolar surface area, captured by increased manual measurements of mean linear intercepts ($p = 0.043$). Parental diet had no effect in circulating inflammatory cytokines of the offspring, but altered the leukocyte structure in pubs ($p < 2.2E-16$). Intergenerational consequences of parental obesity vanished with age. P70 offspring from both LF and HF parents presented similar body weights, similar lung inflammatory dynamics after an LPS challenge of the lung and almost identical gene expression of inflammatory markers in M0 and M1 alveolar macrophages.

Taking these results together, diet-induced obesity presented characteristic sexual dimorphic effects that affected both parents and offspring. Intergenerational repercussions of parental obesity were most evident through prenatal deaths as well as through reduced body weights and altered morphology and leukocyte frequencies in the lungs of HF pubs. However, these effects were transient and disappeared with age. The experimental results presented in this thesis could not support the main hypothesis of a long-term AM pro-inflammatory priming in offspring born to obese parents. Further research on the offspring's lung immunity and development, especially on the consequences of different parental diet regimes and mouse genetic backgrounds with emphasis on the role of leukocyte populations present in the developing lung, could help identify genetic factors and immune cell populations involved in intergenerational consequences of parental obesity for the offspring's lung.

Zusammenfassung

Studien zur Ontogenese von Gewebsmakrophagen haben zu einem Paradigmenwechsel im Bezug auf Alveolarmakrophagen (AMs) geführt. Dabei wurde gezeigt, dass diese die Fähigkeit besitzen, sich unabhängig von zirkulierenden Monozyten selbst zu erneuern. AMs entwickeln sich aus fötalen Monozyten, die die Lunge noch vor der Geburt besiedeln. Sie bleiben an der Grenze zwischen Luft und Lungengewebe, wo sie die Reaktion auf Umweltstimuli koordinieren. Dabei agieren diese Makrophagen nicht nur als erste Verteidigungslinie gegen Pathogene und eingeatmete Partikel, sondern organisieren auch die Initiierung und Auflösung von Entzündungsprozessen. AMs üben zudem zentrale trophische Funktionen aus, die die Lungenentwicklung und Aufrechterhaltung der Homöostase im Gewebe unterstützen. Diese vielfältigen Rollen können AMs dank ihrer bemerkenswerten Plastizität erfüllen.

Studien haben gezeigt, dass Adipositas ein erhöhtes Risiko für Lungenerkrankungen wie Asthma und Lungenfibrose birgt. Auch führt es zu einer erhöhten Sterberate infolge von Influenza. Diese komplexe Krankheit hat generationenübergreifende Auswirkungen. Zum Beispiel wurde Diät-induzierte mütterliche Fettleibigkeit in Mausmodellen mit einer möglichen Beeinträchtigung der Lungenentwicklung in den Nachkommen in Verbindung gebracht.

Entwicklungsstudien zur Immuntoxizität haben zur Annahme einer außerordentlich hohen Empfindlichkeit der Makrophagen auf fötale Programmierung geführt. Mütterliche Fettleibigkeit kann eine systemische Entzündung hervorrufen, die bis in den Uterus hineinreichen und die Genexpression der sich entwickelnden Lunge beeinträchtigen kann. Zudem kann über epigenetische Veränderungen von Gameten der fettleibigen Väter die Embryonalentwicklung negativ beeinflusst werden. Mit der Annahme, dass die elterliche Fettleibigkeit zu einem pro-inflammatorischen Lungenmilieu führen kann, befasst sich die vorliegende Arbeit mit der Hypothese, dass die Entwicklung der AMs ein Zeitfenster erhöhter Anfälligkeit für schädliche Programmierungseffekte durch elterliche Adipositas darstellt. Insbesondere der mögliche Einfluss von pro-inflammatorischen Priming-Effekten der elterlichen Fettleibigkeit auf die Maturation der AMs und die dadurch erwarteten langanhaltenden schädlichen Auswirkungen auf die Lunge der Nachkommen wurden hierfür untersucht.

Für diese Dissertation wurde ein Mausmodell für Diät-induzierte Fettleibigkeit in C57BL/6J Tieren etabliert. Männliche wie weibliche Mäuse wurden 12 Wochen lang entweder mit fettreicher Diät (HFD, 60 kJ% Fett) oder Kontrolldiät (LFD, 11 kJ% Fett) gefüttert und im Alter von 15 Wochen innerhalb der Diätgruppen verpaart. Die HFD führte zu einer sexuell dimorphen Zunahme von Körpergewicht, Körperfett und magerer Körpermasse. Diese Veränderungen wurden von Hyperglykämie und einer systemischen Entzündung mit erhöhtem CXCL1- und IL6-Spiegel im Blutplasma begleitet. Direkte Auswirkungen der Fettleibigkeit auf die Dynamik einer durch

Endotoxin-ausgelösten akuten Entzündung der Lunge wurden untersucht, wobei LPS entzündliche Umweltreize auf die Lunge simulieren sollte. HF Männchen wiesen nicht nur eine geringere Anzahl an AMs unter normalen physiologischen Bedingungen auf, sondern auch eine Verzögerung in der Initiierung und Auflösung der Lungenentzündung. Polarisierungsstudien an AMs zeigten keine Unterschiede zwischen Diätgruppen, jedoch führte HFD zu einer beeinträchtigten Phagozytose. Die beschriebenen Ergebnisse zeigen, dass die verwendete HFD in Mäusen zuverlässig Fettleibigkeit, Hyperglykämie und eine systemische Entzündung auslöst sowie zu Veränderungen von Entzündungsprozessen in der Lunge führen kann.

Obwohl HFD direkte Auswirkungen auf die Elterntiere hatte, führte die elterliche Adipositas weder zu einer Entzündung der Placenta noch hatte sie einen Einfluss auf die Körpergewichte oder Lungenmorphologie der Föten. HF Föten zeigten jedoch eine reduzierte Lebensfähigkeit mit einem relativen Risiko einer pränatalen Resorption von 5.6.

Die Nachkommen wurden zusätzlich zwei (P15) und zehn (P70) Wochen nach der Geburt untersucht. Um intergenerationale Auswirkungen der elterlichen Fettleibigkeit erkennen zu können, wurden die Nachkommen nach dem Absetzen ausschließlich mit der LFD gefüttert. Weibliche HF P15 Nachkommen wiesen ein reduziertes Körpergewicht ($p = 3.16E-3$) sowie eine verminderte innere Alveolaroberfläche auf ($p = 0.043$), erkennbar durch erhöhte Messungen des Mean Linear Intercept. Die elterliche Diät zeigte keine Effekte auf inflammatorische Zytokine im Blutplasma der Nachkommen. Intergenerationale Einflüsse verschwanden mit zunehmendem Alter der Nachkommen. P70 Nachkommen von HF wie LF Eltern wiesen keine Unterschiede in Körpergewicht und Lungenstruktur, der Dynamik einer durch LPS induzierten Lungenentzündung oder der Genexpression von Entzündungsmarkern in M0 und M1 AMs auf.

Zusammengenommen zeigte HFD charakteristische geschlechtsspezifische Auswirkungen, die sowohl Eltern, als auch Nachkommen betrafen. Intergenerationale Beeinträchtigungen zeigten sich am deutlichsten durch die erhöhte pränatale Sterberate sowie das verminderte Körpergewicht und die veränderte Morphologie und Leukozytenstruktur in den Lungen der HF Jungtieren. Jedoch waren diese Effekte nur vorübergehend und verschwanden mit zunehmendem Alter der Nachkommen. Die Haupthypothese eines langfristigen entzündlichen Primings von AMs der Nachkommen fettleibiger Eltern wurde durch die experimentellen Ergebnisse dieser Thesis nicht unterstützt. Weitere Untersuchungen der Effekte elterlicher Fettleibigkeit auf das Lungenimmunsystem und die Lungenentwicklung der Nachkommen, mit Fokus auf die Lungenleukozytenpopulationen vor dem Hintergrund unterschiedlicher Diäten und genetischer Maushintergründe, könnten dazu beitragen, genetische Faktoren und Immunzelltypen zu erkennen, die die intergenerationalen Auswirkungen der elterlichen Adipositas auf die Lungen der Nachkommen vermitteln.

Abbreviations

Ab	antibody
Actb	beta-actin (gene)
AM	alveolar macrophage
AMs	alveolar macrophages
ANOVA	analysis of variance
APC	allophycocyanin
Arg1	arginase 1 (gene)
BAL	bronchoalveolar lavage
BCA	bicinchoninic acid assay
Bmp4	bone morphogenetic protein 4 (gene)
BSA	bovine serum albumin
CCL2	chemokine (C-C motif) ligand 2 (protein)
CD24A	CD24a antigen (protein)
CD45	cluster of differentiation 45 (see PTPRC)
CD64	cluster of differentiation 64 (see FCGR1)
Ch13	chitinase-like 3 (gene)
CO₂	carbon dioxide
COPD	chronic obstructive lung disease
Cox2	cyclooxygenase 2 (gene, see Ptsg2)
CRP	c-reactive protein (protein)
CSF2	colony stimulating factor 2 (protein, see GM-CSF)
Ctrl	control
CXCL1	chemokine (C-X-C motif) ligand 1 (protein)
CXCL2	chemokine (C-X-C motif) ligand 2 (protein)
CXCL5	chemokine (C-X-C motif) ligand 5 (protein)
Da	dalton (unit)
DAMP	damage-associated molecular pattern
DAPI	4',6-diamidino-2-phenylindole
DC	dendritic cell
DCs	dendritic cells
DMEM	Dulbecco's modified eagle medium
DMSO	dimethyl sulfoxide
DNA	deoxyribonucleic acid
DOHaD	developmental origins of health and disease
DTT	dithiothreitol
E18.5	embryonic day 18.5
EDTA	ethylenediaminetetraacetate
ELISA	enzyme-linked immunosorbent assay
EMP	erythro-myeloid progenitor
EtOH	ethanol
FACS	fluorescence activated cell sorting
FBS	foetal bovine serum
FCGR1	Fc receptor, IgG, high affinity I (protein, see CD64)
FFA	free fatty acid
FFPE	formalin-fixed, paraffin-embedded
Fgf	fibroblast growth factor (gene)
FITC	fluorescein isothiocyanate
FL	foetal liver

(continued)

FSC-A	forward scatter (area)
FSC-H	forward scatter (height)
Fzd8	frizzled class receptor 8 (gene)
Gja1	gap junction protein, alpha 1 (gene, also known as connexin 43)
GM-CSF	granulocyte-macrophage colony-stimulating factor (protein, see CSF2)
Gusb	glucuronidase, beta (gene)
H&E	haematoxylin and eosin
H2-AB1	histocompatibility 2, class II antigen A, beta 1 (protein)
HE	haemogenic endothelium
HEPES	4-(2-hydroxyethyl)-1-piperazineethanesulfonic acid
HF	high-fat
HFD	high-fat diet
Hprt	hypoxanthine-guanine phosphoribosyltransferase (gene)
HSC	haematopoietic stem cell
IFNG	interferon gamma (protein)
Il1a	interleukin 1 beta (gene)
IL1A	interleukin 1 beta (protein)
Il1b	interleukin 1 alpha (gene)
IL1B	interleukin 1 alpha (protein)
IL4	IL4 (protein)
Il6	interleukin 6 (gene)
IP	intraperitoneal
IT	intratracheal
Itgad	integrin, alpha D (gene, also known as CD11d)
ITGAM	integrin alpha M (protein, also known as CD11b)
ITGAX	integrin alpha X (protein, also known as CD11c)
kDa	kilodaltons (unit)
Kdr	kinase insert domain protein receptor (gene)
LF	low-fat
LFD	low-fat diet
Lm	mean linear intercept
LMP	lymphoid-myeloid progenitor
LPS	lipopolysaccharide
LY6C	lymphocyte antigen 6 complex, locus C (protein)
LY6G	lymphocyte antigen 6 complex, locus G (protein)
MDS	multidimensional scaling
MF	macrophage
MHCII	major histocompatibility complex class II (see H2-AB1)
MMF	medetomidine, midazolam and fentanyl
MMP9	matrix metalloproteinase-9 (protein)
MRI	magnetic resonance imaging
mRNA	messenger RNA
NaCl	sodium chloride
NLR	nucleotide-binding oligomerization domain-like receptor
Nlrp3	NLR family, pyrin domain containing 3 (gene)
NMR	nuclear magnetic resonance
NO	nitric oxide
P15	postnatal day 15
P70	postnatal day 70

(continued)

PAMP	pathogen-associated molecular pattern
PBS	phosphate buffered saline
Pdgfa	platelet derived growth factor, alpha (gene)
Pdpn	podoplanin (gene)
PE	phycoerythrin
PerCP	peridinin-chlorophyll-protein complex
PFA	paraformaldehyde
PI	propidium iodide
PMN	polymorphonuclear leukocyte
Pparg	peroxisome proliferator-activated receptor gamma (gene)
PRR	pattern recognition receptor
PTPRC	protein tyrosine phosphatase, receptor type, C (protein, see CD45)
Ptsg2	Prostaglandin-endoperoxide synthase 2 (gene)
PUFAs	polyunsaturated fatty acids
qPCR	quantitative polymerase chain reaction
Retnla	resistin like alpha (gene)
RNA	ribonucleic acid
ROS	reactive oxygen species
rpm	rounds per minute
RPMI	Roswell Park Memorial Institute medium
RQ	relative quantity
RT	room temperature
Saa3	serum amyloid A 3 (gene)
SAA3	acute-phase protein serum amyloid A3 (protein)
SC	subcutaneous
Sftpb	pulmonary surfactant-associated protein D (gene)
Sftpc	pulmonary surfactant-associated protein C (gene)
Shh	sonic hedgehog (gene)
Siglecf	sialic acid binding Ig-like lectin F (gene)
SIGLECF	sialic acid binding Ig-like lectin F (protein)
SSC-A	side scatter (area)
TD-NMR	time-domain nuclear magnetic resonance
TF	transcription factor
Timp1	tissue inhibitor of metalloproteinase 1 (gene)
TLR2	Toll-like receptor 2 (protein)
TLR4	Toll-like receptor 4 (protein)
TM	tissue macrophage
TNF	tumor necrosis factor alpha (protein)
Tnfrsf11a	tumor necrosis factor receptor superfamily, member 11a, NFKB activator (gene)
tSNE	t-distributed stochastic neighbor embedding
Vegfa	vascular endothelial growth factor A (gene)
Vegfr2	vascular endothelial growth factor receptor 2 (gene, see Kdr)
WAT	white adipose tissue
Wnt2	wingless-type MMTV integration site family, member 2 (gene)
WT	wildtype

1 Introduction

1.1 Developmental origins of health and disease

Developmental origins of health and disease (DOHaD) aims to decipher how environmental factors act on disease aetiology^[1] with the final goal of preventing non-communicable diseases^[2]. It states that environmental insults on a developing tissue early in life can lead to long-term and sometimes irreversible epigenetic and phenotypic consequences. If stressors happen to take place during critical periods of tissue growth and development they can lead to maximal repercussions^[3]. The DOHaD concept further proposes prevention of diseases and even health enhancement through exposure to positive factors.

Vulnerable developmental periods are characterised by a high tissue plasticity and therefore sensitivity to its environment. This contributes to high responsiveness towards environmental stimuli and ensures a best phenotypic fit to promote survival^[4]. These periods however also pose windows of vulnerability, where tissue might adversely develop upon exposure to stressors^[5].

Programming^[6] processes can take place in-utero^[7], throughout perinatal age^[8] and during early childhood^[9-11] - while organs still continue to adapt and develop. It even can take place pre-conceptually^[12,13].

After plasticity is lost with age, affected tissues might remain permanently committed to phenotypical adaptations and be subject to irreversible developmental damage^[14]. Consequences of this can be diverse, but specially deleterious if a mismatch between environmental stimuli during early and adult life is present^[15].

Epidemiologic observations of transgenerational disease after severe malnutrition in the form of famines, e. g. the Dutch famine between 1944 and 1945^[16] and the longer famine of Leningrad between 1941 and 1944^[17], paved the way for research in the field of DOHaD. Originally, DOHaD focused on nutritional effects on the offspring^[7,16,18]. Knowledge of developmental stressors has since grown^[1]. Today it is well known that exposure to different challenges during development - including inflammation^[19], infection^[20,21], glucocorticoids^[22], hypoxia^[23], stress^[24,25], pesticides^[26], hormonal perturbations^[27,28], heavy metals^[29,30] and other toxins^[31,32] - can disrupt a healthy adult phenotype. Depending on the specific insult, its duration and developmental time point of occurrence, such challenges can impact particular tissues to specific extent, oftentimes in a sexual dimorphic fashion^[17,32]. The resulting physiological and behavioural consequences can carry over beyond the first generation of progeny^[33-36].

Several stressors have already been described around DOHaD of the lung. To name a few, maternal smoking during pregnancy has shown to be a major factor that alters fetal lung development and leads to a long term increased risk of respiratory adverse conditions like asthma^[37], pulmonary hypoplasia (underdeveloped alveoli and altered airway morphology)^[38,39] and chronic obstructive lung disease (COPD)^[40]. Mechanical

ventilation during neonatal age can lead to bronchopulmonary dysplasia^[41,42]. Likewise, the exposure to ambient air pollution (air-borne toxins, including particulate matter from combustion processes) during the final phase of lung development can lead to an impaired lung growth and chronic deficits in lung function^[43-45].

1.2 The lung

As the main organ of the respiratory system, the lung fulfils the vital task of gas exchange. For this, the lung possesses an enormous inner surface with a fine air-blood barrier^[46]. This huge gas exchanging area is mostly made up by the pulmonary alveoli – the smallest functional gas-exchange units of the lung. Alveoli are mostly found within the alveolar sacs at the end of the basic units of respiration (acini)^[47]. Further vital components of the lung include the conducting airways (bronchi and bronchioles) that transport air to the alveoli, a vast and effective vasculature^[46] as well as a surfactant system providing inflation stability^[48] and immune modulation^[49].

Three main periods of lung development are defined based on morphological characteristics of the organ (*Figure 1*) – the embryonic, the foetal and the postnatal periods. In the mouse, lung organogenesis starts with the formation of the anlage of the two lungs, the establishment of the major airways and pleura between embryonic days 9.5 (E9.5) and E12 (human: 4-7 weeks). During this stage, two lung buds pouch out of the ventral wall of the primitive foregut (endoderm) and grow into the surrounding mesenchyme through repetitive cycles of branching morphogenesis^[50]. This process is highly dependent on the correct crosstalk between epithelial and mesenchymal cells through factors like fibroblast growth factor 10 (FGF10), bone morphogenic protein 4 (BMP4), Sonic Hedgehog (Shh) and transforming growth factor beta (TGFb)^[51].

The foetal period of lung development is subdivided into the pseudoglandular, canalicular and saccular stages. During the pseudoglandular phase at the ages E12.5-E16.5 (human: 5-17 weeks) the bronchial tree is formed through further branching morphogenesis and the primitive airway epithelium as well as the first ciliated, goblet and basal and smooth muscle cells begin to emerge^[52,53]. At the end of this stage, the acini are built, even though acinar epithelial cells are not yet fully differentiated^[54].

During the second phase of the foetal lung development – the canalicular phase at the ages of E16.5–E17.5 (human: 16–26 weeks) – the morphological distinction between conducting and respiratory airways becomes possible thanks to the differentiation of the epithelia. During this phase cuboidal epithelial cells differentiate into type I (AECI; squamous, thin and flat cells covering most (>95%) of the inner surface area of the alveolar ducts and sacculi; implicated in gas exchange to the blood) and alveolar epithelial type II cells (AECII; AECI progenitors and surfactant producers)^[55]. This allows for the recognition of the acinus (and in human also of the respiratory bronchioles) for the first time. Further, intensive angiogenesis, the condensation of mesenchyme through apoptosis and the close contact that the alveolar epithelium

acquires with the capillary network lead to development of the primitive air-blood barrier^[51,56]. During this phase increased expression of VEGF and surfactant proteins becomes apparent.

Lastly, during the saccular stage at the ages between E17.5 and postnatal day 4 (P4) (human: 24–38 weeks) branching morphogenesis ceases in order to allow the start of alveolarization^[57]. This is characterized by the expansion of the respiratory area through widening of the sacculi, further condensation of the mesenchyme and the formation of the primary septa to enlarge the gas-exchange area. Depending on the animal species, alveolarization can start already before birth – e. g. in precocial mammals like sheep^[58]. Mice are insessorial mammals born during the saccular stage^[59], while humans present an early alveolar stage during term^[60].

After birth (postnatal period of lung development) alveolarization continues as long as the lungs are growing. The process of alveolarization is of biphasic nature^[61,62]. It is characterized by the formation of immature secondary septae between P4 and P21 (human: week 36, before birth) in a stage termed classical alveolarization and the final maturation of secondary septae with the formation of further alveoli during the stage of continued alveolarization (P14-P36; human: 2-21 years after birth). Septae immaturity can be recognized by the presence of an inefficient double-layered capillary network. Mature septae on the other hand are thinner and undergo a fusion process during microvascular maturation (P4-P36; human: 3-21 years) where the two capillary layers form a single-layer capillary network with high efficiency for gas exchange^[63].

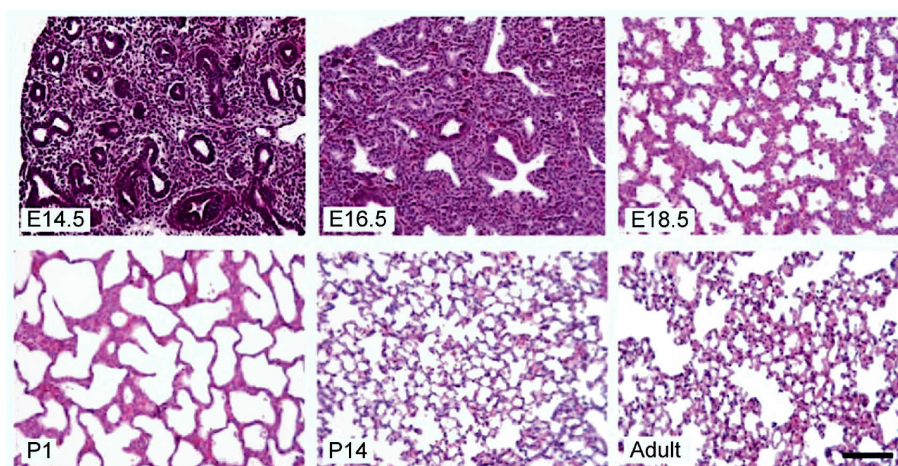


Figure 1: Morphological characteristics of the developing mouse lung. Histology of the murine lung at representative phases of organogenesis: pseudoglandular stage (E14.5); canalicular stage (E16.5); saccular stage (E18.5); terminal sac stage (P1); neonatal lung alveolarization stage (P14); final alveolar maturation stage (adult). Scale bar: 100 μm . (*Adapted from Warburton et al. 2010*)

1.3 Tissue macrophages

Macrophages (MFs, from Greek “big eaters”) are highly specialized leukocytes belonging to the innate immune system of most metazoans. They were first described by the embryologist Ilya Metchnikoff in the late 19th century in his “phagocytosis” (from Greek “phagos” = to eat and “cyte” = cell) and “physiological inflammation” theories. Metchnikoff quickly recognized the MF’s important role in preserving the integrity and ‘harmony’ in the organism by not only protecting it from foreign invaders (pathogens) and clearing the body of unwanted cellular debris (injury repair), but also combating “pathological inflammation”. He also hypothesized an ancient pluripotential autonomy which enabled MFs to have a wide spectrum of functions^[64].

MFs present peculiar morphological characteristics and a core macrophage expression signature, which distinguishes them from other related cell populations like monocytes and dendritic cells (DCs)^[65–67]. MFs can be encountered in all tissues and display a great functional diversity. This is not only evident through specialized functions within different tissues^[68], but also at specific developmental stages of the mouse. During foetal development, MFs orchestrate organogenesis and tissue remodelling, and aid in foetal liver erythropoiesis^[69]. At a perinatal age, MFs further assist in organ development, tissue regeneration and immune surveillance. In adulthood, they tightly regulate inflammatory sequences, including the ones necessary for tissue repair and wound healing^[70].

1.3.1 Tissue macrophage ontogeny

Due to their gargantuan phenotypic heterogeneity, vast efforts have been made to classify MFs. Following their description as phagocytes after 1892, MFs were classified as part of the reticulo-endothelial system (RES).^[71] After several attempts to separate resident phagocytes (MFs) from their antecedents (monocytes), the term mononuclear phagocyte system (MPS) was coined in 1972 by Van Furth and colleagues^[72,73]. However, the MPS was later expanded to encompass monocytes, MFs and DCs^[74,75]. This group of cells were thought to exclusively develop from committed bone marrow (BM) progenitors. Circulating monocytes were said to continuously seed tissues at steady state and replenish local tissue myeloid cell populations. However, this theory was quickly challenged by the recognition of *in situ* “self-reproducing” capacity of MFs^[76] and the relative radioresistance^[77–81] of some tissue macrophages (TMs) which lead to questioning the effectiveness of macrophage depletion analyses.

More contemporary studies presented evidence that MF populations in the adult gut, dermis, spleen, liver, heart and serous cavities indeed partially derive from circulating monocytes and thus could follow Van Furth's model to some extent^[82–88]. Nevertheless, thanks to modern techniques like fate mapping analysis, nowadays it is well recognised that several TMs are long-lived and have the ability to self-renew. TMs do not exclusively derive from blood monocytes, but rather from local precursors established during embryonic development^[74,80,88–93]. TM populations like microglia^[78,94], epidermal Langerhans^[77] and alveolar macrophage (AM)^[81,95] niches are maintained (almost) entirely locally throughout life^[81,95–97].

The identification of different embryonic primordial cells that act as myeloid progenitors during haematopoiesis facilitated a comprehensive division of the haematopoietic process in three different “waves”. These are referred to as primitive, transient-definitive^[98] and definitive embryonic hematopoietic programs^[99,100].

Embryonic haematopoiesis in the mouse starts with the first wave in the extra-embryonic yolk sac (YS) at the embryonic day 7.0 (E7.0)^[101], giving rise to primitive erythroblast, megakaryocyte^[102] and macrophage lineages (“early” Myb⁻ erythro-myeloid progenitors, EMPs)^[103]. The latter develop into YS macrophages, without passing through monocyte intermediates^[101,103,104], and spread in the embryo proper from E8.5 to E10 after blood circulation has been established (E8.5-E9.0)^[105]. However, microglia (brain TMs) has been proposed to be the only adult TM population derived from YS MFs^[94].

The second wave of haematopoietic progenitors arises from the extra-embryonic haemogenic endothelium (HE), formed between E8.0 and E8.25 in the YS. There, multipotent precursors sequentially gain myeloid (EMPs)^[106] then lymphoid (lymphoid-myeloid progenitors, LMPs)^[107] potential. EMPs (Kit⁺, Itga2b⁺, Myb⁺^[103] “late” EMPs) rapidly migrate to the foetal liver (FL) at E9.5, where they develop into different myeloid cells^[108], including FL monocytes (E12.5)^[103]. FL monocytes enter the circulation by E13.5. They colonize every tissue, except the brain (closed blood-brain barrier)^[90], dilute previously seeded YS MFs and give rise to most TM populations^[103].

Definitive haematopoiesis is established with the third haematopoietic wave. The first immature HSCs are observed within the intra-embryonic HE of the para-aortic splanchnopleura, which give rise to foetal HSCs in the aorta, gonads, and mesonephros regions (AGM) between E8.5 and E10.5^[109,110]. Mature-HSCs and pre-HSCs then colonize the FL around E10.5^[111] to establish definitive haematopoiesis after E12.5^[112]. Following E15.5 and E17.5 respectively, they seed the spleen and BM^[107], and drive the generation of adult BM HSCs. However, typical HSC-derived haematopoiesis occur in the BM around perinatal age and possibly only after birth^[113].

Although the embryonic origin of different TMs is well accepted, the exact identity of primordial progenitors, their pathways of differentiation and precise transcription factor specification have yet to be clearly defined. These unknowns have led to slightly different models of TM embryonic ontogeny^[99,103,114,115]. Likewise, the question of the extent in which foetal HSCs or adult HSCs contribute to TM niches, specially during perinatal age, remains unanswered^[99,100].

Monocyte-derived macrophages can indeed complementary replenish prenatally established TM populations under tissue stress circumstances like irradiation, infection, sterile inflammation or macrophage depletion^[116–122]. These monocyte-derived TMs display almost identical gene expression profiles as their foetal-derived counterparts once they have undergone a microenvironment-induced phenotypic transformation^[122]. Nevertheless, even after successful tissue colonisation and acquisition of similar functionality, unique gene-expression profiles and remainings of epigenetic hallmarks can be observed in monocyte-derived TMs^[122,123].

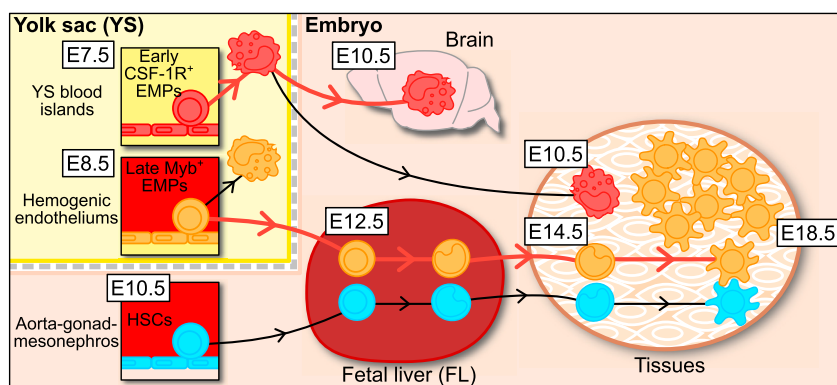


Figure 2: Tissue macrophage ontogeny. Macrophages can be derived from three different embryonic hematopoietic waves. 1) The primitive wave starts at E7.0 in the YS blood and presents the source of YS macrophages from which brain microglia are derived. 2) The transient-definitive wave takes place in the extra-embryonic haemogenic endothelium (HE) between E8.0 and E8.25 from which foetal liver (FL) monocytes will ultimately develop at E12.5. FL monocytes gain access to the circulation around E13.5 and infiltrate every tissue, giving rise to most adult TMs. 3) Definitive haematopoiesis commences between E8.5 and E10.5 within the intra-embryonic HE. Hematopoietic stem cells (HSC) from this program seed the spleen and BM at E15.5 and E17.5 respectively, but HSC-derived haematopoiesis possibly occurs only after birth. HSC-derived blood monocytes can give rise to a minor population of TMs. (*Adapted from Hoeffel & Ginhoux 2018*).

1.4 Alveolar macrophages

AMs are highly specialized mononuclear phagocytic cells located in the alveolar space of the lungs^[124], where they constitute the most abundant haematopoietic cell type at steady state, forming over 90% of its cellular content^[125]. A total of $3E5$ to $1E6$ ^[126] AMs are thought to reside in the alveoli of a mouse lung. Since the mouse lung is roughly estimated to encompass between one and three million alveoli^[127–129], a single AM is said to be found in approximately every third alveolus^[130]. In order to surveil the alveolar lumen, AMs may migrate within a single alveolar sac, but also among multiple alveolar sacs through connecting Kohn pores^[131,132].

The tissue macrophages in the lung can be generally divided into two populations depending on their localization: alveolar macrophages (AMs) that line the surface of alveoli and interstitial macrophages (IMs) that reside in the pulmonary interstitium (lung parenchyme)^[133]. Apart from the location where they reside, AMs can be distinguished from IMs e. g. through flow/mass cytometric characterization based on the expression of surface markers (AMs: ITGAX⁺, SIGLECF⁺, ITGAM⁻, H2-AB1⁻; IMs: ITGAX^{int}, SIGLECF⁻, ITGAM⁺, H2-AB1⁺)^[134]. Additionally, each macrophage population has unique phenotypic and functional profiles. AMs are a particularly competent first line of defence with phagocytic potential, a strong microbicidal activity through large production of reactive oxygen species (ROS), nitric oxide (NO), TNF and IFN γ . On the other hand, IMs can more efficiently release immune-regulatory cytokines like interleukin 1 (IL1), IL6 and IL10, and better stimulate T-cell proliferation^[135]. IMs can inhibit DC maturation and migration, preventing aberrant immune responses to harmless aeroantigens (immunological tolerance in the sensitization phase of lung immune responses)^[136]. By contrast, AMs can restrict the expression of antigen-specific antibodies after sensitization (effector phase of pulmonary immune responses) through the suppression of T-cell activation and the regulation of plasma cell activity^[137], complementing immunosuppressive effects of IMs.

In their role as first line of defence at the air-tissue interface in the lung, AMs are the first immune-competent cells to encounter inhaled antigens and therefore play an important role in regulating immune responses of the lung^[138]. Unquestionable is their role as phagocytes – AMs can engulf viruses, bacteria, fungal cells, and a variety of appropriately sized non-living particulates. Additionally, AMs can clear apoptotic and necrotic cells through recognition of “eat me” signals like exposed phosphatidylserine or calreticulin^[139]. Through this so-called efferocytosis, AMs remove dying cells before they release harmful intracellular content into the local microenvironment. Once engulfed, particulates may be degraded by lysosomal enzymes or retained encapsulated within the macrophages and transferred to lymph nodes draining the site or are cleared from the airway by the mucociliary system^[140]. Phagocytosis of many pathogens is mediated by the AM toll-like receptors (TLRs)^[141]. AMs also present scavenger receptors that facilitate phagocytosis of particles coated with surfactant proteins A^[142] and D^[143], which bind to a wide variety of bacteria and opsonize them.

AMs support lung homeostasis not only through their immune functions, but also through trophic, regulatory and repair functions. Probably one of the most prominent roles of alveolar macrophages include surfactant clearance^[144]. These phospholipoprotein complexes are synthesized and secreted by alveolar epithelial type II cells^[145]. Surfactant is of uttermost importance for the reduction of surface tension and therefore for the correct inflation of the alveoli. Surfactant catabolism requires stimulation of AMs by colony-stimulating factor 2 (CSF2) via the transcription factor SPI1^[146]. Disorders of surfactant homeostasis brought about e. g. by genetic alterations in any of the aforementioned genes can lead to pulmonary alveolar proteinosis and can result in respiratory insufficiency.

1.4.1 Alveolar macrophage ontogeny

Mouse experiments employing a surgical-induced sharing of blood circulation (parabiosis) and the analysis of proliferating cells (BrdU labelling) have shown that the AM population is maintained almost entirely locally throughout life by self-renewal. Williams et al.^[81] could demonstrate in 2013 that this TM niche arises from FL monocytes that seed the developing lung before birth at E14. Lung tissue stress (e. g. irradiation) can indeed lead to replenishment of AMs by circulating adult HSC-derived monocytes^[81,91,92,119,121,123,147]. However, under tissue homeostasis, at least 95% of AMs are of foetal origin in 14 months old mice^[123] and 87% of them can persist at least for 3.5 years after lung transplantation in humans^[148].

FL monocytes are not the only haematopoietic cell population that seeds the foetal lung. YS foetal macrophages populate the developing lung tissue after E8.5^[91]. Even though these foetal cells have the potential to differentiate to mature AMs and colonize the lung before FL monocytes, they underlay a competitive disadvantage in colonizing the AM niche due to a lower expression of the CSF2 receptor and a lower intrinsic proliferative potential^[122]. For this reason, FL monocytes overcompete the YS macrophage population after the first breath and give rise to the stable AM niche. Tan et al. proposed 2016^[149] after analysis of lineage tracing and parabiosis experiments in mice, that the YS MF population remains in the lung interstitium and redistributes to submesothelial and perivascular zones, generating a stable IM population. Together with a third wave of IMs that dispersedly populates the lung interstitium and is maintained by circulating progenitors, these authors propose the presence of three independent populations of TMs in the lung, based on their origin^[149].

Similar to the microglia (brain) and the Langerhans (skin) populations, the AM niche remains stable, without significant displacement by MFs derived from adult HSCs at steady state. This is why the brain, skin and lung are referred to as closed tissues^[99] with respect to such TM populations (see *Figure 3*). Only in extreme cases of tissue stress like irradiation, lung injury or AM depletion, e. g. using diphtheria toxin, monocyte-derived MFs will complementary replenish the prenatally established

the AM population^[91,92,119,121,147]. During this replenishment process, IMs provide an intermediate pool between blood monocytes and AMs^[120,123]. After successful colonisation of the alveoli and the acquisition of a AM phenotype and functionality through imprinting by the lung microenvironment^[150], unique gene-expression profiles and remaining epigenetic hallmarks can be observed in these monocyte-derived AMs^[122,123].

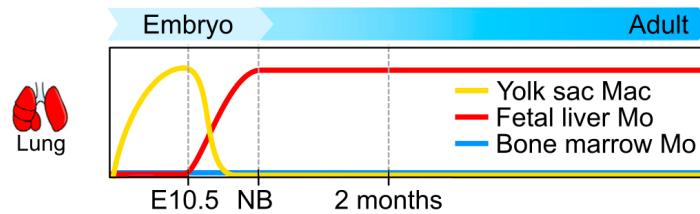


Figure 3: Contribution of macrophage populations to the AM niche. YS foetal macrophages populate the developing lung tissue after E8.5 while FL monocytes arrive at around E14. Both display a potential to differentiate to mature AMs and colonize the lung, however FL monocytes present a competitive advantage due to a higher expression of the CSF2R and a higher intrinsic proliferative potential. YS macrophage population is completely replaced by FL monocytes. The lung is an example of a closed tissue, where the TM niche remains stable, without replacement by adult monocyte-derived MFs. (*Adapted from Ginhoux & Guilliams 2016*).

The maturation of AMs depends strongly on alveolar type-II epithelial cell-secreted CSF2^[151]. The acquisition of a mature phenotype is characterised by, among other features, the upregulation of *Itgax* and *SiglecF*^[81] and the downregulation of *Ly6C*, *Itgam*, *Mmp12* and *Pla2g7*^[152,153]. Interestingly, studies have shown that CSF2 is not only important for the commitment, differentiation and survival of cells^[154], but can also have a dual role, both as a pro-inflammatory as well as a regulatory cytokine^[155]. This duality appears to be dependent on the dose of CSF2, the microenvironment where this cytokine acts on target cells and the presence of other cytokines. While pro-inflammatory molecules like IL1, IL2, TNF, and IFN γ lead to an increased production and secretion of CSF2, immune-regulatory cytokines such as IL10 and TGF β can down-regulate CSF2^[156]. The incorrect regulation of CSF2 has already been implicated in the pathogenesis of different immune disorders. A well described example is rheumatoid arthritis, a chronic pro-inflammatory disease that leads to intense pain and degeneration of the joints due to the uncontrolled expression of pro-inflammatory molecules by M1 macrophages (TNF, IL1, IL6)^[157]. In the context of the lung tissue, a dysregulation of CSF2 can lead to the autoimmune disease pulmonary alveolar proteinosis^[158].

CSF2 signalling in AMs induces the expression of PPAR γ ^[152]. This key transcription factor (TF) acts as a nuclear receptor for several ligands, including polyunsaturated fatty acids like arachidonic acid and its metabolites, and the antidiabetic drug thiazolidinedione. Together with retinoid X receptors, PPAR γ forms heterodimers to regulate gene transcription. PPAR γ is mostly known for its role as master regulator of adipocyte differentiation and control of the expression of genes involved in lipid metabolism^[159].

PPAR γ deficiency is specifically observed in AM from patients with pulmonary alveolar proteinosis^[160]. A similar phenotype can be induced in mice by the conditional knockout of the Pparg^[152], Csf2^[151] or Csf2r genes^[161]. This lung disease exhibits a distinctive accumulation of surfactant in the alveolar space as well as large foam cells – AMs engorged with intracellular lipid droplets due to their inability to metabolize surfactant^[162].

Another central molecule in the maturation of AMs is the actin-bundling protein L-plastin. Its importance was presented by Todd et al. in 2016^[153] with experiments demonstrating that its expression in FL monocytes is crucial for their transmigration into the alveoli by supporting podosome formation. These integrin-based organelles are not only necessary for cell trafficking into the airspace, but also for AM retention. Furthermore, these experiments showed the importance of L-plastin in Csf2 signalling, since its absence resulted in failure to upregulate Pparg in developing AMs, despite abundant presence of CSF2^[153].

While FL monocytes downregulate Ly6C and upregulate Itgax shortly before birth, it is until after the first breath that these maturing AMs express SiglecF^[81] and are recognized as mature AMs. Interestingly, this definitive AM differentiation occurs in parallel with the development of the alveoli, starting in mice around embryonic day E18.5 and completed after birth (as presented in *Section 1.2*). The first breath after birth may be viewed as the lung's first wound^[163] and transforms the lung microenvironment in ways that haven't been fully defined yet. However, it has been demonstrated that the exposure to the external, non-sterile environment and the mechanical stress produced by spontaneous ventilation play an essential role in the alveolar and immune development of the lung^[164]. Ventilation forces mechanically activate alveolar epithelial type 2 cells to produce IL33 which in turn induce IL13 expression on type 2 innate lymphoid cells^[165]. Besides the increased expression of Pparg induced by Csf2 signalling, the presence of IL13 also stimulates AMs anti-inflammatory, and tissue repair and remodelling phenotype. This suggests an important role of M2 AMs in the final lung alveolarization process^[166].

1.4.2 Alveolar macrophage plasticity

Until recent years (1990s)^[167], tissue macrophage's extended functions beyond simply "eating" and as first line of host defence remained unexplored. However, progress in understanding their ontogeny as well as their interactions with other cells and the rest of their microenvironment have lead to recognition of MF's high adaptability. This has allowed an appreciation of their critical roles in tissue health (normal) and disease (abnormal tissue homeostasis).

Similar to other macrophages, AMs have the exceptional ability to quickly undergo a plethora of functional and phenotypic changes as a response to microenvironmental cues. This plasticity allows AMs to undertake their numerous functions in the lung. The final goal of this polarization is the restoration of tissue homeostasis. This response occurs dynamically, following oscillations in the microenvironment. After signalling ceases, AMs will ultimately return to their steady state functional status^[167].

Macrophage polarization has been extensively characterized. However, this has been mostly done *in vitro* using bone marrow derived macrophages and culture conditions that only resemble extreme adverse tissue circumstances. These studies lead to the M1/M2 nomenclature proposed for the polarization statuses of macrophages based on studies of lymphocyte biology. Similar to the Th1/Th2 dichotomy, “classically activated”^[168] AMs (M1) can be induced by the presence of inflammatory factors like TNF, IFN γ , CSF2, microbial, and/or particulate matter^[169], which are used as proxies for lung injury, infection or inflammation. On the other hand, “alternatively activated”^[170] AMs (M2) might be generated by the addition of IL4, IL13, CSF1, and/or components from parasitic organisms^[171] to the culture medium as proxies for injury-resolving, remodelling-inducing, and/or lung parasitic cues. It is important to remark, that such extreme conditions are encountered rather seldom *in vivo*. The continuum^[172,173] of possible polarization statuses of macrophages is dynamic and often presents overlapping M1 and M2 functions, depending on the particular tissue’s physiological condition^[70]. This observation has led to the derivation of more complex nomenclature and experimental guidelines^[174] for the analysis of macrophage polarization and approximation of *in vivo* conditions.

The analysis of fully polarized M1 and M2 macrophages has led to the recognition of polarization biomarkers that help better describe the functional state of AMs *in vivo*^[175]. Polarized macrophages present characteristic cytokine, chemokine and receptor (surface protein) expression. Different biochemical techniques can be employed for the differential expression analysis of such molecules. Possibly the most widely used method for such analysis at the gene expression level (mRNA) is real time polymerase chain reaction. Flow cytometry represents an alternative approach for the characterization of polarization at a protein level as well as for the validation of novel polarization biomarkers^[176].

To name a few examples, M1 AMs display increased expression of the genes Tnf, Il1, Il12b, prostaglandin-endoperoxide synthase 2 (Ptgs2), chemokine (C-C motif) ligand 2 (Ccl2), Cxcl2 and Cxcl10 and of the membrane receptors TLR2, TLR4, CD16, IL1 R type I and CD32. M2 AMs typically produce higher levels of resistin-like alfa (Retnla), chitinase-like 3 (Chil3), Il10, Tgfb as well as of the IL1 receptor antagonist (IL1ra), the type II IL1 decoy receptor, the mannose receptor C type 1 (MRC1), scavenger receptors A

and B, CD163 and CD14^[170,176–178]. It has to be noted that this is not an exhaustive list of polarization markers and that depending on the organism (e. g. human vs. mouse)^[174], strain^[179] and tissue^[65], such polarization markers will vary. It is crucial to take this into account, when comparing results from different experimental setups.

The arginine metabolism represents a central pathway in macrophage polarization^[180]. In this context two enzymes play pivotal roles: arginase 1 (ARG1) and nitric oxide synthase 2 (NOS2). They compete for the catabolism of arginine and ultimately regulate the AM's metabolic and immune response outcome. While ARG1 expression can be induced by M2 cues like IL4, IL13 over signal transducer and activator of transcription 6 (STAT6) or alternatively by IL10, CSF1, and agonists of the peroxisome proliferator-activated receptor transcription factors (PPARg and PPARd)^[181], among others, the transcription of NOS2 is under control of pro-inflammatory factors, such as interferon gamma (INFg), tumour necrosis factor alpha (TNF) and IL1b, and others, that act through STAT1 signalling^[182].

A critical catabolic product of NOS enzymes is nitric oxide, which plays pivotal roles in processes associated with vasodilatation, cytotoxicity and pro-inflammatory immune modulation^[183]. Ornithine on the other hand, is a catalytic product from ARG1 activity and act as precursor for the production of polyamines (via ornithine decarboxylase), which regulate cell proliferation and differentiation, and proline (via ornithine aminotransferase), which is critical for the synthesis of collagen for wound healing and tissue repair^[184].

In this context, it is important to remark once more, that M1 and M2 are only two extreme of a spectrum mostly defined by *in vitro* conditions.

1.4.3 Alveolar macrophages in health and disease

M1 responses are essential in the fight against bacterial and viral pathogens. For an enhanced microbicidal and tumoricidal activity, classically activated AMs produce reactive oxygen species and nitric oxide through the upregulation of NOS2. Together with an increased secretion of pro-inflammatory cytokines as well as neutrophil-recruiting and -activating chemokines, these factors confer AMs their pathogen-killing abilities. Additionally, M1 AMs display enhanced antigen-presentation abilities^[178] as well as increased expression and secretion of matrix metalloproteinases (MMPs) like MMP9, which allow AMs to migrate during inflammatory responses^[185]. M1 AMs can be observed during acute infectious diseases, as in the case of infections with *S. pneumoniae*^[186] or rhinoviruses^[187]. Excessive or prolonged pro-inflammatory activation can however trigger collateral tissue damage due to the toxic activity of M1 products^[172,185] and predispose tissue to neoplastic transformation^[188].

During a “natural resolution of inflammation”^[189] a transition from M1 to M2 polarization and/or apoptosis of M1 macrophages occurs. M2 macrophages are less toxic to microbes and vulnerable host cells. They acquire anti-inflammatory and tissue repair functions that facilitate wound healing after inflammatory processes^[190]. M2 macrophages help clear parasites, reduce inflammation, promote tissue remodelling. These macrophages are characterized by increased phagocytic activity^[191], the expression of the scavenging mannose^[192] and galactose receptors^[193]. The secretion of ornithine and polyamines^[184], cytokines like CCL17 and CCL22, and the expression of molecules associated with development, angiogenesis and fibrogenic activity, e. g. WNT ligands, platelet-derived growth factor (PDGF), TGF β and fibroblast growth factor (FGF)^[194] are important characteristics of M2 macrophages as well. Aberrant and uncontrolled M2 activation of macrophages can however lead to increased microbial survival and pathogenicity^[165], induce fibrosis^[70], exacerbate allergic reactions^[195], promote tumour progression and facilitate metastasis^[196].

Both M1 and M2 macrophages have been implicated in several diseases, including mayor lung diseases like asthma, cystic fibrosis, chronic obstructive pulmonary disease (COPD) and pulmonary fibrosis^[197–199]. Even though the pathogenesis of each of these examples appears to be dominated by the presence of either one of the two polarization statuses, increasing evidence demonstrate the involvement of both phenotypes in disease development, where rather the correct phenotype switch between M1 and M2 becomes compromised.

Asthma is a chronic, heterogeneous and complex inflammatory disease of the airways. It is characterised by increased mucus production, airway remodelling and hyperresponsiveness to different airborne agents, with symptoms like coughing, wheezing, chest tightness and shortness of breath^[200]. Elaborating on the aberrant polarization of AMs during the development and advancement of this disease, it can be observed that while M2-polarized AMs and their biomarkers strongly correlate with asthma and its severity^[201], so do M1-associated molecules. M2 AMs aggravate airway inflammation in asthmatic mice^[202], enhance collagen deposition and increase lower airway hyperresponsiveness, mucus-secreting cell proliferation as well as collagen deposition^[203]. M2 macrophages also promote lung infiltration and activation of inflammatory cells – especially of eosinophils^[204]. M1 AMs on the other hand might promote airway inflammation and hyperreactivity in atopic asthma through TNF^[205,206] and INF γ as well as through the recruitment of eosinophils, but specially of neutrophils^[207]. Additionally, LPS-induced M1 MFs might play an important role in the development of corticosteroid resistance^[208].

In summary, a correct physiologic M1/M2 balance will determine the maintenance of health and tissue homeostasis or the development of disease. Such balance will typically depend on the specific tissue of interest^[65,209] and can be influenced by multiple factors. Studies on developmental immunotoxicity strongly suggest a specially high sensitivity of MFs to alterations by early life environmental insults and foetal programming^[210].

In the case of the lung tissue, M2 polarization of AMs plays a crucial role not only during development, but also during lung homeostasis at steady state. This M2 phenotype is pivotal during the final alveolarization phase, after the first breath^[165,211]. In general, TMs retain an M2 phenotype in healthy tissue^[212,213]. Such quiescent status is important in the lung to hinder unnecessary and tissue-damaging pro-inflammatory signalling upon contact with innocuous airborne molecules. This ground M2 polarization is evidenced by the poor antigen presentation^[214] and lack of co-stimulatory molecules, like CD86^[215] on AMs, which lead to T-cell unresponsiveness and hinder the activation of the adaptive immune system against harmless inhaled antigens. Additionally, AMs at steady state show reduced phagocytic capacity (compared with IMs), decreased respiratory burst and produce immunosuppressive prostaglandins^[209]. During homeostasis, AMs also express other M2-associated biomarkers like TGF^[216], the mannose receptor C type 1 (Mrc1)^[217], stabilin 1 (Stab1), Cd200r^[218], signal-regulatory protein alpha (Sirpa)^[219] as well as reduced M1 markers like Cd14 and H2-Ab^[217].

Aging reduces the responsiveness of MFs to activation stimuli^[213]. This can be observed in aged mice through a blunted IL4 response with diminished Arg1, Chil3 and Retnla expression in MFs compared with young animals^[220]. This might be a reason why correct immune responses progressively deteriorates with age.

1.5 Obesity

Obesity is a complex and multifactorial pathological condition of increased accumulation of excess body fat caused by an imbalance between energy intake and energy expenditure. In humans, such dysregulation of energy balance is complex and has multifactorial aetiologies^[221]. It arises through interactions between the individual's genetics, development, its environment and multiple psycho-social factors. Even though the heritability (portion of phenotype variability explained by genetic variation in a specific environment) of excessive body fat is estimated to be high (40-70%^[222-224]), genetics alone cannot explain the present global rise in obesity^[225,226]. It arises rather as result of an unhealthy lifestyle, which very often is imposed by exposure to modern rural and urban environments^[227].

A myriad of concurrent diseases have been already associated with obesity^[228]. These emphasize the systemic impact of a chronically sustained positive energy balance and why this is highly critical risk factor for non-communicable diseases. Examples of such include: hypertension, type 2 diabetes, cardiovascular disease, gastroesophageal reflux disease, cholelithiasis, non-alcoholic fatty liver disease, osteoarthritis, pancreatitis, gout, multiple forms of cancer, psychological conditions like anxiety and depression, neurodegeneration, urinary incontinence, overall premature death, infertility, obstructive sleep apnoea, and several other disorders of the respiratory system^[228].

Because of these strong comorbidities and its alarmingly high increasing rate during the last four decades worldwide^[229], obesity has been categorized as a pandemic^[230,231]. In an attempt to introduce an easy-to-apply method for determining and categorizing obesity in humans, the world health organization (WHO) has proposed six statuses of nutrition^[232] (see *Table 2*) for adults over 20 years of age by means of the body mass index (BMI). This anthropometric index - also known as the Quetelet index^[233] - is calculated as the ratio of an individual's weight to its squared height (kg/m^2). Each status was defined by its associated risk to different comorbidities^[234,235] and serves as an approximate surrogate of body fat mass.

Table 2: Nutritional status based on BMI. Adapted from *www.euro.who.int*

BMI [kg/m^2]	Nutritional status
Below 18.5	Underweight
18.5 – 24.9	Normal weight
25.0 – 29.9	Pre-obesity
30.0 – 34.9	Obesity class I
35.0 – 39.9	Obesity class II
Above 40	Obesity class III

However simple to measure, the BMI has caveats when applying it not at an individual level, but on different ethnicities and individuals of different age or gender. Its definition assumes that most variation in weight for a population of similar height is due to body fat mass. However, it does not account for differences in body proportions nor

does it discriminate between fat mass and lean mass^[236]. This is why BMI alone is not necessarily the best predictor of metabolic complications and additional data — including waist circumference, skinfold thickness and biochemical analysis of circulating glucose, triglycerides, free fatty acids (FFAs) and inflammatory markers — can leverage the BMI's shortcomings^[237,238].

Historically, the view on obesity has changed from being a sign of wealth and well being to a sign of an unhealthy lifestyle and increased risk for disease. Obesity has become a massive source of economic burden worldwide^[239]. And due to the diverse psychological and physiological effects fat tissue implicates, it has gained increasing scientific interest.

1.5.1 The adipose tissue

Collectively, adipose tissues form a large organ comprised of multiple fat storage sites. In humans, the two largest depots have subcutaneous and visceral locations. Additionally, fat depots can also be found in bone marrow, breast tissue, and ectopic regions like muscle, liver, heart, lung and pancreas^[240]. Increased visceral adipose tissue is associated with an higher risk for metabolic complications like insulin resistance, dyslipidaemia and overall mortality^[241].

Two different types of central parenchymal cells can be distinguished within fat tissue: white and brown adipocytes. Each one presents characteristic morphological and functional traits. The former store energy in form of triglycerides (tri-ester of a glycerol and three fatty acid molecules) and cholesterol in a single cytoplasmic lipid droplet and can produce and secrete a large number of bioactive molecules. The latter contains several smaller lipid droplets and are equipped with numerous uncoupling protein 1 (UCP1)-expressing mitochondria which allow for thermogenesis^[242]. Brown adipocytes can be found in large amounts at birth, but are reduced with age^[243]. Event though these two cell types arise out of two different pathways, white adipocytes can “brown” into paucilocular cells (also referred to as “beige” adipocytes) with mixed characteristics through cold exposure^[244] or physical activity^[245]. Interestingly, adipocyte turnover during adulthood is relatively high, with a renewal rate of around 10% total adipocytes per year^[246].

The stroma supporting and sustaining adipocytes is comprised of connective tissue, nerve, stromovascular, and immune cells. These stromal cells can make up to 50% of the total cell amount in the adipose tissue^[247].

Adipocytes derive from multipotent mesenchymal stem cells, which reside in the vascular stroma of adipose tissue and in the bone marrow. These precursors also have the capacity to develop into myocytes, chondrocytes, and osteocytes^[248]. The process of adipogenesis is initiated with the commitment of precursors to pre-adipocytes

through extracellular activators like insulin, IGF1, TGF β , BMP2 and BMP4^[249]. These signals integrate in the nucleus and culminate in the differentiation of mature adipocytes through the activation of e. g. peroxisome proliferator-activated receptor γ (PPAR γ , known as the “master regulator” of adipogenesis) and CCAAT-enhancer-binding protein α (C/EBP α ^[250]).

1.5.2 The adipose tissue as an endocrine and immune organ

Contrary to previously supposed unique functions as bare energy storage and rather inert protective layer against mechanical damage, white adipose tissue (WAT) has profound local and global metabolic, endocrine and immune effects^[251,252]. This is achieved through the expression and secretion of a large number of bioactive molecules with endocrine, immunological and neurological functions known as adipokines^[253,254]. Several different adipokines — including leptin, adiponectin, resistin, visfatin, glucocorticoids, interleukin 6 (IL6), and tumour necrosis factor (TNF) — have been already described^[254,255], and many hundreds of potential candidates have been identified^[256].

WAT can produce unique profiles of adipokines (adipokinome) depending on its location (e. g. subcutaneous vs visceral^[257]), cellular composition (e. g. presence of activated macrophages or hypertrophic adipocytes) and overall energy conditions (over- vs undernutrition^[258]). Adipocytes are sensitive to metabolic energy changes and can mount multiple feedback loops in a paracrine, autocrine and endocrine fashion. Through such loops, adipocytes control the storage and mobilization of energy via crosstalk with other tissues^[259].

Adipose tissue can adapt to overnutrition through hyperplastic expansion involving adipogenesis and hypertrophy of white adipocytes^[260]. This process involves a transient pro-inflammatory immune activation as part of the adaptive physiological response to increased energy intake^[261]. Inflammation can promote a homeostatic adipose tissue remodelling. This is achieved through angiogenesis — leading to a better nutrient and oxygen supply — and by limiting fat accumulation through temporary insulin resistance^[252]. However, chronic anabolic pressure from overnutrition can mount a pathological and long-term pro-inflammatory immune program. This can induce chronic insulin and catecholamine resistance as well as obesity-related metabolic disorders like type 2 diabetes^[252].

Despite advances in the study of cellular cross-talk mechanisms within the adipose tissue, the precise triggers of long term obesity-associated inflammation are not clear yet. These however encompass different metabolic and immune events^[252]. A well described example involves the paracrine cross-talk between adipocytes and macrophages. Here, macrophage-derived inflammatory mediators^[262], like TNF, directly induce lipolysis and

FFA release in adipocytes^[263]. In turn, chemokines, i. e. leptin,^[255] and FFAs secreted from adipocytes activate and maintain a pro-inflammatory macrophage profile^[264]. It has been shown that FFAs can bind to the pattern recognition receptors (PRRs) Toll-like receptor 4 (TLR4) and TLR2, leading to induction of NF- κ B signalling and cytokine expression in macrophages^[265].

Another pro-inflammatory trigger known to activate TLR4 during obesity is the rise in circulating lipopolysaccharide (LPS) from Gram-negative bacteria in the gut^[266]. This metabolic endotoxaemia results in part from increased intestinal permeability^[267], but also from microbial dysbiosis^[268].

Hypertrophy-induced adipocyte stress can also lead to a pro-inflammatory immune activation. Adipocyte stress emerges in great part from the limited responsiveness of adipose tissue endothelium and extracellular matrix to remodelling needs during the rapid adipocyte hypertrophy^[269]. Hypoxia^[270], mechanical^[271] and oxidative stress^[272] build up as a consequence, which lead to pyroptosis^[273]. This specialized form of caspase-1 dependent pro-inflammatory programmed cell death causes leaking of cytosolic components. Exposing the lipid droplet and other metabolic damage-associated molecular patterns (DAMPs, e. g. ATP, ceramides, cholesterol and urate crystals) from within the adipocyte leads to activation of PRRs, i. e. TLRs and nucleotide-binding oligomerization domain containing protein-like receptors (NLRs), especially the NLRP3 inflammasome^[274]. Pyroptosis and the secretion of pro-inflammatory adipokines and chemokines promote leukocytosis^[251] and the formation of crown-like structures containing pro-inflammatory macrophages^[273].

Pro-inflammatory adipose tissue macrophages can make up to 50% of the cellular content in adipose tissue of obese individuals^[262]. These macrophages are known to secrete large amounts of TNF, IL6 and IL1b — cytokines causally associated with insulin resistance^[262,275–277]. The more this macrophage population expands, the stronger will be the accumulation of pro-inflammatory factors in adipose tissue and their release into the circulation.

Sustained pro-inflammatory stressors can easily disrupt the microenvironment in adipose tissue and perpetuate pro-inflammatory processes^[252]. Such dysregulation leads to the well known phenotype of chronic low-grade inflammation with elevated pro-inflammatory factors in plasma, including leptin, resistin, IL6, IL8, CCL2, TNF and C-reactive protein (CRP), IFNG, plasminogen activator inhibitor 1 and complement component c3^[278,279], and decreased adipokine concentrations with anti-inflammatory properties, like adiponektin^[280]. Interestingly, the anti-inflammatory cytokine IL10 is also elevated during obesity. This appears to happen as an effort to maintain adipocyte metabolic flexibility through suppression of lipolytic signals, amelioration of insulin sensitivity, and recruitment of M2 macrophages to the adipose tissue^[281].

1.6 Obesity and the respiratory system

The ever-growing pandemic of obesity has been positively correlated with the increased pathogenesis of multiple pulmonary diseases^[282,283]. It is comorbid with asthma^[284], acute respiratory distress syndrome (ARDS^[285]), obstructive sleep apnoea, hypoventilation syndrome^[286], pulmonary hypertension^[287], COPD^[288] and lung fibrosis^[289]. It complicates the pathogenesis of COPD^[290] and is associated with primary graft dysfunction after lung transplantation^[291], higher mortality rates from influenza^[292,293], and idiopathic pulmonary fibrosis (IPF^[294]).

Obesity has shown to impair cross-talk mechanisms between adipose tissue and the brain^[295], liver^[296], muscle^[297] and pancreas^[298]. Several hypotheses for the explanation of such pathological cross-talk mechanisms have been proposed^[259]. These include interactions through free fatty acids as well as through endocrine, immune and neural factors. The presence of ectopically stored fat with toxic effects, and the altered endothelial functions have been suggested as well^[259].

Lung homeostasis can be dramatically altered by obesity through a combination of mass loading, endocrine and metabolic factors. A cross-talk between the adipose tissue and the lung based on the mutual influence through inflammatory factors has been proposed^[299]. While pro-inflammatory adipokines in the circulation, e. g. leptin, have shown to modulate lung immune responses^[300], lung-derived pro-inflammatory factors secreted into the circulation may as well amplify inflammation in the adipose tissue^[301].

In terms of mass loading, fat accumulation in the abdomen and thorax can directly reshape biomechanical properties of the respiratory system^[302]. This mechanical load often leads to elevated pleural pressure as well as decreased lung volumes^[303,304]. Consequently, functional residual capacity, compliance, expiratory reserve volume, and total lung capacity tend to decrease with obesity, leading to increased respiratory work load and impairment of the respiratory muscles^[303-305].

Factors secreted by hypertrophic adipose tissue found in the circulation of obese individuals can present pleiotropic effects and contribute to lung disease. An endocrine consequence of obesity known to influence the respiratory system is the reduced circulating concentration of the anti-inflammatory adipokine adiponectin. This factor can inhibit eosinophilia and allergic airway inflammation^[306]. Adiponectin deficiency might be the link between obesity, asthma^[284], COPD^[307], vascular remodelling and pulmonary hypertension^[306] as well as ARDS^[285]. Furthermore, raised levels of TNF have shown to promote both emphysema and pulmonary fibrosis and increase general lung inflammation^[308]. TNF can also reinforce airway neutrophilic inflammation, as showed in a model of ozone-induced lung inflammation^[309].

1.6.1 DOHaD: parental obesity and the offspring lung development

A large body of epidemiological as well as animal experiments have consistently provided evidence of the intergenerational effects of famine on offspring's metabolic, cognitive, developmental and endocrine health^[310]. In face of today's obesity pandemic, DOHaD research has shifted its attention to study long term consequences of parental obesity on offspring. Initial epidemiological and animal studies have shown that offspring born to obese mothers present similar metabolic and developmental outcomes as those born to famine-exposed mothers – especially in terms of adverse metabolic outcomes like increased risk for diabetes, obesity and the metabolic syndrome in later life^[311,312]. The specific effect of parental obesity as well as its plausible molecular causes have been since studied in more detail.

Parental nutrition has become a major predictor of adverse long-term detriment in offspring, including possible immune-related outcomes^[313]. Obesity during pregnancy is associated with higher risk of both maternal and foetal complications^[314,315]. Foetal neural tube defects, macrosomia, shoulder dystocia^[316], increased overall foetal mortality^[317], preeclampsia^[318], risks of cerebral palsy, attention-deficit disorder, cognitive delay, and autism are some well described examples^[319,320].

As the primary metabolic, respiratory, excretory and endocrine organ during pregnancy, the placenta plays an essential role in shaping the intrauterine environment for developmental programming^[321]. For this reason, research on intergenerational effects of obesity has focused on the role of maternal obesity on DOHaD. Metabolic and inflammatory changes brought about by maternal obesity extend to the placenta^[312]. This suggests an exposure of the foetus to an inflammatory environment and elevated levels of free fatty acids during development^[322]. The presence of increased pro-inflammatory molecules (CRP and TNF) in the amniotic fluid of overweight mothers^[323] as well as of a systemic inflammation in offspring – apparent by an increased abundance of pro-inflammatory cytokines in the foetal circulation (IL6, IL17A, and IFN γ ^[324]) – support this hypothesis. Maternal obesity has shown to directly shape the morphology and gene expression in placental tissue^[325]. Obese pregnant mouse dams present an altered thickness of placental tissue layers as well as impaired placental cell proliferation and gene expression^[324]. Obesity also leads to increased placental macrophage activation and elevated cytokine (Tnf, Il1b, Il6, Nlrp3, and Il10) expression^[324,326–328].

Effects of maternal obesity on the offspring's organ development have been previously studied. Metabolic organs like the liver^[329–331], pancreas^[332], muscle^[333] and adipose tissue, but also other organs like the brain^[334–336] and gut have been described. The presence of inflammation as well as increased oxidative stress on these organs is common for foetuses from obese mothers^[324,337–339].

The lung is not absent of parental obesity-induced detriments. Offspring of obese women are at greater risk for respiratory complications at birth^[340]. These include the risk for respiratory distress syndrome (RDS^[341]) as well as for persistent pulmonary hypertension of the new-born^[342]. Maternal obesity is associated with increased susceptibility to wheezing in early childhood^[343,344] and asthma later in life^[345]. Even though the exact mechanisms have not been discovered yet^[346], rodent models corroborate the link between maternal overnutrition and offspring's innate airway hyperresponsiveness^[347,348].

Plausible determinants of maternal obesity that lead to pulmonary challenges in offspring include the foetal exposure to stress hormones, high concentrations of pro-inflammatory cytokines/adipokines, free fatty acids and glucose, oxidative stress, placental inflammation and dysfunction as well as an involvement of intestinal or lung microbiota^[349]. Furthermore, maternal obesity might as well contribute to a maladaptation of the pulmonary L-arginine/NO metabolism in offspring^[350]. This pathway is not only important for vascular contractility, structural integrity of the blood vessels and angiogenesis^[351], but also critical for the innate immune function^[184]. Arginine-catabolizing enzymes, specifically nitric oxide synthases (NOS) and arginases, tightly control the immune response under physiological and pathological conditions. Critical immune, homeostatic and regenerative behaviours of myeloid cells are controlled by the arginine metabolism^[180]. Importantly, many functions of macrophages in the lung (and all other organs) depend on arginine pathways^[184]. Therefore, maladaptations in this metabolic pathway could compromise the lung immunity and possibly the macrophage's role in development and regeneration. Interestingly, rodent models of maternal hypercaloric feeding have shown a detrimental effect on the severity of viral lung infections^[347].

It has been hypothesized that foetal inflammatory exposures may modulate postnatal lung development and function^[352]. Interestingly, in 2013, two authors^[353,354] independently provided experimental results showing that offspring born to HFD dams can experience changes in lung structure and function that may be associated with poorer outcomes in infants of obese mothers. In their publication in 2015, Mayor et al. demonstrated increased expression of inflammatory markers in the placenta and decreased foetal viability in the uterus of HF dams. Their data suggested a reduced foetal lung maturation with diminished expression of surfactant^[354].

Additionally, in a rat model of maternal HFD feeding during pregnancy and lactation, Song et al. could show that maternal HFD exposure might induce the recruitment of inflammatory cells into the offspring lung at 12 weeks of age. HF rat offspring displayed increased lung tissue remodelling with increased collagen deposition and TGF β expression^[355].

1.6.2 Contribution of paternal diet

Due to the importance of the placenta in foetal development, most epidemiological and experimental studies have focused on intergenerational effects from maternal diet on offspring. Thanks to advancements in epigenetic studies, the importance of paternal heritability has also been recognised^[356]. Increasing evidence advocates epigenetic mechanisms (like histone modifications and DNA methylation) in the control not only of intergenerational effects caused by paternal obesity, but also their (transgenerational) transmission to later generations^[357].

It is important to note, that while transgenerational transmission stringently refer to phenotypic consequences effects occurring in the second generation (F2) for male-mediated or third generation (F3) for female-mediate alterations after environmental exposure^[358,359], effects spanning shorter periods are described as parental or intergenerational. Therefore, the effects of parental obesity directly affecting the developing embryo (F1) and the gametes that formed it are referred to as parental (maternal/paternal) or intergenerational transmission.

Observations on the effects of paternal under- and overnutrition on progeny have been made both in animal models as well as in human cohorts. High-fat or hypercaloric diet has not only shown to affect sperm quality and quantity of fathers-to-be^[360,361], but also to reduce embryonic and foetal development, and impair pregnancy efficiency^[362]. Importantly, offspring from obese fathers display increased risk for impaired insulin sensitivity and adiposity^[362]. Moreover, high-fat diet consumption in rats leads to a strong programming effects in the pancreas, especially on female offspring^[356]. These HF female offspring present early β -cell dysfunction with impaired insulin secretion and worsening of glucose intolerance in later life^[363].

Based on such observations and following the idea of DOHaD, the term “Paternal Origins of Health and Disease” (POHaD) has been proposed^[364]. POHaD raises questions about the similarity of disease development based on maternal and paternal transmission and possible additive effect of HF of both parents on the early development of diseases and long term consequences in offspring, especially for lung diseases.

2 Hypothesis and aims

2.1 Background

The view on obesity has changed from a sign of wealth and well being to a sign of an unhealthy lifestyle and increased risk for disease. The ever-increasing pandemic of obesity has been associated with various comorbid disorders, including pulmonary diseases like asthma, lung fibrosis and higher mortality rates from influenza. Mechanical, metabolic and inflammatory changes during maternal obesity extend to the placenta, exposing the foetus to a pro-inflammatory environment.

As a result of studies on the developmental origins of health and disease, today it is well known that environmental insults on a developing tissue early in life can lead to long-term and sometimes irreversible epigenetic and phenotypic consequences, if such stressors happen to take place during critical periods of tissue growth and development. Parental obesity can act as such a developmental stressor.

Obesity is the result of a sustained positive energy balance. A long-lasting anabolic pressure can cause adipose tissue hypoxia, lead to mechanical and oxidative stress with pyroptosis of adipocytes and recruitment of pro-inflammatory cells. This finally elicits a pathological pro-inflammatory immune activation in the adipose tissue with impaired endocrine functions. Chronic overnutrition can therefore often be accompanied by high circulating concentrations of pro-inflammatory cytokines and glucose. Dysregulation of the physiology of in the adipose tissue can profoundly impair not only local, but also global metabolic, endocrine and immune functions. For this reason, the adipose tissue has been described as an endocrine and immune organ.

In addition to the release of inflammatory factors into the circulation, obesity can elicit dyslipidaemia, characterized by increased free fatty acids (FFAs) in blood. Specially saturated FFAs are capable of stimulating a pro-inflammatory reaction through the activation of toll-like receptors 2 (TLR2) and 4 (TLR4) and a downstream nuclear factor kappa B (NF- κ B) activation, leading to pro-inflammatory cytokine expression. FFAs can as well bring about endoplasmic reticulum stress and elevated production of reactive oxygen species. These effects add to the adipocyte-derived inflammatory factors and can lead to the well-known systemic low-grade inflammation associated with obesity.

Maternal obesity can increase placental oxidative stress, inflammation and dysfunction. Due to the presence of pro-inflammatory molecules in the amniotic fluid of obese mothers as well as in the foetal circulation, it is not surprising that parental nutrition has become a major predictor of adverse long-term impairments in offspring, including not only metabolic, but also immune-related adverse outcomes. Additionally, epigenetic mechanisms can as well indirectly transmit detrimental physiological adaptations to later generations. Paternal obesity might therefore as well play a decisive role in the developmental origins of disease. In deed, paternal obesity has shown not

only to affect sperm quality and quantity of fathers-to-be, but also reduce embryonic and foetal development, and impair pregnancy efficiency. This raises the question of possible maternal and paternal additive effects of obesity on the early development of diseases, especially for the lung.

Recent studies around tissue macrophage (TM) ontogeny have led to a paradigm shift around these cells. Contrary to the belief that all TMs are replenished by circulating monocytes, nowadays it is well recognised that, in several tissues, these cells are long-lived and possess the ability to self-renew. The TM population that reside at the air-tissue interface of the lung, the alveolar macrophages (AMs), develop from foetal monocytes. These precursors seed the lung before birth and build a self-renewing independent TM niche.

AMs extended functions beyond simply “eating” include the orchestration of both, the initiation and the resolution of lung inflammation. AMs perform crucial trophic functions that support lung development and lead to overall maintenance of tissue homeostasis. These numerous properties are only possible due to their impressive plasticity. An impairment in such phenotypic versatility can greatly hamper AM's functions, compromising lung homeostasis and leading to disease.

2.2 Objectives

Developmental immunotoxicity studies have suggested a specially high sensitivity of macrophages to alterations by early life environmental insults and foetal programming. Since macrophages exhibit pivotal roles in tissue development and because mouse models of maternal diet-induced obesity suggest an impaired lung development in offspring, this thesis proposes that the period of AM development might present a window of vulnerability for programming effects by parental diet-induced obesity. This hypothesis suggests an impact of parental obesity on AM maturation which leads to a detectable pro-inflammatory AM primed state and long-lasting adverse functions in the offspring's lung. It supports the theory, that such long-term impairments will not only manifest in form of a compromised lung structure, but also become apparent later in life of the mouse offspring through a defective inflammatory response to an LPS challenge.

Based on this proposition, the detection of an impaired AM differentiation (reduced expression of markers like SiglecF), an altered number of AMs at steady state, an impaired AM function (specially in the context of immunity and lung development), and/or a defective AM M1 polarization could be expected. Because of the pro-inflammatory nature of obesity (low-grade systemic inflammation), this work places special emphasis on the pro-inflammatory effects of parental obesity. Therefore, analyses

of the initial M1 AM polarization *in vitro* and the lung's response to intratracheally instilled LPS *in vivo* were performed. Because of the systemic effects of obesity, it is also hypothesised that not only local effects in the lung, but also possible systemic alteration of circulating pro-inflammatory factors are present in high-fat offspring.

The aims of this thesis were divided into two main categories. On one side, direct effects of a HFD on mice body composition, circulating inflammatory factors and inflammatory dynamics in the lung were studied on parent mice. On the other, the inter-generational consequences induced by parental obesity were analysed on offspring animals. For the latter, the impact of parental diet-induced obesity on the offspring's viability, body weight, inflammatory factors in the placenta, lung and blood as well as consequences for their lungs, including their structure, gene expression and response to an acute inflammatory challenge, were studied. In both cases, the consequences of the HFD were specially inspected on the lung inflammatory dynamics and the polarization of alveolar macrophages. In order to reach the goals set for this thesis, three main methods needed to be established in the lab: a mouse model of diet-induced obesity, a mouse model of LPS-induced acute lung inflammation, and a multi-colour flow cytometric approach for analysing immune cell populations in the lung.

2.3 Experimental setting

Based on previous studies and experience from our cooperation partner Dr. Jan Rozman at the German Mouse Clinic, a high-fat diet (HFD) with 60 %kJ fat content was selected. In accordance with Mayor et al.^[327], the duration of the diet was of 12 weeks. However, the contrary to their experimental design, HFD contained a higher energy content (60 %kJ vs. 42 %kJ) for the effective and prompt induction of obesity in C57BL/6J mice. Moreover, in order to narrow down HFD-induced effects, a purified diet for both low-fat (LF) and high-fat (HF) animals was employed. This way, possible effects due to different micronutrient and fibre contents in the HF and control diets were excluded. Similarly to normal chow, the low-fat control diet (LFD) contained 11 %kJ fat. (Refer to *Section 3.1.2* for a detailed feeding protocol).

The characterization of the diet-induced of obesity was centred around three main effects of a HFD on the mouse physiology. First, the consequences of HFD on the body composition, which was analysed by means of NMR. This method provided the granularity needed to detect differences in body composition parameters, not only based on diet, but also on the animal's sex. Second, the presence of a systemic low-grade inflammation was expected to develop after the induction of obesity. For this purpose, circulating cytokine concentrations were analysed in plasma by multiplex immunoassay. The third parameter of interest, was the development of hyperglycaemia as a proxy for a disturbed glucose metabolism. A graphical representation of the overall experimental design can be observed in *Figure 4*.

In order to analyse direct effects of a HFD on the lung's ability to mount an immune response, obese and lean animals were intratracheally challenged with LPS. The goal of this test was to detect possible differences in the dynamics and strength of a pro-inflammatory reaction in the lung. Additionally, direct effects of HFD-induced obesity on the murine AM population were analysed *in vitro* by polarizing these cells with LPS. Their characterization was performed by the analysis of gene expression with qPCR. The presence of a systemic low-inflammation as well as hyperglycaemia and hyperlipidaemia was expected to alter the normal pro-inflammatory reaction against LPS.

The main hypothesis in this thesis was centred around the impact of parental obesity on the offspring's AM population. These effects were inspected by introducing an LPS challenge to the offspring's lungs as well as the *in vitro* polarization of their AMs. However, further inter-generational effects of parental HFD feeding were analysed, too. In order to detect the repercussions of parental obesity along the offspring's development, three different time points of analysis were selected: the foetal age of embryonic day 18.5 (E18.5), the neonatal age of two weeks after birth (P15) and a young-adult^[365] time point in the mouse life of 10 weeks of age (P70). While the strongest effects of parental obesity were expected to appear during the foetal development, long-term consequences were also anticipated. In order to recognise sequelae of parental obesity and prevent direct diet-induced outcomes, offspring animals were exclusively fed with LF control diet after weaning. Body weights, the lung structure and inflammatory gene expression in the lung were analysed at all three of the time points selected. Additionally, circulating cytokines were measured at the ages of P15 and P70. Long-term inter-generational effects of parental diet were inspected in P70 offspring, especially during the induction of lung inflammation and polarization of AMs with LPS.

Previous reports have consistently shown the presence of a strong sexual dependence on effects brought about by HFD and/or obesity. In order to recognize possible sexual dimorphic consequences of the experimental design employed for this thesis, all comparisons were performed not only after grouping individual subjects by diet, but also by sex.

During planning and execution of all animal experiments, following the 3Rs (**R**eplacement, **R**eduction and **R**efinement) guiding principles for more ethical use of animals had paramount priority.

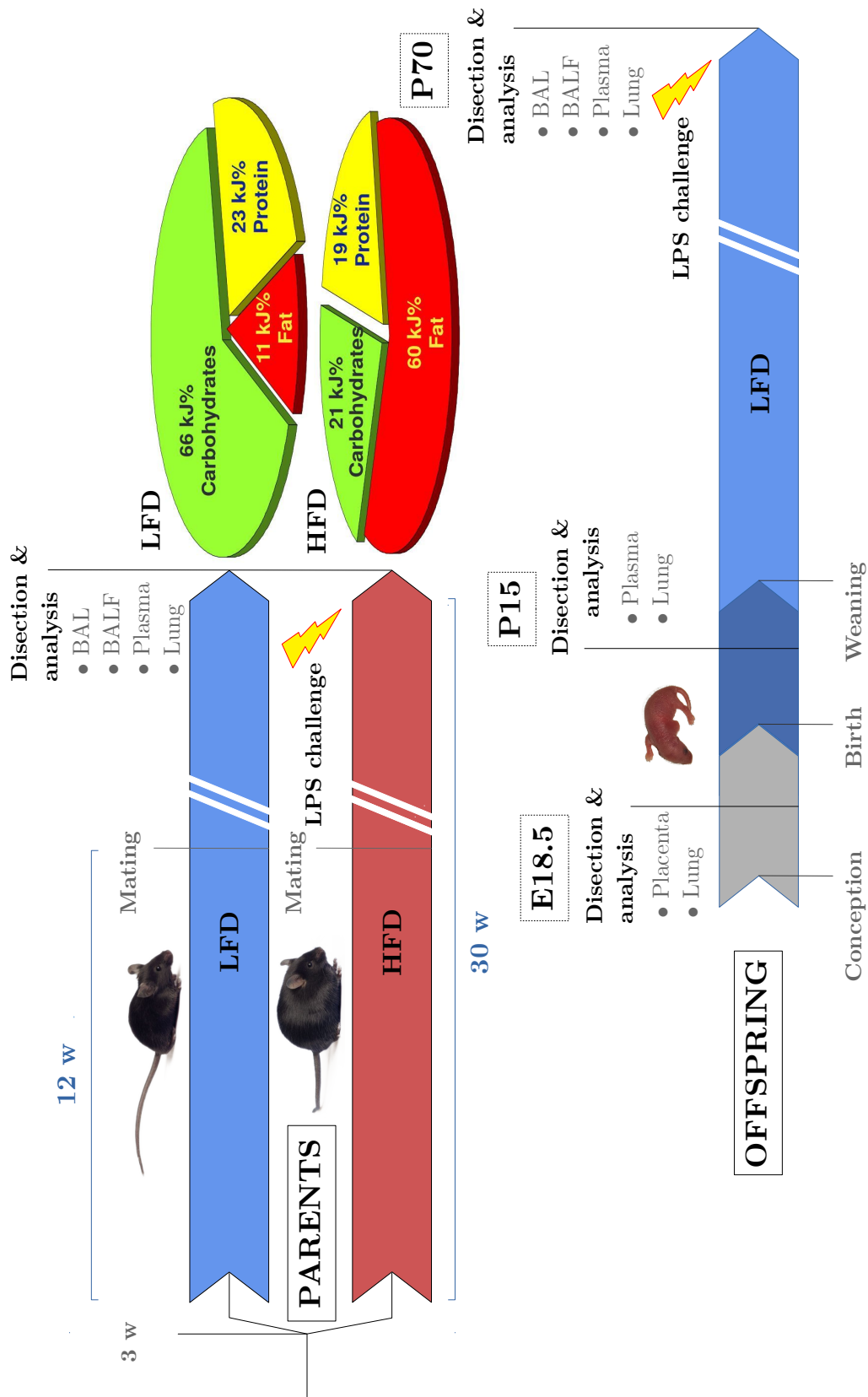


Figure 4: Experimental design. Parent WT C57BL/6J mice were fed with either HFD (60 kJ% fat) or LFD (11 kJ% fat) for 12 weeks before mating. During this time, body composition was monitored weekly by NMR. Parent animals were kept on the same diet until their sacrifice. Mating took place at 15 weeks of age with a female:male ratio of 2:1. Breeding efficiencies of 3.2 offspring per dam for the HF group and of 3.9 for the LF control group were taken into account. Both HF and LF offspring were exclusively fed with LFD after weaning. Parent mice were sacrificed and dissected at 30 weeks of age, while offspring at E18.5 (embryonic day 18.5), P15 (postnatal day 15) or P70 (postnatal day 70).

3 Materials and methods

3.1 Animal experiments

3.1.1 Ethics statement

All animal experiments were conducted in conformity with the FELASA Guidelines and Recommendations, the German animal welfare law and approved by the institutional animal welfare committee (“committee for animal experiments and animal facility” of the Helmholtz Zentrum München) as well as by the District Government of Upper Bavaria (approval number: 55.2-1-54-2532-46-2016)

3.1.2 General mouse housing and feeding

Wildtype (WT) C57BL/6J mice were obtained from Charles River, Sulzfeld, Germany, housed and bred in the animal facilities at the Institute of Lung Biology and Disease (iLBD) or the German Mouse Clinic (GMC), Helmholtz Zentrum München, Neuherberg, Germany, under specific-pathogen-free (SPF) conditions. Animals had access to food (standard chow, Altromin 1314; high-fat (HF), Ssniff EF D12492(II) mod. 60 kJ% fat (tallow) E15741-347; low-fat (LF), Ssniff EF control E15000-047) and water *ad libitum*. Special diet composition is presented on *Figure 4* and in *Table 3*.

A maximum of 3-4 animals were kept in isolated ventilated cages (IVC-Racks, BioZone, Margate, UK) supplied with filtered air. Housing rooms were maintained at room temperature of 23 ± 2 °C and constant humidity (relative humidity 60 ± 5 %) with a 12 h light/dark cycle (lights on from 06:00 to 18:00).

Possible outbreaks of infectious diseases in animal groups were controlled by constant monitoring of the mouse well being (appearance, mood and feeding). Additionally, for every study group, sentinel animals were tested for the presence of pathogens. There were no pathogenic outbreaks during any of the studies.

3.1.3 High-fat diet feeding protocol

WT C57BL/6J mice were purchased directly after weaning at 3 weeks of age. Special dieting of animals started on the same day of delivery. Individual animals were randomly assigned to either HF diet (HFD, 60 kJ% fat) or LF control diet (LFD, 11 kJ% fat) and fed for 12 weeks before mating. Parent animals were kept on the same diet assigned at the beginning of the experiment until their sacrifice.

To better follow the principles of the 3Rs (**R**eplacement, **R**eduction and **R**efinement), number of matings needed for diet experiments were calculated using breeding efficiencies of 3.2 offspring per dam for HFD-fed mice and of 3.9 for LFD control groups.

Breeding took place at 15 weeks of age with a female:male ratio of 2:1. Daily matutinal vaginal plug and delivery checks were performed, and day of plug and delivery were recorded for mouse age calculation. The day of plug detection was defined as day 0.5 of gestation. On day 18.5 of gestation (E18.5), females were euthanised, and the number of gestational and resorbed sacs were documented.

Born offspring from both groups (HF and LF) were fed after weaning exclusively with LFD. Offspring were analysed at embryonic day 18.5 (E18.5), 2 weeks after birth (postnatal day 15, P15) or at the age of 10 weeks (postnatal day 70, P70). Please refer to *Figure 4* for a graphical representation of the experimental design.

Table 3: Diet composition

	Chow [Altromin 1314]	LFD [Ssniff EF control E15000-047]	HFD Ssniff [EF D12492(II) mod. E15741-347]
Crude Nutrients	[%]	[%]	[%]
Crude fat	5	4.2	34
Crude protein	22.6	20.8	24.1
Crude fibre	4.5	5	6
Crude ash	7.1	5.6	6.1
Polysaccharide(s)	34.3	46.8	2.2
Di- and monosaccharide(s)	5.4	10.8	22.4
Metabolizable Energy	13.8 MJ/kg	15 MJ/kg	21.4 MJ/kg
Fatty acids	[%]	[%]	[%]
C12:0	—	—	0.03
C14:0	—	0.02	1.03
C16:0	0.52	0.45	8.06
C16:1	—	0.02	0.78
C17:0	—	—	0.38
C18:0	0.16	0.19	5.61
C18:1	0.9	1.07	12.13
C18:2	2.14	2.12	2.37
C18:3	0.29	0.26	0.33
C20:0	0.014	0.02	0.04
C20:1	0.018	—	0.01
C20:4	—	—	0.07
Amino acids	[%]	[%]	[%]
Lysine	1.14	1.71	1.98
Methionine	0.32	0.73	0.83
Met+Cys	0.64	0.82	1.28
Threonine	0.83	0.93	1.07
Tryptophan	0.29	0.27	0.31
Arginine	1.49	0.76	0.88
Histidine	0.55	0.66	0.76
Valine	1.07	1.42	1.64

Table 3: Diet composition (*continued*)

	Chow [Altromin 1314]	LFD [Ssniff EF control E15000-047]	HFD Ssniff [EF D12492(II) mod. E15741-347]
Isoleucine	0.97	1.09	1.25
Leucine	1.71	2.05	2.36
Phenylalanine	1.06	1.11	1.29
Phe+Tyr	1.82	2.22	2.57
Glycine	0.96	0.43	0.5
Glutamic acid	4.37	4.69	5.41
Aspartic acid	2.19	1.55	1.79
Proline	1.39	2.39	2.76
Alanine	1.03	0.68	0.79
Serine	1.13	1.24	1.43
Vitamins	per kg	per kg	per kg
Vitamin A	15000 IU	15.000 IU	15.000 IU
Vitamin D3	600 IU	1.500 IU	1.500 IU
Vitamin E	143 mg	150 mg	150 mg
Vitamin K	3 mg	20mg	20mg
Vitamin C	36 mg	30 mg	30 mg
Thiamin (B1)	18 mg	16 mg	16 mg
Riboflavin (B2)	12 mg	16 mg	16 mg
Pyridoxine (B6)	9 mg	18 mg	18 mg
Cobalamin (B12)	0.024 mg	30 µg	30 µg
Nicotinic acid	36 mg	49 mg	45 mg
Pantothenic acid	21 mg	56 mg	55 mg
Folic acid	2.4 mg	19 mg	19 mg
Biotin	250 µg	310 µg	310 µg
Choline-Chloride	600 mg	1.040 mg	2.300 mg
Inositol	not indicated	80 mg	80 mg
Minerals	[%]	[%]	[%]
Calcium	0.71	0.9	1.05
Phosphorus	0.51	0.63	0.61
Sodium	0.2152	0.19	0.2
Magnesium	0.2	0.21	0.17
Potassium	1.02	0.97	1
Trace elements	per kg	per kg	per kg
Iron	191 mg	166 mg	139 mg
Manganese	77 mg	98 mg	82 mg
Zinc	84 mg	65 mg	56 mg
Copper	14 mg	14 mg	12 mg
Iodine	1.5 mg	1.2 mg	0.97 mg
Selenium	0.25 mg	0.14 mg	0.13 mg
Cobalt	0.37 mg	0.15 mg	0.13 mg

3.1.4 Body mass and body composition analysis

Weight and body composition of parent animals were weekly monitored for 12 weeks after start of special dieting. Body mass was assessed by a scale, while body fat and body lean mass were measured with a time-domain nuclear magnetic resonance (TD-NMR) analyser (MiniSpec LF50, Bruker BioSpin MRI, Ettlingen, Germany).

TD-NMR provided precise measurements of lean tissue and body fat in live mice without the need of anaesthesia. To conduct the measurement, unsedated single mice were placed in a plastic restrainer (sample tubes with a diameter of 50 mm) and introduced into the magnet of the scanner for up to 5 minutes until measurement was completed. Prior to data acquisition the analyser was calibrated using a mixture of seeds with known fat and water content.

3.1.5 Embryonic tissue dissection

18 days after a positive vaginal plug test (E18.5), dams were euthanised by cervical dislocation. Uteri of dams were carefully exposed and excised using ring-shaped tip forceps (Carl Roth, Karlsruhe, Germany) to prevent puncturing the embryos.

Foetal tissue dissections were performed on a glass petri dish (dish diameter 13 cm, dish height 3 cm) coated with 3-5 mm of the silicone rubber Elastosil RT 601 (Wacker, Munich Germany) and filled up with 1x DPBS. Phosphate-buffered saline prevented tissue drying, while the elastomeric rubber allowed anchoring of foetuses with 1 cm long stainless steel minuten pins with a rod diameter of 0.2 mm (Fine Science Tools, Heidelberg, Germany).

Following the excision of uteri, foetuses were quickly euthanised under a binocular (Leica Microsystems, Singapore) by carefully cutting the cervical nerves directly after separation from the placenta. Special attention was paid not to cut through the trachea to prevent bleeding into the lung septum. Placentas were collected, snap frozen in liquid nitrogen and kept at -80 °C until further analysis.

Left lobes of foetal lungs were incubated at 4 °C over night in 4% PFA and histologically prepared (see *Section 3.3.2*). Right lung lobes were snap frozen and stored at -80 °C until further processing.

3.1.6 Intratracheal intubation and instillation

P70 (or older) mice were IP administered with completely antagonizable anaesthesia using the combination of medetomidine (12-20 µg/kg), midazolam (0.12-0.2 mg/kg) and fentanyl (1.2-2 µg/kg) (MMF). MMF injection volumes were calculated based on individual mouse body weights. Drying of animal eyes was prevented with eye cream (Bayer Vital, Leverkusen, Germany).

After assessment (e. g. with toe-pinch test) of anaesthetic depth (surgical anaesthesia), mice were intubated non-surgically^[366] using a olive-tipped 23 G reusable feeding needle (UNIMED, Lausanne, Switzerland) inserted 10 mm into the trachea. For this, animals suspended at a 60° angle by the upper incisors with a string attached to a plexiglass support. The trachea was then transilluminated with a cold light LCD fibre optic illuminator (Schott, Duesseldorf, Germany) while holding the mouse's tongue with a curved micro-spatula for the effective intratracheal insertion of the cannula.

50 μ l of air, followed by 0.1 μ g E. coli O55:B5 endotoxin (Sigma-Aldrich, Saint Louis, USA) diluted in 50 μ l PBS, and further 100 μ l of air were instilled with a 1 ml syringe (B. Braun Melsungen, Germany) after verifying the successful placement of the cannula through inspection of pressure changes (animal breathing) with a self-constructed pneumotachograph. Control mice were instilled only with PBS, applying the same instillation volumes (50 μ l of air, followed by 50 μ l PBS and further 100 μ l of air).

After careful removal of the cannula from the trachea, the animal was delicately dismantled from the support and SC injected with an MMF-antagonizing mixture of antipamezol (0.06-0.1 mg/kg), flumazenil (12-20 μ g/kg) and naloxon (28.8-48 μ g/kg) (antagonist; concentrations for mouse body weights ranging between 24 and 40 g). Animal health condition was monitored 1, 3 and 24 h after MMF-antagonization.

3.1.7 Blood and plasma analysis

After effective euthanasia with an IP injection of a lethal dose of anaesthesia (500 mg/kg ketamine, 6 mg/kg xylazine), the retro-bulbar vein plexus of the mouse was punctured with a glass capillary coated with lithium-heparinat (Hirschmann Laborgeräte, Eberstadt, Germany). Up to 1 ml of blood from each animal was collected in lithium-heparinat-coated tubes (Kabe Labortechnik, Nümbrecht-Eisenroth, Germany). After mixing by inversion, blood was incubated at room temperature (RT) for 30-60 min and centrifuged for 15 min at 3500 g. Plasma (supernatant) was separated, snap-frozen and kept at -80 °C until further analysis.

The concentrations of pro-inflammatory mouse cytokines (IFN γ , IL1b, IL2, IL4, IL5, IL6, CXCL1, IL10, IL-12p70, and TNF) in the plasma were determined by high-performance multiplex (10 assay spots per well) electrochemiluminescence immunoassay (Mesoscale MESO QuickPlex SQ 120) in cooperation with Dr. Aguilar-Pimentel at the Institute of Experimental Genetics (IEG), Helmholtz Zentrum München.

Quantitative blood glucose measurements from freshly isolated whole blood samples were performed with the Accu-Chek Aviva Connect blood glucose monitoring system (Roche Diagnostics, Mannheim, Germany).

3.1.8 Bronchoalveolar lavage

Mice were euthanised with an IP injection of a lethal dose of anaesthesia (see *Section 3.1.7*) and their death was ensured by exsanguination. Bronchoalveolar lavage (BAL) was performed by cannulating the trachea with a plastic catheter (Introcan Safety IV 20 G, B. Braun Melsungen, Melsungen, Germany) and infusing the lungs ten times with 1 ml of cold PBS lacking the bivalent cations Ca^{2+} and Mg^{2+} (DPBS 1X, Gibco, Dublin, Ireland).

Lavages of each animal were collected into two separated pools – one from the first and second lavages, another from the third to the tenth lavages – and centrifuged (350 g, 10 min, 4 °C). The cell-free supernatant from the first pool was separated into three tubes, snap-frozen in liquid nitrogen and kept at -80 °C until further biochemical analysis.

For each animal the cell pellets from both BAL pools were resuspended in 1 ml Roswell Park Memorial Institute (RPMI) 1640 medium (Gibco, Dublin, Ireland) supplemented with 10% foetal bovine serum (FBS; gibco, New Zealand) and the number of living cells was determined with the trypan blue exclusion method.

3.1.9 Differential counting of bronchoalveolar lavage cells

3×10^4 BAL cells per animal were centrifuged (400 rpm, 6 min) on a glass slide with a bench-top cytocentrifuge (Shandon Soudern Products, Cheshire, England). Preparations were stained with May-Grünwald-Giemsa (Merck KGaA, Darmstadt, Germany). Two differential cell counts per animal were manually performed by counting two hundred cells with the aid of a differential cell counter (Karl Hecht, Sondheim, Germany). With this method, polymorphonuclear leukocytes (PMNs), mononuclear cells (alveolar macrophages, monocytes and dendritic cells), eosinophils, and multinucleated giant cells were distinguishable.

Alternatively, cell pellets from both lavage pools were resuspended in 1 ml FACS buffer (see formulation on *Table 12*) and counted by flow cytometry using CountBright absolute counting beads (Thermo Fisher Scientific, Eugene, USA) (refer to *Equation 1*). Living cells were distinguished with DAPI (1:400, 5 min, Miltenyi Biotec, Bergisch Gladbach, Germany).

3.2 Flow cytometry

3.2.1 Compensation controls

After setting PMT voltages on cytometer and prior to flow cytometric analyses, compensation controls were performed. For each fluorochrome, a mixture of one drop of blank beads and one drop of anti-REA compensation beads for REA antibodies (Miltenyi Biotec, Bergisch Gladbach, Germany), or one drop of OneComp eBeads compensation beads (Invitrogen, California, USA) for any other antibody, were mixed with 1-2 μl of antibody and incubated at room temperature for 10 minutes. The suspension was diluted with 1 ml of FACS buffer and measured for instrument calibration.

Live/dead compensation controls were achieved with a 1:1 mixture of live:death PBMCs, cell culture cells, or primary cells. For the generation of the dead fraction, cells were incubated for 10 min at 95 °C, or treated with 5 μM staurosporin for 1.5 h, and washed with 1 ml FACS buffer (350 g, 5 min) prior to treating with DAPI (1:400, 5 min, Miltenyi Biotec, Bergisch Gladbach, Germany) or fixable “Viability Dye” (1:100, 15 min, RT, Miltenyi Biotec, Bergisch Gladbach, Germany). Fixable viability dye-treated cells were again washed with 1 ml FACS buffer (350 g, 5 min) before mixing with the live fraction. DAPI stained cells were analysed without prior washing.

Compensation matrices were calculated automatically on the BD FACSDiva software (BD Biosciences, San Jose, USA) after manually selecting (1D gating) for the negative and positive populations for each of the 8 or 10 fluorochromes.

3.2.2 Flow cytometric immunophenotyping of bronchoalveolar lavage cells

Flow cytometric immunophenotyping of BAL cells presents a precise method to reliably analyse single cells within the alveoli. Differential cell counting of BAL cells by flow cytometry was accomplished following an 8-color staining protocol. The selection of the markers and the manual gating protocol employed in this thesis was based on previous works from Misharin et al.^[217], Ellis et al.^[367] and Yu et al.^[368].

Up to 2e5 lavage cells of each animal were transferred to a 5 ml FACS tube, washed with 1 ml FACS buffer (350 g, 5 min) and resuspended in 100 μl of a 1:100 viability fixable dye:FACS buffer solution. After mixing, cells were incubated at RT for 15 min in the dark and washed with 1 ml FACS buffer. After centrifugation (350 g, 5 min), BAL cells were resuspended in 50 μl antibody cocktail (see panel on *Table 4*) and incubated on ice for 15 min in the dark. After washing (1 ml FACS buffer; 350 g, 5 min), cell pellet was resuspended in 300 μl FACS buffer and 50 μl of CountBright Absolute counting beads (Molecular Probes, Eugene, USA) were added for the quantification of absolute cell numbers in the lavages (refer to *Equation 1*).

Stained cells were analysed on a BD FACSCANTO II cytometer (BD Biosciences, San Jose, USA) at the iLBD of the Helmholtz Zentrum München. Compensated single cell data was exported as FCS files using the BD FACSDiva software. Flow cytometry data

sets were manually gated with FlowJo (FlowJo LLC, Ashland, USA) to distinguish cell populations based on the expression of the 8 markers. Alternatively, unsupervised learning algorithms were applied to single cell data after manual quality control to semi-automatedly distinguish BAL cell populations. Statistics were computed using R (The R Foundation for Statistical Computing, Vienna, Austria).

Calculation of the absolute cell concentration of each lavage was performed following the equation:

$$\frac{A}{B} \times \frac{C}{D} = \text{concentration of sample as cells}/\mu\text{l} \quad (1)$$

where :

A = number of cell events

B = number of bead events

C = assigned bead count of the lot used (beads/50 μl)

D = lavage volume used for analysis (μl)

Table 4: 8-color staining panel for flow cytometric immunophenotyping of mouse bronchoalveolar lavage cells

Antigen	Fluorochrome	Host/ Isotype	Clone/ ID	Final conc.	Dilution
FCGR1	PE	rh / IgG1	REA286	3 $\mu\text{g}/\text{ml}$	1:50
H2-AB1	APC-Vio770	rh / IgG1	REA813	1 $\mu\text{g}/\text{ml}$	1:150
ITGAM	PE-Vio770	rh / IgG1	REA592	1.2 $\mu\text{g}/\text{ml}$	1:25
ITGAX	FITC	rh / IgG1	REA754	3 $\mu\text{g}/\text{ml}$	1:50
LY6C	PerCP-Vio700	rh / IgG1	REA796	3 $\mu\text{g}/\text{ml}$	1:50
LY6G	VioBlue	rh / IgG1	REA526	3 $\mu\text{g}/\text{ml}$	1:10
SIGLECF	APC	rh / IgG1	REA798	3 $\mu\text{g}/\text{ml}$	1:50
Viability	405/520		Viability Fixable Dye		1:100

3.2.3 Flow cytometric immunophenotyping of whole lung cells

In order to acquire a thorough view of the immune system in mouse lung, the the BAL staining protocol was augmented to a 10-color panel for the differential cell counts of whole lung immune cells.

After euthanasia with an IP injection of a lethal dose of anaesthesia and exsanguination through an incision in the *inferior vena cava*, mice lungs and heart were exposed by carefully opening the thoracic cavity. Lungs were perfused with 5-10 ml cold PBS. PBS was injected into the right ventricle and allowed to exit through an incision in the left atrium. 1 ml dispase (Corning, Massachusetts, USA) was instilled into the lungs after intratracheal intubation of mice. Spilling of dispase out of the lung was prevented with two sutures on the trachea. Lungs were prepared out of the chest cavity and incubated at RT in 1.5 ml dispase in a 50 ml tube.

Dispase-treated lungs were filtered through 70 μm strainers (Miltenyi Biotec, Bergisch Gladbach, Germany) and collected in a 50 ml tube. Not fully digested tissue was scraped through the filter with a cell scraper while rinsing with FACS buffer until 7 ml cell suspension was obtained. Cell suspensions were again filtered through 70 μm strainer. Cells were pelleted by centrifugation (350 g, 5 min), resuspended in 5 ml FACS buffer and counted by flow cytometry using CountBright Absolute counting beads (see Equation 1).

5e5 dissociated whole lung cells per animal were transferred to a 5 ml FACS tube and washed with 1 ml FACS buffer (350 g, 5 min). BAL cells were incubated with unlabelled anti-CD16/CD32 antibody (rat/IgG2a, clone 93, 0.5 mg/ml, eBioscience, San Diego, USA) for 5 min in order to reduce Fc-receptor mediated binding of test antibodies and resuspended in 100 μl antibody cocktail (see panel on Table 5). For staining, cells were incubated on ice for 15 min in the dark. After washing with 1 ml FACS buffer (350 g, 5 min), the cell pellet was resuspended in 400 μl of a 1:400 DAPI:FACS buffer solution.

Stained cells were analysed with a BD FACSLSR II cytometer (BD Biosciences, San Jose, USA) at the Comprehensive Pneumology Center (CPC) of the Helmholtz Zentrum München. Compensated single cell data was exported as FCS files using the BD FACSDiva software. FCS files were manually gated with FlowJo and population numbers and statistics were computed using R. Alternatively, immune cell populations were semi-automatedly clustered and counted using unsupervised machine learning algorithms.

Table 5: 10-color staining panel for flow cytometric immunophenotyping of mouse whole lung cells

Antigen	Fluorochrome	Host/ Isotype	Clone/ ID	Final conc.	Dilution
CD24A	Alexa Fluor700	rat / IgG2b	M1/69	5 $\mu\text{g}/\text{ml}$	1:100
FCGR1	PE	rh / IgG1	REA286	3 $\mu\text{g}/\text{ml}$	1:50
H2-AB1	APC-Vio770	rh / IgG1	REA813	1 $\mu\text{g}/\text{ml}$	1:150
ITGAM	PE-Vio770	rh / IgG1	REA592	1.2 $\mu\text{g}/\text{ml}$	1:25
ITGAX	FITC	rh / IgG1	REA754	3 $\mu\text{g}/\text{ml}$	1:50
LY6C	PerCP-Vio700	rh / IgG1	REA796	3 $\mu\text{g}/\text{ml}$	1:50
LY6G	VioBlue	rh / IgG1	REA526	3 $\mu\text{g}/\text{ml}$	1:10
PTPRC	VioGreen	rh / IgG1	REA737	3 $\mu\text{g}/\text{ml}$	1:50
SIGLECF	APC	rh / IgG1	REA798	3 $\mu\text{g}/\text{ml}$	1:50
Viability	DAPI	-	-	25 ng/ml	1:400

3.2.4 Gating strategy

The manual gating strategy generated for this thesis was based on previous works from Misharin et al.^[217], Ellis et al.^[367] and Yu et al.^[368]. Compensated single cell fluorescent data was imported to FlowJo using its graphical user interface. Each fluorescent channel was transformed with FlowJo's biexponential function and its axis minimum and maximum were adjusted to the range of the fluorescent intensities.

Sequential manual gates were applied on bivariate histograms. In order to better distinguish cell clusters, two-parameter histograms were displayed in density plots. Refer to *Figure 31* for the gating strategy of whole lung leukocytes.

After removing cell debris (FCS-A, SSC-A) and dead cells (SSC-A, viability/DAPI), (live) singlet cells were selected (FCS-A, FSC-H). Leukocytes (PTPRC⁺) were gated from the singlet population and lymphocytes (ITGAX⁻, ITGAM⁻) were subdivided into B (CD24A⁺, H2-AB1⁻) and T-cells. Inflammatory T-cells could be distinguished by the presence of LY6C.

From the not-lymphocytes, singlet cells group (notLymph), neutrophils (PMNs) could be identified by the expression of LY6G. From the not-PMN cell population (notPmn), monocytes (FCGR1⁺, ITGAM⁺) and natural killer cells (NK cells, FCGR1⁻, ITGAM^{med}) were identified by their low SSC-A and missing expression of H2-AB1 (monoNk). Inflammatory and resident monocytes were separated on a LY6C-ITGAX density plot, where inflammatory cells were recognized by the presence of LY6C.

The not-monocyte/NK population (notMonoNk) was further split into macrophages (FCGR1⁺), dendritic cells (CD24A⁺, FCGR1⁻, H2-AB1⁺) and eosinophils (CD24A⁺, SIGLECF⁺, H2-AB1⁻). Lastly, alveolar (SIGLECF⁺), inflammatory (SIGLECF⁻, LY6C⁺) and interstitial macrophages (SIGLECF⁻, LY6C⁻) were identified on a SIGLECF-LY6C-histogram.

3.2.5 Semi-automated immunophenotyping of lavage and whole lung cells

Manual gating has been the standard procedure to analyse low dimensional single cell data for many years. However, with the technical advancements in mass^[369] and flow cytometry^[370] and the increasing capacity to generate large and high-dimensional data sets, manual analysis of single cell data becomes harder to reproduce due to its subjectiveness^[371], its susceptibility to bias^[372] and the difficulty to recognize small cell populations^[373]. Computational methods based on dimensionality reduction have proven^[374] to help the analysis of big flow cytometric data^[375], allowing automation, standardization and reproducibility of procedures for the recognition of cell populations, especially small/rare ones^[373].

The semi-automated method for immunophenotyping of lavage and whole lung cells applied in this thesis was inspired by the work of Nowicka et al.^[376] published in 2017.

Fluorescent channels of compensated flow cytometry data were transformed with FlowJo's biexponential function and its axis minimum and maximum were adjusted to the range of the fluorescent intensities. Single cell data was cleaned by manually gating for the singlet cell population, as mentioned in *Section 3.2.4*. This "gating set" was imported into R using the packages CytoML^[377] and flowWorkspace^[378]. Cytometry data was analysed by applying three different unsupervised learning algorithms for clustering and dimensionality reduction. Data was scaled and centred before it was

clustered by training a self-organizing map and building a minimal spanning tree with the FlowSOM package^[379]. 20 subclusters were built applying consensus clustering^[380] on the 100 flowSOM clusters. Finally, t-distributed stochastic neighbour embedding^[381] (tSNE) was performed on 8e3 randomly selected cells to visually inspect the subclusters. Analysing these plots, together with 1D and 2D histograms of the clustered cells and their marker expression, the clusters were manually grouped and labelled with expected immune cell population names.

3.3 Histology

3.3.1 May-Grünwald-Giemsa staining of cytopspins

Cytocentrifuged specimens were left at RT to dry over night. Four glass cuvettes containing 1) undiluted May-Grünwald's eosine-methylene blue solution (Merck, Darmstadt, Germany), 2) tap water, 3) 1:20 dilution of Giemsa's azur eosin methylene blue solution:tap water (Merck, Darmstadt, Germany), and 4) tap water were prepared for staining.

Cytospin slides were successively immersed in the four cuvettes and incubated for 1) 10 min, 2) 2 min, 3) 15 min, and 4) 2 min. Excessive water on sample slides was carefully removed with a tissue and cytopspins were let dry at RT over night before covering stained cells with Entellan (Merck, Darmstadt, Germany) and cover slips. Manual cytopspin counts were performed after hardening of mounting medium over night.

3.3.2 Lung tissue preparation

Mice were euthanized and intratracheally intubated. After lung perfusion (see *Section 3.2.3*), lungs were filled with formaldehyde solution made from 4% paraformaldehyde powder in PBS (4% PFA) with a constant pressure of 25 cm 4% PFA for 10 min. The trachea was sutured to prevent spilling of fixing solution, and lungs were incubated at 4 °C in 4% PFA over night. Fixing solution was exchanged with 70% ethanol and lungs were kept at 4 °C until further preparation.

Fixed lobes were cut into 2 mm thick slices. For each subject, slices were pooled in embedding cassettes and automatedly embedded in a Leica TP1020 benchtop tissue processor (Leica Biosystems Nussloch GmbH, Nussloch, Germany) following the protocol presented on *Table 6*.

After completing the process of dehydration, clearing and infiltration, tissue samples were externally embedded in paraffin wax (Merck, Darmstadt, Germany) using a cold module (Thermo Scientific, Runcorn, UK).

Formalin-fixed, paraffin-embedded (FFPE) tissues were hardened at 4 °C over night. 6 μm thick tissue sections were cut with a ZEISS HYRAX M 55 rotary microtome (MICROM, Walldorf, Germany) and stretch-dried on glass slides with a specimen stage-stretching table (MEDAX, Neumünster, Germany). Dried sections were then deparaffinized through two 5 min changes of xylene and re-hydrated through a descending series of alcohol to water, consisting of two changes of absolute ethanol, and one 1 min change of each 90%, 80% and 70% ethanol solutions.

Slides were briefly washed in distilled water, nuclear-stained with Mayer's hemalum solution (Merck, Darmstadt, Germany) for 5 min, and briefly dipped in alkalinized water, and 0.1% HCl-EtOH. After washing for 10 min with tap water, specimens were dipped in distilled water and incubated in 0.5% eosin (Merck, Darmstadt, Germany) for 8 min.

For better preservation, tissue sections were dehydrated again through a series of alcohol solutions in ascending concentration. Sections were briefly dipped in 70%, 80%, 90% and 96% EtOH, and two 1 min changes of absolute ethanol. After two 5 min changes in xylene, slides were mounted with Entellan and cover slips.

Table 6: Lung tissue embedding protocol

Station	Medium	Time
1	70% EtOH	1 h
2	80% EtOH	1 h
3	96% EtOH	1 h
4	96% EtOH	2 h
5	96% EtOH	2 h
6	100% EtOH	1 h
7	100% EtOH	2 h
8	100% EtOH	2 h
9	xylene	1 h
10	xylene	2 h
11	paraffin wax	1 h
12	paraffin wax	2 h

3.3.3 Stereological analysis

Quantitative morphometric analysis of neonatal (P15) and young-adult^[382] (P70) mouse lungs was performed on 6 μm thick hematoxylin and eosin (HE) stained FFPE tissue sections (see *Section 3.3.2*). Slides were blindly analysed by design-based stereology on an Olympus BX51 light microscope equipped with the new Computer Assisted Stereological Toolbox (newCAST, Visiopharm, Hoersholm, Denmark).

Tissue sections were mounted on the microscope and a “super image” was created by stitching images captured with the 2x objective. Lung tissue area was manually defined using the selection tool of the software. Using the 20x objective, 20-30 fields of view per subject were selected by the software using simple uniform random sampling across multiple sections.

A line grid (line spacing of $530.57 \mu\text{m}$) and points (line length per point of $88.08 \mu\text{m}$) were superimposed on lung section images. Intercepts of lines with alveolar septa (I_{septa}) and points lying on air space (P_{air}) were manually counted (for an example of manual counting see *Figure 5*). Mean linear intercepts (L_m) were calculated for each animal following *Equation 2*.

Since this measure (L_m) is partly dependent on the structural size of the lung (absolute surface area) as well as on changes on the lung volume. Changes in the latter may be induced by disease (e. g. due to loss of elastic recoil in emphysematous lungs)^[383], but can also be introduced by technical errors during isolation and fixation – e. g. by irregular pressures during inflation with PFA or during bronchoalveolar lavage, due to lung puncture and other errors. For this reason, lung volumes were measured after fixation and samples with outlying measurements in volume were excluded from the stereological analysis. For this, only lungs with volumes within the 25th and 75th percentiles of the volume measurements were randomly sampled.

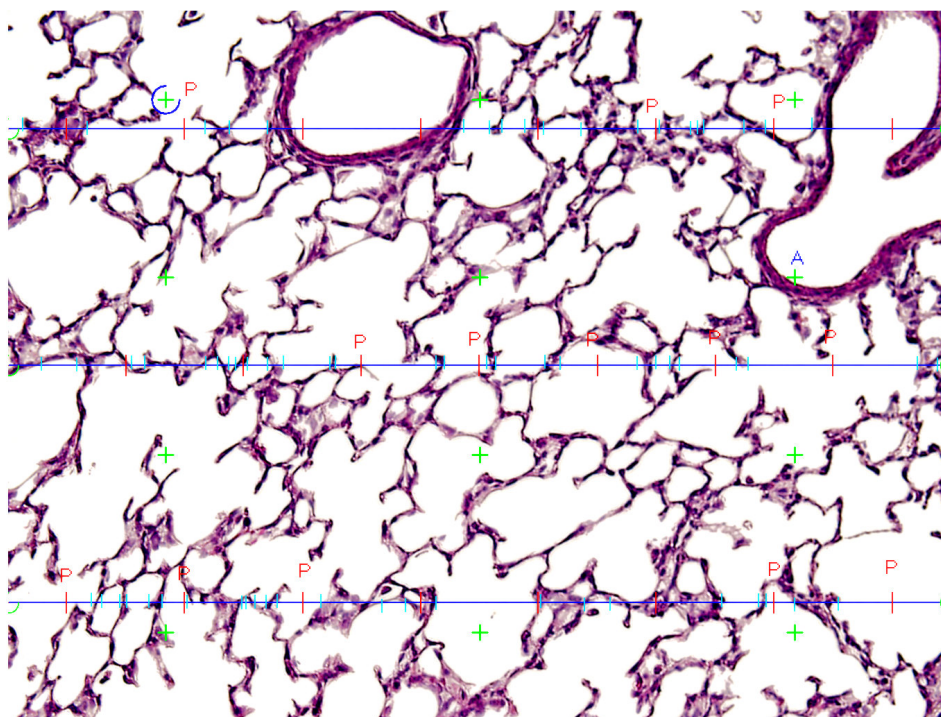


Figure 5: Manual quantitative morphometric analysis of mouse lung tissue. Example of an HE stained FFPE tissue sections of a young-adult (P70) mouse lung under the 20x objective of an Olympus BX5 light microscope. A line grid (line spacing of $530.57 \mu\text{m}$) and points (line length per point of $88.08 \mu\text{m}$) were superimposed on lung section images. Intercepts of lines with alveolar septa (I_{septa} , blue lines) and points lying on air space (P_{air} , red "P") were manually counted. Mean linear intercepts (L_m) were calculated following *Equation 2*.

$$L_m = \frac{\sum P_{air} \times L_p}{\sum I_{septa} \times 0.5} \quad (2)$$

where :

P_{air} := grid point lying on air space

L_p := line length per point (88.08 μm)

I_{septa} := intercept between alveolar septum and grid lines

3.3.4 Digital image analysis

Digital image analysis was performed in cooperation with Dr. Annette Feuchtinger and Dr. Andreas Falko Parzefall at the Core Facility Pathology and Tissue Analytics of the Helmholtz Zentrum München. After visual inspection for quality control of the stained tissue sections Dr. Andreas Falko Parzefall, histological slides were scanned with an AxioScan.Z1 digital slide scanner (Zeiss, Jena, Germany) equipped with a 20x magnification objective. Images were evaluated using the commercially available image analysis software Definiens Developer XD2 (Definiens AG, Munich, Germany) by Dr. Annette Feuchtinger following a previously published procedure^[384] at the Core Facility Pathology and Tissue Analytics.

A rule set was defined to detect and quantify the alveolar space within each lung lobe, based on morphology, size, pattern, shape, neighbourhood and special colour features. The quantified parameter were the alveolar and septal area [μm^2], the length of border between septum and air [μm], the total lung area [μm^2], the total number of alveoli as well as the ratio between air and septal areas. Statistical analysis of digital image analysis results were performed with R.

3.4 Enzyme-linked immunosorbent assay

Cytokine concentration in BAL fluid was analysed by sandwich enzyme-linked immunosorbent assay (ELISA). All ELISA kits were purchased from R&D Systems, Wiesbaden-Nordenstadt, Germany (refer to *Table 10* for a list of all ELISA kits used in this work). Assays were performed following all recommendations and the general ELISA protocol from the provider. All incubation periods were performed at RT, in the dark and covering the 96-well microplate with an adhesive sealer. Between each assay step, all wells of the microplate were washed with an auto-washer three times with 400 μl of a PBS dilution of 0.05% Tween 20 (Sigma-Aldrich, Taufkirchen, Germany) with a pH of 7.4. All measurements were performed in duplicate.

After dilution of capture antibody to the working concentration in PBS, the microplate was coated with 100 μl of the dilution and incubated at RT over night. Wells were blocked for 1 h with 300 μl of a 1% BSA solution in PBS, pH 7.4, and filled with 100 μl BALF or cytokine standards diluted in PBS containing 1% BSA. After an incubation of 2 h at

RT, 100 μ l of the detection antibody, diluted in PBS containing 1% BSA, were added to each well and microplate was incubated for another 2 h. 100 μ l of the working dilution of streptavidin conjugated to horseradish-peroxidase were added to each well and after 20 min incubation 100 μ l of a 1:1 mixture of H₂O₂ : Tetramethylbenzidine was added to each well. The colour reaction was carefully monitored for a maximum of 15 min and 50 μ l of a 2 N H₂SO₄ solution was added to the colour mixture in each well to stop the colour reaction.

After ensuring that no bubbles were present in any of the wells, optical density was measured at 450 (signal) and 570 nm (correction) using a Tecan NanoQuant infinite M200 PRO microplate reader (Tecan Austria, Salzburg, Austria). After subtracting the correction from the signal OD values and normalizing all signals by subtracting the OD values from wells without sample (PBS), OD values were exported using the Magellan Software V7.1 SP1 (Tecan Austria, Grödig, Austria) and analysed in R. For the creation of a calibration curve, a second-order polynomial regression was fit using the exported values. The cytokine concentration of each BALF sample was then predicted by applying the fitted model to each normalized OD value and averaging the predicted concentrations of the technical duplicates.

3.5 Analysis of alveolar macrophages

3.5.1 Alveolar macrophage isolation

Freshly isolated BAL cells (see *Section 3.1.8*) of two mice were resuspended in RPMI-1640 medium supplemented with 10% FBS (gibco, New Zealand), 0.05 mM 2-mercaptoethanol (Sigma-Aldrich, Taufkirchen, Germany), 100 U/ml Penicillin and 100 μ g/ml Streptomycin (Gibco, Dublin, Ireland) (MHS-medium; *Table 12*). AMs were purified by plating 1-2E5 cells with 1 ml MHS medium per well on plastic 12-well plates at 37 °C and 5 % CO₂ for 60 min and washing off non-adherent cells twice with 37 °C-warm PBS.

3.5.2 Alveolar macrophage polarization

In vitro polarization of primary alveolar macrophages (AMs) was performed exclusively on cells isolated from (LPS-)untreated healthy mice. Classical activation (M1) of AMs was achieved by incubating the adherent cell fraction with MHS medium containing 1 μ g/ml LPS (Sigma-Aldrich, Taufkirchen, Germany) for 50 min or 24 h. For an alternative (M2) activation, AMs were incubated with MHS medium containing 20 ng/ml IL-4 for 24 h. Control cells (M0) were incubated for the same period of time as M1 or M2 AMs in plain MHS medium. All incubation steps were performed at 37 °C and 5 % CO₂.

After washing twice with 37 °C-warm PBS and carefully aspirating the remaining supernatant, cells were directly lysed with lysis solution of RNA preparation kit in their wells while scraping with the pipette tip. Lysed suspensions of each pool was collected into a 1.5 ml reaction tube, snap frozen and stored at -80 °C until RNA isolation.

3.5.3 Alveolar macrophage phagocytosis assay

1E5 freshly isolated primary AMs (see *Section 3.5.1*) per well were incubated on a 96-well plate for 1 h at 37 °C and 5 % CO₂. All wells were filled with 200 µl MHS-medium (see formulation on *Table 12*). Culture medium in control wells was supplemented with 10 µM of the mycotoxin and F-actin polymerization inhibitor cytochalasin D (Gibco, Dublin, Ireland) to suppress phagocytosis. AMs were washed with 1x live cell imaging solution (Molecular Probes, Eugene, USA) and incubated with 100 µl of a suspension containing 0.5 mg/ml pHrodo red zymosan A bioparticles (life technologies, Eugene, USA) in 1x live cell imaging solution for 60 min. For a correct dispersion of the particles, the suspension was briefly vortexed and sonicated for 5 minutes in an ultrasonic water bath directly before pipetting it to the wells. The incubation of the cells with the zymosan particles was performed in an incubator without CO₂ influx to avoid artificial acidification of the buffer.

After washing cells with 37 °C-warm 1x live cell imaging solution, 100 µl Accutase (Sigma-Aldrich, Taufkirchen, Germany) were added to each well and AMs were placed back in the incubator for up to 10 min to detach cells from the plate. 300 µl FACS buffer were added to each well and fluorescence intensities of uptaken particles (585 nm emission maximum) were measured on a BD FACSCANTO II cytometer at the iLBD of the Helmholtz Zentrum München (488 nm blue laser, 585/42 “PE” filter).

3.6 RNA isolation and reverse transcription

RNA from lung and placenta tissues was isolated using the RNeasy Plus Mini Kit (QIAGEN, Hilden, Germany), while RNA from AMs was isolated using the Quick-RNA MicroPrep kit (ZYMO RESEARCH, California, USA) following the manufacturer’s recommendations. Lung and placenta tissues were mechanically homogenized in 600 µl lysis buffer in a tube containing Lysing Matrix D (MP Biomedicals) for 30 s at a speed of 6500 on a MagNA Lyser Instrument (Roche Diagnostics GmbH, Mannheim, Germany). Directly after homogenization, lysates were centrifuged at maximum speed for 3 min and supernatant transferred to gDNA eliminator columns for further RNA preparation.

For the RNA isolation of AMs, bronchoalveolar lavages from two animals were pooled, plated on 12-well plates and incubated with MHS-medium at 37 °C and 5 % CO₂ for 60 min. After washing off non-adherent cells with warm PBS, AMs were lysed with 200 µl lysis buffer. Lysates were collected in 1.5 ml reaction tubes, shock-frozen in liquid nitrogen and stored at -20 °C until further RNA preparation.

After total RNA purification, tissue RNA was eluted in 50 μl and AM RNA in 12 μl RNA free water. Directly after elution, RNA concentration and purity was quantified with a NanoDrop ND-1000 spectrophotometer (peqlab Biotechnologie, Erlangen, Germany).

For synthesis of complementary DNA (cDNA), up to 1 μg in 10 μl total RNA were transferred to 0.2 ml thin-walled microtubes for PCR (Thermo Fisher Scientific, UK) incubated with 1 μl of random nonamers with a concentration of 0.1 mM for 5 min at 70 °C on a PCR- thermal cycler (MJ Research, Hamburg, Biozym, Germany). After 5 min incubation on ice and 10 min at RT, 9 μl of a master mix containing 4 μl 5x first strand buffer, 2 μl 10x dithiothreitol 0.1 M, 1 μl Superscript II reverse transcriptase 200 U/ μl (Invitrogen, California, USA), 1 μl RNase inhibitor 40 U/ μl and 1 μl 4 dNTP mix 10 mM each NEB (Thermo Fisher Scientific) were added to each sample and reaction tubes were incubated for 1 h at 42 °C. After inactivation of the reverse transcriptase at 70 °C for 15 min, samples were diluted 1:5 in DEPC- and nuclease-free UltraPure Distilled Water (Invitrogen, California, USA) and stored at -20 °C until qPCR analysis.

3.7 Real-time polymerase chain reaction

Primer design was performed online with the *NCBI's primer blast tool*^[385] targeting primer melting temperatures around 61.5 °C with a maximal melting temperature difference between primer pairs of 1.5 °C. Primer selection was also limited to primer pairs binding to exon junctions or exon-spanning regions and leading to PCR product sizes between 80 and 140 base pairs. Please refer to *Table 7* for the list of primer sequences employed in this thesis.

qPCR analysis was performed with a LightCycler 480 II (Roche Diagnostics, Rotkreuz, Switzerland). For each sample, 10 μl of a qPCR master mix containing 6 μl LightCycler 480 SYBR Green I Master (Roche, Mannheim, Germany), 3.5 μl DEPC- and nuclease-free UltraPure Distilled Water (Invitrogen, California, USA) and 0.5 μl primer mix (10 μM each), were pipetted to each sample well of a 96-well Lightcycler plate (SARSTEDT AG & Co. KG, Nürnberg, Germany). 2 μl cDNA (see *Section 3.6*) or water as no template controls were added to wells containing master mix and the plate was sealed with an optically clear adhesive seal (Thermo Scientific, Wilmington, USA). All samples were analysed using two technical replicates.

The qPCR protocol consisted of a pre-incubation period of 6 min at 95 °C, followed by 45 amplification cycles composed of a denaturation phase of 8 s at 95 °C, an hybridization period of 12 s at 60 °C and an polymerization interval of 15 s at 72 °C. A single acquisition of the SYBR green fluorescence intensity was performed at the end of the polymerization interval. For quality control, a melting curve program was run directly

after amplification. This consisted of a continuous increase of temperature from 65 °C to 97 °C with a ramp rate of 0.11 °C/s and the acquisition of the SYBR green fluorescence intensity every 5 s. The LightCycler protocol was finished with a cooling period of 10 s at 40 °C.

The identification of the threshold cycle (C_T) was performed automatically by the LightCycler 480 software (Roche Diagnostics, Rotkreuz, Switzerland) with the second derivative maximum method. C_T values were exported as text files and analysed with R. Three house keeping genes (Actb, Hprt, Gusb) were used as internal control. These three genes were selected after identifying the most stably expressed control genes in the tissues of interest employing the geNorm method^[386].

The quantification of the relative expression of the genes of interest was performed using the ΔC_T method^[387]. For each sample, the average of the C_T values from technical replicates was computed and the average of all control genes was subtracted from it (ΔC_T). The relative quantity of each gene of interest was then calculated by exponentiating 2 to the power of $-\Delta C_T$ ($2^{-\Delta C_T}$).

Table 7: Primer sequences

Gene	RefSeq	Forward (5'→3')	Reverse (5'→3')
Arg1	NM_007482.3	ggcagagggtccagaagaatgg	tgagcatccaccaaatgacac
Bmp4	NM_007554.3	acttcgaggcgacacttctacag	actggagccggtaaagatccc
Ccl17	NM_011332.3	ctctgcttctggggacttttct	agtaatccaggcagcactctc
Ccl2	NM_011333.3	ttaaaaacctggatcggaaccaa	gcattagcttcagatttacgggt
Chil3	NM_009892.3	atggcctcaacctggactgg	tgctttctccacagattcttctc
Cxcl2	NM_009140.2	aagtttgcttgaccctgaagc	gttctccggttgaggacagc
Fgf10	NM_008002.4	tgagaagaacggcaaggtcag	gacggcaacaactccgatttc
Fzd1	NM_021457.3	actttgtgccgaagcactcc	tccagcaaccaagcagcag
Fzd10	NM_175284.3	cgccgatcatggagcagttc	ctcatccgagccgttgttg
Fzd7	NM_008057.3	ggtgtgtggcagtgctgtg	tgggtcgctctggatagctg
Ifng	NM_008337.4	aggaactggcaaaaggatggt	atgttgttctgatggcctg
Igf1r	NM_010513.2	cccacctcgctgtgg	agctgctgatagctgttgcg
Ii12b	NM_001303244	ttgaactggcgttggaaagcac	tcttgggcggttctggtttg
Ii6	NM_031168.2	ggagcccaccaagaacgatag	cagcatcagtcaccaagaaggc
Kdr	NM_010612.3	ctagctgtcgctctgtggttc	ttgtcagtatgctttctgtgtgc
Lef1	NM_010703.4	ctcaggagccctaccacgac	cgggtcgctgttcatattggg
Mmp2	NM_008610.3	tggcaccaccgaggactatg	gttggccaggaaagtgaaggg
Mmp9	NM_013599.4	ctattcgccctgcaccacag	cttctccgttccctgtctc
Nkx2-1	NM_009385.3	caggacaccatgcggaacag	ccgccatgccactcatattc
Nlrp3	NM_001359638	gtaccaaggctgctatctgg	gcagcccttctcagggtctc
Nos2	NM_001313921	atgactcccagcacaagg	ctcttgcggacctctctctg
Pdgfa	NM_008808.4	gtgccattcgaggaagag	caggaagttggccgatgtgg
Pdgfra	NM_001083316	cgcggaacctcagagaaatcg	ctgaggaccagaagacctgtgtg
Pdpm	NM_010329.3	aacaaccacaggtgctactgg	tgctgaggtggacagttctc
Pparg	NM_001127330	gagatcatcacgatgctggc	cgcaggctttgaggaactc
Ptsg2	NM_011198.4	caacacctgagcgggttac	gttccaggaggatggagt
Retnla	NM_020509.3	gctaactatccctcactgtaacg	caagcacaccagtagcagtc

Table 7: Primer sequences (*continued*)

Gene	RefSeq	Forward (5'->3')	Reverse (5'->3')
Saa3	NM_011315.3	agccaaagatgggtccagttc	atgtcagagtaggctcgcca
Sftpb	NM_147779.2	aggctatgccacaggcaatg	caggtgatgtggcatcctg
Sftpc	NM_011359.2	caaagaggtcctgatggagagtc	accacaaccacgatgagaagg
Sftpd	NM_009160.2	tggtcgtgatggacgggatg	gttcgccagcagagccattc
Shh	NM_009170.3	gcaggtttcgactgggtctac	aacagccgccgatttgg
Tgfb1	NM_011577.2	taatggtggaccgcaacaacg	tgctcccgaatgtctgacg
Timp3	NM_011595.2	cacatgctctcccagccatc	accagctctttcccaccac
Tnf	NM_001278601	gatcgggcccaagggatg	gtggtttgtgagtgtgagggt
Tnfrsf11a	NM_009399.3	tgcagctcaacaagatacgg	ccctggtgtctctagcttcc
Vegfa	NM_001025250	agccagcacataggagagatgag	tgctttgtctgtcttcttgg
Wnt10b	XM_006520892	cgcggttccgtgagagtg	ccgttaccaccagcttgcc
Wnt2	NM_023653.5	tcggtggaatctggctctgg	tcacacatcacctggaggag
Wnt3a	NM_009522.2	tcggatactcttagtgctctgc	gcacagagaatgggctgagtg
Wnt5a	NM_009524.4	ggcatcggagatggaactgc	ctcggctcatggcgttcac
Wnt7b	NM_009528.3	acaatgaggcgggcagaaag	cctcgcggaacttaggtagc

3.8 Statistical analysis

Experimental raw data was imported, wrangled and analysed over the integrated development environment (IDE) RStudio 1.3.959^[388] in the language for statistical computing and graphics R, versions 3.5.2 or 4.0.0^[389]. R packages employed are listed in the references^[378,379,390-409]. Graphical representations of analysed data were generated also in R. This thesis was written making use of the R Markdown framework^[399,403,408] and L^AT_EX^[410].

Descriptive statistical analysis of experimental results consisted of the following steps:

After loading raw data files into R, a first exploratory examination was performed. This consisted of the identification of the type of variables in the data, the presence of missing values and potential outliers as well as the qualitative visualization of the distribution of the data points along their respective scales. Outlier removal was performed only in cases where there was a strong evidence of technical errors. The visualization of data was an important step during exploratory analysis, which also allowed for a first qualitative impression of possible differences between groups. Data wrangling allowed the organization of observations (samples) and variables (measured attributes) into a “tidy”^[411] format for downstream analytics. Data compression was achieved by the computation of summary statistics to recognize the central tendency, dispersion, shape of the underlying distribution and dependence between variables. Depending on the type of variable analysed, assumptions of appropriate statistical inference tests were assessed before the actual statistical comparison between groups

(hypothesis testing). The evaluation of the normal distribution and, for instance, was an important step in the control of the required assumptions. This was performed qualitatively with the help of QQ-plots as well as quantitatively by applying the Shapiro-Wilk normality test. In order to test for the homogeneity of variance across groups, the Levene test was also employed.

The significance level α was set to 0.05. The test decision was based on p-values from hypothesis testing results. To prevent the inflation of false positive rates, p-value correction techniques were implemented in the case of multiple comparisons. The more conservative Bonferroni correction (family-wise error rate correction) was used in confirmatory analyses – i. e. results that were already published somewhere else and experimentally verified – while the Benjamini-Hochberg correction (false discovery rate correction) in rather exploratory analyses.

Table 8: Software

Software Name	Manufacturer
BD FACSDiva Software Version 6.1.3	BD Biosciences, San Jose, USA
BD FACSDiva Software Version 8.0	BD Biosciences, San Jose, USA
FlowJo 10.5.3	FlowJo LLC, Ashland, USA
LightCycler 480 Software SP4 version 1.5.0.39	Roche Diagnostics, Rotkreuz, Switzerland
Magellan Software V7.1 SP1	Tecan Austria, Grödig, Austria
OLYMPUS cellSens Dimension 1.14	OLYMPUS CORPORATION, Tokyo, Japan
R versions 3.5.1 and 4.0.0	The R Foundation for Statistical Computing, Vienna, Austria
RStudio version 1.3.959	RStudio, Boston, USA
Tecan NanoQuant infinite M200 PRO	Tecan Austria, Salzburg, Austria
VIS - Visiopharm Integrator System Version 6.0.01765	Visiopharm, Medicon Valley, Denmark

Table 9: Equipment

Equipment Name	Cat. No.	Company
ABI PRISM® 7500 detection system		Applied Biosystems, Foster city, CA, USA
Accu-Chek Aviva Connect	06919138001	Roche Diagnostics GmbH, Mannheim, Germany
Axioplan	451887	Carl Zeiss Microscopy GmbH, Jena, Germany
BD FACSCanto II	338962	BD Biosciences, San Jose, USA
CB 150 incubator	9140-0001	Binder, Tuttlingen, Germany
Centrifuge: Eppendorf 5415D		Eppendorf, Hamburg, Germany
Centrifuge: Sigma 3K18		Sigma, Osterode am Harz, Germany
Cold Module for Embedding	A81000105	Thermo Scientific, Runcorn, UK
Counter AC-12	345-12	Karl Hecht, Sondheim, Germany
CR422 refrigerated centrifuge	23173	Pabisch, München, Germany

Table 9: Equipment (*continued*)

Equipment Name	Cat. No.	Company
Ferrari manual counter	L10	ferrari
Forceps with ring-shaped tip	L00.1	Carl Roth, Karlsruhe, Germany
HistoStar cold module	HS0147B1103	Thermo Scientific, Runcorn, UK
Incubator Heraeus BBD 6220	51020241	Thermo Electron, Langensfeld, Germany
KL 1500 LCD fiber optic illuminator	KL1500LCD	Schott, Duesseldorf, Germany
Lacrymal olive-tipped needles (0.60 x 33 mm. 23G x 1 3/8")	27.140	UNIMED, Lausanne, Switzerland
Leica M80 binocular	MEB132	Leica Microsystems, Singapore
Leica TP1020-1-1 benchtop tissue processor	042230535	Leica Biosystems Nussloch GmbH, Nussloch, Germany
LightCycler 480 II /96	28340	Roche Diagnostics, Rotkreuz, Switzerland
MagNA Lyser Instrument	41337317	Roche Diagnostics GmbH, Mannheim, Germany
Mastercycler nexus eco / nexus gradient	6332	Eppendorf, Hamburg, Germany
MESO QuickPlex SQ 120	AI0AA-0	MESO SCALE DIAGNOSTICS, Maryland, USA
Mikro-Dismembrator S	00313	Sartorius Stedim, Göttingen, Germany
MIKRO 220R centrifuge	2205	Hettich, Tuttlingen, Germany
MiniSpec body composition analyzer	LF50	Bruker BioSpin MRI, Ettlingen, Germany
Minutien pins	26002-20	Fine Science Tools, Heidelberg, Germany
Multipipette E3	H42845F	Eppendorf, Hamburg, Germany
NanoDrop® ND-1000 spectrophotometer	ND-1000	peqlab Biotechnologie, Erlangen, Germany
Neubauer improved bright-line OLYMPUS BX51TF	BR717810	Brand, Wertheim, Germany
OLYMPUS DP72		OLYMPUS CORPORATION, Tokyo, Japan
PCR- thermal cycler : PTC-225		MJ Research, Hamburg, Biozym, Germany
Reusable feeding needles	18064-20	Fine Science Tools, Heidelberg, Germany
Sartorius precision scale	R160P	Sartorius, Göttingen, Germany
Shandon cytospin 2 cytocentrifuge	59900101	Shandon Soudern Products, Cheshire, England
Specimen stage-stretching table	14332	MEDAX Gmbh & Co. KG, Neumünster, Germany
Thermomixer compact	5350	Eppendorf, Hamburg, Germany
Universal 32 R centrifuge	1610	Andreas Hettich, Tuttlingen, Germany
XS205 DualRange precision scale	X205BDU	Mettler Toledo, Greifensee, Switzerland
ZEISS Axiovert 135	LCB 0725	Lauda, Lauda-Königshofen, Germany
ZEISS HYRAX M 55	43773	MICROM, Walldorf, Germany

Table 9: Equipment (*continued*)

Equipment Name	Cat. No.	Company
Zetasizer Nano Series	ZEN3600	Malvern instruments limited, Worcestershire, UK

Table 10: Biochemical isolation and analysis kits

Kit Name	Catalog Number	Manufacturer
Annexin V Apoptosis Detection Kit- APC	88-8007-74	eBioscience, San Diego, USA
Mouse CCL17/TARC DuoSet ELISA	DY529	R&D Systems, Minneapolis, USA
Mouse CCL2 DuoSet ELISA	DY479	R&D Systems, Minneapolis, USA
Mouse CSF2 DuoSet ELISA	DY415	R&D Systems, Minneapolis, USA
Mouse CXCL1 DuoSet ELISA	DY453	R&D Systems, Minneapolis, USA
Mouse Fas Ligand/TNFSF6 DuoSet ELISA	DY526	R&D Systems, Minneapolis, USA
Mouse IL1a/IL-1F1 DuoSet ELISA	DY400	R&D Systems, Minneapolis, USA
Mouse IL1b/IL-1F2 DuoSet ELISA	DY401	R&D Systems, Minneapolis, USA
Mouse Lactate Dehydrogenase, LDH ELISA Kit	E1864m	USCNLIFE
Mouse LIX DuoSet ELISA	DY443	R&D Systems, Minneapolis, USA
Mouse Serum Amyloid A Quantikine ELISA Kit	MSAA00	R&D Systems, Minneapolis, USA
Pierce BCA Protein Assay Kit	23225	Thermo Fisher Scientific
Quick-RNA MicroPrep kit	R1051	ZYMO RESEARCH, California, USA
RNeasy Plus Mini Kit	74136	QIAGEN, Hilden, Germany

Table 11: Chemicals and reagents

Reagent	Cat. No.	Manufacturer
1x live cell imaging solution	A14291DJ	Molecular Probes, Eugene, USA
2-mercaptoethanol	M3148	Sigma-Aldrich, Taufkirchen, Germany
3,3',5,5'-Tetramethylbenzidine (TMB) Liquid Substrate System for ELISA	T0440	Sigma-Aldrich, Taufkirchen, Germany
Accutase	A6964	Sigma-Aldrich, Taufkirchen, Germany
Antisedan (Atipamezol) 5 mg/ml	10000449	Prodivet pharmaceuticals, Barcelona, Spain
BEPANTHEN Eye and Nose Cream	1578681	Bayer Vital, Leverkusen, Germany
Bovine Serum Albumin (BSA)	A2153	Sigma-Aldrich, Taufkirchen, Germany
CD16/ CD32 (93)	14-0161-81	eBioscience, San Diego, USA
CD24A-Alexa Fluor 700 (M1/69)	101836	BioLegend, San Diego, USA
cell tracker red CMTX	C34552	Invitrogen, California, USA
CountBright Absolute Counting Beads	C36950	Molecular Probes, Eugene, USA
cytochalasin D	PHZ1063	Gibco, Dublin, Ireland

Table 11: Chemicals and reagents (*continued*)

Reagent	Cat. No.	Manufacturer
DAPI staining solution	130-111-570	Miltenyi Biotec, Bergisch Gladbach, Germany
Dispase	354235	Corning, Massachusetts, USA
DNaseI	A3778	AppliChem, Darmstadt, Germany
dNTP Mix (10 mM each)	R0192	Thermo Fisher Scientific
Dormicum (Midazolam) 5 mg/1 ml	10145376	Roche, Mannheim, Germany
Dulbecco's Phosphate Buffered Saline (DPBS) (1X)	14190-094	Gibco, Dublin, Ireland
Elastosil RT 601 A	9104437067	Wacker, Munich Germany
Elastosil RT 601 B	9104437067	Wacker, Munich Germany
Entellan new	107961	Merck KGaA, Darmstadt, Germany
Ethanol absolute for analysis	100983	Merck KGaA, Darmstadt, Germany
Ethylenediaminetetraacetic acid disodium salt dihydrate (EDTA)	ED2SS	Sigma-Aldrich
FCGR1-PE (REA286)	130-118-684	Miltenyi Biotec, Bergisch Gladbach, Germany
Fentanyl 0.1 mg/2 ml injection solution	2084366	Janssen, Neuss, Germany
Fetal Bovine Serum (FBS)	10091148	Gibco, New Zealand
Flumazenil injection solution 1 mg/10 ml	4470990	HEXAL, Holzkirchen, Germany
Giemsa's azur eosin mthylene blue solution	109204	Merck KGaA, Darmstadt, Germany
H2-AB1-APC-Vio770 (REA813)	130-112-233	Miltenyi Biotec, Bergisch Gladbach, Germany
HEPES Buffer Solution (1 M)	02968	Gibco, Dublin, Ireland
high-fat, Ssniff EF D12492(II) mod. 60 kJ% fat (tallow)	E15741-347	SSniff Spezialdiäten, Soest, Germany
Histosec pastilles	111609	Merck KGaA, Darmstadt, Germany
ITGAM-PE-Vio770 (REA592)	130-109-287	Miltenyi Biotec, Bergisch Gladbach, Germany
ITGAX-FITC (REA754)	130-110-837	Miltenyi Biotec, Bergisch Gladbach, Germany
ketamine 10%	00218	medistar, Ascheberg, Germany
LightCycler 480 SYBR Green I Master	04887352001	Roche, Mannheim, Germany
Lipopolysaccharides from <i>Escherichia coli</i> O55:B5	L2880	Sigma-Aldrich, Saint Louis, USA
low-fat, Ssniff EF control E15000-047	E15000-047	SSniff Spezialdiäten, Soest, Germany
LY6C-PerCP-Vio700 (REA796)	130-111-920	Miltenyi Biotec, Bergisch Gladbach, Germany
LY6G-VioBlue (REA526)	130-110-449	Miltenyi Biotec, Bergisch Gladbach, Germany
MACS Comp Bead Kit, anti-REA	130-104-693	Miltenyi Biotec, Bergisch Gladbach, Germany

Table 11: Chemicals and reagents (*continued*)

Reagent	Cat. No.	Manufacturer
May-Grünwald's eosine-methylene blue solution modified	101424	Merck KGaA, Darmstadt, Germany
Mayer's hemalum solution	109249	Merck, Darmstadt, Germany
Mistosec pastilles	1.11609.2504	Merck, Darmstadt, Germany
Narcanti (Naloxon) 0.4 mg/ml injection solution	3338219	Braun, Melsungen, Germany
Omnifix-F 1 ml syringe	9161406V	Braun, Melsungen, Germany
OneComp eBeads Compensation Beads	01-1111-42	Invitrogen, California, USA
PBS Dulbecco w/o calcium w/o magnesium	L182-10	Biochrom, Berlin, Germany
Penicillin-Streptomycin	15140122	Gibco, Dublin, Ireland
pHrodo Red Zymosan Bioparticles Conjugate for Phagocytosis primers (see primer table)	P35364	Thermo Fisher Scientific metabion international, Planegg, Germany
ProLong Gold antifade with DAPI	P36935	Invitrogen, California, USA
Proxylaz (Xylazin)	3100408.00.00	bela-pharm, Vechta, Germany
PTPRC-VioGreen (REA737)	130-110-803	Miltenyi Biotec, Bergisch Gladbach, Germany
RNase away	7005-11	Molecular BioProducts, San Diego, USA
RnaseOUT Recombinant Ribonuclease Inhibitor	10777019	Invitrogen, California, USA
Roswell Park Memorial Institute (RPMI) 1640 medium	21875-034	Gibco, Dublin, Ireland
Roticlear	A538.2	Carl Roth, Karlsruhe, Germany
SEDIN 1 mg/ml injection solution (medetomidine hydrochloride)		Pharma partner, Hamburg, Germany
SIGLECF-APC (REA798)	130-112-333	Miltenyi Biotec, Bergisch Gladbach, Germany
standard chow	1314	Altromin, Lage, Germany
SuperScript II reverse transcriptase	18064014	Invitrogen, California, USA
tri-sodium citrate dihydrate	6430	Merck, Darmstadt, Germany
TWEEN 20	T2700	Sigma-Aldrich, Taufkirchen, Germany
UltraPure Distilled Water	10977-035	Invitrogen, California, USA
Viability 405/520 Fixable Dye	130-109-814	Miltenyi Biotec, Bergisch Gladbach, Germany
ZEISS HYRAX M 55 Microtome	9905120	MICROM GmbH

Table 12: Buffer formulations

Buffer	Compound	Concentration
FACS buffer		
	BSA	2%
	DNase I	25 µg/ml
	DPBS w/o Ca ⁺² w/o Mg ⁺²	1x
	EDTA	0.5 mM
	FBS	2%
	HEPES	25 mM
MHS medium		
	2-mercaptoethanol	0.05 mM
	FBS	10%
	Penicillin	100 U/ml
	RPMI 1640	1x
DPBS		
	Streptomycin	100 U/ml
	KCl	2.7 mM
	KH ₂ PO ₄	2 mM
	Na ₂ HPO ₄	10 mM
	NaCl	137 mM

4 Results

4.1 HFD induces obesity, systemic inflammation and hyperglycaemia

4.1.1 HFD leads to increases in body weight, body fat and body lean mass in a sexual dimorphic fashion

To test the hypothesis of transgenerational high-fat diet (HFD)-induced alveolar macrophage (AM) priming, a mouse model for obesity in C57BL/6J mice was generated. Animals were fed with purified diets containing either 60 kJ% fat (HF) or 10 kJ% fat (LF). Before mating at the age of fifteen weeks, their body composition was monitored weekly for a total of twelve weeks with a time-domain nuclear magnetic resonance (TD-NMR) analyser. HF diet led to increases in body weight and body fat in both male and female animals (*Figure 6*). When comparing diet groups, these increments, especially in body fat and body lean mass, occurred in a sexual dimorphic fashion.

In HF females, differences in all three body composition parameters were obvious from week five on after start of diet (*Figure 6A, C and E*). In HF males, substantial differences in body fat were detected already after the first week on diet (*Figure 6D*), and in body weight after the seventh week on diet (*Figure 6B*) compared to LF control mice. Interestingly, no obvious differences between diet groups were seen in body lean mass of males.

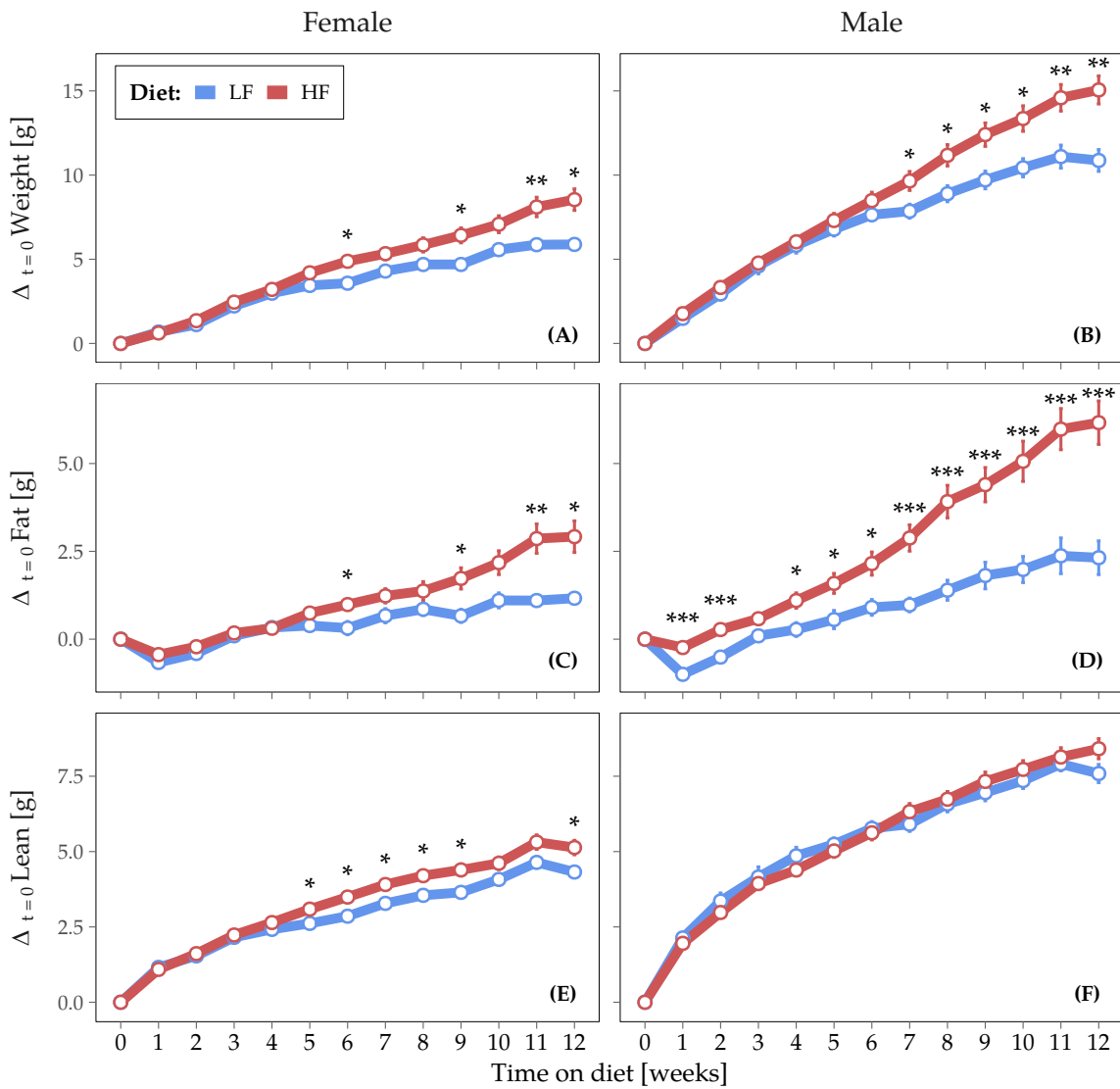


Figure 6: High-fat diet leads to an increase in body composition parameters in a sexual dimorphic way. Body weight, body fat and body lean mass of HF (red) and LF (blue) diet fed animals were monitored weekly with a time-domain nuclear magnetic resonance (TD-NMR) analyser. Body composition differences compared to week 0 (starting time point of dieting) are displayed as a function of time under diet ($n_{LF} = 12$, $n_{HF} = 20$). Mean composition values and SEM for each time point are mapped on the plot. While an increase of all three body composition values of HFD female animals was obvious from week 5 on, an increment in body fat of HFD male mice compared to LF control group was evident from week 1 on, and in body weight from week 7 on. Sexual dimorphism was especially prominent on body fat and body lean mass differences between HF and LF groups. Wilcoxon rank sum test with Benjamini-Hochberg p-value correction for multiple testing (78 comparisons): * $p < 0.05$, ** $p < 0.01$, *** $p < 0.001$.

4.1.2 HFD induces systemic inflammation and hyperglycaemia

HF-induced obesity in C57BL/6J mice is characterized by the presence of pro-inflammatory factors in the circulation and insulin resistance.^[412] To further characterise the established model of diet-induced obesity, the ability of HFD to induce signs of systemic inflammation and metabolic deregulation was tested. For this, plasma concentrations of pro-inflammatory cytokines C-X-C motif chemokine ligand 1 (CXCL1), interferon gamma (IFNG), interleukin 1 beta (IL1B), IL2, IL4, IL5, IL6, IL10,

IL12 (p70) and tumour necrosis factor (TNF) were evaluated by 10-plex immunoassay (Figure 7). At 25 weeks of age, elevated levels of blood glucose and plasma levels of the pro-inflammatory cytokines CXCL1 and IL6 revealed signs of hyperglycaemia and systemic inflammation in HF animals. While these observations were similar for both sexes, HF male mice (Figure 7B) exhibited to some extent higher concentrations of IL6 (15.7 pg/ml; median difference of 12.6 pg/ml between diet groups) than females (8.11 pg/ml; median difference of 4.2 pg/ml between diet groups) and increased levels of IL2 compared to LF controls. On the other hand, HF female animals presented less IFNG compared to LF control groups (Figure 7A).

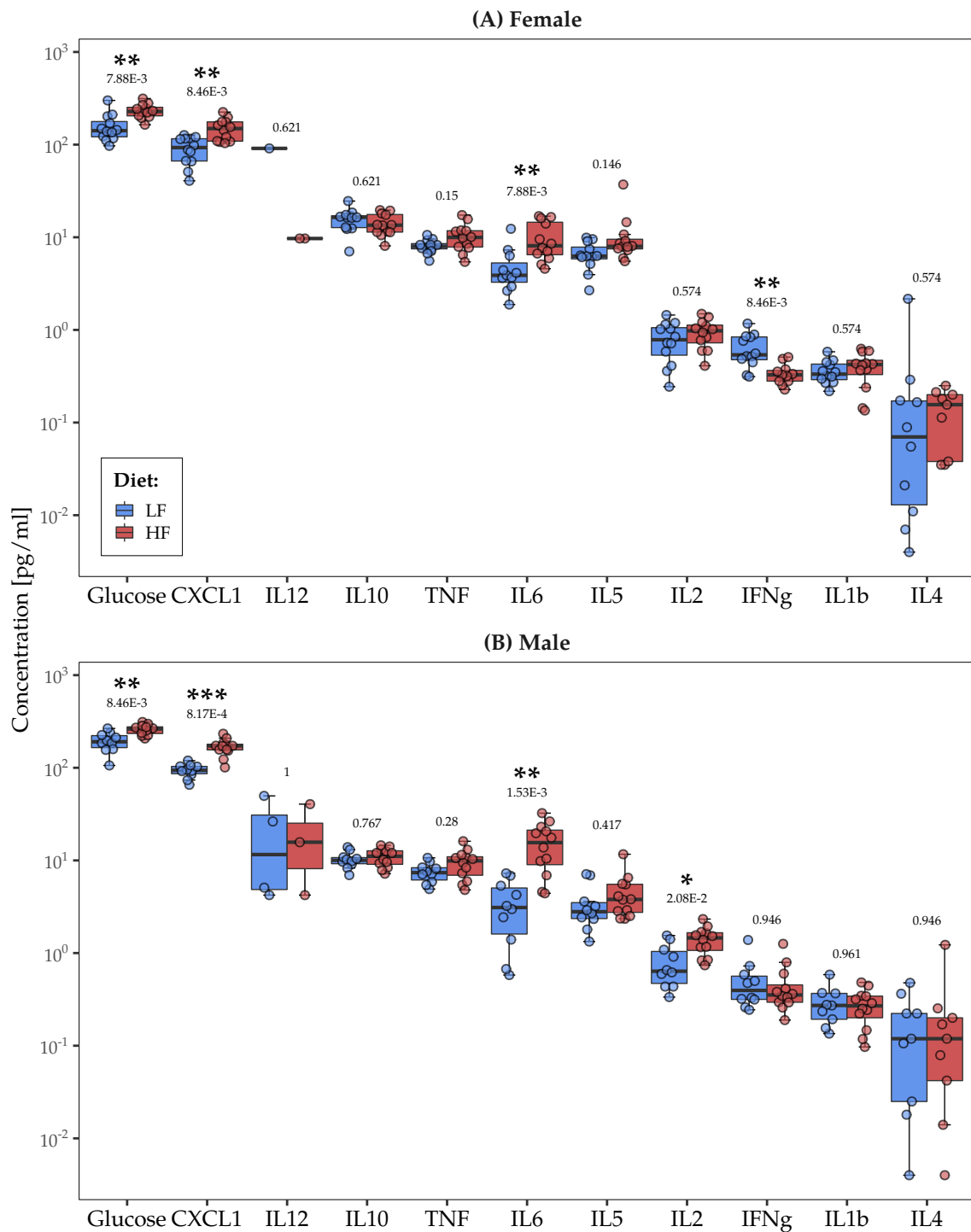


Figure 7: Increased levels of glucose in blood and pro-inflammatory cytokines in plasma evidence presence of a systemic inflammation and glucose metabolism impairment by HFD feeding. At 25 weeks of age, cytokine concentrations in plasma were measured by 10-plex immunoassay, glucose concentrations in blood with a blood glucose meter. Female (A) and male (B) HF mice (n = 10-12) presented elevated glucose, CXCL1 and IL6 concentrations. Interestingly, only male HF animals showed increases in IL2, and female LF animals raised INF γ concentrations. Wilcoxon rank sum test with Benjamini-Hochberg p-value correction for multiple testing (20 comparisons): * p < 0.05, ** p < 0.01, *** p < 0.001.

4.2 HFD distorts the course of lung inflammation and alveolar macrophage's phagocytosis

4.2.1 HF males display altered inflammatory lung dynamics

Knowing that the exposure to HFD elicits systemic metabolic and inflammatory changes in mice, its effect on lung inflammatory dynamics was tested by a model of endotoxin-induced acute lung inflammation. 30-week old female and male mice were intratracheally instilled with 0.1 μ g LPS and the numbers of bronchoalveolar lavage (BAL) neutrophils and macrophages as well as the concentration of protein in BAL fluid (BALF) were followed for 72 h (*Figure 8*). HF females did not show any differences in any of the three parameters compared to LF control groups (*Figure 8A, C and E*). These female mice were previously bred at the age of 15 weeks.

Inflammatory dynamics of HF male animals were shifted to the back of the time course. I. e. male HF mice presented a delayed initiation of inflammation with decreased counts of BAL neutrophils 24 h after LPS instillation as well as a delayed resolution 72 h after the challenge with increased neutrophils counts (*Figure 8B*). The macrophage numbers of both PBS-instilled and LPS-challenged HF males were lower than those of its corresponding LF control groups 24 h after instillation. Furthermore, mononuclear cell counts ("macrophages") of HF males 72 h after instillation were increased, compared to cell numbers of the control diet group (*Figure 8D*). Differences in the start and resolution of lung inflammation between HF and LF males were not visible at the protein level in the cell-free fraction of the lavages (*Figure 8F*).

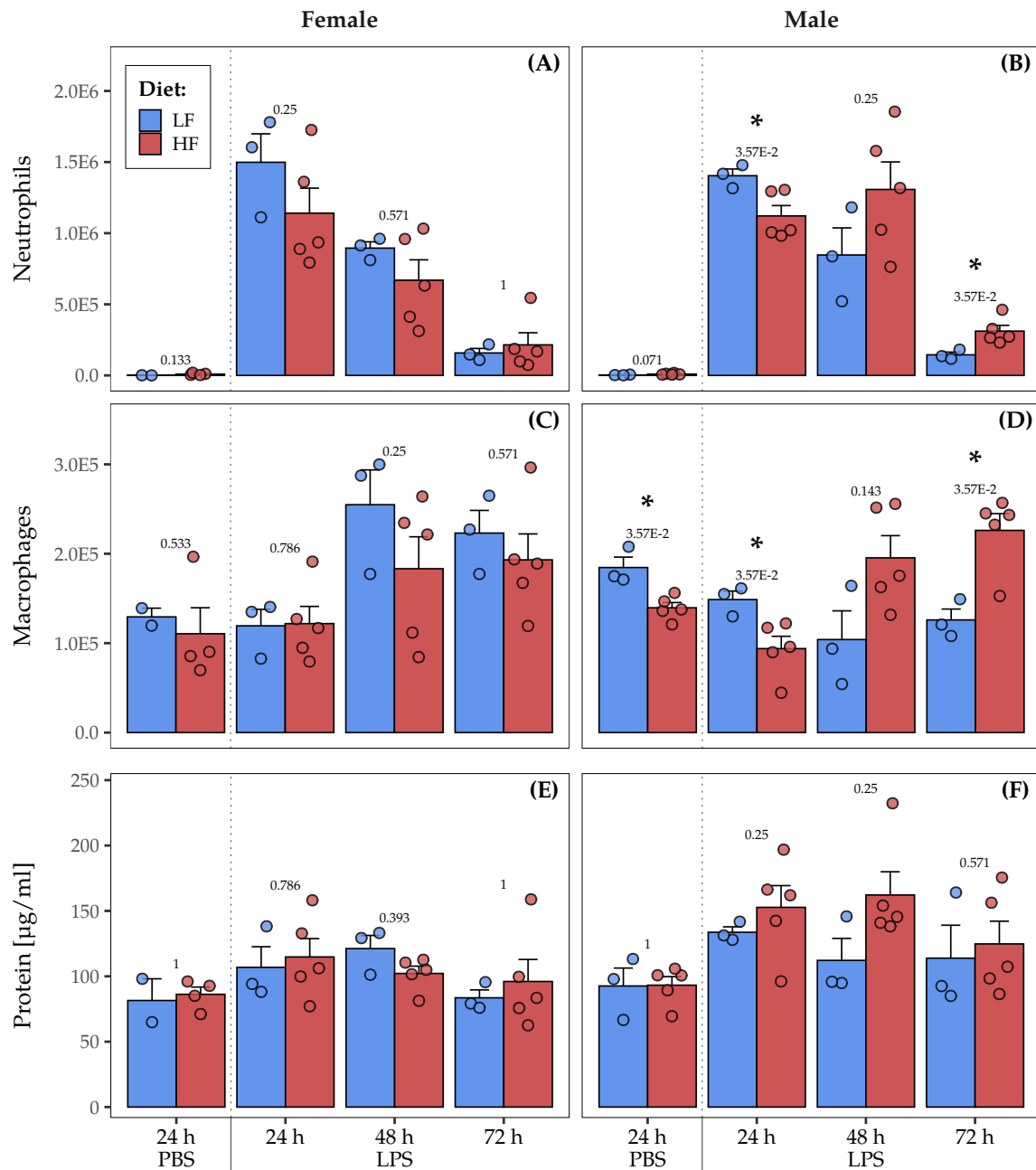


Figure 8: HFD shifts lung inflammatory dynamics during endotoxin-induced acute lung inflammation in male mice. 30 week old animals were intratracheally challenged with 0.1 μg LPS. (A-D) Neutrophils and macrophages were counted on cytocentrifuged preparations from BAL. (E,F) Protein concentrations acquired by BCA analysis of BALF showed no difference between diet groups. (B) HF males presented a shift in the inflammatory response with delayed recruitment of neutrophils to the lung 24 h after LPS instillation (delayed initiation of inflammation) and increased cell counts 72 h after the challenge (delayed resolution). (D) Reduced number of macrophages were measured in BAL 24 h after PBS and LPS instillation, while these counts increased 72 h after the start of the challenge. Wilcoxon rank sum test: * $p < 0.05$, ** $p < 0.01$, *** $p < 0.001$.

4.2.2 HFD impairs phagocytosis in alveolar macrophages of male mice

Next, in order to describe the extent to which alveolar macrophages (AMs) are involved in initial phase of the previously described shift of LPS response in the lung (delayed initiation of inflammation), these tissue macrophages (TMs) were isolated from untreated mice and analysed by qPCR. For this, lavage cells from 25-week old mice were plated with MH-S medium and purified by adherence. AMs were either classically activated (M1) with 1 μ g/ml LPS for 50 min for the analysis of their pro-inflammatory polarizability or incubated in MH-S medium for the examination of their ground polarization status at steady state (M0 AMs). Pro- (M1: Cxcl2, Il12b, Il1b, Nlrp3, Saa3, Tnf) and anti-inflammatory (M2: Chil3, Pparg) marker expression was quantified by qPCR for each of the 8 groups (*Figure 9* and *Figure 10*).

The incubation of AMs with LPS effectively led to increased expression of pro-inflammatory markers when comparing respective M0 and M1 data ($p < 0.001$, *Appendix, Table 14*). However, comparisons of the marker expression between diet groups displayed no differences at steady state (M0, *Figure 9*) nor after M1 polarization (*Figure 10*).

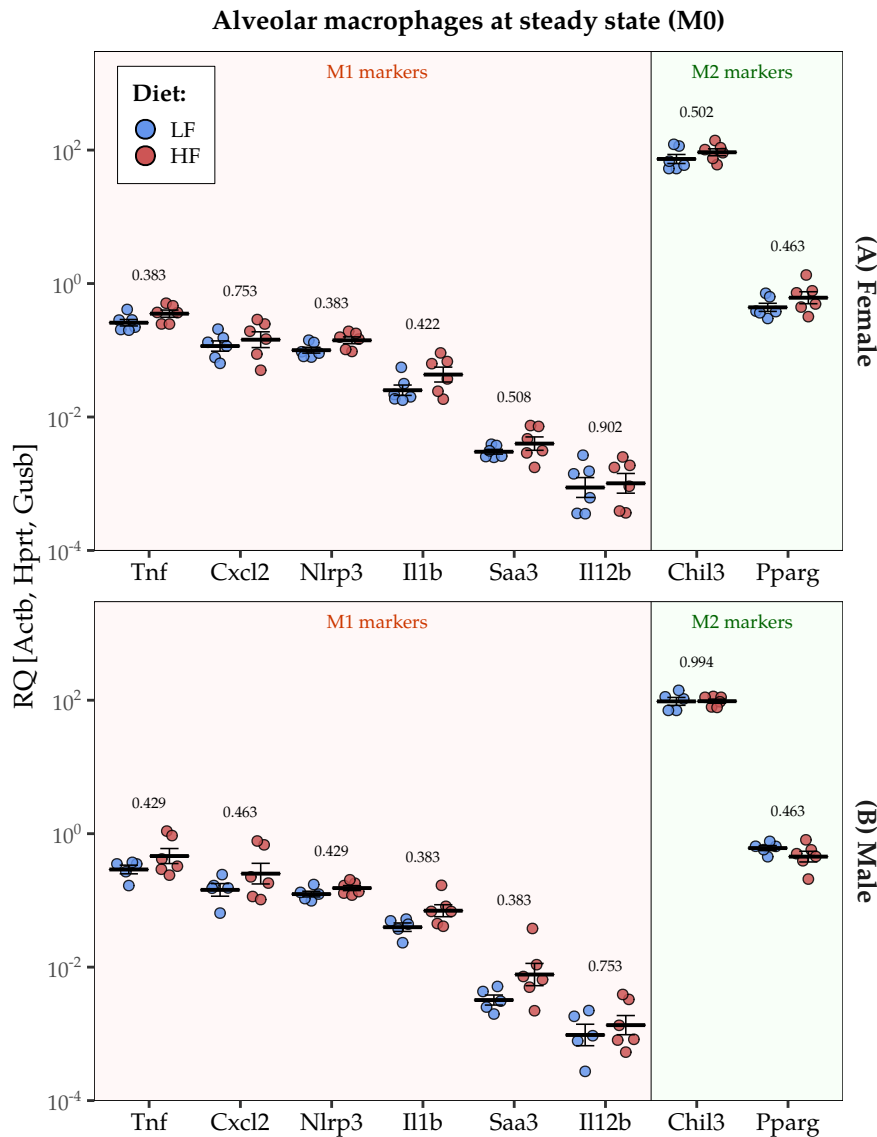


Figure 9: No effect of HFD on expression of AM polarization markers at steady state. AMs were isolated from untreated mice (n = 5-6) at 25 weeks of age by bronchoalveolar lavage and purified by adherence. Pro- (M1: Cxcl2, Il12b, Il1b, Nlrp3, Saa3, Tnf) and anti-inflammatory (M2: Arg1, Chil3, Pparg, Retnla) marker expression was quantified by qPCR and normalized (relative quantity, RQ) to three housekeeping genes (Actb, Hprt, Gusb). Neither female (A) nor male (B) mice presented any changes in gene expression due to HFD feeding. Welch two sample t-test with Benjamini-Hochberg p-value correction for multiple testing (16 comparisons).

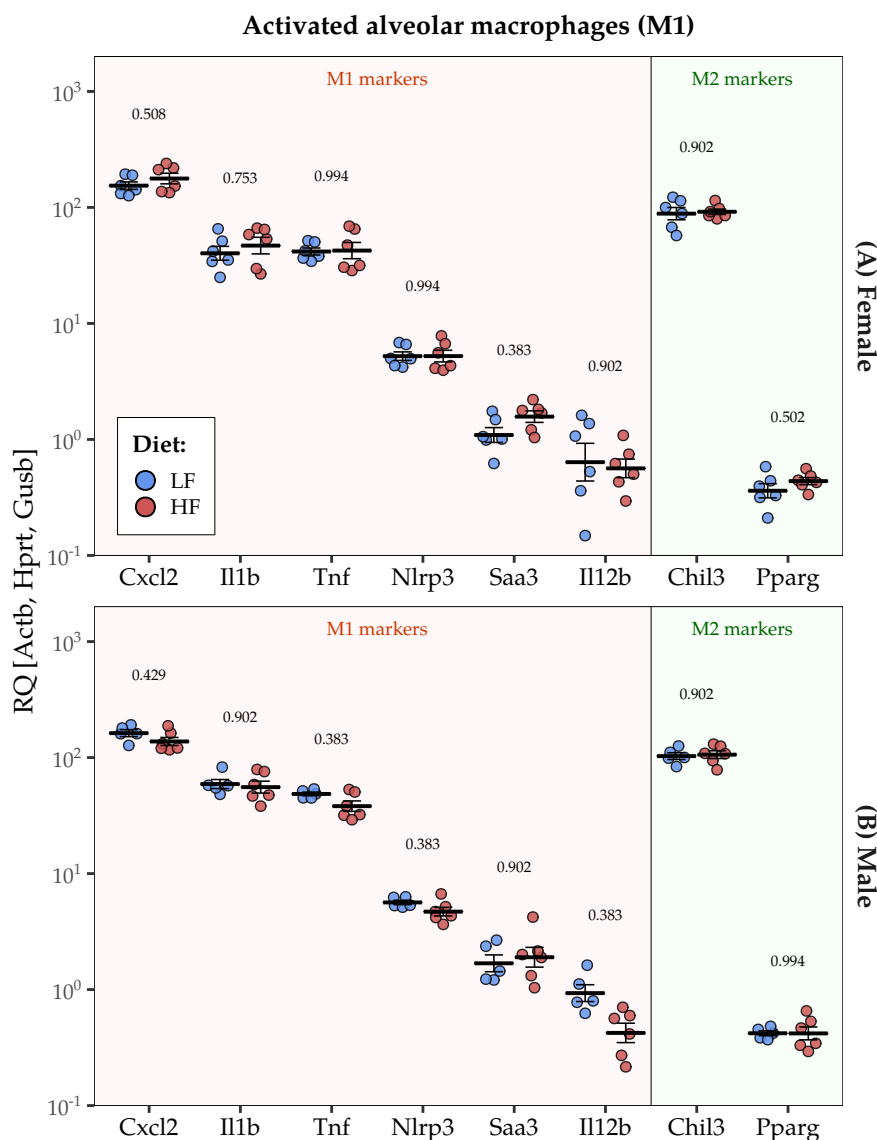


Figure 10: No effect of HFD on the *in vitro* M1 polarizability of AMs. AMs isolated from untreated mice ($n = 5-6$) at 25 weeks of age were incubated with $1 \mu\text{g/ml}$ LPS for 50 min for M1 (classical/pro-inflammatory) activation. Gene expression of pro- (M1: Cxcl2, Il12b, Il1b, Nlrp3, Saa3, Tnf) and anti-inflammatory (M2: Arg1, Chil3, Pparg, Retnla) markers was analysed by qPCR and normalized (relative quantity, RQ) to three housekeeping genes (Actb, Hprt, Gusb). Polarization of AMs was successful with clear increases in gene expression of M1 markers ($p < 0.001$, Appendix, Table 14). Neither female (A) nor male (B) mice presented any changes in the polarizability of their AMs *in vitro* due to HFD feeding. Welch two sample t-test with Benjamini-Hochberg p-value correction for multiple testing (16 comparisons).

As mentioned in Section 1.4.2, AMs are not only of highest importance for the initiation, but also for the resolution of lung inflammation. Processes of utmost relevance in the resolution of lung inflammation are the efferocytosis of apoptotic neutrophils^[413] and removal of debris by phagocytosis^[414]. To investigate the effect of HFD on AM phagocytosis and phagosome maturation, AMs isolated from BAL were incubated with pHrodo zymosan particles and analysed by flow cytometry. These particles emit fluorescence in the presence of an acidic milieu, like the one present

in mature phagolysosomes^[415]. Cell counts of fluorescence-emitting AMs in females were unaffected by HFD. However, pHrodo-positive AMs numbers from HF male mice were reduced compared to the control group (*Figure 11*). This pointed to either an impaired phagocytic uptake of particles or to a delayed or defective phagosome acidification/maturation in alveolar macrophages from HF male mice.

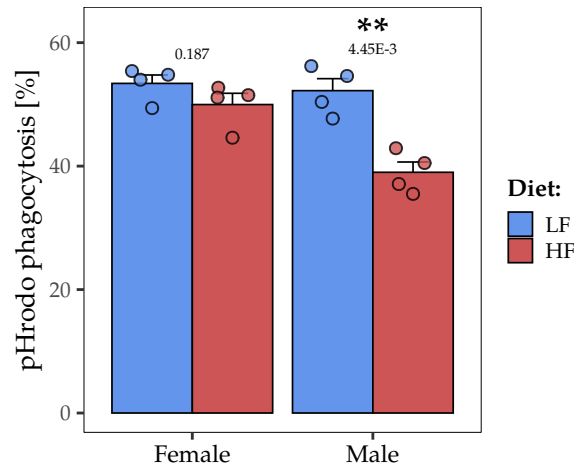


Figure 11: HFD impairs phagocytosis in HF males. AMs were isolated from bronchoalveolar lavages of mice, incubated with pHrodo zymosan particles and analysed by flow cytometry. Zymosan particle phagocytosis by AMs female animals remained unaffected by diet. The amount of AMs from HF males positive for the phagocytosis test were reduced, pointing to impaired phagocytic uptake or defective phagosome maturation (n = 4). Welch two sample t-test with Benjamini-Hochberg p-value correction for multiple testing (2 comparisons): ** p < 0.01.

4.3 Parental obesity reduces foetal viability and delays weight gain after birth

Parent mice were mated 12 weeks after continuous feeding with either HFD or LFD. Aiming to describe the effect of parental diet-induced obesity on foetal outcomes, viable foetuses were counted and weighted 18.5 days after positive vaginal plug test. Additionally, the number of resorbed foetal sacs were quantified. HF dams exhibited increased foetal death (22%) compared to LF dams (4%) (Figure 12A). However, foetal body weights did not differ between parental diet groups (Figure 12B).

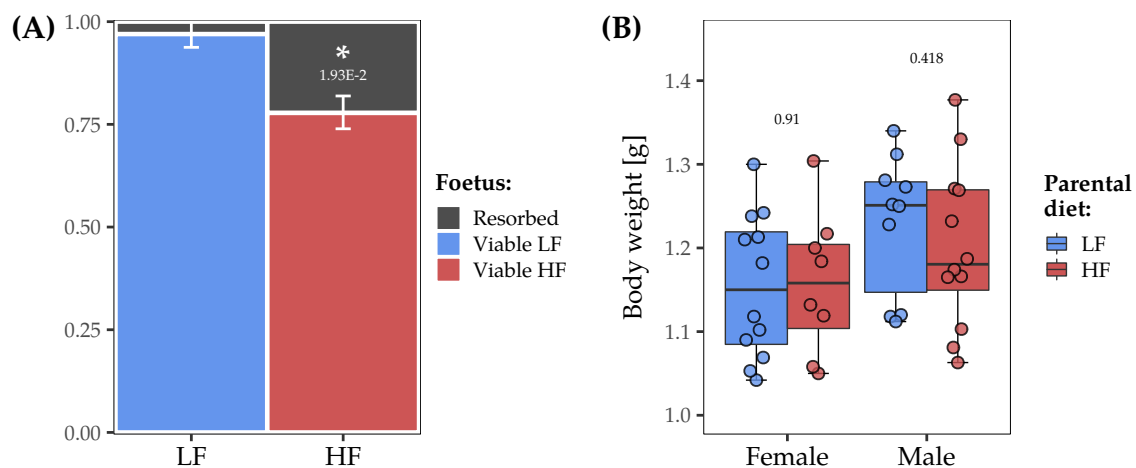


Figure 12: Parental obesity increases E18.5 foetal sack resorption with no repercussions on body weights of viable foetuses. (A) 18 days after positive vaginal plug test, number of vital E18.5 foetuses and resorbed sacs (miscarriages) per dam ($n = 3$) were counted. Ratios between miscarriages and viable foetuses pointed to increased number of miscarriages during gestation and consequently a decreased total number of vital foetuses from dams fed with HFD (ratio_{HF} = 77.8%) compared to the female LF control group (ratio_{LF} = 96.0%). Fisher's exact test for count data: * $p < 0.05$. (B) E18.5 foetal body weights ($n_{E18.5} = 10-12$) were not affected by parental diet-induced obesity. Wilcoxon rank sum test.

Offspring's body weights were further determined at two weeks (postnatal day 15, P15), and at ten weeks (P70) of age (Figure 13). No differences in body weights were observed in P15 male offspring nor at the age of P70. Yet, body weights of HF female offspring were reduced at the age of P15 compared to the LF control group (Figure 13A). These observations were transient, since a catch-up in body weight occurred after the age of two weeks, leading to similar body weight measurements of the HF and LF female offspring at the age of P70 (Figure 13B).

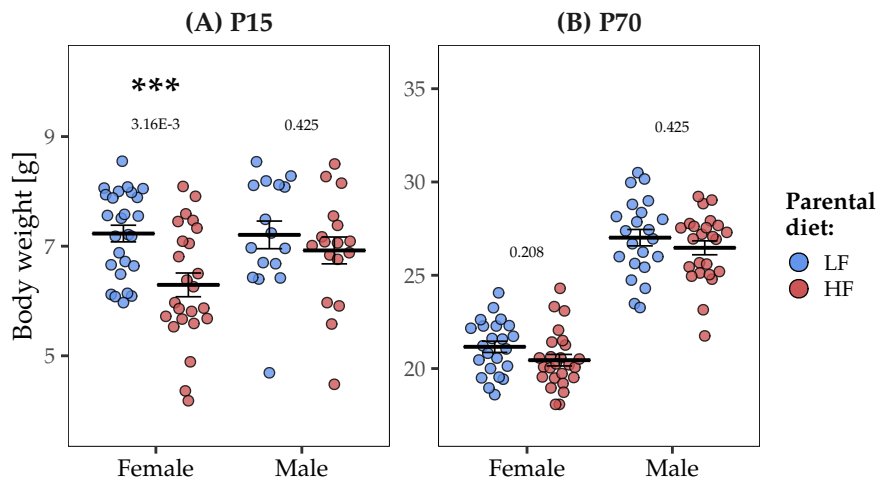


Figure 13: Non-persistent body weight reduction of female offspring by parental obesity. Offspring body weights ($n_{P15} = 16-26$, $n_{P70} = 22-25$) were assessed at postnatal day 15 (A) and postnatal day 70 (B). Only a transient decrease in body weights of HF female offspring was observed at two weeks of age (P15) compared to the female LF control group (A). Two sample t-test with Benjamini-Hochberg p-value correction for multiple testing (4 comparisons): *** $p < 0.001$.

4.4 No effect of parental obesity on placental inflammatory gene expression

Different authors have previously suggested sexual dimorphic alterations in the placentas from HFD dams. Importantly, mRNA expression of several pro-inflammatory cytokines has shown to be increased after maternal HFD feeding, including Il1b, Nlrp3 and Tnf^[324,327,416]. The presence of an altered pro-inflammatory environment in the placenta of E18.5 HF foetuses could in part explain the observed increase in foetal sack resorption. To analyse the effect of parental diet-induced obesity on the expression of inflammatory markers in the placenta 18.5 days after conception, placentas from HF and LF dams were collected and analysed by qPCR. The relative expression of the pro-inflammatory markers Saa3, Nos2, Ptgs2, Ccl2, Il6, Il1a, Il1b, Tnf, Cxcl2, Nlrp3 and Il12b as well as of anti-inflammatory markers Tgfb, Chil3, Retnla and Arg1 was assessed (Figure 14). In order to stratify the data and test for sexual dimorphic effects, sex of the E18.5 embryos was determined by analysis of their internal reproductive organs.

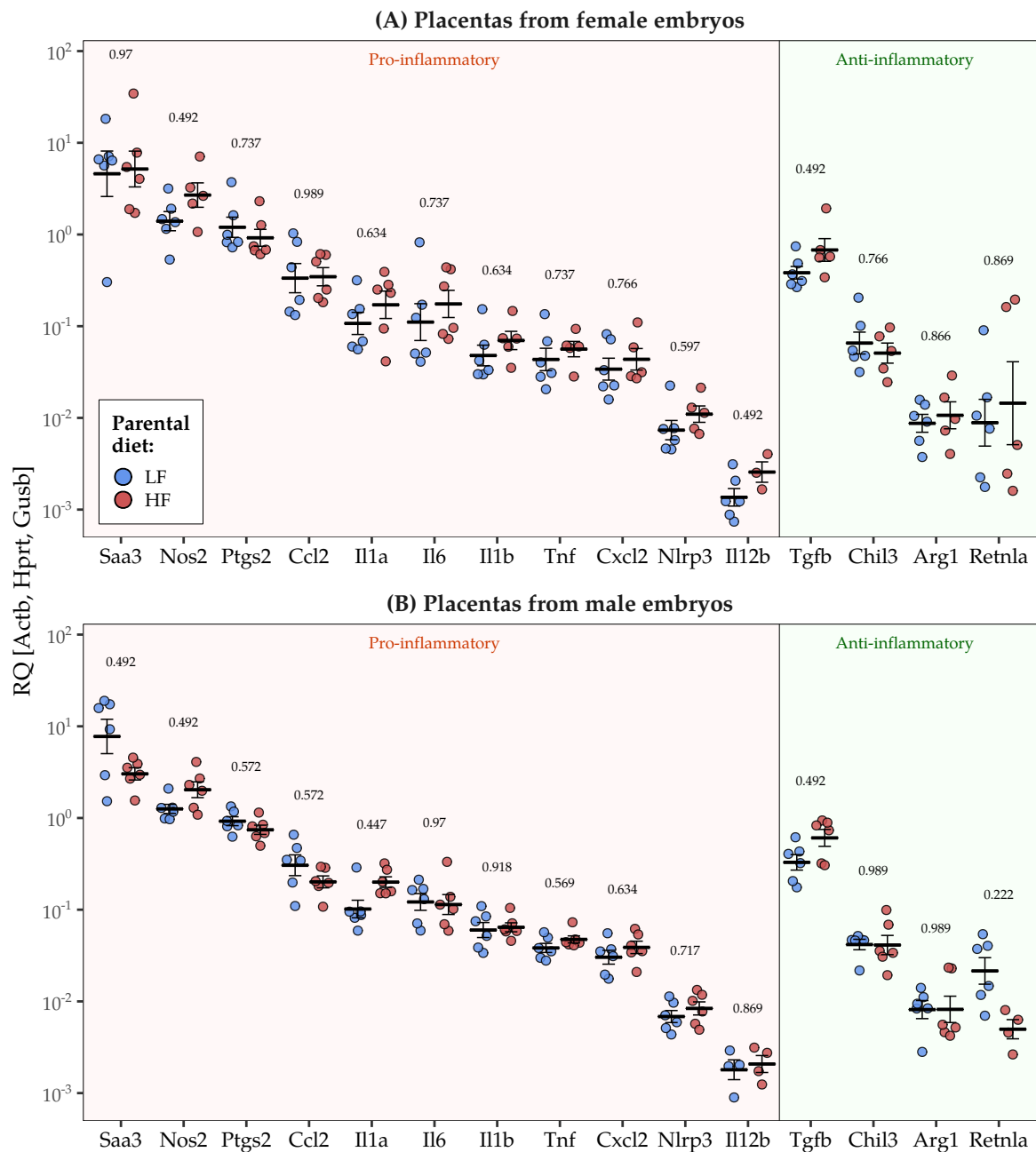


Figure 14: No effect of parental obesity on E18.5 placental gene expression. 18.5 days after positive vaginal plug test, LF and HF dams ($n = 3$) were euthanized and placentas were collected ($n_{\text{Female}} = 9-12$, $n_{\text{Male}} = 11-12$). Foetal sex was determined by the analysis of embryonic internal reproductive organs. Pro- (Ptgs2, Ccl2, Il1a, Il6, Il1b, Cxcl2, Nlrp3, Il12b, Nos2, Saa3, Tnf) and anti-inflammatory (Chil3, Arg1, Retnla, Tgfb) gene expression was quantified by qPCR and normalized (relative quantity, RQ) to three housekeeping genes (Actb, Hprt, Gusb). No differences in gene expression was observed for any of the analysed genes in E18.5 female (**A**) nor in male (**B**) placentas. Welch two sample t-test on log-transformed data with Benjamini-Hochberg p-value correction for multiple testing (30 comparisons).

Placentas from HF animals presented no alterations in the expression levels of any of the analysed inflammatory markers compared to LF control placentas. A sexual dimorphic qualitative trend of increased gene expression of pro-inflammatory markers was observed in placentas from HF female embryos compared to LF control placentas (*Figure 14A*). However, differences between parental diet groups did not lead to rejection of the null hypothesis. No difference in expression nor a trend was detected for the expression of inflammatory markers in placentas from male E18.5 fetuses (*Figure 14B*).

4.5 Parental obesity has no effect on offspring's circulating cytokine levels

Even though there was no evidence pointing to the presence of inflammation in the placenta at an embryonic age, the possibility of its systemic onset after birth due to parental obesity could not be excluded. In order to assess long-term effects at a systemic level, the concentration of 10 cytokines were examined in the plasma of P15 and P70 offspring by multiplex immunoassay (*Figure 15* and *Figure 16*). No difference in circulating offspring's cytokine concentrations between respective parental diet groups were measured, neither at the age of P15 nor at P70. A trend of increased concentrations in the TH2 cytokines IL4, IL5 and IL10 was observed in plasma of P70 HF female offspring. However, this trend was not sufficiently pronounced to reject of the null hypothesis (*Figure 16A*).

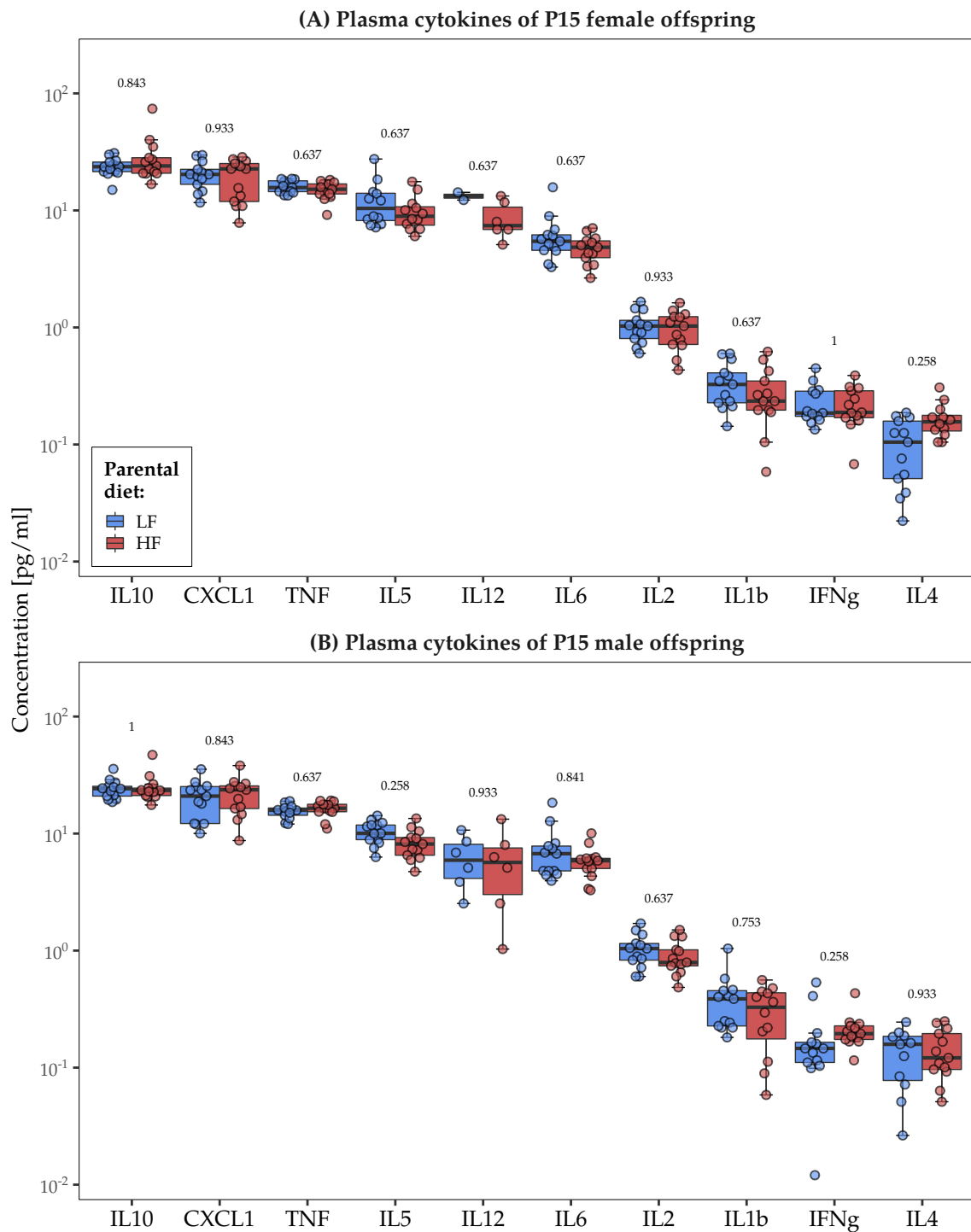


Figure 15: No effect of parental diet-induced obesity on circulating cytokines of P15 offspring. Cytokine concentrations in plasma from two weeks old offspring were measured by 10-plex immunoassay ($n = 13$). Cytokine levels were not affected by parental obesity, neither in female (A) nor in male (B) P15 offspring. Wilcoxon rank sum test with Benjamini-Hochberg p-value correction for multiple testing (20 comparisons).

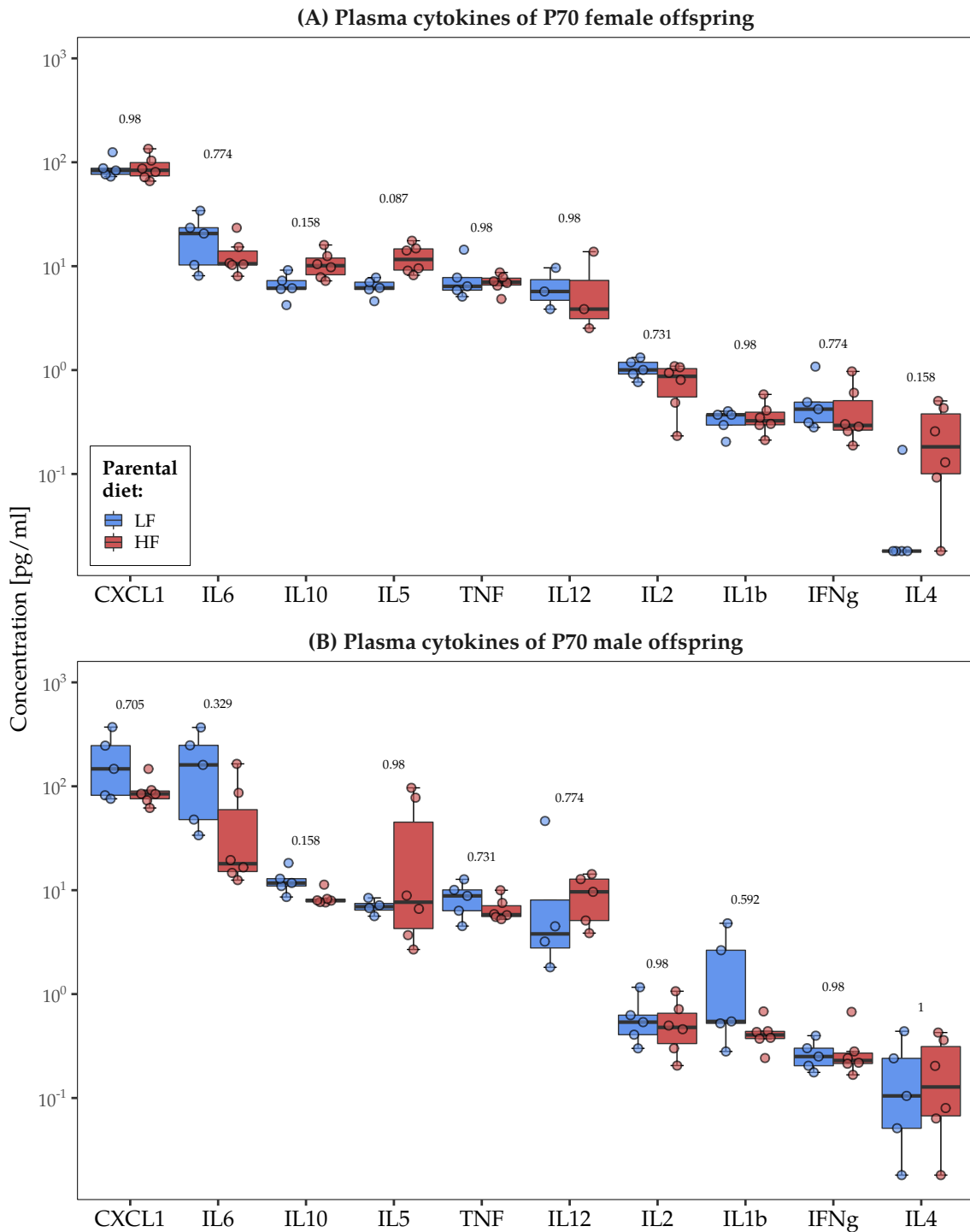


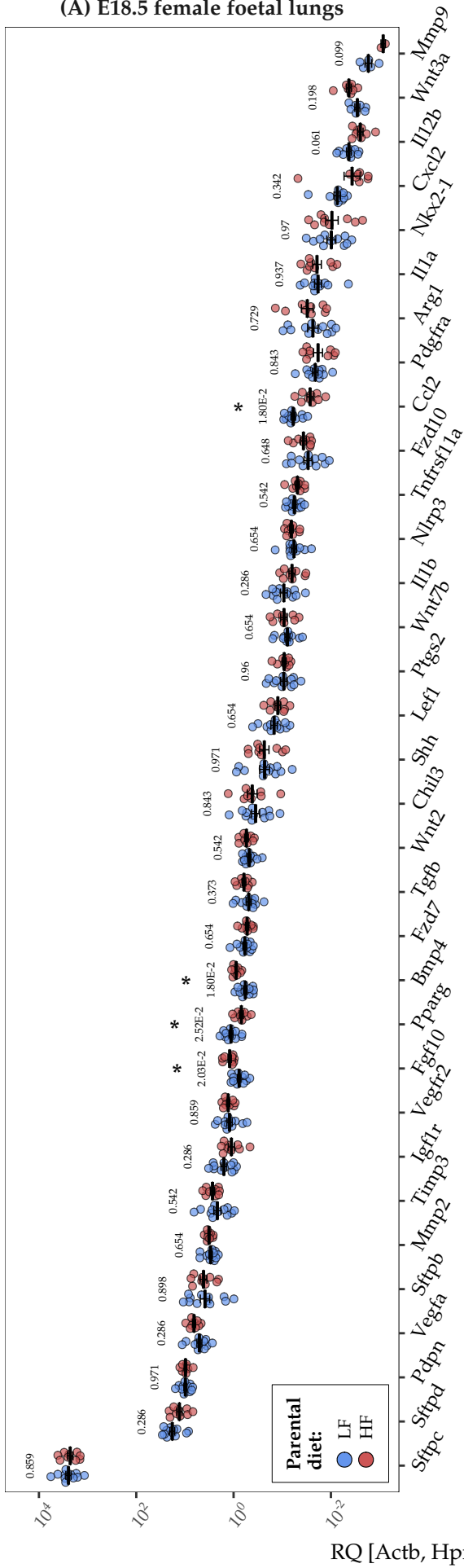
Figure 16: No effect of parental diet-induced obesity on circulating cytokines of P70 offspring. Plasma cytokine concentrations of P70 mice were measured by 10-plex immunoassay ($n_{LF} = 5$, $n_{HF} = 6$). No differences between parental diet groups in plasma cytokine levels of P70 female (A) nor male (B) offspring were detected. A trend of increased concentrations in the TH2 cytokines IL4, IL5 and IL10 was observed in plasma of P70 HF female offspring (A). Wilcoxon rank sum test with Benjamini-Hochberg p-value correction for multiple testing (20 comparisons).

4.6 Parental obesity delays final alveolarization in lungs of female offspring

Additionally to the increases in pro-inflammatory marker expression in placentas of HF dams, Mayor et al.^[327] presented in their publication an impaired foetal lung development which extended until postnatal day 15. Lungs from HF-fed dams presented reduced structural maturation and lower expression of surfactant mRNA. To test whether the gene expression of selected developmental and inflammatory markers in the foetal lung was affected by parental HFD, lungs from E18.5 foetuses were isolated and analysed by qPCR. The developmental stage as well as the morphology of these lungs were additionally investigated by semiquantitative grading and image analysis of FFPE, HE-stained lung specimens, respectively.

Out of 33 markers inspected in E18.5 lungs by qPCR, the gene expression of *Fgf10*, *Pparg*, *Bmp4* and *Ccl2* was influenced by parental diet-induced obesity in a sexual dimorphic fashion (*Figure 17*). Gene expression patterns of these four markers were similar for both sexes, with increased mRNA levels of *Fgf10* and *Bmp4* and lower gene expression of *Pparg* and *Ccl2*. However, while mRNA quantities of these four genes displayed differences between parental diet groups in lungs from female foetuses (*Figure 17A*), this was only the case for *Bmp4* and *Ccl2* in male lungs (*Figure 17B*).

(A) E18.5 female foetal lungs



(B) E18.5 male foetal lungs

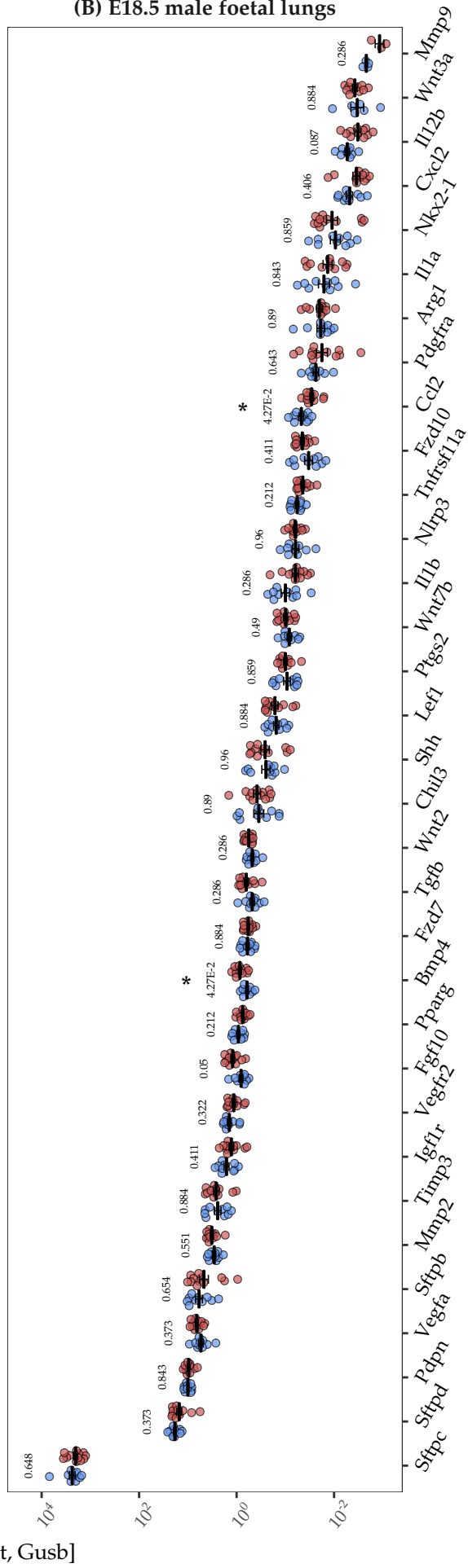


Figure 17: Gene expression of developmental and inflammatory markers is altered by parental obesity in E18.5 foetal mouse lungs. Lungs from E18.5 foetuses were isolated and their right lobes were analysed by qPCR. Gene expression of developmental and inflammatory markers (Bmp4, Fgf10, Fzd1, Fzd10, Fzd7, Igf1r, Lef1, Mmp2, Mmp9, Nkx2-1, Pdgfra, Pdpn, Sftpb, Sftpc, Sftpd, Shh, Timp3, Tnfrsf11a, Vegfa, Vegfr2, Wnt2, Wnt3a, Wnt7b, Ccl2, Ptgs2, Cxcl2, Il12b, Il1a, Il1b, Nlrp3, Arg1, Chil3, Pparg, Tgfb) was quantified relative to three housekeeping genes (Actb, Hprt, Gusb). Lungs (n = 12) from both female (A) and male (B) E18.5 HF groups displayed elevated expression of Bmp4 and decreased levels of Ccl2 compared to LF control groups. Additionally, female embryos presented higher expression of Fgf10 and lower mRNA levels of Pparg compared to its respective LF control group (A). Welch two sample t-test on log-transformed data with Benjamini-Hochberg p-value correction for multiple testing (66 comparisons): $p < 0.05$.

In spite of the observed alterations in gene expression of Fgf10, Pparg, Bmp4 and Ccl2 by parental obesity, no signs of relevant morphological pathological alterations were visible during semiquantitative grading of lung maturity in E18.5 foetuses (Table 13). Lungs of all E18.5 groups were categorized as being in the terminal saccular phase of lung development. Additionally, image analysis of the lung slides (Appendix, Table 15) corroborated negative findings from semiquantitative grading, displaying no effect of parental diet on foetal lung morphology.

Table 13: Semiquantitative grading of foetal lung maturity. Tissue sections (n = 9) from left lobes of FFPE E18.5 foetal lungs were HE-stained and semiquantitatively graded. Grading stages were defined based on the work of Warburton *et al.* 2010 and Mayor *et al.* 2015. Grade 0: pseudoglandular stage of lung development; Grade 1: canalicular stage; Grade 2: canalicular/terminal saccular stage; Grade 3: terminal saccular stage; Grade 4: terminal saccular/alveolar stage.

Group	Male-LF	Male-HF	Female-LF	Female-HF
Grade (mean \pm SD)	3 \pm 0	3 \pm 0	3 \pm 0	3 \pm 0

To test for effects of parental obesity on lung alveolarization, left lung lobes from P15 and P70 offspring lungs were also fixed, HE stained and examined by histology and automatic image analysis. For histological investigation, blind analysis by design-based quantitative morphometric stereology was performed (Figure 18). Mean linear intercept (Lm) measurements of P15 HF female offspring were increased compared to the LF control group (Figure 18A). Similar to the effect on body weights of these female offspring, alveolar lung structure differences between parental diet groups were detectable only at two weeks of age. Lm measurements of P70 HF female were similar to their corresponding LF controls (Figure 18B). No evident differences in Lm were observable for HF male offspring at any of the two ages analysed.

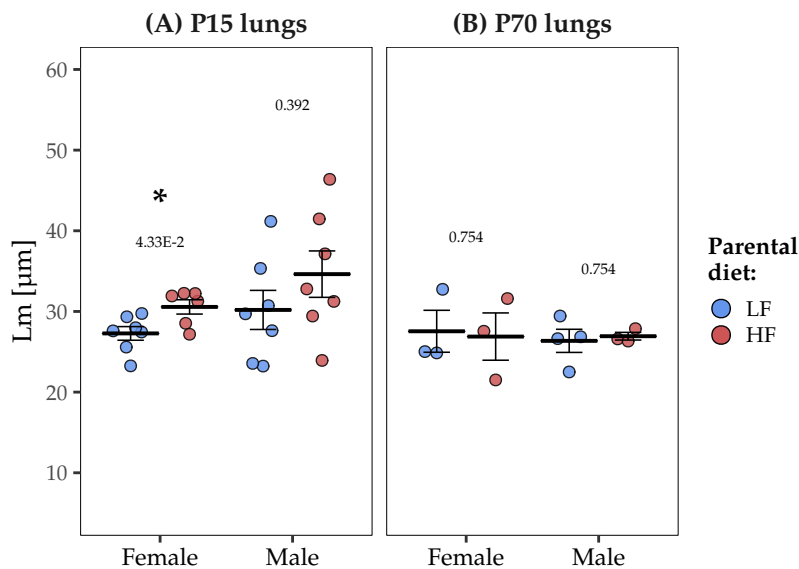


Figure 18: Transient sexual dimorphic impairment of lung alveolar structure by parental obesity at P15. Left lungs ($n_{P15} = 6-7$, $n_{P70} = 3-4$) from P15 and P70 offspring were isolated, filled with formaldehyde solution with a constant pressure of 25 cm 4% PFA for 10 min and fixed overnight. 6 μm thick FFPE tissue slices were HE stained, and blindly analysed by design-based quantitative morphometric stereology. (A) Mean linear intercepts (Lm) of HF female P15 offspring were remarkably increased compared to its corresponding LF control group. (B) Comparable Lm measurements between parental diet groups at 10 weeks of age. One-sided two sample t-test with Holm p-value correction for multiple testing (4 comparisons): * $p < 0.05$.

In order to verify manual Lm measurements, automatic image analysis of the lung slides was performed (*Appendix, Table 15*). This assay included the quantification of the alveolar, septal and lung areas as well as the total number of alveoli, the total length of the border between septum and the air space (border septum-air). After multiple test correction, no differences in the automatic image analysis measurements were detected. Therefore, automatic analyses could not corroborate the results from manual Lm quantification.

4.7 Parental obesity transiently alters the gene expression and leukocyte population composition in the offspring's lung

Having observed the morphological changes in the lungs of HF pups, in order to determine further impact of parental obesity on the offspring's lung after birth, right lungs lobes from P15 offspring were isolated and inspected by qPCR. Gene expression levels of eleven markers of lung development and/or inflammation in the P15 offspring lung were evaluated by qPCR (Arg1, Ccl2, Cxcl2, Fgf10, Il12b, Il1b, Pparg, Retnla, Tnf, Tnfrsf11a and Wnt3a). Parental diet induced sexual dimorphic changes in the gene expression of Ccl2, Il1b, Pparg, Tnfrsf11a, and Wnt3a (*Figure 19*). The expression of

Pparg, Ccl2 and Il1b was reduced in the lung of P15 HF male offspring, compared to the respective LF control group (Figure 19B). On the other hand, the gene expression of Tnfrsf11a and Wnt3a was increased by parental HFD in the P15 offspring lung from both sexes.

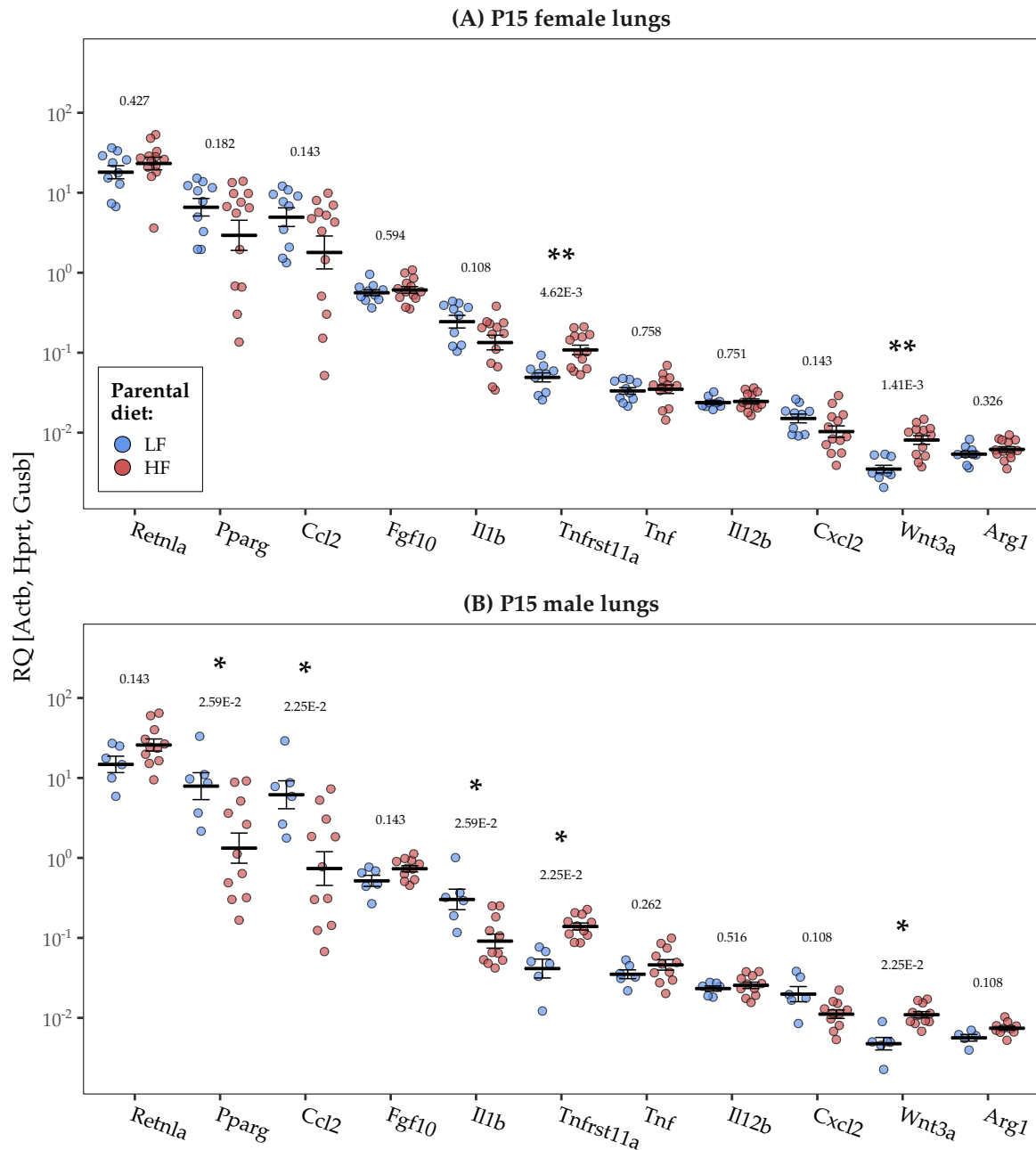


Figure 19: Parental HFD alters gene expression of developmental and inflammatory markers in the P15 mouse lung. Lobes from right lungs from P15 mice were isolated ($n_{\text{Female}} = 10-13$, $n_{\text{Male}} = 6-11$) and the gene expression of developmental and inflammatory markers was analysed by qPCR. Gene expression levels were normalized relative to three housekeeping genes (Actb, Hprt, Gusb). Gene expression of developmental markers Tnfrsf11a and Wnt3a in lungs from HF diet groups of both sexes was increased compared to LF control group. (B) Additionally, male offspring presented prominent decreases in gene expression of pro-inflammatory cytokines Ccl2 and Il1b as well as of the anti-inflammatory-acting, developmental marker Pparg compared to LF control group. Welch two sample t-test with Benjamini-Hochberg p-value correction for multiple testing (22 comparisons): $p < 0.05$, $p < 0.01$.

4.7.1 Parental obesity alters leukocyte population frequencies in the P15 offspring's lung

Murine alveolar macrophages finish their maturation after birth^[81]. To control for the presence of mature AMs and test for the influence of parental diet-induced obesity on the development of leukocyte populations in the lung, whole lungs from 2-week old offspring were analysed by flow cytometry. A 10-colour panel was employed for staining whole lung cell suspensions from P15 mice. After quality control and pre-processing, three unsupervised learning algorithms were applied to single cell fluorescence data. Pre-processing steps of flow cytometry data included biexponential transformation, removal of doublets, debris and dead cells as well as gating for leukocytes (PTPRC⁺). A self-organizing map was used for dimensionality reduction and unsupervised generation of 100 initial clusters. Consensus clustering, together with manual merging of clusters were then employed to further aggregate initial clusters. t-distributed stochastic neighbour embedding (tSNE) was utilized to graphically control for correct subclustering. Eleven leukocyte populations (*Figure 20A*) with unique marker expression patterns (*Figure 20B*) were identified in the P15 lungs.

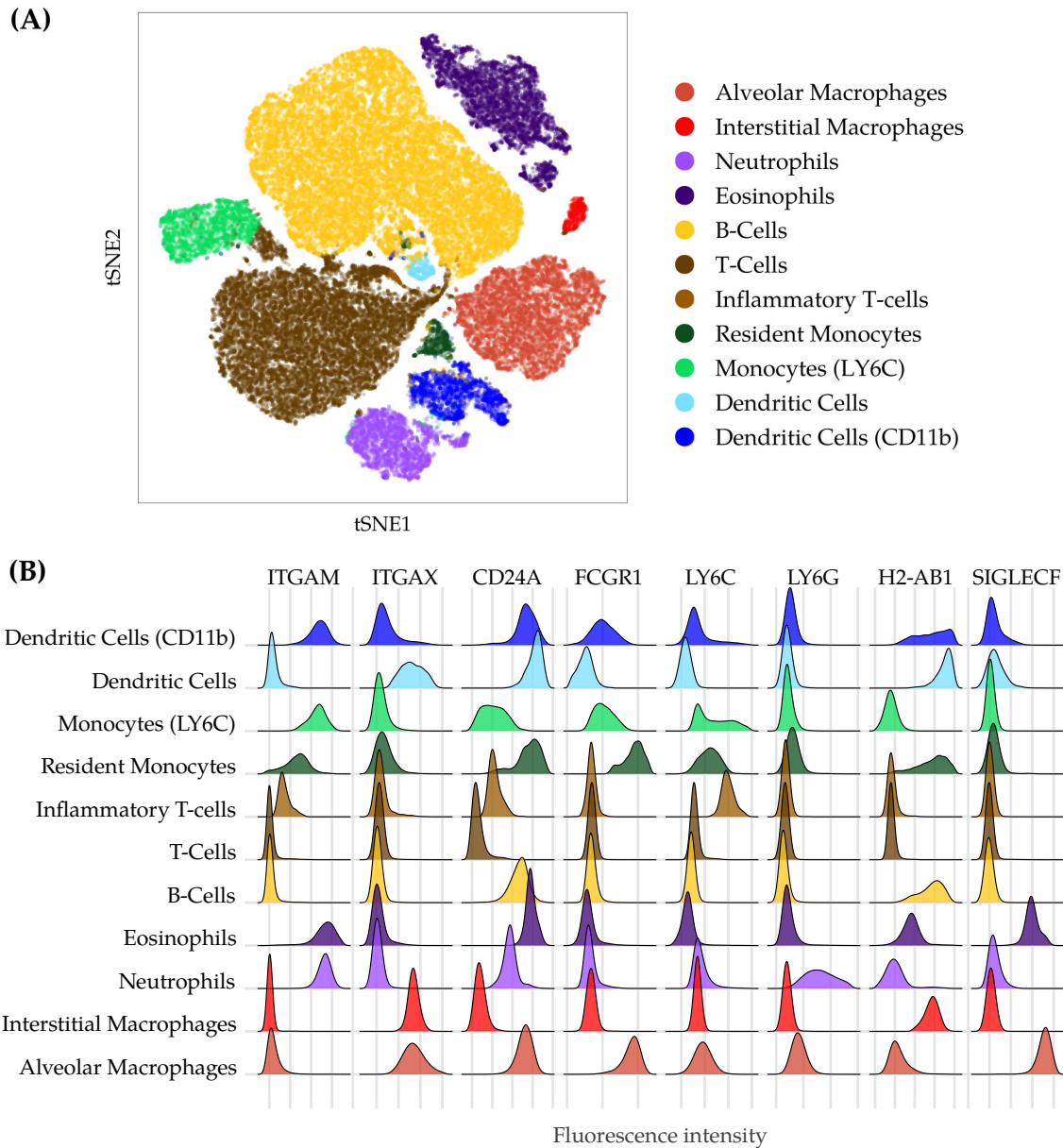


Figure 20: Flow cytometric immunophenotyping of the P15 mouse lung revealed eleven leukocyte populations. Whole lungs from 28 P15 offspring mice ($n_{LF} = 5-6$, $n_{HF} = 7-10$) were perfused, isolated and dissociated. Lung cell suspensions were analysed with a 10-colour flow cytometry panel (ITGAM, ITGAX, CD24A, PTPRC, H2-AB1, LY6C, LY6G, FCGR1, SIGLECF and Viability). Quality-controlled single-cell data was analysed with unsupervised machine learning. **(A)** Two-dimensional tSNE projection of lung cells displays a good separation of the eleven cell clusters. **(B)** Self-organizing map and consensus clustering algorithms for semi-automated cell clustering were applied on the collected single-cell fluorescence data for the identification of eleven cell clusters with unique marker expression patterns. One-dimensional density plots (flow cytometry histograms) present the relative expression of ITGAM, ITGAX, CD24A, PTPRC, H2-AB1, LY6C, LY6G, FCGR1 and SIGLECF on each of the leukocyte populations identified in the P15 mouse lung.

Out of the eleven leukocyte populations, six of them presented frequencies greater than 5% of the total leukocyte cell numbers. Five minor populations with frequencies smaller than 5% of the total leukocyte cell numbers were also detected (*Figure 21B*). Alveolar macrophages were detected in the P15 lungs of both female and male P15

offspring. This TM population presented the expected expression patterns of cell surface molecules (*Figure 20B*) typical for AMs of adult mice (ITGAX⁺, FCGR1⁺, SIGLECF⁺, *Figure 25B*). The comparison of these markers between parental diet groups displayed no differences in mean fluorescence intensity (data not shown). Compared to the total number of leukocytes detected in whole lungs, AMs exhibited relative cell frequencies of 10 - 12 %. The contrast in cell frequencies of AMs measured between parental diet groups did contribute to the overall differences between observed in the omnibus chi-squared test, but these were not as marked (around 1 %) as for other of the populations detected (*Figure 21B*)).

Inference on differences between parental diet groups was performed with a chi-squared test on relative population counts. Considerable differences in cell frequencies were observed between parental HF and LF groups of both female and male offspring (*Figure 21A*). T-cells displayed the highest contribution (standardized Pearson's residuals) to the magnitude of the computed chi-squared values ($\chi^2_{\text{female}} = 4768.4$, p-value < 2.2e-16 ***, $\chi^2_{\text{male}} = 7373.8$, p-value < 2.2e-16 ***), followed by eosinophils and LY6C⁺ monocytes (*Figure 21A*). Interestingly, the B-cell leukocyte population was the most prominent in the lungs of P15 offspring in term of cell frequencies (*Figure 21B*)) comprising up to 40.2 % of the total leukocyte cell numbers.

Sexual dimorphism was observed during the comparison of the relative cell numbers of the eleven leukocyte populations. While differences in T-cells and eosinophils contributed to the overall discrepancy in cell numbers between parental diet groups of both sexes, LY6C⁺ monocytes played a more important role for these differences in males, while this was the case for neutrophils in female offspring (*Figure 21A*). Furthermore, B-cells, interstitial macrophages as well as resident monocytes played a bigger role in these differences rather for male than female offspring.

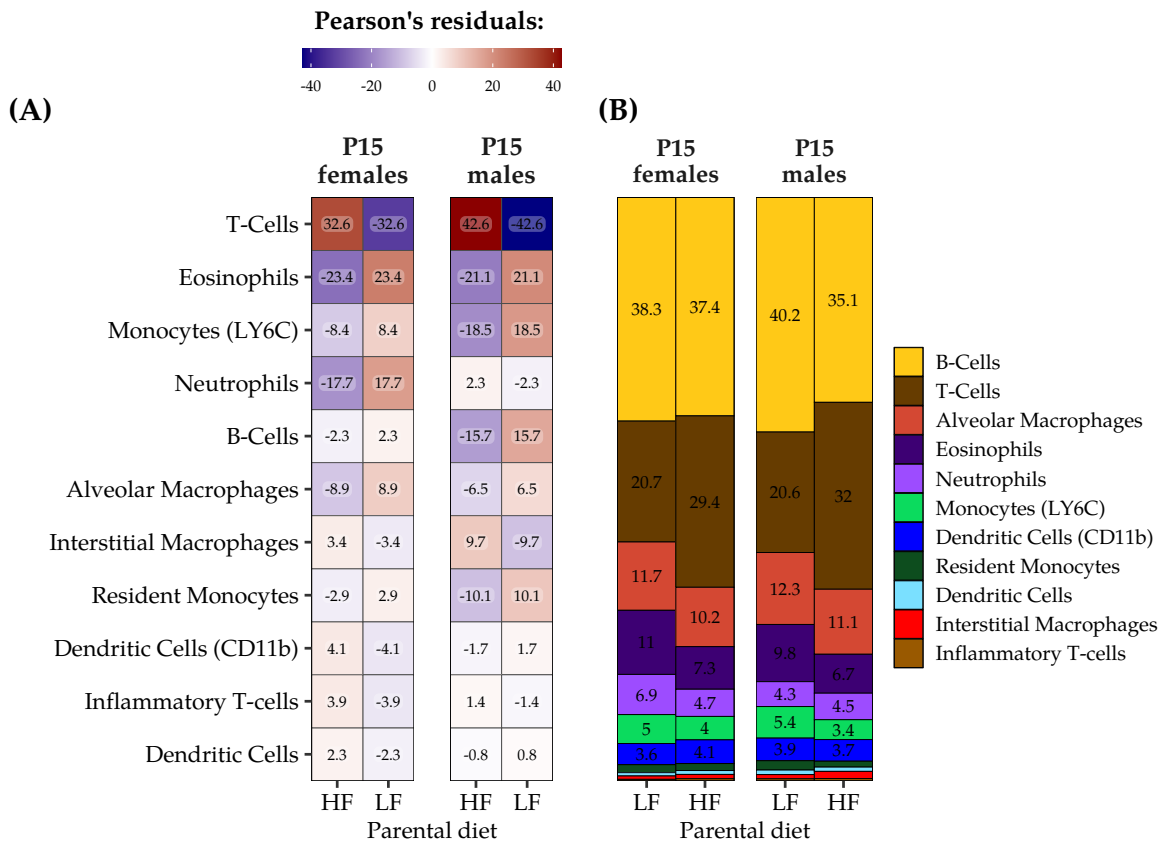


Figure 21: Analysis of single standardized Pearson's residuals from chi-squared tests discloses contribution of individual cell clusters to the observed differences between P15 diet groups. Cell cluster proportions were compared between parental diet groups for female (A) and male (B) offspring mice with the Pearson's chi-squared test of homogeneity. Frequency counts showed not to be identically distributed across different populations ($\chi^2_{\text{female}} = 4768.4$, p-value $< 2.2e-16$, $\chi^2_{\text{male}} = 7373.8$, p-value $< 2.2e-16$). To further investigate the statistically significant omnibus chi-squared test results, the contribution of each cell cluster to the magnitude of the computed chi-squared values was weighed with their standardized Pearson's residuals. Immune cell cluster two exhibited the greatest standardized Pearson's residual for both male and female groups. It also showed to be the second largest cell cluster for all groups.

Overall, the impact of parental obesity on the relative composition of leukocyte populations in the lungs from P15 offspring was more pronounced in male than female animals (Figure 21A and Figure 22). In order to visualize the distance (dissimilarity) between individual mice based on leukocyte population structure, multidimensional scaling (MDS) was performed on population frequencies and plotted on a 2-dimensional space (Figure 22). 2-D mapping of MDS dimensions showed high similarity between individual P15 offspring belonging to the same parental diet group and evident distance (high dissimilarity) between offspring of different parental diet groups. Such dissimilarity between HF and LF offspring was more obvious for male (Figure 22B) than for female offspring.

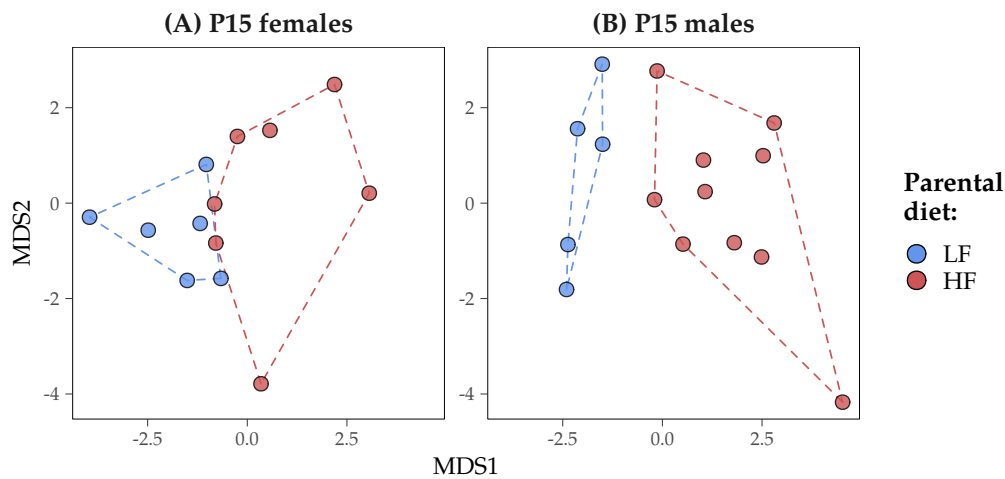


Figure 22: Multidimensional scaling based on leukocyte frequencies exhibit distance between LF and HF P15 offspring in a sexual dimorphic fashion. Kruskal’s non-metric multidimensional scaling (ordinal MDS) of standardized Euclidean distances was computed from the proportion matrix of the eleven identified immune cell populations in the P15 offspring lung. Similarity between individual mice was mapped on a two-dimensional space. To further stress the distance between offspring belonging to different parental diet groups, convex hulls were plotted around the individual samples. HF offspring presented high similarity to each other and high dissimilarity to LF offspring. This pattern was more pronounced for male (B) than female (A) offspring. As presented in *Figure 21*, frequencies in T-cells displayed the highest contribution to the observed differences between parental diet groups.

4.8 No effect of parental obesity on endotoxin-induced acute lung inflammation

As stated in *Section 1.4.2*, AMs have critical roles in the initiation and resolution of lung inflammation. Hence, pro-inflammatory priming effects on offspring’s AMs by parental obesity were expected to influence the inflammatory dynamics during an *in vivo* endotoxin-induced acute lung inflammatory challenge. To test for such changes that could hint at long-term priming effects of AMs, young-adult male LF and HF offspring were exposed at ten weeks of age (P70) to a “mild” intratracheal LPS-induced acute lung inflammatory challenge.

In order to find an adequate dose of LPS, an initial dose response analysis in chow-fed C57BL/6J mice was performed. This examination revealed a dose-dependent neutrophil recruitment to the airspace. Higher LPS concentrations were associated with increased neutrophil counts (*Figure 23A*). Furthermore, macrophage counts on cytocentrifuged preparations from BAL decreased with increasing concentrations of LPS (*Figure 23B*). A dose of 0.1 μg LPS per mouse (equivalent to a dose of 4.3 $\mu\text{g}/\text{kg}$ at an average body weight of 23.1 g) induced a considerable level of acute lung inflammation, characterized by an increase in the absolute numbers of neutrophils in BAL without macrophage depletion within 24 h after intratracheal instillation.

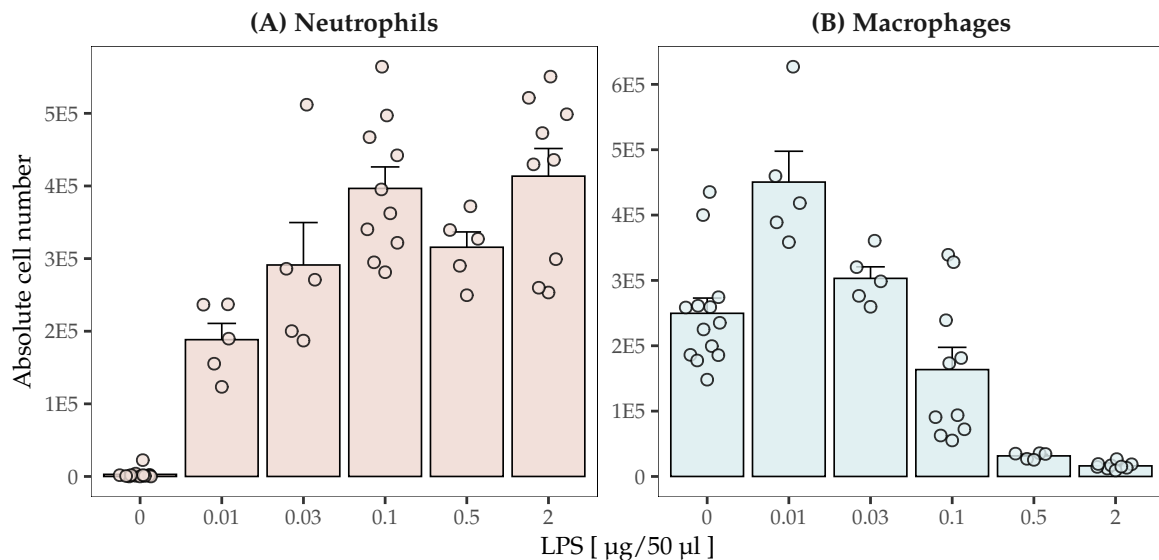


Figure 23: LPS dose response analysis on C57BL/6J mice. Chow-fed C57BL/6J mice were intratracheally instilled with five different doses of LPS (n = 5-13). Single instillations with LPS concentrations ranging from 0.01 to 2 µg were performed and total neutrophils (A) and macrophages (B) in bronchoalveolar lavages were counted on cytocentrifuged preparations 24 h after instillation. A dose of 0.1 µg LPS per mouse (equivalent to a dose of 4.3 µg/kg at an average body weight of 23.1 g) induced a strong influx of neutrophils without macrophage depletion within 24 h after intratracheal instillation. Doses higher than 0.1 µg lead to a severe loss in macrophage counts in BAL.

To test for the effect of parental diet-induced obesity on lung inflammatory dynamics, 10-week old male offspring were intratracheally challenged with the selected dose of 0.1 µg LPS per animal. Directly before (0 h) and during the inflammatory challenge (6, 24, 48 and 72 h post instillation), the presence of inflammatory factors secreted into the lung air space was analysed by ELISA. The concentration of seven pro-inflammatory cytokines (colony stimulating factor 2 (CSF2), CXCL1, CXCL2, CXCL5, IL1b, IL1a and TNF) and the acute-phase protein serum amyloid A3 (SAA3) were quantified in BALF (Figure 24). Most pro-inflammatory mediators analysed in the BAL fluid (CXCL1, CXCL2, CSF2, IL1a, TNF) reached a maximum in concentration 6 h after instillation and returned to baseline levels at 72 h. Especially TNF displayed a strong peak at 6 h after LPS instillation. Two of the mediators analysed – CXCL5 and SAA3 – reached their highest concentration not at 6 h, but at 24 h after instillation.

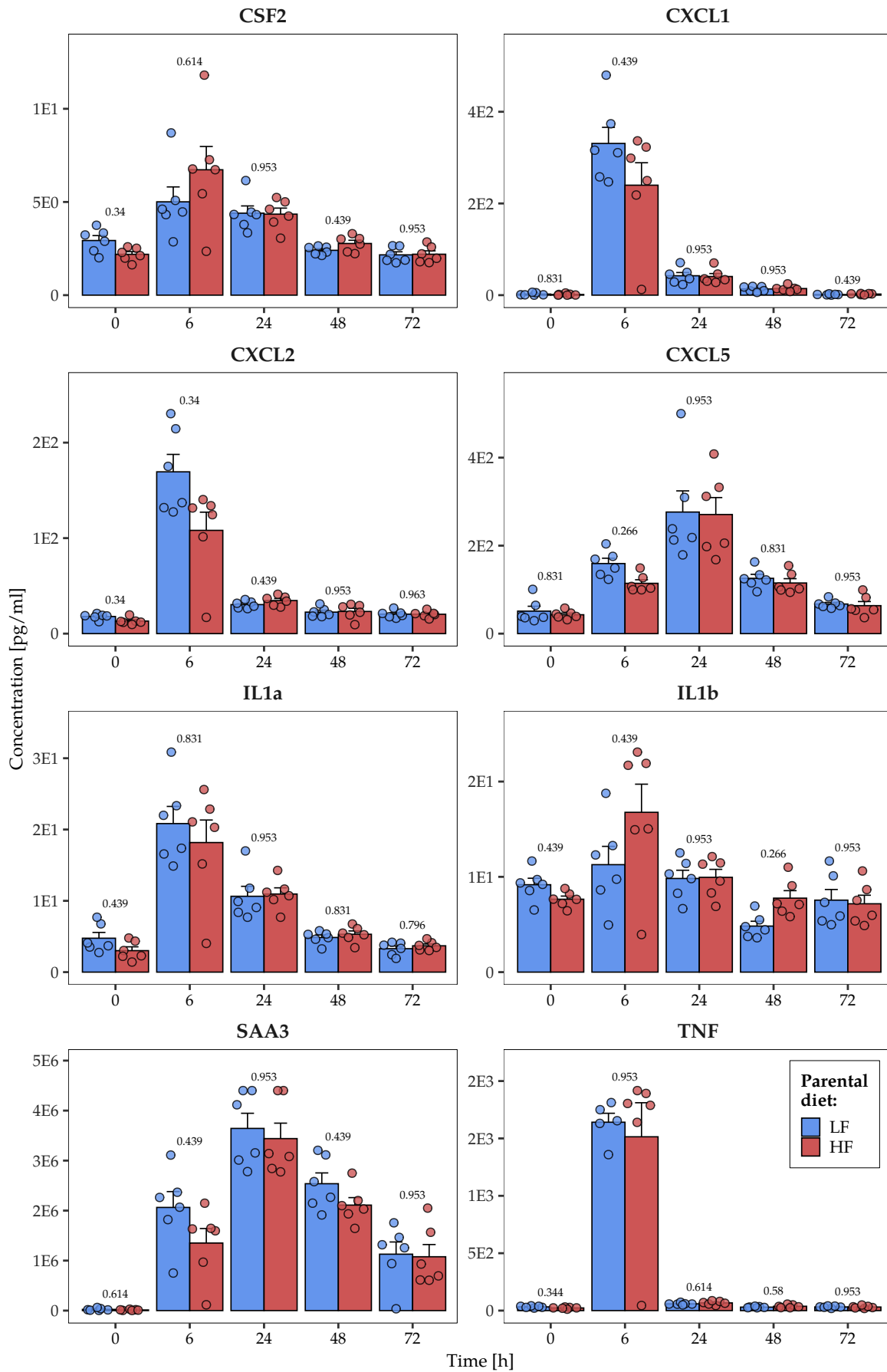


Figure 24: Parental high-fat diet has no effect on chemokine release in bronchoalveolar lavage of P70 male offspring after LPS instillation. 10-week old male offspring were intratracheally challenged with 0.1 μ g LPS (n = 6). Inflammatory dynamics were monitored for 6, 24, 48 and 72 hours after instillation. Concentrations of the inflammatory factors CXCL1, CXCL2, CXCL5, GM-CSF, IL1a, IL1b, SAA3 and TNF in bronchoalveolar lavages were analysed by sandwich ELISA. With the exception of CXCL5 and SAA3, pro-inflammatory mediators in the BAL fluid reached a maximum in concentration 6 h after instillation and returned to baseline levels at 72 h. CXCL5 and SAA3 reached their highest concentration at 24 h after instillation. No differences in the concentration of the examined factors in the air space were observed between parental-diet groups at any time point. Welch Two Sample t-test with Benjamini-Hochberg p-value correction for multiple testing (40 comparisons)

A trend of decreased concentrations of CSF2, CXCL2, IL1a, IL1b and TNF in the parental HF diet group was noticed before the the start of the acute lung inflammation (0 h). However, no differences in the secretion of pro-inflammatory cytokines were observed between parental diet groups at any of the analysed time points. Contrary to results from previous publications showing that LPS induced acute lung inflammation does not cause increases of IL1b in the air space^[417], the comparison between time points 0 and 6 did display higher concentrations of the bioactive form of IL1b (p = 0.013) after LPS instillation. If split by parental diet, a trend in higher IL1b quantities was observed for the HF group at 6 h compared to 0 h. However, after such split, differences between both time points did not reach statistical significance.

In order to test for a complete return of the concentrations of inflammatory factors secreted into the lung air space at the end of the challenge, their levels were compared between untreated mice (0 h) and animals 72 h after LPS instillation. The concentrations of all factors, except SAA3 (p = 0.039 for both parental diet groups) and CXCL2, returned to steady state levels. Interestingly, differences in CXCL2 levels between both time points were only observed for the HF group (p = 0.039).

Because of the similar release of pro-inflammatory factors into the airspace after LPS instillation, LF and HF offspring were expected to present a similar recruitment of immune cells into the lumen of the lung during the LPS challenge. Leukocyte dynamics in the airspace were followed by flow cytometric analysis of BAL cells. An eight-colour antibody panel was employed to analyse cell surface markers on BAL leukocytes (PTPRC⁺) and track the presence of 14 immune cell populations at 0, 6, 24, 48 and 72 h after LPS instillation (*Figure 26* and *Figure 27*). BAL cells were isolated and directly stained with fluorochrome-conjugated antibodies targeting the surface markers protein tyrosine phosphatase, receptor type, C (PTPRC), integrin alpha M (ITGAM), integrin alpha X (ITGAX), Fc receptor IgG high affinity I (FCGR1), lymphocyte antigen 6 complex, locus G (LY6G), lymphocyte antigen 6 complex, locus C1 (LY6C), histocompatibility 2, class II antigen A, beta 1 (H2-AB1) and sialic acid binding Ig-like lectin F (SIGLECF). Flow cytometric immunophenotyping was performed with the help of unsupervised clustering algorithms (*Figure 25A*) and names of immune cell clusters were assigned based on expression patterns of surface markers (*Figure 25B*).

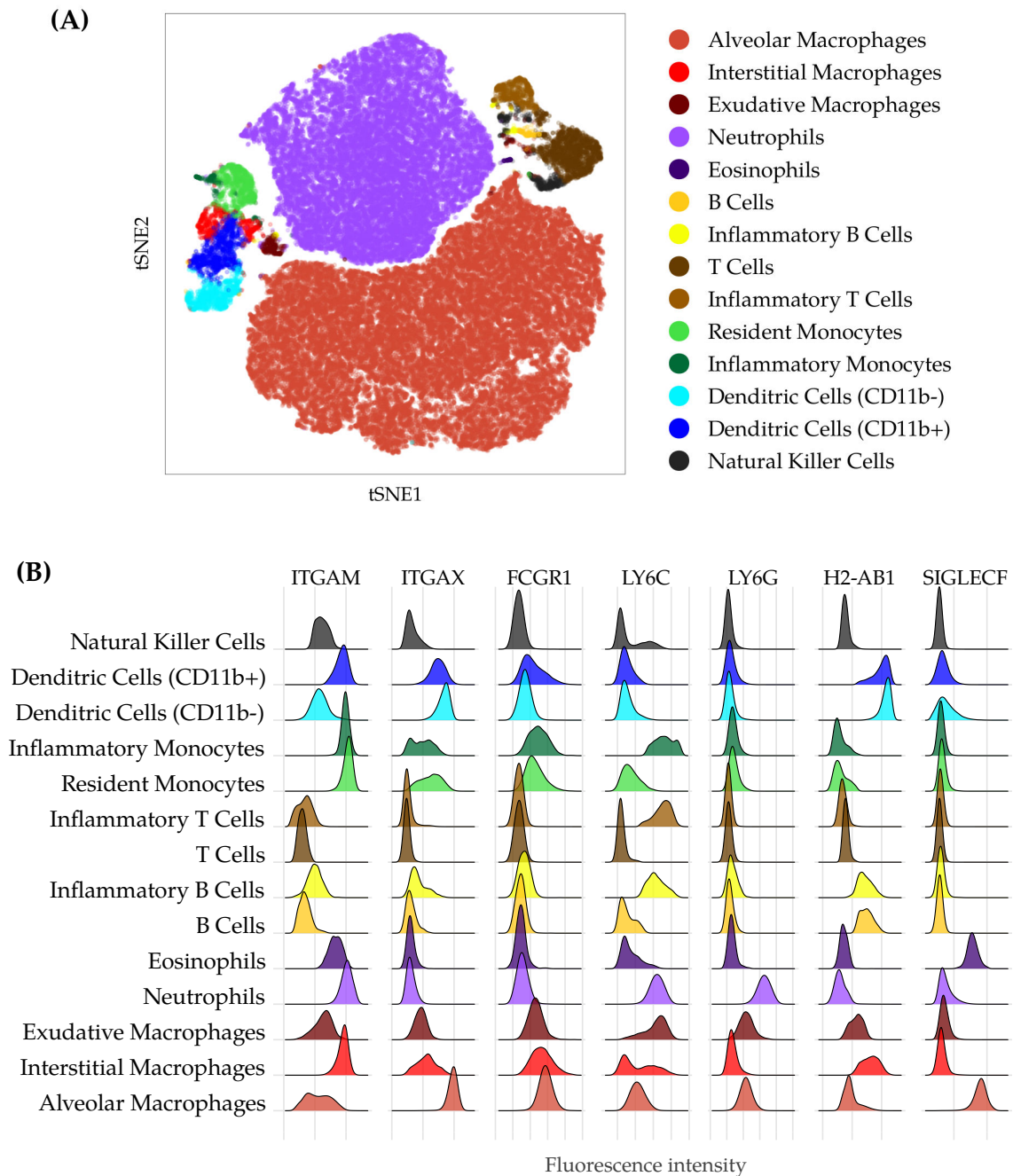


Figure 25: t-SNE projection of cell populations identified by flow cytometric immunophenotyping in BAL after endotoxin challenge. (A) 14 cell populations were identified in the lavage of male animals. Flow cytometric immunophenotyping was performed with the help of the three unsupervised clustering algorithms as described in *Section 3.2.5*: self-organizing map and consensus clustering aided in the definition of leukocyte cell clusters, while t-distributed stochastic neighbour embedding (t-SNE) helped for the dimensionality reduction and improved visualization of FACS data on a two-dimensional projection. (B) Names of immune cell clusters were assigned based on expression patterns of the surface markers ITGAM, ITGAX, FCGR1, H2-AB1, SIGLECF, LY6C and LY6G.

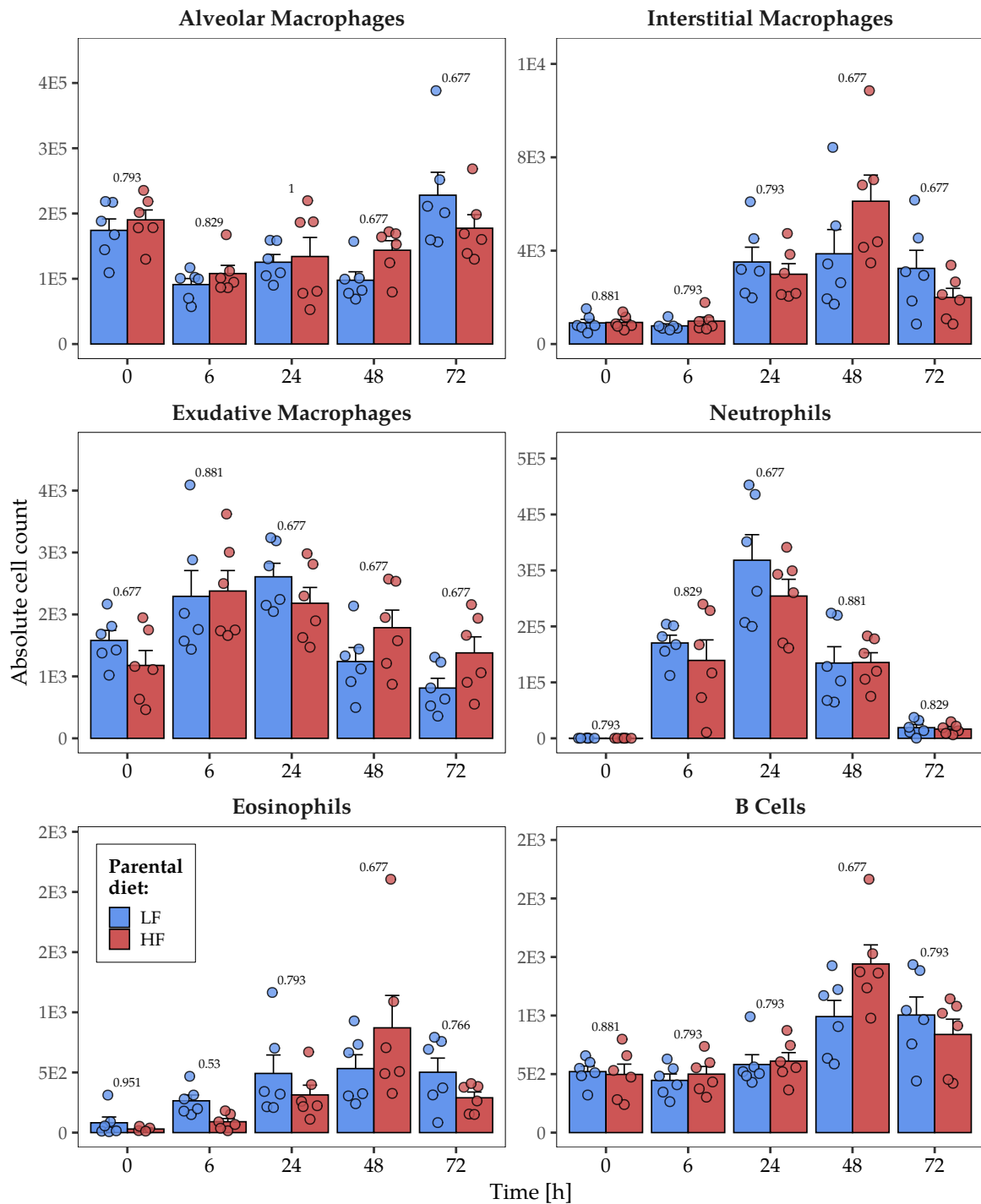


Figure 26: Parental obesity does not alter immune cell dynamics during an endotoxin-induced acute inflammation in the P70 male offspring lung. Flow cytometric immunophenotyping of lavage cells from 10-week old male offspring challenged with $0.1 \mu\text{g}$ endotoxin was performed at 6, 24, 48 and 72 hours after instillation. 14 leukocyte populations in the lavage were identified with the help of unsupervised clustering algorithms (self-organizing maps, consensus clustering and t-distributed stochastic neighbour embedding) by their expression of the antigens ITGAM, ITGAX, FCGR1, H2-AB1, SIGLECF, LY6C and LY6G. Absolute cell numbers were calculated with absolute counting beads. An alternative qualitative representation of the inflammatory dynamics is presented in *Appendix, Figure 30*. Wilcoxon rank sum test with Benjamini-Hochberg p-value correction for multiple testing (70 comparisons).

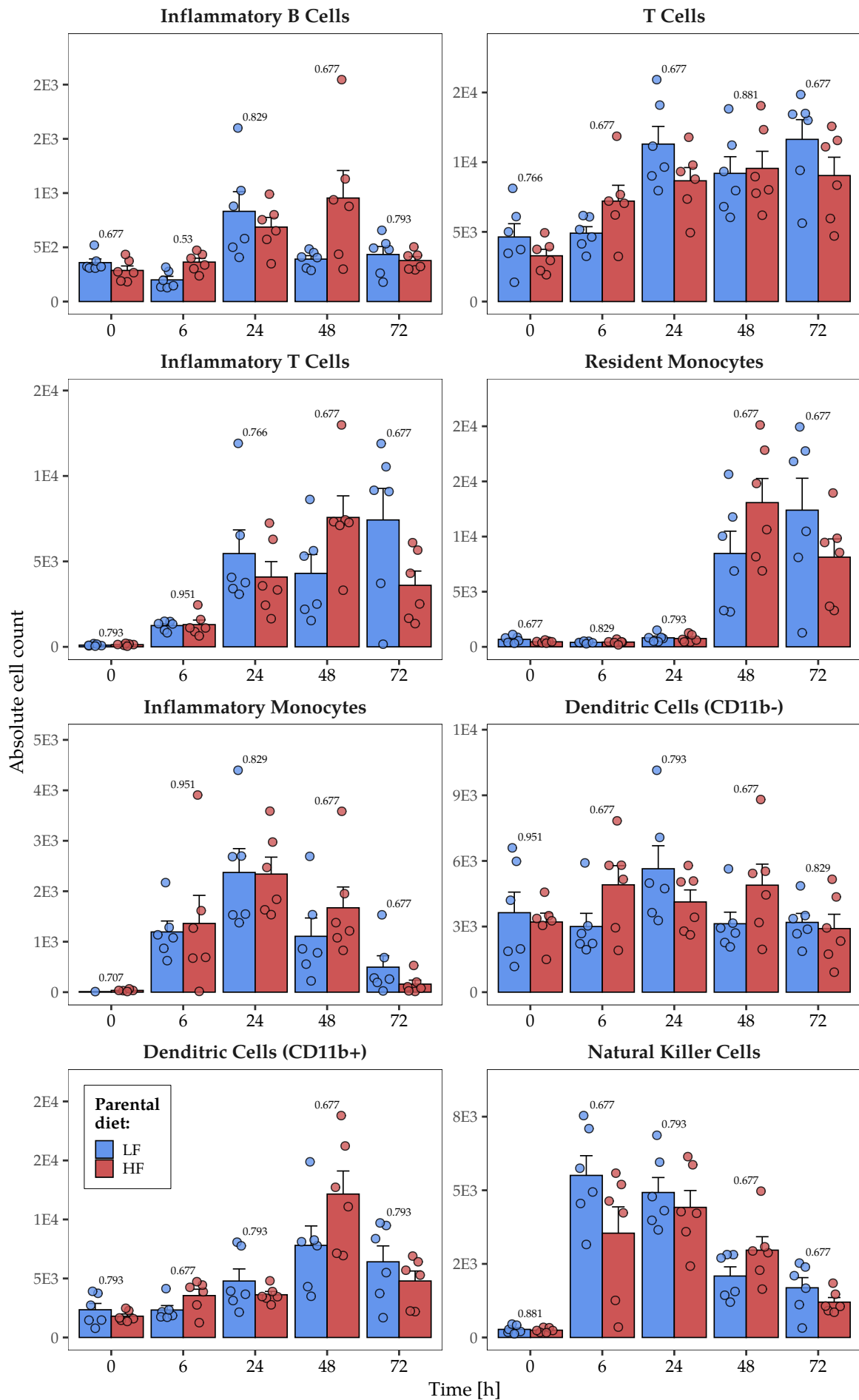


Figure 27: Parental obesity does not alter immune cell dynamics during an endotoxin-induced acute inflammation in the P70 male offspring lung. (continued)

As expected, absolute counts of neutrophils (ITGAM⁺, LY6C⁺, LY6G⁺) peaked at 24 h after LPS instillation. The AM population (ITGAX⁺, FCGR1⁺, SIGLECF⁺) was only slightly reduced by LPS during the first 48h of inflammation, followed by a full recovery of absolute cell numbers 72 h after instillation. Inflammatory monocytes (ITGAM⁺, FCGR1⁺, LY6C⁺), exudative macrophages (FCGR1⁺, LY6C⁺, H2-AB1⁺) and natural killer cells (ITGAM⁺, LY6C⁺) were recruited to the airspace in a similar fashion to neutrophils, peaking at 24 h after instillation. Cell dynamics of eosinophils (ITGAM⁺, SIGLECF⁺), interstitial macrophages (ITGAM⁺, FCGR1⁺, ITGAX⁺, H2-AB1⁺), B cells (H2-AB1⁺), inflammatory T cells (LY6C⁺), dendritic cells (ITGAM⁺, ITGAX⁺, H2-AB1⁺) were similar to each other, with the highest absolute cell counts 48 h after LPS instillation. While most of the aforementioned cell types were present in only small numbers in the lung lavages/air space, only AMs and neutrophils reached absolute cell counts above 1E5. Flow cytometric analysis of BAL revealed no effect of parental HFD on dynamics of mayor cells populations after pulmonary challenge with LPS in male offspring. However, challenged HF offspring mice presented 3.04-fold (median) lower absolute numbers of eosinophils (ITGAM⁺, SIGLECF⁺) and 2.15-fold (median) increased numbers of inflammatory B cells (LY6C⁺, H2-AB1⁺) 6 h after LPS instillation compared to the LF control group. No differences in absolute cell counts of any of the 14 populations were observed at steady state (0 h) between HF and LF offspring.

4.9 No evidence of long-term pro-inflammatory alveolar macrophage priming by parental obesity

Even though no differences in cytokine release nor in cell dynamics in the air space during endotoxin-induced acute lung inflammation was detected, the hypothesized pro-inflammatory AM priming through parental diet-induced obesity could still be present. Therefore, AMs from P70 female and male offspring were analysed by qPCR in order to study their polarization characteristics at steady state (M0) and their pro-inflammatory polarizability (M1). Bronchoalveolar lavage cells from (LPS-)untreated HF and LF offspring were isolated, pooled (two mice per pool) and plated in MH-S medium for purification by adherence. AMs were either M1 polarized with 1 µg/ml LPS for 50 min or incubated in MH-S medium (M0 AMs). Pro- (M1: Il6, Nlrp3, Cxcl2, Ptgs2, Ccl2, Il1a, Il1b, Il12b) and anti-inflammatory (M2: Retnla, Arg1, Pparg, Chil3) marker expression was quantified by qPCR.

M1 polarization proved to be effective by the comparison of M0 and M1 AMs (*Appendix, Table 16*). M1 AMs presented a clear increase in the expression of M1 markers compared to M0 AMs (p-value < 0.001) after incubation in medium containing LPS.

The comparison of marker expression of M0 AMs from offspring, grouped by sex, presented no differences between parental diet groups. Parental diet-induced obesity had no impact on the long-term ground polarization status of the offspring's AMs at steady state (Figure 28). After classical AM activation with LPS, a trend in decreased pro-inflammatory gene expression was noticed in M1 AMs isolated from HF offspring (Figure 29). However, differences in gene expression observed between M1 AMs from LF and HF P70 offspring were not large enough to reject the null hypothesis.

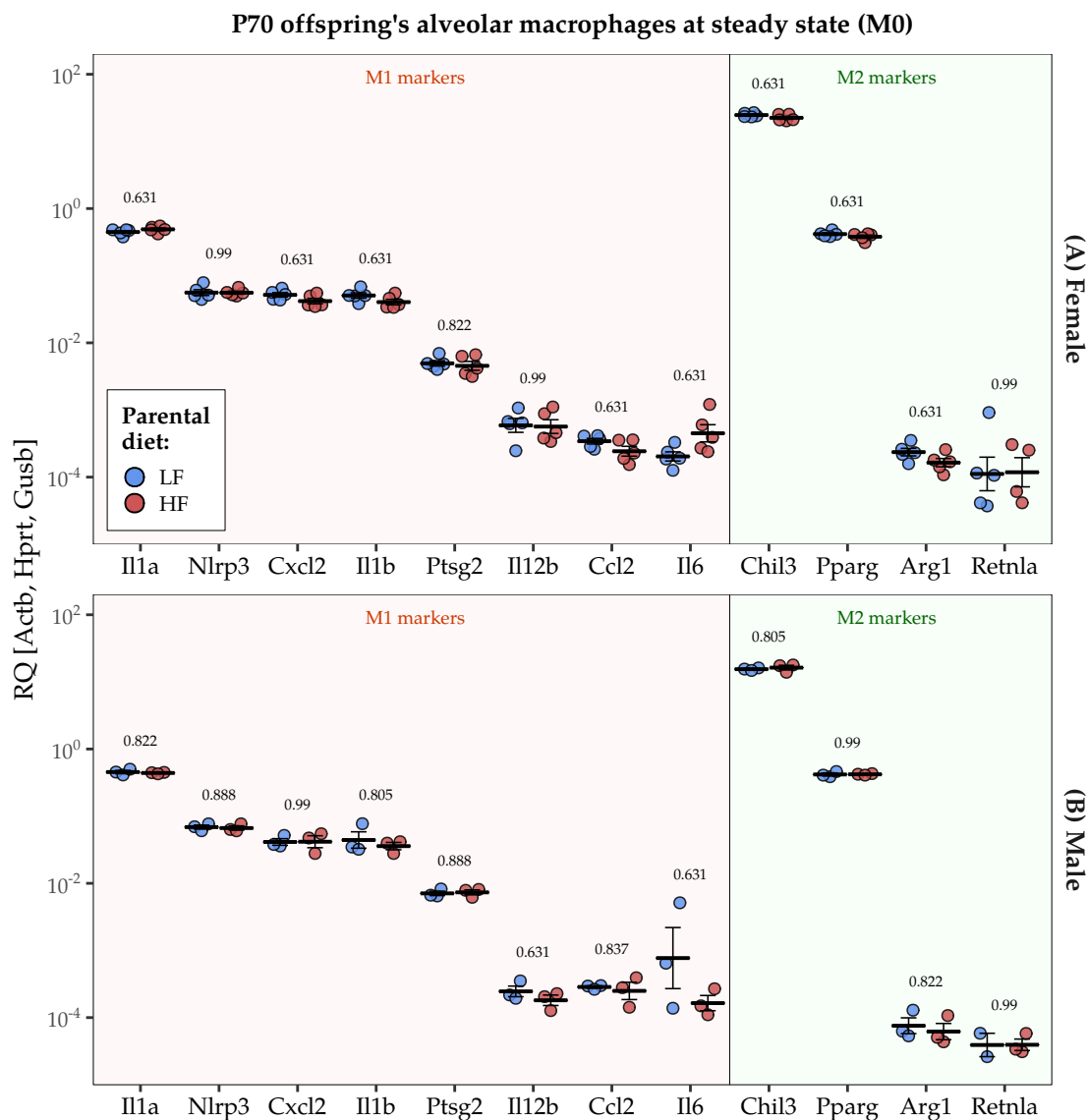


Figure 28: Parental obesity has no effect on ground polarization status of AMs at steady state. AMs isolated from bronchoalveolar lavages from 10-week old offspring mice at steady state were pooled (2 animals per pool), adherence-purified and incubated in MHS-medium for 50 min before gene expression analysis by qPCR. No difference in the expression of pro-inflammatory (M1: Il6, Nlrp3, Cxcl2, Ptsg2, Ccl2, Il1a, Il1b, Il12b) nor pro-resolution (M2: Retnla, Arg1, Pparg, Chil3) markers relative to three house-keeping genes (Actb, Hprt and Gusb) were observed between HF offspring's AMs and LF control groups at steady state ($n_{\text{female}} = 3$, $n_{\text{male}} = 5$). Welch two sample t-test with Benjamini-Hochberg correction (48 comparisons).

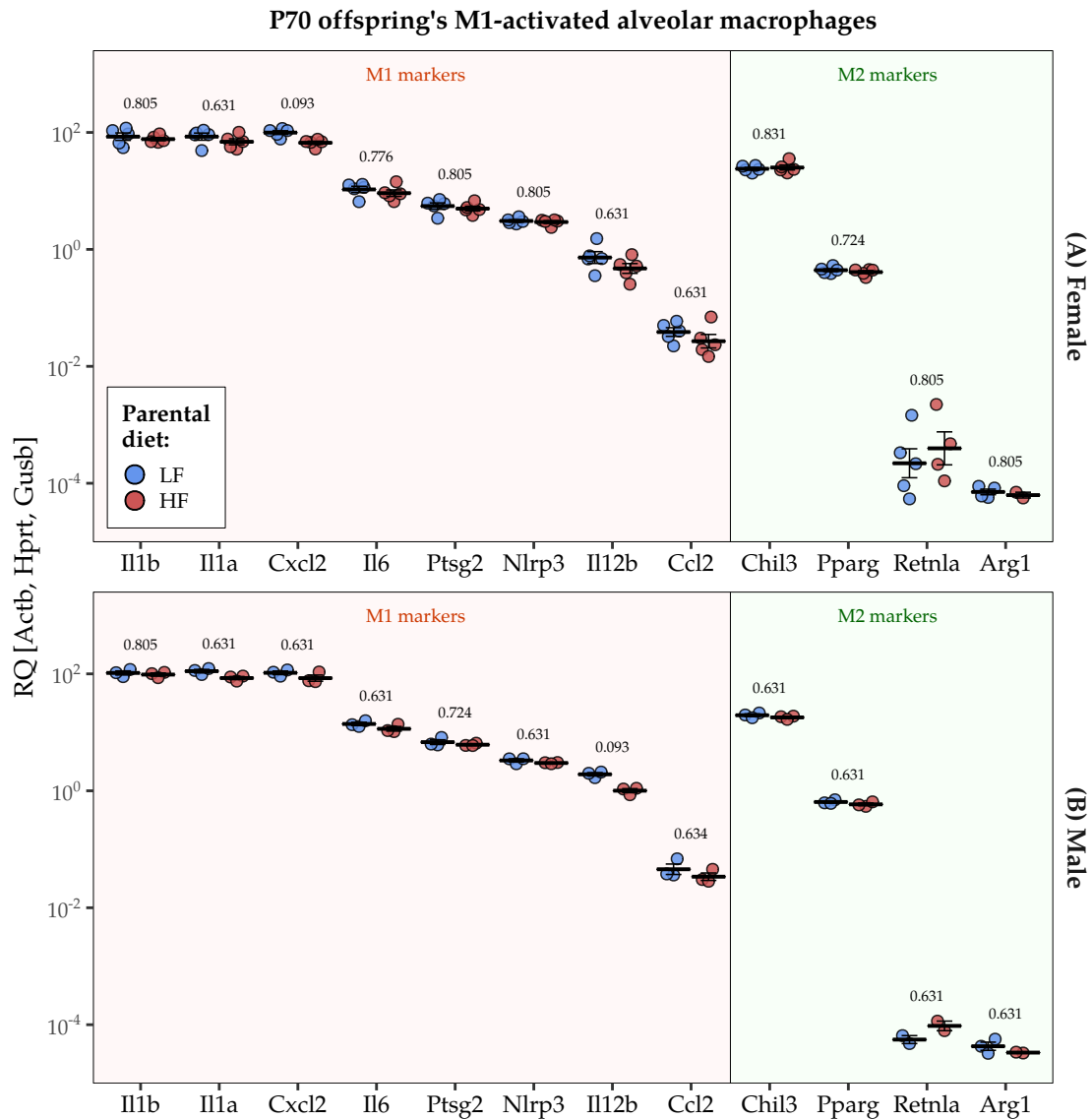


Figure 29: Parental obesity has no effect on M1-polarizability of AMs by LPS. AMs isolated from bronchoalveolar lavages from 10-week-old untreated offspring mice were pooled (2 animals per pool), adherence-purified and incubated in 1 $\mu\text{g/ml}$ LPS for 50 min before analysis by qPCR. M1 polarizability of AMs was not affected by parental diet ($n_{\text{female}} = 3$, $n_{\text{male}} = 5$). No difference in gene expression of pro-inflammatory (M1: Il6, Nlrp3, Cxcl2, Ptsg2, Ccl2, Il1a, Il1b, Il12b) nor pro-resolution (M2: Retnla, Arg1, Pparg, Chil3) markers relative to three house-keeping genes (Actb, Hprt and Gusb) were observed between parental HF and parental LF control groups after classical activation. Welch two sample t-test with Benjamini-Hochberg correction (48 comparisons).

5 Discussion

The paradigm shift around tissue macrophage ontogeny, the ever-growing pandemic of obesity and evidence of developmental origins of disease brought about by obesity led to the formulation of the hypothesis presented in this work. This hypothesis states that parental high-fat diet (HFD) induced obesity can have priming effects on developing alveolar macrophages (AMs) of the offspring and lead to an adverse immune response later in life.

AMs are not only the first line of defence at the air-tissue interface in the lung, with the ability to initiate and resolve inflammation, but are also of utmost importance for lung development and homeostasis. AMs display self-renewal capabilities and are long-lived. At tissue steady state, this tissue macrophage (TM) population is very stable. Only less than 5% of the AM population is replaced at steady state by circulating monocytes within 14 months of a mouse life^[123].

Applying mouse models of maternal diet-induced obesity (DIO), recent publications have described maternal obesity-dependent impairments in offspring lung development^[327,353]. Maternal obesity can induce the overexpression of pro-inflammatory markers, which are not only observable in the mother's circulation, but spill over to the placenta^[324] and even reach the foetal lung^[354]. Additionally, research on developmental immunotoxicity suggests a especially high sensitivity of MFs to alterations by early life environmental insults and foetal programming^[210].

In this thesis, the period of AM development was proposed to present a window of vulnerability for programming effects by parental DIO. This hypothesis suggests an impact of parental obesity on AM maturation which leads to a detectable pro-inflammatory AM primed state and long-lasting adverse functions in the offspring's lung. It also implies that such long-term impairments become apparent later in life of the mouse offspring, not only through a mal-development of their lungs, but also through a defective inflammatory response to an LPS challenge.

Both dams and sires were expected to contribute to the proposed AMs pro-inflammatory priming effects in offspring. Stress^[270,271], pyroptosis and pro-inflammatory activation^[273] can build up in the adipose tissue of obese individuals of both sexes and lead to high circulating concentrations of pro-inflammatory cytokines, free fatty acids and glucose^[252,278,279]. This pro-inflammatory metabolic deregulation can impair systemic metabolic, endocrine and immune functions which can be directly or indirectly transferred to the developing offspring either through the placenta (placental oxidative stress, inflammation and dysfunction) or through epigenetic mechanisms, respectively.

The first step in the analysis of the role of parental obesity on the offspring's lung development and AM priming was the generation and characterization of a mouse model of DIO.

5.1 Mouse model of high-fat diet-induced obesity

In order to test the hypothesis presented in this thesis, a mouse model of DIO was established employing the C57BL/6J mouse strain. Previous publications^[418–420] as well as experience from our cooperation partner Dr. Jan Rozman^[421] have consistently proven the high genetical susceptibility of this strain to metabolic and physiologic alterations through diet, even more so than other mouse strains^[422], e. g. BALB/c or A/J^[423,424].

Animals were fed with purified diets containing either 60 kJ% fat (HF) or 11 kJ% fat (LF) for 12 weeks. To avoid confusion, it is important to note that the fat content of the so-called “low-fat diet” conforms to the fat content of a standard mouse chow. This term is used here to remark the comparison with the high-fat diet and in concordance with previous literature presenting DIO studies using similar purified control diets^[425,426]. For future projects and publications, possibly the term “control diet/CD” would be more suitable.

For this work, purified ingredient HF and LF diets were employed and not grain-based chow diet alternatives. Comparing the purified ingredient LF control diet with the standard chow diet for instance, it can be observed that both diets present a very similar energy content of around 10-13 %KJ in form of fat^[427,428]. However, primary components of chow diets are natural ingredients, such as grains and meals. Therefore micro- and macronutrient content does not always completely match between them. Additionally, standard chow nutritional content can vary from batch to batch^[429], complicating the reproducibility of results.

The use of 60% kcal in form of fat for murine feeding has been criticized of being of too high fat content^[430]. This is especially because HFD does not reflect the normal human dietary fat intake – neither the energy content in form of fat nor its fat source^[431]. Often, only a single fat source (e. g. lard, as in the present study) is used. According to NHANES, the typical human “western” diet contains around 35%, 49% and 16% of energy from fat, carbohydrates, and protein, respectively^[432]. 60% of energy as fat might be tolerable for humans, however the difference to a normal rodent diet is of a much greater magnitude. Nonetheless, the use of 60% HFD leads to faster and more pronounced physiological and metabolic effects. This reduces the time in which animals need to be fed, housed and maintained, diminishing the overall caging costs and experimental time.

Mice on HFD with 60% of its energy content in form of fat become more rapidly obese than on diets with lower fat contents (e. g. 45% of energy from fat)^[433,434]. Previous studies have confirmed the higher efficiency of 60% HFD in inducing obesity in C57BL/6J mice compared to other high-caloric diets that try to mimic unhealthy food consumption in humans^[431,435].

The so-called “cafeteria diet” is an example which includes along with chow diet high palatable human food like chocolate, peanuts, corn-starch crackers and others^[436],

depending on the provider. The cafeteria diet has proven to be a relatively robust alternative to the feeding of purified HFDs to induce obesity^[437,438]. Probably the main reason for this is that cafeteria diet provides a substantial amount of sugar and salt, which increases appetite and excess food intake^[439]. Of course, its employment could prevent the solely use of a particular type of fat while inducing continuous hyperphagia and increased energy intake. On the other hand, it can be a challenge to attribute induced physiologic, metabolic and transgenerational effects to specific components, since such diets are less well defined in terms of nutrient content and because of the presence of several additives^[431]. Nonetheless, previous studies from Dr. Stöger's lab have shown that HFD can more strongly induce increases in body composition parameters and lead to an higher immune activation in C57BL/6J mice compared to a cafeteria diet^[440], even for feeding periods as short as six weeks. Additionally, rodents fed with a cafeteria diet develop the greatest dysbiosis compared to other high caloric diets^[431]. This effect by itself can strongly impact immune homeostasis and lead to systemic diseases^[441].

5.1.1 Effects of high-fat diet on the mouse body composition

The presented model of murine HF diet feeding showed to be very effective for inducing body weight and body fat increases on parent animals from both sexes (*Figure 6*). However, an obvious sexual dimorphism was noticed, especially on gains of body fat and body lean mass. While differences in fat mass between HF and LF groups were promptly evident after one week of diet in males, these changes were not as fast nor were they as pronounced for HF female animals. An increase of 49.3% in body fat (12.2% in body weight and 6.7% in body lean mass) was observed between diet groups in males at week 12 after start of diet, while a 32.3% difference in body fat (10.2% in body weight, 3.5% in body lean mass) was measured between LF and HF females. It was striking to notice, that although males presented such marked differences in body fat measurements, no changes in their lean body mass were evident by comparing diet groups. This was not the case for female mice. HF female animals did indeed display increases in lean mass compared to LF control groups. Curiously, no statistical significance for comparisons of the parameters body weight and body fat between HF and LF females was reached at weeks 7, 8 and 10 after start of diet. Nonetheless, differences in these body composition measurements were large at the end of the 12-week feeding period (*Figure 6*) before mating, which corroborated the presence of obesity during mating.

Longer feeding periods might have led to more stable weight and body fat differences in female mice – possibly resembling more closely human obesity. In a protocol from 2012 by Wang and Liao^[442], recommendations for diet induced obesity models include diet times of 16 weeks to reach a full picture of obesity with adipocyte hyperplasia, visceral fat deposition, increased body fat mass, signs of diabetes and hypertension^[442]. However, other authors working with mouse models of DIO, specifically employing the C57BL/6J strain, have applied very different periods of feeding times. Dieting periods in current literature range from short-term feeding of only 3 days^[443,444] to long-term

diets of over 20 weeks, including studies with up to one year of dieting^[445]. While short diet periods lead to increases in body weight gains, body fat mass and insulin resistance, longer dieting times are necessary to induce systemic inflammatory changes^[443]. Again, the onset and strength of the phenotypes induced by different dieting times will depend on the specific mouse strain under study^[446]. Interestingly, while C57BL/6J is said to be highly sensitive to DIO, studies show an even higher sensitivity of other strains, including C57BL/6N and 129P2/OlaHsd^[446].

However not determined, it is possible that obesity in males could have led to reduced activity (e. g. less movement in cages), promoting muscle mass loss. On the other hand, if fat mass increases in females were not marked enough to reduce their activity, augmented force production due to increased mass loads could have led to muscle mass gains^[447]. Furthermore, obesity has shown to reduce circulating testosterone levels^[448,449] and depress anabolic effects of insulin in the stimulation of protein synthesis, contributing to loss of muscle mass^[450]. Inflammatory adipokines like IL6 also exhibit catabolic effect on muscle^[451]. These results suggest possible sexual dimorphic effects of DIO on muscle mass development in C57BL/6J mice.

Large variations in obesity phenotypes have been reported for C57BL/6J mice despite their inbred and isogenic genetic status^[452,453]. Especially the parameters body weight and body fat were affected by such high variability, showing increased variance over feeding time^[453]. In this thesis, an increase in variance from 0.27 to 13.8 g² between the start of diet and after week 12 on diet was observed for HF male animals (from 0.59 to 8.19 g² for HF females). Authors have also observed, that body lean mass remains relatively stable along diet^[453]. This results were also detected in the present work, where in the case of HF males variances increased only from 0.2 to 2.2 g² between week 0 and 12 on diet (0.22 to 1.14 g² for HF females).

5.1.2 Impact of diet-induced obesity on sexual interest and mating

During mating of diet-treated parent mice, a qualitative difference in sexual activity and sexual interest between diet groups was observed. This was not surprising, since such effects were known to cooperation partners and since obesity has been associated with reduced circulating testosterone^[449]. Such reduction is partly brought about by the increased expression of aromatase in adipocytes, an enzyme known to convert testosterone to oestrogens^[448].

Longer mating times were noticed for the HF group. The possibility of a too strong decay in the sexual interest of mice could hinder breeding and consequently the analysis of offspring. Especially male mice were qualitatively affected by HFD. In order to avoid such decline, while achieving obesity in both sexes, a feeding duration of 12 weeks was selected. It has already successfully been proven that such feeding time, implementing similar contents of fat in diet (60 kJ%) and with the same mouse strain (C57BL/6J), effectively leads to systemic symptoms of obesity and inflammation. These symptoms

include increased body weight and fat, elevated blood concentrations of glucose and decreased circulating levels of adiponectin^[454] as well as diabetic cardiomyopathy symptoms^[455]. Additionally, this duration of 12 weeks overlapped with the time of three to five months during which the mice were kept on diet before mating in the work of Mayor et al.^[327], which lead to increased placental pro-inflammatory gene expression and changes in the offspring's lung morphology (reduced maturation).

Alternatively to the experimental design for mouse feeding employed in this work, only dams could have been fed with a HFD before mating with age-matched LF males. However, the effect of parental HFD on increased offspring's body weight is suggested to be of additive nature^[13,456]. Since a stronger priming effect of the metabolism and immune system in offspring was expected when both parents belonged to the HF group, a possible alternative could be the mating of non-matching aged mice. For instance, females fed for 20 weeks mated with males fed for 10 weeks. However, due to lack of housing space and because this was not the main question in this work, no analysis of mating times nor combinations of different feeding periods were performed. Such supplementary animal work was also avoided in order to follow the 3Rs guiding principles for more ethical use of animals^[457].

5.1.3 Immunological consequences of obesity at steady state

HF parent animals presented metabolic-driven systemic inflammation and hyperglycaemia at the age of 25 weeks (*Figure 7*). While elevated pro-inflammatory plasma cytokines CXCL1 and IL6 were observed in HF parent animals, other authors have suggested additional increases in pro-inflammatory cytokines in the circulation, e. g. IL1B and IL10, and TNF^[412,458] with mouse models on similar diets. Such differences could be partly attributed to genetic background of the animal model, differences in diet composition – content of sugar, polyunsaturated fatty acids (PUFAs) and cholesterol – and duration of HFD feeding.

Employing the mouse model of DIO used in this thesis, increased sample number would most likely have lead to measurable differences in TNF concentrations (80 % power: $n_{\text{female}} = 20$; $n_{\text{male}} = 27$). Interestingly, if these cytokine measurements were not grouped by sex, overall plasma TNF levels of HF animals resulted elevated during statistical analysis ($p = 0.035$) compared to LF controls after multiple test correction. Unfortunately, circulating levels of pro-inflammatory cytokines were not analysed at the time point of conception due to the lack of animals, and in order to reduce handling-related stress and prevent further reduction in mating efficiencies.

Lung homeostasis can be dramatically altered by obesity, not only through mass loading, but also through endocrine and metabolic factors. A cross-talk between the adipose tissue and the lung based on the mutual influence through inflammatory factors has been proposed^[299]. Interestingly, even though the DIO model implemented in this thesis lead to obesity, systemic inflammation and hyperglycaemia, the analysis of

CXCL2, TNF (data not shown) as well as total protein concentrations in the airspace of the lung (*Figure 8*) did not show any changes brought about by obesity at steady state. These results provided no signs of gross alterations of the pulmonary air-tissue barrier or strong pro-inflammatory activation of the lung tissue by obesity alone that could be measured in BALF. Interestingly, even though the counts of alveolar macrophages in bronchoalveolar lavages was reduced in obese male animals under basal conditions (*Figure 8D*), the polarization status of these AMs did not show any differences in pro- or anti-inflammatory gene expression at steady state (M0, *Figure 9*). Nonetheless, a trend of increased pro-inflammatory gene expression was observed on M0 AMs of both sexes. Even though mRNA quantities did not reach detectable changes between diet groups, this trend could be hint on the possible impact of AM homeostasis through obesity-induced alterations in the adipose tissue-lung cross-talk.

5.1.4 Contribution of free fatty acids to systemic inflammation

Obesity is not only associated with a systemic low-grade inflammation, but also with dyslipidaemia – hypertriglyceridemia and increases in free fatty acids (FFAs)^[459]. It has been shown that FFAs, specifically saturated ones^[460], are capable of stimulating a pro-inflammatory reaction and can thus contribute to the inflammatory state of obese individuals. FFAs can bring about the activation of toll-like receptor 2 (TLR2) and the TLR4 (canonical LPS receptor) signalling pathways^[461]. Such induction leads to a downstream activation of the nuclear factor kappa B (NF- κ B) transcription factor^[462] in order to elicit pro-inflammatory cytokine expression. Additionally, FFAs can cause the induction of endoplasmic reticulum stress^[463] and the stimulation of reactive oxygen species (ROS) production^[464]. An inhibition of the immune system to properly mount a response to fight an infection might arise from the constant presence of pro-inflammatory stimuli that reach the lung tissue.

Saturated fatty acids are an essential component of bacterial endotoxins – specifically of the lipid A portion of LPS. Lauric, myristic and palmitic fatty acids constitute the most common type of FFAs in the lipid A fragment^[465]. Interestingly the deacylation of these fatty acids from LPS results in loss of endotoxic activity^[466]. Importantly, it has been shown that their substitution by mono- or polyunsaturated counterparts blocks the pro-inflammatory activity of LPS^[467]. This denotes an additional important role of saturated fatty acids in LPS-mediated signalling. Strikingly, partial structures resulting from such deacylation can even inhibit responses to LPS in MFs without inhibiting its uptake^[468].

5.2 LPS challenge of the parental generation

5.2.1 Selection of the *in vivo* LPS challenge model

Contrary to other models of acute lung injury, the LPS challenge presented in this work targeted directly the lung. This was achieved by a local instillation of endotoxin into the lung and not, like other works^[469–472], indirectly over a intraperitoneal injection of a very high concentration of endotoxin. The latter induces a systemic pro-inflammatory challenge, affecting not only the lung, but every other tissue.

The LPS model established for this thesis did not aim to induce a lung injury. Most importantly, the endotoxin concentration was selected low in order to avoid AM loss due to excess necrosis^[417] and a radical alteration of the AM microenvironment. Such alterations would probably override the expected priming effects from parental obesity on their offspring (discussed in *Section 5.3.12* and *Section 5.4*).

In order to meet this criteria, while maintaining the pro-inflammatory activity of the instillation solution, an initial dose response analysis in chow-fed C57BL/6J mice was performed. This examination revealed a dose-dependent neutrophil recruitment to the airspace with higher neutrophil counts for increasing LPS concentrations (*Figure 23A*). Concurrently, macrophage counts decreased with greater concentrations of LPS (*Figure 23B*). This was not surprising, since LPS has shown to induce AM necrosis via Ca^{2+} influx upon TLR activation^[417].

A dose of 0.1 μg LPS per mouse induced a considerable level of acute lung inflammation, characterized by an increase in the absolute numbers of neutrophils in BAL, without macrophage depletion within 24 h after intratracheal instillation. Using this model of mild LPS-induced acute lung inflammation, the effect of obesity and obesity-induced low-grade inflammation on inflammatory dynamics in the lung was analysed.

Relatively high variation in cell counts and protein concentrations were observed during the examination of inflammatory dynamics in the lung (*Figure 8*). Different sources of variability could be listed, including differences in body weights, lung volumes, body fat mass, and systemic and local inflammatory states of the mice.

The LPS dose employed for the intratracheal instillation of 0.1 μg per animal corresponded to body weight-normalized doses between 1.9 to 3.8 $\mu\text{g}/\text{kg}$, depending on the specific body weight of the mouse (range: 26 - 52 g). It could be argued that the use of LPS doses based on animal body weight could have led to more stable results and less variation of measurements between animals.

In fact, estimations of the total surface area of mammals is based on their body weights. Correlation studies suggest a value of 1 m^2/kg body weight as a realistic estimate of the lung surface in mammals^[473]. However, when looking at a single species, especially while looking at a single mouse strain, the strongest determinant of the lung area of a subject will be its respiration state^[474]. To date, there is no evidence of a

correlation between lung volumes and the body weight of a mouse. Contrarily, weight gain has a more complex relationship to lung volumes and function^[303], especially considering that changes in mediators produced by adipose tissue can modulate the lung function^[475].

Since only local effects in the lungs were the target of the mild LPS challenge used in these analyses, and because rather in the case of an expected systemic reactivity would make sense to correct for the animal's body weight, the decision of using the same amount of LPS for every mouse challenged was taken. Additionally, a normalization of cell count during the course of inflammation against body weight alone (data not shown) actually lead to higher variations in the results. Unfortunately, a normalization against lung weights was not possible, since lavage (introduction of PBS into the airspace) and perfusion (introduction of PBS into the lung blood capillaries) were performed on the mouse lungs.

5.2.2 The role of obesity in the course of endotoxin-induced acute lung inflammation

Intratracheally LPS-challenged 30-week old HF male animals presented delayed inflammatory dynamics with decreased counts of BAL neutrophils and macrophages 24 h after LPS instillation and increased cell counts of both types 72 h after the challenge compared to LF controls (*Figure 8*). At this time point, a full resolution of inflammation in the lungs of male animals was not completed. It would be very interesting to measure the extent to which the shift of inflammatory dynamics occurs in these animals. Especially intriguing would be to know if HFD on these males could have had chronic lung implications after the challenge – in the form of a chronic inflammation or the development of emphysema or fibrosis due to possible tissue damage through the extended presence of inflammatory factors and neutrophils in the alveoli.

It is well known, that obesity is a risk factor for infectious lung diseases. Obesity leads to increased susceptibility, severity, morbidity and mortality from viral lung diseases^[476–478]. Additionally, influenza vaccinations strategies have shown to be less effective on obese individuals^[479]. During the current COVID-19 pandemic in 2020, obesity has also been identified as a mayor risk factor for hospitalization, mechanical ventilation and mortality from an infection with the novel severe acute respiratory syndrome coronavirus 2 (SARS-CoV-2)^[480–482]. An inhibition of the immune system to properly respond to an infection can be observed through reduced antiviral and pro-inflammatory cytokine expression in the lungs of influenza-infected obese mice^[292,483,484]. Immune responses involved in the fight against viral and bacterial infections are subject to different regulatory pathways^[485]. However, the delay in the inflammatory response in HF males during the *in vivo* LPS challenge (*Figure 8B*)

suggests a similar hindrance of the immune system by the presence of obesity. Further analysis of the distortion of immune responses by obesity could better help understand this risk factor and improve treatment strategies of obese individuals during lung infections.

Unfortunately, due to the low number of animals available for the analysis of inflammatory dynamics in the lung, no further time points could be examined during the LPS challenge. The evaluation of cytokine concentrations in the lung (BALF) of these animals, specifically of CXCL2 and TNF (data not shown), did not exhibit any noteworthy increases during the course of the inflammation. Further investigation of the apparent lack of regulation of these cytokines in the LPS model made evident that the incorporation of at least one additional earlier time point in the analysis was needed in order to be able to recognize changes in these inflammatory factors. This modification was therefore introduced in the evaluation of the offspring animals (*Figure 24*).

Female animals appeared to be protected from perturbations in inflammatory dynamics during the LPS challenge. These animals showed no differences between diet groups in BAL cell counts nor on BALF protein concentrations (*Figure 8A, C and E*), even though obesity and a metabolic inflammation was present. Unluckily, no HF females that did not go through pregnancy were analysed. It would be intriguing to find out, if such protection originated from the female sex physiology (e. g. oestrogens) or was specific to protective effects from the undergone pregnancy.

Studies from previous betacoronavirus outbreaks, e. g. of the so-called Middle East respiratory syndrome-related coronavirus (MERS-CoV)^[486] and SARS-CoV(-1)^[487], have shown a correlation between pregnancy and more severe and fatal cases of infection. Such results could be partly attributed to the bias toward a systemic Th2 dominance (immune tolerance/suppression) found in pregnant women^[488]. This Th2 bias is necessary for foetal development and protection against foetal rejection^[489,490], but leaves the mother vulnerable to viral infections, which are more efficiently confronted by the Th1 system^[491]. During the postpartum period, a reversal of the Th2/Th1 balance takes place^[492]. The protective effect of pregnancy proposed here is subject of revision, however, in case of a validation, it is conceivable that pregnancy and the immunological changes brought about by it might act as a “resetting” event that leads to strengthening of the immune system and to improved outcomes during an infection after such reset. It would be intriguing to observe, if in the human population, women show similar protective effects of an undergone gravidity against adverse effects of a SARS-CoV-2 infection.

It is important to remark, that no p-value correction for multiple comparison was applied on the results from the LPS challenge data from parent animals (*Figure 8*). This was not performed, since all comparisons were planned beforehand, sample sizes were small, and rejecting the alternative hypothesis too readily by the use of for example the conservative Bonferroni correction was avoided^[493,494]. This correction method would

have been especially severe in this analysis due to the use of the Wilcoxon test. This non-parametric statistical test provides a lower statistical power when compared to e. g. a standard parametric two sample t-test. This issue underlines the necessity of bigger group sizes for future analyses of similar interventions in mice as well as the need of validation of the presented results. Unfortunately, for this thesis, the use of larger animal numbers was not possible.

5.2.3 No impact of obesity on alveolar macrophage M1 polarization

Alveolar macrophages are key effector cells in the initiation and resolution of lung inflammatory responses^[495]. To better understand the delay in the initiation of lung inflammation observed during the LPS challenge of HF mice (*Figure 8*) and assess the possible impact of obesity on the initial phase of M1 AM polarization, AMs were examined by qPCR 50 min after *in vitro* incubation with LPS. At that moment, M1 AMs showed very pronounced increases in pro-inflammatory marker expression compared to steady state AMs (*Appendix, Table 14*).

Previous work from Prof. Dr. Meiners' and Dr. Stöger's groups^[496] show that the *in vitro* M1 polarization of AMs for 24 h presents comparable increases in pro-inflammatory gene expression when comparing M0 and M1 AMs to the differences presented in this thesis 50 min after the start of polarization (*Appendix, Table 14*). Additionally, time course analysis of *in vitro* M1 activation of MFs with LPS (and INF γ) by these groups^[496] and others^[497] for times between 0 and 24 h have shown a dynamic M1 marker expression. In these studies, maximal increases in mRNA quantities were captured at around 4-6 h. A subsequent decrease in pro-inflammatory gene expression was observed until 24 h after incubation. In order to capture changes in AM polarization as closely to the *in vivo* conditions as possible (*ex vivo* incubation presents a completely different microenvironment compared to the lung), and because the polarization study of AMs in this thesis aimed the description of the initial phase of M1 AM polarization that could explain the delay of *in vivo* inflammation during the LPS instillation in obese mice, the time point of 50 min after AM incubation with LPS was selected.

As expected, the M2 markers Pparg and Chil3 were not differentially expressed between M1 and M0 macrophages. Furthermore, obesity, systemic inflammation and increased plasma glucose levels in HF animals had no effects on the initial M1 AM polarization *in vitro*. The similar expression in pro-inflammatory markers, especially of Cxcl2, measured between M1 and M0 AMs 50 min after their incubation with LPS could indicate that the delay in the initial influx of neutrophils was not directly caused by the expression of the inspected pro-inflammatory molecules in AMs. Interestingly, qPCR analyses of AMs isolated from C57BL/6J mice fed for up to a year with HFD did not show any differences in the expression levels of polarization markers at steady state either (data not shown).

It would be intriguing to find out if the expression of M1 markers in AMs are affected during later time points of the *in vitro* incubation with LPS. Especially interesting would be an analysis of such expression during the time point of “maximal polarizability” of AMs. As presented 2016 by Chen et al.^[496] and Xie et al.^[497], such maximum in expression might be observed 4-6 h after the start of *in vitro* polarization with LPS.

Another possible explanation of the delayed inflammatory response *in vivo* could be the smaller numbers of MFs observed in the lavages of mice at the time point 0 h of the LPS time course. This would mean that, even if single AMs expressed the same amount of pro-inflammatory factors, the overall concentrations in the lung would be reduced in HF (male) animals.

5.2.4 M1 alveolar macrophage adherence to the lung epithelium

The cause for the reduction in AM counts in obese mice could also have been caused by a stronger adherence of AMs to the lung epithelium. This adherence process can be integrin α_D -mediated (Itgad) and therefore dependent on the polarization status of AMs^[498]. M1 MFs demonstrate a higher expression of Itgad and therefore stronger adhesive characteristics^[498]. Interestingly, AMs presented a trend of increased expression of pro-inflammatory genes at steady state (*Figure 9*). Further gene expression analysis could provide information on effects of obesity on the regulation of Itgad and possibly explain a stronger adherence of AMs in obese mice.

Yet another known process involved in AM binding to the epithelium is the expression of gap junction protein α_1 (Gja1). During endotoxin-induced lung inflammation, M1 AMs can adhere to the alveoli and initiate immunosuppressive, Ca^{2+} -dependent intercommunication employing GJA1-based gap junctional channels to the lung epithelium as communication route^[130]. Impaired Gja1-mediated signalling in AMs can impact the secretion of pro-inflammatory cytokines by epithelial cells (CXCL1, CXCL5) and neutrophil recruitment to the airspace^[130]. Such impairment could have led to the observed alteration in BAL macrophages numbers *in vivo*. In addition to Itgad, Gja1 could be an interesting research candidate for this model. Intriguingly, Gja1 have shown to be involved in obesity-related processes within other organs, like white adipose tissue being^[499] and hypothalamic control of feeding behaviour^[500]. For this reason it could present an additional link between obesity and inflammation.

5.2.5 AM phagocytosis and the resolution of inflammation

An equally important, but often overlooked function of AMs, additionally to the initiation of an inflammatory response in the lung, is the induction of its resolution. Even though the analysis of polarization markers did not show any differential gene expression between diet groups at steady state nor 50 min after LPS exposure, the phagocytosis test implemented in this work displayed a reduced uptake of zymosan particles by HF male AMs (*Figure 11*).

It was not possible to distinguish with this assay alone exactly which mechanisms of phagocytosis were perturbed by HFD. Possible impairments in phagocytosis could occur for example in the uptake of particles, but also on the maturation of the phagolysosome – specifically on its acidification. Both types of phagocytosis impairment would lead to a reduced fluorescence in AMs and lower counts of pHrodo-positive AMs^[415].

Even though the phagocytosis analysis presented differences between LF and HF males, it is important to mention that only the uptake of particles was tested and not the engulfment of apoptotic neutrophils. Differences in the latter would present a direct explanation of the delay in resolution of inflammation observed 72 h after the *in vivo* LPS challenge of obese male animals. In contrast to the phagocytosis of bacteria, particulate matter or necrotic cells, efferocytosis of apoptotic cells runs “quietly”, without evoking inflammatory or immunogenic reactions^[501]. Most importantly, the efferocytosis of apoptotic neutrophils by AMs promotes anti-inflammatory signalling not only by preventing cell lysis of neutrophils and release of their content, but also by acting as a strong inducer of anti-inflammatory and pro-resolution pathways in macrophages^[413].

5.2.6 Possible contributors to immune alterations during obesity

Taking into account that obesity can not only lead to a systemic low-grade inflammation^[278,279], but also dyslipidaemia^[241], impairment of the endocrine functions of the adipose tissue^[253], and gut microbiome dysbiosis^[268], three possible contributors to the distortion of the lung’s inflammatory dynamics (*Figure 8*) could be listed: immune cell exhaustion, endotoxin tolerance and deregulation of immunoregulatory adipokines.

Immune cell exhaustion is a process characterized by a progressive and hierarchical loss of effector functions following chronic exposure to pro-inflammatory signals^[502]. Exhausted cells present decreased proliferative potential, attenuated cytokine production, and diminished self-renewal capacity^[502]. Additionally, exhausted macrophages are characterized by an impairment of their phagocytic activity^[503,504]. Immune exhaustion of AMs could be involved in the observed decrease in macrophage counts in the lungs of HF males at steady state (*Figure 8D*) as well as to the delayed initiation and resolution of inflammation (*Figure 8B*).

Endotoxin tolerance involves the continuous activation of TLR2 and TLR4 pathways on myeloid cells through repeated exposure to bacterial LPS. This phenomenon is characterized by hyporesponsiveness to a subsequent pro-inflammatory activation^[505,506] and is thought to be an adaptive mechanism that protects from tissue injury by repeated subjection to Gram-negative bacteria^[507]. Since FFAs can act as TLR agonists and because obesity can induce gut dysbiosis, increase gut permeability and lead to leaking of LPS into the circulation (endotoxemia)^[508,509], the question of possible endotoxin tolerance in the presented mouse model of DIO arises.

Lastly, adipokines have shown to play a pivotal role for the correct function of the immune system. Adiponectin, for instance, facilitates the uptake of apoptotic cells by MFs^[510], but its concentration is reduced in C57BL/6J mice subjected to DIO^[511]. Additionally, leptin is of great importance for the development and function of immune cells^[512,513], but obesity can lead to its deregulation and resistance, directly affecting the lung immunity^[514]. Importantly, AMs express the leptin receptor and the leptin signalling pathway promotes their phagocytic activity^[515]. During C57BL/6J DIO, peripheral leptin insensitivity starts at week eight^[516]. This is why (at least) leptin and adiponektin could play important roles in an immune deregulation in the lung during obesity.

5.3 Intergenerational effects of diet-induced parental obesity

More often than not, the terms “intergenerational” and “transgenerational” are used interchangeably. However, it is important to remark that a true transgenerational epigenetic transmission stringently refer to phenotypic consequences that cannot be attributed to immediate influences of a particular trigger (e. g. an environmental exposure) on the altered organism. Specifically, only effects occurring in the second generation (F2) for male-mediated or third generation (F3) for female-mediated alterations after environmental exposure can be described as transgenerational inheritance^[358,359]. On the other hand, effects spanning shorter periods are described as parental or intergenerational. The impact of parental obesity directly affecting the developing embryo (F1) and the gametes that formed it is therefore defined as a parental or intergenerational effect.

After the successful generation and characterization of a parental mouse model of diet-induced obesity (DIO), the intergenerational effect of parental obesity was analysed at three different time points in the offspring’s life. The first two – embryonic day 18.5 (E18.5) and postnatal day 15 (P15) – were selected in accordance with previous publications on the effects of maternal DIO on the placenta and the offspring’s lung^[324,327]. Additionally, an age of ten weeks (P70) was inspected for the study of long-term effects of parental obesity at a young-adult^[365] mouse age.

Following human developmental terminology, the denomination “embryo” indicates a developing human between the time of implantation and the onset of bone marrow generation in the humerus^[517], i. e. around the ninth week after conception. Posterior to this phase and until birth, the term “foetus” is used. Such distinction in the mouse is however less strict. Since the term embryo can be applied to all stages of mouse development between conception and birth^[517], here “foetus” and “embryo” are used interchangeably to describe E18.5 offspring.

5.3.1 Impact of experimental design on high-fat diet outcomes

The hypothesis proposed in this thesis as well as the constellation of analyses performed on offspring were designed based on the premise that a high-fat diet (HFD) not only can induce obesity in parent animals, but also induce placental inflammation and cause a disruption of the normal lung development in offspring. I. e. parental HFD feeding was expected to lead to the reproduction of results from previous publications (see *Section 5*), especially of the findings from Mayor et al. from 2015^[327].

Contrary to named publication, a HFD containing a higher fat content (60 %KJ vs. 42 %KJ) and exclusively purified diets (low-fat diet vs. standard mouse chow) were employed for the present work. This decision was made following suggestions from our

cooperation partners at the German Mouse Clinic (see *Section 2.3* and *Section 5.1*) and because of the higher efficacy of such HFD in inducing obesity in mice. Additionally, scientists have previously mentioned an impact of maternal DIO on the offspring's lung morphology employing purified diets^[353].

Since a grain-based, standard mouse chow (like the one employed by Mayor et al. as control diet) presents a completely different source of carbohydrates, has a higher content in fibre and contains different plant chemicals, such as phytoestrogens (isoflavones)^[518], it is likely that spurious effects of parental diet on the offspring's physiology might arise not from parental obesity, but from differences in nutrient and chemical content between diets. Such elements can modify endocrine functions^[519,520] and affect the gut microbiome^[520]. It has been shown, that the latter can directly modulate important immune functions in a sexual dimorphic manner^[521].

Further differences between the two experimental designs included the possibly reduced feeding period of parents (12 weeks vs. "3-5 months"), the earlier start of parental feeding (directly after delivery at three weeks of age vs. "6-8 week old" mice), the application of the DIO model on parents from both sexes (vs. only dams), and potentially the use of a different mouse genetic background (C57BL/6J vs. "C57/Bl6", see article "*There is no such thing as a C57BL/6 mouse!*"^[522]). The presence of such differences would lead to critical repercussions, since these not only can define the susceptibility of animals to DIO^[446], but also dictate specific immune responses^[523-525].

5.3.2 No effects of maternal obesity on placental inflammation

As presented in *Section 2.2*, the main hypothesis of this thesis proposes that the period of AM development can present itself as a window of vulnerability for programming effects by parental DIO.

Studies of maternal DIO have demonstrated alterations in the gene expression and morphology of placentas from HF dams in a sexual dimorphic fashion^[324,327,416]. Particularly, authors propose an increased expression in pro-inflammatory cytokines after maternal HFD feeding, including higher mRNA levels of Ccl2, Il6, Il1b, Tnf and Nrlp3^[324,327,416].

Placental inflammation has shown to induce placental dysfunction and intrauterine growth restriction, among other pregnancy complications^[526]. Because the precursors of the AM niche (foetal monocytes) seed the lung before birth, it is very likely that placental inflammation plays a critical role in the hypothesized pro-inflammatory priming of this tissue macrophage (TM) population.

In this thesis, the analysis of the gene expression of inflammatory markers in the placenta of E18.5 foetuses, including the genes mentioned above, displayed no effect of parental diet (*Figure 14*). Even though a qualitative trend of higher expression levels of

pro-inflammatory genes in placentas from HF female embryos (*Figure 14A*) compared to LF control placentas was observed, these differences did not reach statistical significance. Such trend was not as clear for male embryos (*Figure 14B*).

Based on the findings of sexual dimorphic expression of pro-inflammatory molecules in the placenta^[324,327,416] as well as on the detrimental effects of placental inflammation on foetal survival, in order to categorize this trend as biological relevant, differences in the sex distribution of surviving offspring between diet groups could be expected. This was however not the case ($p=0.563$, Fisher's exact test).

Calculations of the number of samples needed to reach a statistical power of 80 % using the observed standard deviation and difference in mean gene expression between diet groups of female placentas resulted in sample sizes of 11 for *Il12b*, 16 for *Nos2*, 29 for *Nlrp3* and 38 for *Il1b*. Based on these estimates, it could be argued that higher samples sizes or longer feeding times of dams might have led to the observations demonstrated in the work from Kim et al.^[324]. It has to be noted however, that the disruption of placental morphology, cell proliferation and the presence of inflammation in placentas detected by these authors took place after merely 8 weeks of feeding purified diets (both HFD and LFD).

Similarly to Mayor et al.^[327], the fat content of the HFD used by Kim et al. was lower (45% kcal as fat) compared to the present work, and the reported mouse strain employed was also "C57BL/6". Because mouse strains with a C57BL/6N background display more pronounced responses in the development of DIO upon HFD feeding^[446], it is likely that Kim et al. as well as Mayor et al. have made use of strains with such a genetic background (6N).

Several studies have previously identified distinct phenotypic consequences based on the specific genetic background of C57BL mice (6N vs. 6J)^[446,527-529]. For instance, comparing these two mouse strains, Bourdi et al. could demonstrate in 2011^[528] seriously contradicting findings of studies on liver injury. These discrepancies were attributed solely to differences in the genetic background of these two "C57BL/6" mouse strains^[528].

Since Kim et al.^[324] employed purified diets as in the case of this thesis, rather the genetic background of the mice used and less the differences in diet composition (standard chow vs. LFD) led to the inconsistencies observed in the placental consequences of maternal DIO among the different studies presented.

5.3.3 No effects of parental obesity on systemic inflammation in offspring

Even though the gene expression analysis demonstrated no evidence of inflammation in the placenta, these results did not exclude the possible emergence of systemic inflammation in HF offspring after birth as a consequence of epigenetic inheritance.

Nevertheless, in accordance to the negative results from the gene expression examination in placentas, none of the ten inflammatory cytokines measured in the offspring's circulation after birth at P15 (*Figure 15*) nor at P70 (*Figure 16*) presented any differences between HF and LF offspring groups.

Unfortunately, some of the observed cytokine concentrations were close to the detection limit of the measurement system. This hindered their interpretability. For that reason, the relevance of qualitative differences between parental diet groups, especially of the apparently higher levels of INF γ in P15 male offspring (*Figure 15B*) and the seemingly higher concentration in IL4 in HF P70 female offspring (*Figure 16A*), could not be clearly stated. Furthermore, since no standard control levels of plasma cytokines from standard chow-fed mice were measured, no conclusions on the effect of the purified LFD on plasma cytokine concentrations in offspring could be made.

Cytokine measurements in offspring's plasma were performed at steady state. It could be imaginable that a "second hit" could expose systemic effects brought about by parental DIO, which otherwise were not detectable during homeostasis. Systemic challenges could include the intravenous injection of LPS to induce a systemic acute inflammation as well as a continued HFD feeding regime, similar to the HF parents.

5.3.4 Parental obesity and foetal deaths

The causes for stillbirths have been extensively studied both in human and mouse. Maternal stress caused by factors like air pollution^[530], nutrient imbalance^[531], cigarette smoke^[532], bacterial^[533] or viral infections^[534] and exposure to gold nanoparticles^[535], among others, have been previously described. Common to these environmental exposures is the promotion of intrauterine stress. Such stress can alter the embryonic homeostasis through malfunctions in nutrient, oxygen and waste exchange/transport of the placenta^[536]. Maternal obesity is also a well known predictor of pregnancy complications like preterm birth^[537], preeclampsia^[538] and foetal deaths^[317].

Rodent models of maternal DIO have demonstrated increased pro-inflammatory gene expression, and altered morphology and vasculature of placentas from HF dams^[324,327,539]. These placental changes are thought to be responsible for poor neonatal survival. Therefore, it was very surprising to notice that even though pro-inflammatory gene expression in placentas from HF animals was not altered (*Figure 14*), HF embryos presented a more pronounced resorption 18 days after conception than the LF control groups (*Figure 12A*).

Inflammation has shown to induce placental dysfunction and intrauterine growth restriction, among other pregnancy complications^[526]. The possibility that any other form of disturbance could have changed placental function or uteroplacental blood flow

and led to the observed increase in foetal resorption could not be discarded. It is plausible, that the loss in number of embryos could have stabilized nutrient and blood flow to the surviving foetuses and prevented thereby the expected pro-inflammatory phenotype in their placentas.

While HF dams exhibited 22% of miscarriages, only 4% of foetal sacks in LF dams were resorbed (*Figure 12A*). This represented a relative risk of 5.6 for a HF E18.5 foetus of dying (being resorbed) before birth compared with the LF group.

In order to quantify breeding efficiencies, the total number of living offspring at weaning were assessed and divided by the total number of female mice mated. Breeding efficiencies of 3.2 offspring per HF female and 3.9 for LFD control groups were observed. Interestingly, the 18% decrease in foetal viability in the HF group could explain the 18% reduction in breeding efficiency. This suggests that the time before birth presents the highest risk of death for a HF offspring.

5.3.5 Effects of parental obesity on the offspring's body weight

Reduction in foetal viability in HF mice has been previously observed by Mayor et al.^[327] and by other authors^[334,349,434,540,541]. Compared to their results, foetal weights did not differ between diet groups in the present work (*Figure 12B*). This was surprising, since many models of HFD in rodents have led to signs of foetal growth retardation/restriction and to the phenotype "small for gestational age" in HF offspring^[327,334,542-545]. Similar effects as the ones observed in this thesis (no differences in weight) were noticed in other animal models as well^[347,348,546].

There have been many inconsistent reports on the effects of parental HFD feeding on foetal growth^[545] and offspring's body weight outcomes^[547], showing both increased^[349,548,549] and non-affected^[325,348,550,551] foetal body weights. Such observations took place in spite of increased fat mass, glucose intolerance and placental morphological alterations in HF dams^[325].

Not only the species, strain and age of the animal model^[424], but also the duration of feeding^[453] and the specific composition of the animal's diet, e. g. carbohydrate and fat content^[552-554], fat origin (animal vs. vegetal)^[554,555], and the presence of mono- and polyunsaturated fatty acids^[556-558], can differently affect the metabolism and physiology of the animal model and lead to variable intergenerational consequences. Therefore, it can be expected that even small differences in rodent diets lead to the aforementioned inconsistencies in physiologic and inter-/transgenerational outcomes.

Further efforts should continue to be made in order to standardize rodent models of diet induced obesity. This is especially important since more often than not, the ultimate goal of such models resides in their application in translational medicine. Since the

numbers of rodent studies implementing similar fat contents as the one used in these analyses – HFD with 60 % of its caloric content coming from fat, and LF control diets with around 10 % of fat – are increasing^[547,559], such standardized model of rodent obesity might lead to more homogeneous results in future studies with C57BL/6J mice.

Writing a review article on the topic in 2019, Chistians et al.^[545] described a plausible relationship between maternal HFD feeding times and their effects on the offspring's body weight. While feeding mice a HFD (60 %) for 4–9 weeks prior to pregnancy favoured larger foetal body weights, longer feeding periods tended to reduce foetal growth^[545]. This remains to be definitely validated, however, following this hypothesis, the duration of the HFD used in this thesis could overlap with a period “in-between”, where no foetal weight differences can be observed between HF and control animals.

Similar to male E18.5 foetuses, no differences in body weights were observed in P15 male offspring nor at the age of P70 (*Figure 13*). Yet, body weights of P15 HF females were reduced compared to the LF offspring control group (*Figure 13A*). This effect appeared to be temporary, since a catch-up in weight followed, leading to comparable body weights between parental diet groups at P70. Even though a trend in lower mean weights for all HF groups compared to LF controls was visible, these differences were not substantial.

Previous studies have shown that male offspring have a higher susceptibility to transgenerational perturbations by parental diet^[560–562]. It was striking to observe that only the P15 female offspring group presented alterations in body weight due to parental diet. Also interesting was the recovery in body weights until the age of ten weeks. Unfortunately, no differential analysis of body composition parameters was performed on offspring mice. Such data could help understand, if the catch-up observed was due to increases in body fat or in all three body composition values. Since offspring were exclusively fed with a LF control diet after weaning, the latter could rather be expected.

5.3.6 Implications of parental obesity on the embryonic lung inflammatory and developmental status

Developmental and/or inflammatory gene expression interrogation in foetal lungs by qPCR demonstrated altered levels of *Fgf10*, *Pparg*, *Bmp4* and *Ccl2*. While E18.5 HF female lungs displayed increased mRNA levels of *Fgf10* and *Bmp4* and lower gene expression of *Pparg* and *Ccl2*, these differences were only visible for *Bmp4* and *Ccl2* in male foetal lungs (*Figure 17*).

Contrary to the results presented in 2015 by Mayor et al.^[327] no differences in the expression of *Il1b* nor of *Nlrp3* were observed in the HF E18.5 lungs (*Figure 17*). The results from Mayor et al. were conform with the previous publication by Bry et al.^[563] and Hogmalm et al.^[564], who proposed that perinatal overexpression of *Il1b* in the lung

can lead to respiratory insufficiency with increased postnatal mortality and impaired postnatal growth. These authors suggested a disruption of alveolar morphogenesis in the lungs of neonatal mice and increased expression of pro-inflammatory cytokines like CXCL1, CXCL2 and CCL2, consistent with neutrophilic and monocytic infiltration of the lungs. Intriguingly, the expression of the pro-inflammatory marker Ccl2 was decreased by HFD in the present work. Also, levels of Cxcl2, Il1b and Il12b presented a trend of lower expression in the HF group compared to LF control foetal lungs (*Figure 17*). This was astonishing, since an opposite tendency was expected.

The expression of the nuclear hormone receptor and transcription factor (TF) peroxisome proliferator-activated receptor gamma (PPAR γ) has been reported in a number of pulmonary cell types, including inflammatory, mesenchymal, and epithelial cells. PPAR γ expression is prominent in the airway epithelium in the mouse lung and its deficiency results in defective postnatal lung maturation with enlarged airspaces^[565]. It also plays a role in the regulation of inflammation. Lung macrophage Pparg deregulation in a genetic model of obesity (db/db) has shown to increase host susceptibility to an influenza virus infection in obese mice. These mice displayed attenuated lung antiviral immunity, hampered recovery from the infection and reduced survival^[566].

PPAR γ has an anti-inflammatory activity, promoting transcription of genes coding for anti-inflammatory factors such as Arg1 and Clec10a^[567]. It also inhibits the activity (transrepression) of pro-inflammatory transcription factors like NF- κ B^[568] and the production of pro-inflammatory cytokines such as TNF, IL1b as well as other MF M1 markers like MMP9 and the macrophage scavenger receptor 1 (MSR1)^[569]. PPAR γ activation controls the function of several immune cells, including monocytes and macrophages, acting as negative regulator of pro-inflammatory activation^[568].

Importantly, the induction of PPAR γ is critical for the differentiation of AMs from foetal monocytes^[152], which, as mentioned before, play an important role in lung development^[211]. Based on the roles of PPAR γ , its central position connecting obesity, immunity, metabolism and lung development is clearly recognizable. Therefore, it was very striking to observe, that despite the presence of alterations in gene expression of Pparg as well as Fgf10, Bmp4 and Ccl2, no relevant morphological pathological alterations were visible during semiquantitative grading (*Table 13*) nor after quantification by image analysis of maturity in E18.5 foetal lungs (*Appendix, Table 15*).

5.3.7 Parental obesity does not necessarily induce a pro-inflammatory environment during AM development

As presented in *Section 2* and *Section 5.3.1*, the generation of the hypothesis of a pro-inflammatory priming of AMs by parental obesity started from the premise that the implementation of parental HFD feeding in mouse would lead not only to obesity in dams and sires, but would also increase the expression of pro-inflammatory genes

in placentas from obese dams as well as in the lungs from HF embryos. These pro-inflammatory alterations were expected to cause the disruption of the normal lung development in offspring observed by Mayor et al.^[327] as well as induce the hypothesised pro-inflammatory priming of AMs.

Because of the missing inflammation, both in the placentas as well as in the E18.5 offspring's lung, especially the absent up-regulation of Il1b and Nlrp3, the assumptions for this hypothesis were violated. In case of a detection of alterations in lung development or in the polarization AMs of HF offspring, a connection to a pro-inflammatory milieu in the lung during AM maturation would not be possible.

5.3.8 Implications of parental obesity on the P15 offspring's lung inflammatory and developmental gene expression

Additionally to the altered expression of Fgf10, Pparg, Bmp4 and Ccl2 in the HF embryonic lungs, parental DIO reshaped the mRNA levels of Ccl2, Il1b, Pparg, Tnfrst11a, and Wnt3a in the lungs from P15 offspring in a sexual dimorphic fashion (*Figure 19*). Pparg, Ccl2 and Il1b expression levels in the P15 lungs were decreased by parental HFD-induced obesity, but only in the male offspring's lung. Parental HFD raised the expression of Tnfrsf11a and Wnt3a in the P15 HF offspring lungs from both sexes.

Even though the presence of sexual dimorphism was observed in the altered gene expression by parental obesity in both the E18.5 as well as the P15 lungs, no evident trend in the impact of a specific offspring's sex was observed. While differences in the mRNA quantities in the offspring's lungs were more evident in HF females during an embryonic age compared to the LF control group (*Figure 17*), this was rather the case for lungs from P15 male offspring (*Figure 19*).

Compared to the qPCR analysis of E18.5 lungs (*Figure 17*), it can be observed that a less exhaustive interrogation of markers was performed for the P15 lungs. This was decided, since most of the markers analysed in E18.5 lungs presented no differences in the gene expression between diet groups. The strongest impact of parental obesity on developmental signalling in the offspring's lung was expected to appear during foetal development. Additionally, the more comparisons are performed, the stronger the burden due to multiple test correction is on the results from statistical comparisons. I. e. the less genes are compared, the higher is the statistical power of the analyses that are performed.

Interestingly, even though no increase in levels of Il1b mRNA were observed in neither the E18.5 nor the P15 offspring's lungs, the expression of the anti-inflammatory marker Pparg during both time points was decreased. Notwithstanding that the presence of a decreased Pparg gene expression did not affect both sexes consecutively at during the two time points analysed (compare *Figure 17* and *Figure 19*), a consistent trend of its reduced presence was evident.

5.3.9 Impact of maternal obesity on the early postnatal lung maturation

It was striking to notice that parental obesity effects on marker expression were more pronounced at the age of two weeks than during foetal development. Since solely LFD was used to feed offspring, it could be expected that direct parental obesity effects would diminish after birth and only priming/epigenetic effects would persist for a longer term. Even though the offspring development is no longer under the influence of the maternal intrauterine HF environment after birth, it has been shown, that nursing by foster HF dams can as well induce physiologic changes in rodents^[570]. HFD can directly impact the composition of the mother's milk^[571,572], especially in terms of fatty acid composition, nutritional content and the presence of inflammatory mediators.

The neonatal age is a crucial developmental time point for the lung and for alveolar macrophages. It is after the first breath that sacculi expansion concludes and alveolarization takes place. At the age of two weeks, both classical and continued alveolarization as well as microvascular maturation continue to progress^[573]. The final AM maturation takes place around this period of time, too^[81]. In turn, deregulation of the neonate's nutrition can also present itself as a window of vulnerability for developmental origins of lung disease^[570].

Even though no clear pro-inflammatory conditions were detected in the placenta nor in the E18.5 offspring's lung, a possible connection between maternal obesity and inflammation in the offspring after birth might be made. This would result from alterations in the composition of the maternal milk. The transmission of pro-inflammatory factors during this second window of vulnerability could affect the final phase of alveolarization and AM maturation. Therefore, it would be fascinating to evaluate the contribution of the maternal milk to the possible impact on these developmental processes.

5.3.10 Transient delay in the final alveolarization by parental obesity

Additionally to gene expression analysis, P15 and P70 lungs were tested for parental obesity effects in terms of their alveolarization. Histological examination by design-based quantitative morphometric stereology demonstrated increased mean linear intercept (Lm) measurements in P15 HF female offspring lungs compared to the LF control group (*Figure 18A*). Lm is an estimator of the mean path within the alveolar complex. As such, it represents an estimate of the internal alveolar surface area^[574]. Contrary to the believe that Lm can represent the alveolar size, it rather characterizes the entire acinar air space and not just alveoli^[574].

Similar to the effect on weights of female offspring, parental obesity only transiently affected Lm values at the age of P15. This pointed to a possible alteration of the final lung alveolarization after birth. Lm values of P70 HF female were similar to their corresponding LF controls (*Figure 18B*). No evident differences in Lm measurements were observable for HF male offspring at any of the two ages. Even though a similar

tendency as for P15 females of higher Lm values for the P15 HF male offspring was observed, differences to LF controls did not reach statistical significance (for 80 % power, the sample size needed would be of $n_{\text{Male,P15}} = 41$).

The observed changes on both the body weight as well as lung histology patterns on HF female neonates resolved with age. As presented in *Section 5.3.9*, these sexual dimorphic alterations in the lung structure of the HF female offspring might have been actually caused by an altered content of nutrients and inflammatory factors in the mother's milk. Such alterations in the new-born feeding might be seen as a "second hit", which transiently affects both the offspring's global weight gain and local lung development. Cross-fostering HF offspring with LF dams could be employed to corroborate this hypothesis.

It has been demonstrated, that lungs of mice can actually completely regenerate and restore the lost lung volume and total alveolar area after a pneumonectomy within 21 days after the operation^[575]. This fact supports the hypothesis of a complete catch-up in alveolar development until the age of P70. It would be very intriguing to analyse possible overlaps between pathways of regeneration and the alveolarization catch-up observed after P15.

A drawback of this thesis was the small animal numbers employed. Larger sample sizes could have increased the power of the statistical tests and better displayed group variances. Even though the histological results suggested a possible delay in the final phase of the offspring's lung development, more studies would be needed in order to understand the consequences of parental obesity on the neonatal lung development. Additionally, since other parameters affected by parental diet could act as confounders and bias the results from lung morphology analyses, it would be advisable to take these into account in possible follow-up experiments. Examples of them include body weight and body size, but especially lung volume, size and weight – to which morphometry data could be normalized against.

Similarly to the contrast between the results presented in this thesis and the publication from Mayor et al.^[327], several inconsistent outcomes of parental obesity on the offspring's lung development have been published. I. .e in a study of rat offspring born to dams fed preconceptionally and during lactation with a HFD, Smoothy et al. could not show any difference in Lm measurements in offspring at two weeks of age^[349]. Interestingly, these authors rather detected a trend of lower Lm sizes on HF offspring. In spite of the low sample size ($n = 4-6$) implemented in the study, Smoothy et al. interpreted this measurement as a possible increase in lung development due to maternal HFD – an opposite effect to that displayed by Mayor et al.^[327]

In accordance with the results presented in this thesis, MacDonald et al.^[348] could not show in 2017 any gross differences in lung structure or airway thickness at ten weeks of age in a mouse model of maternal HFD either. In their study, no structural differences in the offspring's lung were observed, even after a second hit of HFD on the

offspring. Comparable negative results were presented also by Baack et al.^[541] in a rat model of maternal HFD. Even though the expression of surfactant protein B was reduced by maternal HFD feeding, no histological consequences were observed on the offspring's lung. These effects were analysed after birth and at three weeks of age.

Upadhyay et al. proposed 2019 to qualitatively have observed a detrimental effect of parental diet on the E18.5 rat foetal lung^[576]. Even though the study could show the positive effects of time restricted feeding on HFD dams in terms of improved placental oxidative stress, inflammation and apoptosis, the results presented did not confirm a detrimental effect of parental HFD on the offspring's lung development, especially long-term consequences, since the mentioned effects were not quantified in any form.

It is possible that the adverse effects of parental obesity on the offspring's lung observed in this thesis could have continued to be present or even worsen through a continued HFD after weaning, similarly to the results from Heyob et al. from 2019^[549]. In their study, these authors demonstrated a long-term impairment of the offspring's lung development. Not surprisingly, a second hit of HFD on the offspring presented an additive detrimental effect. Unfortunately, no information about the mouse strain employed was given by Heyob et al. (strictly speaking, this was not presented by Mayor et al.^[327] either, see article "*There is no such thing as a C57BL/6 mouse!*"^[522]). On the other hand, the effects proposed by Heyob et al.^[549] appeared to be rather dependent on the second HFD hit, since LF (CD, control diet) and HF offspring presented comparable phenotypes after being fed with HFD (so called CD/HFD and HFD/HFD). Finally, is also possible that the data presented by these authors did not meet the assumptions of the statistical algorithms selected, especially the assumption of normality and homogeneity of variances, possibly leading to spurious results.

Unfortunately, Mayor et al.^[327] did not analyse the lung morphometry from offspring older than two weeks of age. However, these authors propose an arrest of the structural and functional foetal lung maturation. Results from the present thesis, suggest rather a transient delay in alveolarization due to parental obesity. Since this process of alveolarization continues in mice until around P36^[61], morphometric studies between the first breath (P0) and P36 could help better understand effects of parental diet on the final phase of lung development.

Summarising the presented literature, it can be noticed, that studies of the effects of parental obesity on the offspring's lung development do not always lead to results congruent with the findings presented by Mayor et al. Not only differences in feeding regimes are observable among the studies, but importantly, the inconsistent employment of rodent genetic backgrounds. Further studies will be necessary to define a strain (e. g. C57BL/6N) and feeding rules for the reproducible study of the impact of parental obesity on the offspring's lung development. Such findings could then be applied to translational medicine research.

5.3.11 Impact of parental obesity on leukocyte frequencies of the P15 lung

With the aid of flow cytometry, it has been shown that murine alveolar macrophages appear in the alveolar space in the first week of life^[81]. During this time, AMs finish their maturation and differentiate into long-lived tissue macrophages in a process highly dependent on CSF2^[81]. In order to confirm the presence of mature AMs (ITGAX⁺, FCGR1⁺, SIGLECF⁺), and test for differences in frequencies and expression of surface markers by lung tissue leukocytes, whole lungs were analysed with a ten-colour flow cytometry panel.

The analysis of flow cytometry data sets by means of unsupervised machine learning lead to the recognition of eleven leukocyte (PTPRC⁺) populations (*Figure 20*). Among them, mature alveolar macrophages with characteristic expression of adult AM signature of ITGAX, ITGAM, FCGR1, SIGLECF was observed (*Figure 25B*). The expression levels of these markers were not affected by parental obesity. Neither were extreme contrasts measured in frequencies between parental diet groups (around 1 % difference, *Figure 21B*)) in comparison with other leukocyte populations.

Notwithstanding that discrepancies in the relative cell numbers of AMs were present between parental diet groups, their effects on the observed reduction in lung maturation and bulk gene expression in lung tissue were not directly measured. Since differences in the frequencies of AMs between parental diet groups were more pronounced in female (1.5 %) than in male (1.2 %) offspring (*Figure 21*)) and contributed differently to the overall contrast between diet groups (Person's residuals of 8.9 and 6.5, respectively), it could be imaginable that AMs might be partially responsible for the morphological and gene expression divergence detected between offspring groups after segregation by parental diet and sex. For this reason, the in-depth analysis of AMs between birth and weaning would be utterly valuable in the recognition of their contribution to the postnatal lung development.

The more granular analysis of individual cells, e. g. by means of single-cell mRNA sequencing, could better help identify functions of differentially observed leukocyte populations in the lungs of HF pups. This technique could help describe the possible contributions of the individual cell populations in the lung to the phenotypes observed in offspring at two weeks of age, especially the putative influence of AMs. Additionally, this method could aid in further subdivision of the populations recognized by flow cytometry and even spot other ones which were not detected with the antibody panel selected (ITGAM, ITGAX, CD24A, PTPRC, H2-AB1, LY6C, LY6G, FCGR1, SIGLECF), including epithelial cell populations.

A fascinating publication of such analysis was actually published a few months before the submission of this thesis^[577]. Employing single-cell mRNA sequencing, Domingo-Gonzalez et al. studied the homeostatic and immune-modulatory functions

of leukocytes in the developing mouse lung. They presented a single-cell atlas of the C57BL/6J lung immune compartments and examined the changes in leukocyte populations at several time points between an embryonic (E18.5) and a weaning (P21) age.

As expected, Domingo-Gonzalez et al. detected proliferative MFs during the embryonic age of the mice. They additionally could show a remarkable physical interaction between these MFs and the developing vasculature^[577]. After birth, this MF population faded and was replaced by a dynamic mixture of leukocytes that included different macrophage subtypes, dendritic cells, granulocytes, and lymphocytes, as detected during the flow cytometry examination of P15 lungs of this thesis. These authors corroborated the context-specific functions of MFs in tissue remodelling, angiogenesis, and immunity. Interestingly, they also recognised naive lymphocytes that populate the lung at birth, which comprised 60 % of total immune populations, in accordance to the results presented in this thesis.

Because of the limited resolution of the analysis of only ten surface markers, the most prominently affected cell population by parental obesity (called here “T-cells”) could not be further subdivided into other leukocyte subtypes. Following the results from Domingo-Gonzales et al.^[577], who could distinguish several lymphocyte populations, including innate lymphoid cells (ILC2s), natural killer (NK) cells, B-cells and T-cells, it could be argued that this “T-cell” population actually consists of several other leukocyte cell types, like ILC2s. Importantly, the observed lymphocytes by Domingo-Gonzales et al. maintained a naive phenotype until P21, which presented a skewed Th2 immunity. This findings overlapped with results from Saluzzo et al.^[165], who showed an AM M2 phenotype, promoted specially by ILC2-derived IL13 after the first breath.

Maternal obesity has been associated with increased susceptibility to wheezing in early childhood^[343,344] and asthma later in life^[345]. The link between maternal overnutrition and offspring’s innate airway hyperresponsiveness has been corroborated in rodent models.^[347,348] Eosinophils play a crucial role in the pathogenesis of asthma. Eosinophilic asthma develops from complex immunologic and pro-inflammatory mechanisms, mainly driven by Th2 responses (IL5, IL4, and IL13). Th2-mediated airway eosinophilia derives from a intricate interaction between the innate and adaptive immunity^[578]. Importantly, the activity of both type 2 helper T (Th2) and type 2 innate lymphoid (ILC2) cells play utterly important roles in the development of eosinophilic allergic and nonallergic asthma^[579].

Neither asthma nor eosinophils were the main research targets for this thesis, however, these results could hint on the possibility of the here implemented C57BL/6J mouse model of parental DIO in the study of asthma and other M2-related diseases. Lastly,

further analysis of leukocyte populations in the lungs from diet-treated parents between an embryonic age and weaning could further explain the contribution of individual immune cell types to the observed morphological and gene expression differences between parental diet groups at the age of P15.

5.3.12 No evidence of long-term pro-inflammatory AM priming at steady state by parental obesity

The main hypothesis in this thesis states that parental obesity can induce a pro-inflammatory priming of developing AMs. Here, the period of AM development was proposed to present a window of vulnerability for M1 programming effects by parental DIO. For this reason, pro-inflammatory consequences of the established parental DIO on the offspring lung were studied, with especial emphasis on AMs. An impact of parental obesity on AM maturation and priming was expected to be a long-lasting.

In order to analyse these long-term effects and prevent an uninterrupted direct influence from parental obesity through the placenta or the mothers milk, a young-adult mouse age^[365] of ten weeks was selected. Since diet alone did impact inflammatory dynamics in the lungs of obese mice (*Figure 8*), offspring were exclusively fed a LFD after weaning.

Under tissue homeostasis, at least 95% of AMs have shown to be of foetal origin in 14 months old mice^[123]. This further stresses the long life and self-renewal abilities of the AM niche^[81,91,95,96]. In the case that the hypothesised pro-inflammatory priming of AMs has taken place as a consequence of parental obesity during AM development – either perinatally through maternal obesity or prenatally through paternal obesity – primed AMs were expected to remain present in the airspace of HF offspring.

In order to test for the presence of priming effects on AMs at steady state, these TMs were isolated from LF and HF offspring, and their pro- (M1) and anti-inflammatory (M2) gene expression was analysed without any form of treatment (M0, *Figure 28*). During the isolation process of cells from the airspace of HF and LF control mice at steady state, no differences in cell numbers of AMs (*Figure 26*) nor any other cell type identified in the lung lumen (*Figure 27*) were detected between parental diet groups. This pointed to possible catch-up in leukocyte frequencies from the observed differences at an age of two weeks until P70.

It is possible, that priming effects from parental diet could have had an effect on the adhesion of AMs to the epithelium, leading to similar cell counts of lavaged cells. This however is unlikely, since AMs from P70 offspring at steady state did not show any sign of long-term impacts in their M1 nor M2 gene expression (M0 AMs, *Figure 28*). A similar analysis of whole lung leukocyte populations employed for the study of P15 offspring could be employed for P70 animals to corroborate this.

The absent differences in gene expression of M0 AMs as well as the comparable cell counts observed between LF and HF P70 offspring did not present any evidence of long-term pro-inflammatory AM priming at steady state by parental obesity.

5.4 LPS challenge of the offspring generation

5.4.1 No impact of obesity on alveolar macrophage M1 polarization

AM pro-inflammatory priming effects may remain “dormant” during homeostasis and become visible during inflammation of the lung. The hypothesis of this thesis additionally stated that pro-inflammatory AM priming can lead to long-lasting adverse functions in the offspring’s lung which might become apparent later in life through a defective inflammatory response to an LPS challenge. Therefore, AMs from P70 female and male offspring were analysed by qPCR after their initial *in vitro* polarization (“polarizability”).

Similarly to the polarization of AMs of parent animals, M1 activation of the offspring’s AMs *in vitro* proved to be very effective after just a 50 min incubation period in medium containing 1 $\mu\text{g}/\text{ml}$ LPS (*Appendix, Table 16*), presenting a clear increase in the expression of M1 markers compared to M0 AMs (p-value < 0.001). However, comparisons of gene expression between parental diet groups could not demonstrate any differences in mRNA quantities of M1 nor M2 markers.

5.4.2 Lung inflammatory responses in offspring of obese parents

In addition to the *in vitro* polarization of AMs, the lungs of P70 offspring were challenged *in vivo* by the mild model of endotoxin-induced acute inflammation discussed in *Section 5.2.1*. Contrary to the analyses during the challenge of parent animals (*Figure 8*), a more exhaustive interrogation in the P70 offspring could be made. For this, the dynamics of the seven pro-inflammatory cytokines CSF2, CXCL1, CXCL2, CXCL5, IL1b, IL1a and TNF as well of SAA3 were analysed at time points 0, 6, 24, 48 and 72 hours post instillation (*Figure 24*). Additionally, the cell populations in the airspace during the challenge were not examined by manual counting, but by means of flow cytometry (*Figure 26* and *Figure 27*).

During the *in vivo* challenge of offspring animals with endotoxin, the analysis of cytokine secretion into the airspace demonstrated two different waves of pro-inflammatory factors. The first one presented a very quick response, with highest concentrations at 6 h after instillation. It is however possible, that even higher concentrations were present in the lung during earlier time points of the challenge.

Especially for TNF, a strong peak at 6 h was observed. CXCL1, CXCL2 and IL1a (and IL1b) demonstrated similar dynamics with peak concentrations at 6 h. On the other hand, CXCL5 and SAA3 reached their highest concentration not at 6 h, but at 24 h after instillation (*Figure 24*).

Concentrations of the cytokine IL1b remained within the detection limit of the test (*Figure 24*). These results appeared to accord with previous publications showing that LPS induced acute lung inflammation did not induce increases of IL1b in the air space^[417]. Since the active form of IL1b was targeted by antibodies of the ELISA kit, these results could suggest that inflammasomes (Caspase 1-activating multicomplex proteins) are not involved in the LPS-induced acute lung inflammation. This absence of inflammasome involvement was previously proposed by Dagvadorj et al. in 2015^[417]. Interestingly, experiments from Moreland et al. from 2001 additionally suggested that IL1b is not an essential factor for the inflammatory response towards LPS in the lung^[580].

On the other hand, these authors measured an increased gene expression after LPS inhalation. In this thesis, the comparison between time points 0 h and 6 h (*Figure 24*) did indeed display higher concentrations of the bioactive form of IL1b after LPS instillation ($p = 0.013$, not split by parental diet). It would be interesting to analyse BALF samples isolated with lower amounts of PBS or by means of other detections systems with higher sensitivity. This could help test for the involvement of the inflammasome during an endotoxin-induced acute lung inflammation and distinguish possible differences in concentrations of this cytokine in the lung due to parental diet effects as well as its dynamics.

The family of CXC chemokines constitute essential ligands for neutrophil influx into inflamed tissues^[581]. Six hours after LPS instillation during the *in vivo* pro-inflammatory lung challenge, HF male offspring presented a trend of lower concentrations of the chemokine CXCL2 compared to the LF control group (*Figure 24*). This tendency suggested the presence of a possible long-term alteration of AMs by parental diet, as presented in the main hypothesis. Importantly, a similar trend was also present for the Cxcl2 expression in M1 activated AMs from both male and female offspring (*Figure 29*) and the number of neutrophils recruited to the airspace of challenged P70 offspring (*Figure 26*).

The neutrophil-recruiting chemokine with the highest (not statistically significant) difference in concentration between the HF and LF groups was CXCL5, followed by CXCL2 and CXCL1. While the chemokine CXCL5 is expressed by AECII cells^[582], CXCL1^[583] and CXCL2^[584] are mainly expressed by AMs (and neutrophils)^[585] after a pro-inflammatory stimulation. A test revealed sample sizes needed of 6 and 10 to reach a power of 80% for CXCL5 and CXCL2, respectively.

These observations were unexpected, since the hypothesis proposed in this thesis was of an increased inflammatory response as a consequence to pro-inflammatory AM priming by parental obesity. Additionally, MacDonald et al. could demonstrate in a study from 2017^[348] that offspring born to mothers on a hypercaloric diet present not

only elevated airway resistance, but, importantly, increased neutrophil infiltrates at ten weeks of age as well as increased levels of total BALF protein. In line with the hypothesis presented on this thesis, results from MacDonald et al. suggest an increased baseline presence of inflammatory cells in the air space and compromised air-tissue integrity in the lung.

Similar to the results from the *in vitro* M1 polarization of their AMs, the statistical analyses of data collected during the *in vivo* challenge of P70 male offspring displayed no differences in the concentrations of the inflammatory factors secreted into the airspace of the lung between parental-diet groups at any time point. Together with the negative results from the qPCR analyses of AMs at steady state, these data could not corroborate the hypothesis of a pro-inflammatory AM priming by parental obesity. Nonetheless, the tendencies observed during both the *in vitro* and *in vivo* pro-inflammatory challenges led to question these negative results. Higher animal numbers, but also the use of other mouse strains with an alternative genetic background could help definitely accept or reject the hypothesis presented here.

5.4.3 Cellular dynamics during the *in vivo* LPS challenge of the offspring generation

Looking at the cellular fractions recognized during the lung inflammatory challenge, it could be argued that two of the populations inferred by the analysis of the flow cytometry data could not be present in the alveoli of the lungs: interstitial MFs and resident monocytes. Both cell types are expected to reside within the interstitium of the lung^[586]. Historically speaking, the characterization and naming of different cell populations has not only been done based on their histological localization at steady state, but also on their function and expression of biomarkers.

The definition of cells populations by flow cytometry alone is exclusively based on the expression of such biomarkers. For the identification of the different cell types presented in this work, the expression patterns of lung cells previously described by Misharin et al.^[217], Ellis et al.^[367] and Yu et al.^[368] were employed (*Figure 25B*). Interestingly, both interstitial MFs and resident monocytes displayed similar migration dynamics into the airspace of the lung, presenting a peak in cell numbers at around 48 h after instillation (*Figure 26* and *Figure 27*). It would be interesting to trace these two cell types to better understand their function and fate during lung inflammation. The presence of these two leukocyte populations in the lung lumen is most likely of ephemeral nature. While monocytes probably undergo apoptosis and are uptaken by AMs, mature interstitial macrophages could rather differentiate into AMs or migrate back into the interstitium. Additionally, while it is possible that their presence of resulted from an active migration from the interstitium into the airspace, it is also likely that these cells were washed out of the LPS-damaged tissue during lavage.

The dynamics of dendritic cells (DCs) was also interesting to observe. While cell numbers of ITGAM⁻ DCs remained relative stable, ITGAM⁺ DCs reached a peak 48 h after instillation with LPS (*Figure 27*). ITGAM⁺ DCs are known to migrate from the blood into the lung in response to *Cryptococcus neoformans*^[587] as well as to influenza^[588] or respiratory syncytial virus (RSV)^[589] infections. This migration takes course in a CCR2-dependent manner^[590]. It has been shown that these cells play an important role in the clearance of pathogens^[587]. The measured dynamics of ITGAM⁺ DCs took place in accordance with previous literature.

The observed dynamics of the 14 leukocyte populations detected by flow cytometry during the LPS challenge support a correct differentiation of the cell types in the airspace by means of unsupervised clustering methods. Even though such methods have proven^[374] to outperform manual gating of cell populations in terms of reproducibility and accuracy, especially for the recognition of rare cell populations^[375], the fidelity of these methods depend on expert knowledge of the analyst. Such expert knowledge is crucial for the correct assignment of cell type names to the identified clusters of cells. Alternative methods include supervised and semi-supervised machine learning methods^[591]. Recent improvements in computational efficiency can even enable a fast “online” inference of cell types and aid cell sorting, e. g. via deep learning^[592]. A downside of supervised methods however, is the need of rather big datasets in order to train the models for achieving adequate prediction performance^[593].

In order to corroborate the accuracy of the inferred cell types, both the comparison with cell numbers from manual gating (*Figure 31*) as well as cell sorting experiments were performed. The analysis of flow cytometry data by means of manual gating resulted in very similar numbers to the ones obtained by means of unsupervised machine learning algorithms (data not shown). This was especially the case for cell populations with high numbers in the airspace. AMs and neutrophils, the two most prominent cell types in the alveoli during the LPS challenge, were detected with a similar fidelity with both methods. The overlap of counts between the semiautomated method and the manual gating process was lower for smaller cell populations, since their correct manual detection was difficult. This comparison corroborated the superior performance of unsupervised clustering for recognizing rare cell populations compared to manual gating of flow cytometry data.

Unluckily, the characterization of cell types by means of cell sorting for the validation of detection of leukocytes in the airspace was not possible. Two sources of cellular stress hindered the successful sorting of whole lung cells: the stress caused by the lung dissociation (treatment with the protease and mechanical dissociation through a filter) as well as the mechanical shear burden implicated by the use of a 100 μm nozzle. A reduction of time between dissociation of the lung tissue and cell sorting as well as the use of a 120 μm nozzle for cell sorting to reduce shear forces on sorted cells could help in future implementations of the manual gating strategy presented in this thesis for sorting experiments of lung leukocytes.

6 Outlook

The main hypothesis in this work suggested that the presence of a pro-inflammatory developmental microenvironment induced by parental obesity can lead to an altered AM development with pro-inflammatory programming consequences (priming). This thesis was based on previous studies showing that metabolic and inflammatory changes brought about by maternal DIO can extend to the placenta and expose the developing foetus to a pro-inflammatory environment. This milieu is characterised by elevated levels of free fatty acids^[322] and placental macrophage activation, displaying increased cytokine (Tnf, Il1b, Il6, Nlrp3, and Il10) expression^[324,326–328]. Offspring to obese dams present higher abundance of pro-inflammatory cytokines (IL6, IL17A, and IFN γ) in the circulation^[324] as well as an increased expression of Il1b in the lung^[354] at a foetal age. Most importantly, Mayor et al.^[327] showed in a mouse model of maternal DIO an impaired foetal lung development with reduced structural maturation both at an embryonic age as well two weeks after birth.

The hypothesis presented here was centred around AM, since studies on developmental immunotoxicity^[594] suggest a peculiar sensitivity of macrophage populations to early life insults^[210]. As presented in *Section 1.4*, AMs play multiple crucial trophic and immune roles during and after lung development in order to maintain tissue homeostasis. Therefore, AMs might act as central players in the impairment of the lung development in offspring. Taking into account the long life of AMs^[123,595], the isolated nature of this TM niche^[99], and their self-renewal capabilities^[81], pro-inflammatory priming effects through parental DIO were expected to persist until a young-adult mouse age^[365] of ten weeks, even after feeding HF offspring exclusively a control LF diet after weaning.

The experimental results presented in this thesis could not support the main hypothesis of long-term pro-inflammatory priming effects of parental DIO on AMs of HF offspring mice. These analyses did not provide evidence of consequences from parental DIO on an endotoxin-induced acute inflammatory challenge of the ten-week old offspring's lung nor on the *in vitro* pro-inflammatory polarization of their AMs. Importantly, the assumptions this hypothesis was based on were not met. No impact on the pro-inflammatory gene expression in placentas from obese dams nor in the lungs of their offspring were found. Consequently, the premise of a pro-inflammatory environment during foetal AM development was not fulfilled.

To our knowledge, this is the first time a mild intratracheal LPS challenge is used for the analysis of transgenerational diet-induced effects on the immune system of the lung. Even though a limited number of animals were available for the experiments presented in this thesis, they helped making very interesting findings. A peculiar sexual

dimorphism could be recognized accompanying the outcomes observed from direct and intergenerational diet-induced obesity. Further studies on sex-specific consequences of (parental) DIO could help better understand possible protective factors against the repercussions of obesity.

A transient delay in the final alveolarization phase of the HF offspring's lung was detected at two weeks of age. This delay was exclusive to the early postnatal phase and was accompanied by differences in gene expression of inflammatory and developmental markers as well as altered leukocyte population frequencies in the lung. Since these effects were not observed at the embryonic nor at the young-adult mouse age selected, it could be proposed, that an altered composition of the maternal milk might have triggered these consequences. Cross-fostering HF offspring with LF dams could be employed to corroborate this hypothesis. A more granular study of the process of alveolarization in offspring between their first breath and 36 days after birth^[61] could also be performed to better understand effects of parental obesity on this final phase of lung development. Moreover, the detailed analysis of leukocyte populations in the offspring lung during this time, e. g. by means of single-cell mRNA analysis might better explain the physiological consequences of the differences observed in cell frequencies between parental diet groups.

As mentioned in *Section 5.3.1*, differences between the experimental designs, especially differences in the setup between this thesis and the work from Mayor et al.^[327] could explain discrepancies in the results obtained between the two works. Not only differences in diet regimes, but most importantly possible differences in the genetic background of the mice employed could help identify the specific (genetic) factors which prevented placental and foetal inflammation.

The final aim of this study was not only to gain a better understanding of intergenerational inflammatory consequences of parental DIO on mice, but support future translational medicine studies to ultimately improve human health, quality of life and longevity. Further research in the inter- and transgenerational effects of developmental origins of health and disease as well as the effective communication of past and future research outcomes on the topic, especially to the general public, could help motivate the adoption of a healthier life style and help live a more fulfilling life thanks to well-informed decisions made with future generations in mind.

Appendix

This section contains tables and figures supplementary to the data already presented in the main results part of this thesis.

In vitro alveolar macrophage polarization with LPS

Table 14: Assessment of gene expression differences after AM M1 polarization by qPCR. AMs from untreated mice (n = 5-6) at 25 weeks of age were isolated by bronchoalveolar lavage and purified by adherence. Cells either M1 polarized (classical/pro-inflammatory AMs) with 1 µg/ml LPS for 50 min or incubated in MH-S medium (M0 AMs). Gene expression of pro (M1: Cxcl2, Il12b, Il1b, Nlrp3, Saa3, Tnf) and anti-inflammatory (M2: Chil3, Pparg) markers was analysed by qPCR. Polarization of AMs was successful with clear increases in gene expression of M1 markers. Welch two sample t-test on log extsubscript10-transformed expression data with Bonferroni p-value correction for multiple testing (8 comparisons): *** p.adj < 0.001.

Gene	Marker	mean.M0	mean.M1	sd.M0	sd.M1	p.value	p.adj	sig
Nlrp3	M1	0.13	5.28	0.04	1.13	2.69E-38	2.15E-37	***
Il1b	M1	0.05	52.11	0.03	16.17	8.01E-34	6.41E-33	***
Tnf	M1	0.37	43.66	0.22	11.23	1.84E-32	1.47E-31	***
Il12b	M1	1.37E-3	0.72	1.01E-3	0.42	4.02E-30	3.21E-29	***
Saa3	M1	5.76E-3	1.66	7.37E-3	0.76	7.10E-30	5.68E-29	***
Cxcl2	M1	0.2	160.49	0.18	35.01	5.92E-27	4.74E-26	***
Pparg	M2	0.56	0.42	0.24	0.1	2.10E-2	0.168	
Chil3	M2	92.68	98.63	26.46	19.16	0.273	1	

Digital image analysis of offspring's lung morphology

Table 15: Quantification of lung morphology parameters by digital image analysis. Images from HE stained FFPE lung slides from E18.5, P15 and P70 offspring mice were acquired and automatically segmented with Definiens Developer XD2 software at the the Core Facility Pathology and Tissue Analytics ($n_{E18.5} = 9$, $n_{P15} = 10$, $n_{P70} = 5-7$). No signs of disturbances of the morphology of the offspring's lungs due to parental diet could be observed. Mean and standard deviation for each diet, age and sex group. Wilcoxon rank sum test with Benjamini-Hochberg p-value correction for multiple testing.

Age	Sex	Parameter	LF	HF	p.value	p.adj
E18.5	Female	Alveolar area [μm^2]	4.55E5 \pm 1.37E5	4.21E5 \pm 8.92E4	0.79	0.92
E18.5	Female	Border septum-air [μm]	1.06E5 \pm 2.57E4	1.03E5 \pm 1.64E4	0.79	0.92
E18.5	Female	Lung area [μm^2]	2.12E6 \pm 4.14E5	2.20E6 \pm 2.51E5	0.6	0.83
E18.5	Female	n alveoli	519.11 \pm 128.92	499.89 \pm 84.93	0.69	0.9
E18.5	Female	Ratio air/septum	0.27 \pm 0.05	0.24 \pm 0.05	0.19	0.39
E18.5	Female	Septal area [μm^2]	1.67E6 \pm 2.98E5	1.78E6 \pm 2.16E5	0.54	0.77
E18.5	Male	Alveolar area [μm^2]	4.72E5 \pm 1.38E5	3.94E5 \pm 5.75E4	0.29	0.58
E18.5	Male	Border septum-air [μm]	1.16E5 \pm 2.29E4	1.00E5 \pm 8.18E3	0.16	0.38
E18.5	Male	Lung area [μm^2]	2.11E6 \pm 2.59E5	2.19E6 \pm 2.37E5	0.72	0.9
E18.5	Male	n alveoli	523.78 \pm 67.4	498.89 \pm 51.65	0.19	0.39
E18.5	Male	Ratio air/septum	0.29 \pm 0.08	0.22 \pm 0.04	0.08	0.23
E18.5	Male	Septal area [μm^2]	1.64E6 \pm 1.71E5	1.80E6 \pm 2.34E5	0.16	0.38
P15	Female	Alveolar area [μm^2]	1.50E7 \pm 1.21E6	1.40E7 \pm 2.24E6	0.38	0.7
P15	Female	Border septum-air [μm]	2.63E6 \pm 4.18E5	2.32E6 \pm 3.17E5	0.03	0.12
P15	Female	Lung area [μm^2]	2.77E7 \pm 2.19E6	2.50E7 \pm 2.44E6	0.03	0.12
P15	Female	n alveoli	1.20E4 \pm 2.74E3	1.04E4 \pm 1.87E3	0.03	0.12
P15	Female	Ratio air/septum	1.19 \pm 0.15	1.28 \pm 0.21	0.43	0.7
P15	Female	Septal area [μm^2]	1.27E7 \pm 1.52E6	1.10E7 \pm 7.41E5	0.01	0.12
P15	Male	Alveolar area [μm^2]	1.26E7 \pm 1.10E6	1.40E7 \pm 1.25E6	0.02	0.12
P15	Male	Border septum-air [μm]	2.18E6 \pm 4.18E5	2.18E6 \pm 4.33E5	0.91	0.99
P15	Male	Lung area [μm^2]	2.42E7 \pm 2.08E6	2.48E7 \pm 1.83E6	0.52	0.77
P15	Male	n alveoli	1.00E4 \pm 2.64E3	9.26E3 \pm 2.55E3	0.43	0.7
P15	Male	Ratio air/septum	1.1 \pm 0.14	1.31 \pm 0.13	0.01	0.12
P15	Male	Septal area [μm^2]	1.16E7 \pm 1.40E6	1.08E7 \pm 9.60E5	0.12	0.34
P70	Female	Alveolar area [μm^2]	1.47E7 \pm 5.83E5	1.66E7 \pm 1.49E6	0.04	0.12
P70	Female	Border septum-air [μm]	2.91E6 \pm 1.24E5	3.25E6 \pm 1.76E5	0.02	0.12
P70	Female	Lung area [μm^2]	2.72E7 \pm 1.17E6	3.03E7 \pm 1.97E6	0.04	0.12
P70	Female	n alveoli	1.49E4 \pm 870.46	1.65E4 \pm 895.68	0.02	0.12
P70	Female	Ratio air/septum	1.18 \pm 0.07	1.21 \pm 0.07	0.4	0.7
P70	Female	Septal area [μm^2]	1.25E7 \pm 7.85E5	1.37E7 \pm 5.15E5	0.04	0.12
P70	Male	Alveolar area [μm^2]	1.83E7 \pm 1.81E6	1.86E7 \pm 2.32E6	0.72	0.9
P70	Male	Border septum-air [μm]	3.69E6 \pm 2.86E5	3.59E6 \pm 3.44E5	0.52	0.77
P70	Male	Lung area [μm^2]	3.15E7 \pm 2.68E6	3.19E7 \pm 2.63E6	1	1
P70	Male	n alveoli	1.70E4 \pm 1.04E3	1.64E4 \pm 1.71E3	0.83	0.93
P70	Male	Ratio air/septum	1.39 \pm 0.09	1.39 \pm 0.18	0.94	1
P70	Male	Septal area [μm^2]	1.32E7 \pm 1.03E6	1.34E7 \pm 7.99E5	1	1

Inflammatory dynamics during LPS-induced acute lung inflammation in P70 male offspring

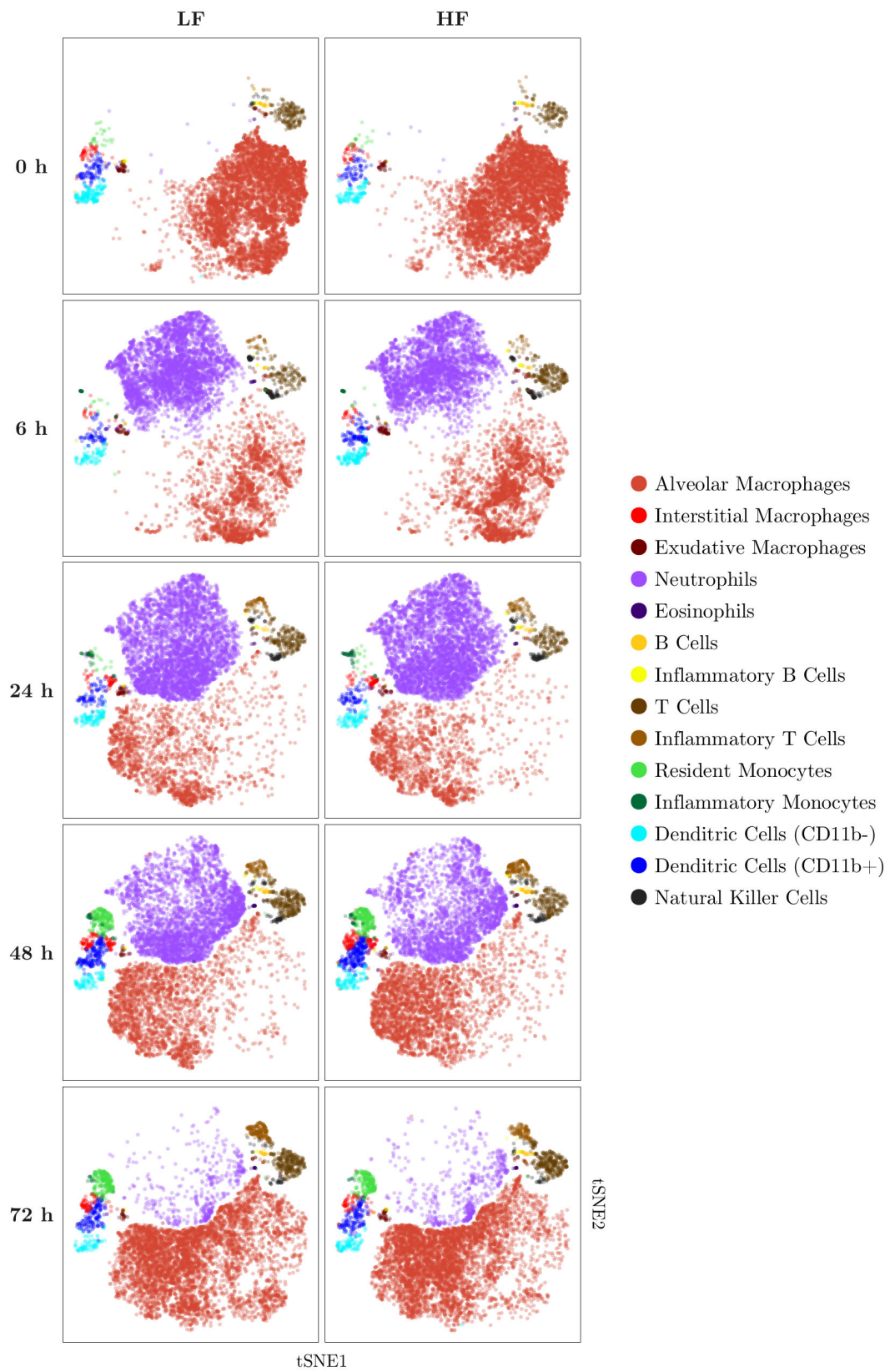


Figure 30: Visualization of inflammatory cell dynamics in form of two-dimensional embeddings. Cell populations in the lavage of male animals were identified based on the expression of the antigens ITGAM, ITGAX, FCGR1, H2-AB1, SIGLECF, LY6C and LY6G (see expression pattern in *Figure 25*) using unsupervised machine learning. Lavage cells (each dot represents a cell) were separated based on diet and time point of the lung inflammation in order to better recognize cell dynamics on two-dimensional tSNE projections.

***In vitro* M1 polarization of alveolar macrophages from P70 offspring**

Table 16: Effective AM polarization by *in vitro* incubation with LPS. AMs from untreated mice at 10 weeks of age (P70) were isolated by bronchoalveolar lavage and purified by adherence. Pooled cells (2 animals per pool) were either M1-polarized (classical/pro-inflammatory AMs) with 1 $\mu\text{g/ml}$ LPS for 50 min or incubated in MH-S medium (M0 AMs). Gene expression of pro- (M1: Il6, Nlrp3, Cxcl2, Ptsg2, Ccl2, Il1a, Il1b, Il12b) and anti-inflammatory (M2: Retnla, Arg1, Pparg, Chil3) markers was analysed by qPCR. An effective polarization of AMs with clear increases in gene expression of M1 markers was achieved by incubation with LPS ($n = 16$). Welch two sample t-test on \log_{10} -transformed expression data with Bonferroni p-value correction for multiple testing (12 comparisons): *** p.adj < 0.001.

Gene	Marker	mean.M0	mean.M1	sd.M0	sd.M1	p.value	p.adj	sig
Cxcl2	M1	0.05	88.09	0.01	20.26	3.21E-38	3.85E-37	***
Il1b	M1	0.04	89.66	0.01	19.42	4.37E-36	5.24E-35	***
Ptsg2	M1	5.78E-3	5.79	1.65E-3	1.2	3.43E-33	4.12E-32	***
Nlrp3	M1	0.06	3.07	0.01	0.31	6.11E-31	7.34E-30	***
Il12b	M1	4.84E-4	0.96	3.17E-4	0.58	2.77E-25	3.32E-24	***
Ccl2	M1	2.94E-4	0.04	8.65E-5	0.02	2.28E-24	2.74E-23	***
Il1a	M1	0.46	86.57	0.04	21.82	4.15E-24	4.98E-23	***
Il6	M1	6.38E-4	11.16	1.23E-3	2.73	1.42E-18	1.70E-17	***
Arg1	M2	1.58E-4	5.58E-5	8.87E-5	1.94E-5	7.77E-5	9.32E-4	***
Pparg	M2	0.41	0.5	0.04	0.11	5.55E-3	0.067	
Retnla	M2	1.49E-4	4.22E-4	2.37E-4	6.61E-4	0.056	0.677	
Chil3	M2	20.77	22.57	4.34	4.66	0.241	1	

Manual gating strategy for flow cytometric immunophenotyping of lung cells

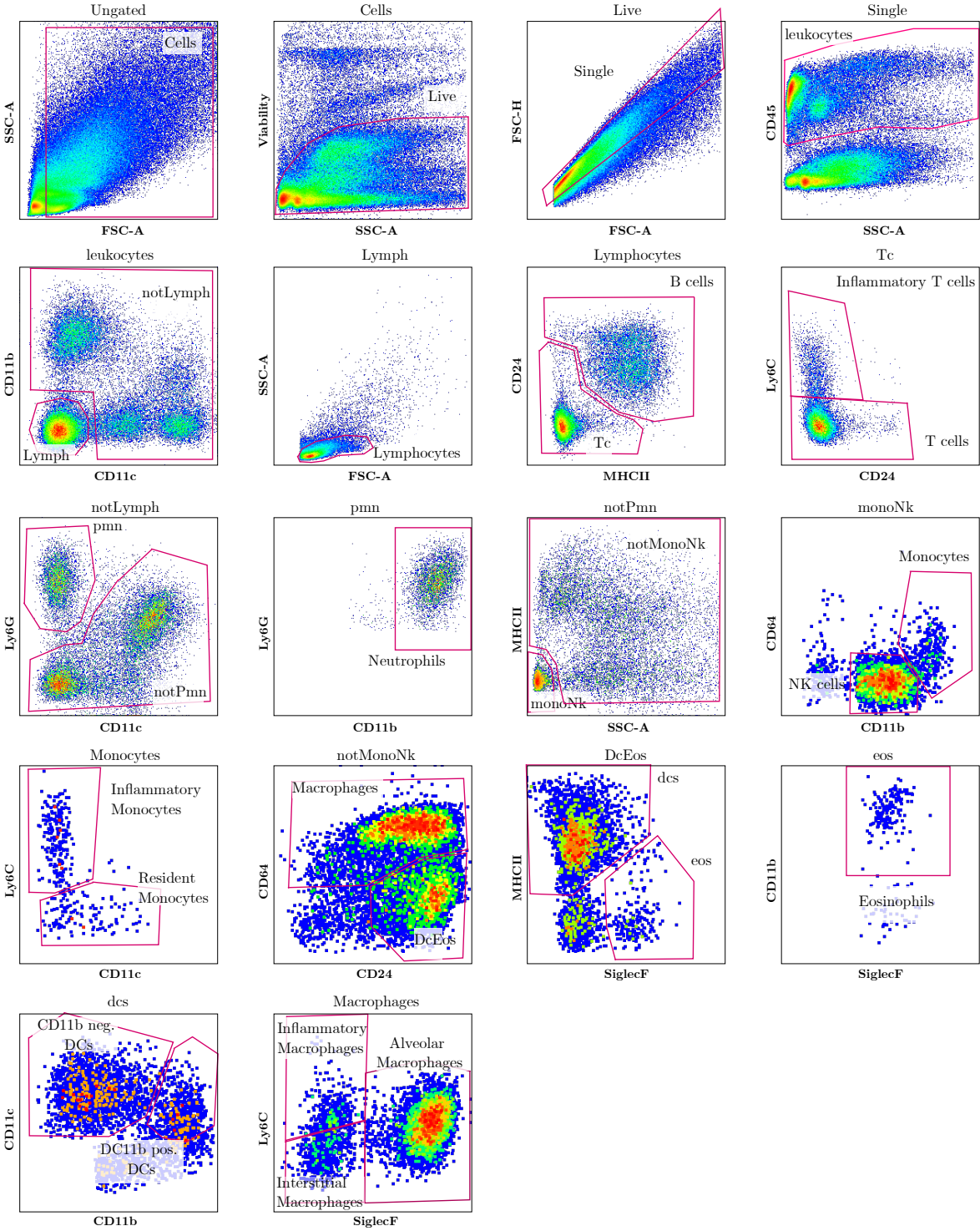


Figure 31: Manual gating strategy for flow cytometric immunophenotyping of lung cells

References

- 00 1. Haugen *et al.* (2015). Evolution of DOHaD: the impact of environmental health sciences. *Journal of Developmental Origins of Health and Disease*. DOI:10.1017/s2040174414000580.
2. Gillman *et al.* (2007). Meeting Report on the 3rd International Congress on Developmental Origins of Health and Disease (DOHaD). *Pediatric Research*. DOI:10.1203/pdr.0b013e3180459fcd.
3. Schug *et al.* (2013). PPTOX III: Environmental Stressors in the Developmental Origins of Disease—Evidence and Mechanisms. *Toxicological Sciences*. DOI:10.1093/toxsci/kfs267.
4. Hales & Barker (2001). The thrifty phenotype hypothesis. *British Medical Bulletin*. DOI:10.1093/bmb/60.1.5.
5. Michels (2017). Developmental plasticity: Friend or foe? *Evolution, medicine, and public health*. DOI:10.1093/emph/eox022.
6. Lucas (1991). Programming by early nutrition in man. *The childhood environment and adult disease* 1991, 38–55.
7. Barker *et al.* (1993). Fetal nutrition and cardiovascular disease in adult life. *The Lancet*. DOI:10.1016/0140-6736(93)91224-a.
8. Tamashiro & Moran (2010). Perinatal environment and its influences on metabolic programming of offspring. *Physiology & Behavior*. DOI:10.1016/j.physbeh.2010.04.008.
9. Eriksson *et al.* (1999). Catch-up growth in childhood and death from coronary heart disease: longitudinal study. *BMJ*. DOI:10.1136/bmj.318.7181.427.
10. Eriksson *et al.* (2001). Early growth and coronary heart disease in later life: longitudinal study. *BMJ*. DOI:10.1136/bmj.322.7292.949.
11. Singhal *et al.* (2003). Low nutrient intake and early growth for later insulin resistance in adolescents born preterm. *The Lancet*. DOI:10.1016/s0140-6736(03)12895-4.
12. Lane *et al.* (2015). Peri-conception parental obesity, reproductive health, and transgenerational impacts. *Trends in Endocrinology & Metabolism*. DOI:10.1016/j.tem.2014.11.005.
13. Huypens *et al.* (2016). Epigenetic germline inheritance of diet-induced obesity and insulin resistance. *Nature Genetics*. DOI:10.1038/ng.3527.
14. Mcmillen & Robinson (2005). Developmental Origins of the Metabolic Syndrome: Prediction, Plasticity, and Programming. *Physiological Reviews*. DOI:10.1152/physrev.00053.2003.
15. Godfrey *et al.* (2007). Epigenetic Mechanisms and the Mismatch Concept of the Developmental Origins of Health and Disease. *Pediatric Research*. DOI:10.1203/pdr.0b013e318045bedb.
16. Ravelli *et al.* (1976). Obesity in Young Men after Famine Exposure in Utero and Early Infancy. *New England Journal of Medicine*. DOI:10.1056/nejm197608122950701.
17. Stanner *et al.* (1997). Does malnutrition in utero determine diabetes and coronary heart disease in adulthood? Results from the Leningrad siege study, a cross sectional study. *BMJ : British Medical Journal*. DOI:10.1136/bmj.315.7119.1342.
18. Wadhwa *et al.* (2009). Developmental origins of health and disease: brief history of the approach and current focus on epigenetic mechanisms. *Seminars in reproductive medicine*. DOI:10.1055/s-0029-1237424.
19. Rosenberg (2018). Baby brains reflect maternal inflammation. *Nature Neuroscience*. DOI:10.1038/s41593-018-0134-0.
20. Mazumder *et al.* (2010). Lingering prenatal effects of the 1918 influenza pandemic on cardiovascular disease. *Journal of Developmental Origins of Health and Disease*. DOI:10.1017/s2040174409990031.
21. Mlakar *et al.* (2016). Zika Virus Associated with Microcephaly. *New England Journal of Medicine*.

DOI:10.1056/nejmoa1600651.

22. Harris & Seckl (2011). Glucocorticoids, prenatal stress and the programming of disease. *Hormones and Behavior*. DOI:10.1016/j.yhbeh.2010.06.007.
23. Giussani & Davidge (2013). Developmental programming of cardiovascular disease by prenatal hypoxia. *Journal of Developmental Origins of Health and Disease*. DOI:10.1017/s204017441300010x.
24. Frideric et al. (1986). Effects of prenatal stress on vulnerability to stress in prepubertal and adult rats. *Physiology & Behavior*. DOI:10.1016/0031-9384(86)90172-1.
25. Niknazar et al. (2013). Parents' adulthood stress induces behavioral and hormonal alterations in male rat offspring. *Behavioural Brain Research*. DOI:10.1016/j.bbr.2013.05.026.
26. Eskenazi et al. (2007). Organophosphate Pesticide Exposure and Neurodevelopment in Young Mexican-American Children. *Environmental Health Perspectives*. DOI:10.1289/ehp.9828.
27. Timms et al. (2005). Estrogenic chemicals in plastic and oral contraceptives disrupt development of the fetal mouse prostate and urethra. *Proceedings of the National Academy of Sciences of the United States of America*. DOI:10.1073/pnas.0502544102.
28. Ho et al. (2006). Cancer Research. *Cancer Res*. DOI:10.1158/0008-5472.can-06-0516.
29. Gilbert & Grant-Webster (1995). Neurobehavioral effects of developmental methylmercury exposure. *Environmental health perspectives*. DOI:10.1289/ehp.95103s6135.
30. Guilarte et al. (2003). Environmental enrichment reverses cognitive and molecular deficits induced by developmental lead exposure. *Annals of neurology*. DOI:10.1002/ana.10399.
31. Koopman-Elseboom et al. (1996). Effects of Polychlorinated Biphenyl/Dioxin Exposure and Feeding Type on Infants' Mental and Psychomotor Development. *Pediatrics*.
32. Broberg et al. (2014). Arsenic exposure in early pregnancy alters genome-wide DNA methylation in cord blood, particularly in boys. *Journal of Developmental Origins of Health and Disease*. DOI:10.1017/s2040174414000221.
33. Burdge et al. (2007). Dietary protein restriction of pregnant rats in the F0 generation induces altered methylation of hepatic gene promoters in the adult male offspring in the F1 and F2 generations. *The British journal of nutrition*. DOI:10.1017/s0007114507352392.
34. Galler & Rabinowitz (2014). The intergenerational effects of early adversity. *Progress in molecular biology and translational science*. DOI:10.1016/b978-0-12-800977-2.00007-3.
35. Nowacka-Woszek et al. (2019). Hepatic DNA methylation and expression profiles under prenatal restricted diet in three generations of female rat fetuses. *PLoS ONE*. DOI:10.1371/journal.pone.0215471.
36. Rousseau-Ralliard et al. (2019). Effects of first-generation in utero exposure to diesel engine exhaust on second-generation placental function, fatty acid profiles and foetal metabolism in rabbits: preliminary results. *Scientific Reports*. DOI:10.1038/s41598-019-46130-x.
37. Gilliland, Frank D. Li, Yu-Fen Peters (2001). Effects of Maternal Smoking during Pregnancy and Environmental Tobacco Smoke on Asthma and Wheezing in Children. *American Journal of Respiratory and Critical Care Medicine*. DOI:10.1164/ajrccm.163.2.2006009.
38. Milner et al. (2007). The effects of antenatal smoking on lung function and respiratory symptoms in infants and children. *Early Human Development*. DOI:10.1016/j.earlhumdev.2007.07.014.
39. Maritz & Harding (2011). Life-long Programming Implications of Exposure to Tobacco Smoking and Nicotine Before and Soon After Birth: Evidence for Altered Lung Development. *International Journal of Environmental Research and Public Health*. DOI:10.3390/ijerph8030875.
40. Beyer et al. (2009). Maternal smoking promotes chronic obstructive lung disease in the offspring as adults. *European Journal of Medical Research*.

DOI:10.1186/2047-783x-14-s4-27.

41. Cunha *et al.* (2005). Risk Factors for Bronchopulmonary Dysplasia in very Low Birth Weight Newborns Treated with Mechanical Ventilation in the First Week of Life. *Journal of Tropical Pediatrics*. DOI:10.1093/tropej/fmi051.
42. Keszler & Sant'Anna (2015). Mechanical Ventilation and Bronchopulmonary Dysplasia. *Clinics in Perinatology*. DOI:10.1016/j.clp.2015.08.006.
43. Dockery *et al.* (1989). Effects of Inhalable Particles on Respiratory Health of Children. *American Review of Respiratory Disease*. DOI:10.1164/ajrccm/139.3.587.
44. Schwartz (1989). Lung function and chronic exposure to air pollution: A cross-sectional analysis of NHANES II. *Environmental Research*. DOI:10.1016/s0013-9351(89)80012-x.
45. Gauderman *et al.* (2004). The Effect of Air Pollution on Lung Development from 10 to 18 Years of Age. *New England Journal of Medicine*. DOI:10.1056/nejmoa040610.
46. Gehr *et al.* (1978). The normal human lung: ultrastructure and morphometric estimation of diffusion capacity. *Respiration Physiology*. DOI:10.1016/0034-5687(78)90104-4.
47. Storey & Staub (1962). Ventilation of terminal air units. *Journal of applied physiology*. DOI:10.1152/jappl.1962.17.3.391.
48. Clements (1957). Surface tension of lung extracts. *Proceedings of the Society for Experimental Biology and Medicine*. *Society for Experimental Biology and Medicine (New York, N.Y.)*. DOI:10.3181/00379727-95-23156.
49. Sano & Kuroki (2005). The lung collectins, SP-A and SP-D, modulate pulmonary innate immunity. DOI:10.1016/j.molimm.2004.07.014.
50. Schittny & Burri (2007). Development and growth of the lung. <https://boris.unibe.ch/id/eprint/20368>.
51. Swarr & Morrisey (2015). Lung Endoderm Morphogenesis: Gasping for Form and Function. *Annual Review of Cell and Developmental Biology*. DOI:10.1146/annurev-cellbio-100814-125249.
52. Merkus *et al.* (1996). Human lung growth: A review. DOI:10.1002/(sici)1099-0496(199606)21:6<383::aid-ppul6>3.0.co;2-m.
53. Burri (John Wiley & Sons, Inc., 2011). Development and Growth of the Human Lung. in *Comprehensive physiology*. DOI:10.1002/cphy.cp030101.
54. Barré *et al.* (2016). The total number of acini remains constant throughout postnatal rat lung development. *American Journal of Physiology - Lung Cellular and Molecular Physiology*. DOI:10.1152/ajplung.00325.2016.
55. Bachofen & Weibel (1977). Alterations of the gas exchange apparatus in adult respiratory insufficiency associated with Septicemia. *American Review of Respiratory Disease*. DOI:10.1164/arrd.1977.116.4.589.
56. Rogelj *et al.* (1989). Basic fibroblast growth factor is an extracellular matrix component required for supporting the proliferation of vascular endothelial cells and the differentiation of PC12 cells. *Journal of Cell Biology*. DOI:10.1083/jcb.109.2.823.
57. Morrisey *et al.* (2013). Molecular Determinants of Lung Development. *Annals of the American Thoracic Society*. DOI:10.1513/annalsats.201207-036ot.
58. Alcorn *et al.* (1981). A morphologic and morphometric analysis of fetal lung development in the sheep. *The Anatomical Record*. DOI:10.1002/ar.1092010410.
59. Amy *et al.* (1975). Post-natal growth of the mouse lung. *Tubercle*. DOI:10.1016/0041-3879(75)90060-4.
60. Zeltner *et al.* (1987). The postnatal development and growth of the human lung. I. Morphometry. *Respiration Physiology*. DOI:10.1016/0034-5687(87)90057-0.
61. Mund *et al.* (2008). Developmental alveolarization of the mouse lung. *Developmental Dynamics*.

DOI:10.1002/dvdy.21633.

62. Herring *et al.* (2014). Growth of alveoli during postnatal development in humans based on stereological estimation. *American Journal of Physiology - Lung Cellular and Molecular Physiology*. DOI:10.1152/ajplung.00094.2014.
63. Schittny (2017). Development of the lung. DOI:10.1007/s00441-016-2545-0.
64. Tauber (2003). Metchnikoff and the phagocytosis theory. *Nature Reviews Molecular Cell Biology*. DOI:10.1038/nrm1244.
65. Gautier *et al.* (2012). Gene-expression profiles and transcriptional regulatory pathways that underlie the identity and diversity of mouse tissue macrophages. *Nature Immunology*. DOI:10.1038/ni.2419.
66. Mass *et al.* (2016). Specification of tissue-resident macrophages during organogenesis. *Science (New York, N.Y.)*. DOI:10.1126/science.aaf4238.
67. T'Jonck & Bonnardel (2018). Niche signals and transcription factors involved in tissue-resident macrophage development. *Cellular Immunology*. DOI:10.1016/j.cellimm.2018.02.005.
68. Gordon & Plüddemann (2017). Tissue macrophages: heterogeneity and functions. *BMC Biology*. DOI:10.1186/s12915-017-0392-4.
69. McGrath *et al.* (2008). Enucleation of primitive erythroid cells generates a transient population of 'pyrenocytes' in the mammalian fetus. *Blood*. DOI:10.1182/blood-2007-08-107581.
70. Wynn & Vannella (2016). Macrophages in Tissue Repair, Regeneration, and Fibrosis. *Immunity*. DOI:10.1016/j.immuni.2016.02.015.
71. Aschoff (Springer Berlin Heidelberg, 1924). Das reticulo-endotheliale System. in *Ergebnisse der inneren medizin und kinderheilkunde*. DOI:10.1007/978-3-642-90639-8_1.
72. Furth & Cohn (1968). The origin and kinetics of mononuclear phagocytes. *The Journal of experimental medicine*. DOI:10.1084/jem.128.3.415.
73. Furth *et al.* (1972). Mononuclear phagocytic system: new classification of macrophages, monocytes and of their cell line. *Bulletin of the World Health Organization* 47, 651–8.
74. Hume (2006). The mononuclear phagocyte system. *Current Opinion in Immunology*. DOI:10.1016/j.coi.2005.11.008.
75. Varol *et al.* (2015). Macrophages: Development and Tissue Specialization. *Annual Review of Immunology*. DOI:10.1146/annurev-immunol-032414-112220.
76. Czernielewski & Demarchez (1987). Further Evidence for the Self-Reproducing Capacity of Langerhans Cells in Human Skin. *Journal of Investigative Dermatology*. DOI:10.1111/1523-1747.ep12464659.
77. Merad *et al.* (2002). Langerhans cells renew in the skin throughout life under steady-state conditions. *Nature Immunology*. DOI:10.1038/ni852.
78. Ajami *et al.* (2007). Local self-renewal can sustain CNS microglia maintenance and function throughout adult life. *Nature Neuroscience*. DOI:10.1038/nn2014.
79. Geissmann *et al.* (2010). Unravelling mononuclear phagocyte heterogeneity. *Nature Reviews Immunology*. DOI:10.1038/nri2784.
80. Ginhoux *et al.* (2010). Fate mapping analysis reveals that adult microglia derive from primitive macrophages. *Science (New York, N.Y.)*. DOI:10.1126/science.1194637.
81. Guillems *et al.* (2013). Alveolar macrophages develop from fetal monocytes that differentiate into long-lived cells in the first week of life via GM-CSF. *The Journal of experimental medicine*. DOI:10.1084/jem.20131199.
82. Tamoutounour *et al.* (2013). Origins and Functional Specialization of Macrophages and of Conventional and Monocyte-Derived Dendritic Cells in Mouse Skin. *Immunity*. DOI:10.1016/j.immuni.2013.10.004.
83. Bain *et al.* (2014). Constant replenishment from circulating monocytes

- maintains the macrophage pool in the intestine of adult mice. *Nature Immunology*. DOI:10.1038/ni.2967.
84. Haldar *et al.* (2014). Heme-Mediated SPI-C Induction Promotes Monocyte Differentiation into Iron-Recycling Macrophages. *Cell*. DOI:10.1016/j.cell.2014.01.069.
 85. Molawi *et al.* (2014). Progressive replacement of embryo-derived cardiac macrophages with age. *The Journal of experimental medicine*. DOI:10.1084/jem.20140639.
 86. Bain *et al.* (2016). Long-lived self-renewing bone marrow-derived macrophages displace embryo-derived cells to inhabit adult serous cavities. *Nature Communications*. DOI:10.1038/ncomms11852.
 87. Scott *et al.* (2016). Bone marrow-derived monocytes give rise to self-renewing and fully differentiated Kupffer cells. *Nature Communications*. DOI:10.1038/ncomms10321.
 88. Shaw *et al.* (2018). Tissue-resident macrophages in the intestine are long lived and defined by Tim-4 and CD4 expression. *The Journal of Experimental Medicine*. DOI:10.1084/jem.20180019.
 89. Takahashi *et al.* (1989). Differentiation, Maturation, and Proliferation of Macrophages in the Mouse Yolk Sac: A Light-Microscopic, Enzyme-Cytochemical, Immunohistochemical, and Ultrastructural Study. *Journal of Leukocyte Biology*. DOI:10.1002/jlb.45.2.87.
 90. Hoeffel *et al.* (2012). Adult Langerhans cells derive predominantly from embryonic fetal liver monocytes with a minor contribution of yolk sac-derived macrophages. *The Journal of experimental medicine*. DOI:10.1084/jem.20120340.
 91. Schulz *et al.* (2012). A Lineage of Myeloid Cells Independent of Myb and Hematopoietic Stem Cells. *Science*. DOI:10.1126/science.1219179.
 92. Yona *et al.* (2013). Fate mapping reveals origins and dynamics of monocytes and tissue macrophages under homeostasis. *Immunity*. DOI:10.1016/j.immuni.2012.12.001.
 93. Ginhoux & Jung (2014). Monocytes and macrophages: developmental pathways and tissue homeostasis. *Nature Reviews Immunology*. DOI:10.1038/nri3671.
 94. Ginhoux *et al.* (2010). Fate Mapping Analysis Reveals That Adult Microglia Derive from Primitive Macrophages. *Science*. DOI:10.1126/science.1194637.
 95. Murphy *et al.* (2008). The Prolonged Life-Span of Alveolar Macrophages. *American Journal of Respiratory Cell and Molecular Biology*. DOI:10.1165/rcmb.2007-0224rc.
 96. Tarling *et al.* (1987). Self-Renewal of Pulmonary Alveolar Macrophages: Evidence From Radiation Chimera Studies. *Journal of Leukocyte Biology*. DOI:10.1002/jlb.42.5.443.
 97. Röszer (2018). Understanding the Biology of Self-Renewing Macrophages. *Cells*. DOI:10.3390/cells7080103.
 98. McGrath *et al.* (2011). A transient definitive erythroid lineage with unique regulation of the β -globin locus in the mammalian embryo. *Blood*. DOI:10.1182/blood-2010-12-325357.
 99. Ginhoux & Guilliams (2016). Tissue-Resident Macrophage Ontogeny and Homeostasis. *Immunity*. DOI:10.1016/j.immuni.2016.02.024.
 100. Hoeffel (2018). Fetal monocytes and the origins of tissue-resident macrophages. *Cellular Immunology*. DOI:10.1016/j.cellimm.2018.01.001.
 101. Palis *et al.* (1999). Development of erythroid and myeloid progenitors in the yolk sac and embryo proper of the mouse. *Development (Cambridge, England)* 126, 5073–84.
 102. Tober *et al.* (2007). The megakaryocyte lineage originates from hemangioblast precursors and is an integral component both of primitive and of definitive hematopoiesis. *Blood*. DOI:10.1182/blood-2006-06-031898.
 103. Hoeffel *et al.* (2015). C-Myb+ Erythro-Myeloid Progenitor-Derived Fetal Monocytes Give Rise to Adult Tissue-Resident Macrophages. *Immunity*. DOI:10.1016/j.immuni.2015.03.011.

104. Goldmann *et al.* (2016). Origin, fate and dynamics of macrophages at central nervous system interfaces. *Nature Immunology*. DOI:10.1038/ni.3423.
105. McGrath *et al.* (2003). Circulation is established in a stepwise pattern in the mammalian embryo. *Blood*. DOI:10.1182/blood-2002-08-2531.
106. Frame & McGrath (2013). Erythro-myeloid progenitors: 'Definitive' hematopoiesis in the conceptus prior to the emergence of hematopoietic stem cells. *Blood Cells, Molecules, and Diseases*. DOI:10.1016/j.bcmd.2013.09.006.
107. Lin *et al.* (2014). Lymphoid Progenitor Emergence in the Murine Embryo and Yolk Sac Precedes Stem Cell Detection. *Stem Cells and Development*. DOI:10.1089/scd.2013.0536.
108. Palis *et al.* (2001). Spatial and temporal emergence of high proliferative potential hematopoietic precursors during murine embryogenesis. *Proceedings of the National Academy of Sciences of the United States of America*. DOI:10.1073/pnas.071002398.
109. Medvinsky & Dzierzak (1996). Definitive Hematopoiesis Is Autonomously Initiated by the AGM Region. *Cell*. DOI:10.1016/s0092-8674(00)80165-8.
110. Taoudi & Medvinsky (2007). Functional identification of the hematopoietic stem cell niche in the ventral domain of the embryonic dorsal aorta. *Proceedings of the National Academy of Sciences*. DOI:10.1073/pnas.0700984104.
111. Kieusseian *et al.* (2012). Immature hematopoietic stem cells undergo maturation in the fetal liver. *Development (Cambridge, England)*. DOI:10.1242/dev.079210.
112. Christensen *et al.* (2004). Circulation and Chemotaxis of Fetal Hematopoietic Stem Cells. *PLoS Biology*. DOI:10.1371/journal.pbio.0020075.
113. Coşkun *et al.* (2014). Development of the Fetal Bone Marrow Niche and Regulation of HSC Quiescence and Homing Ability by Emerging Osteolineage Cells. *Cell Reports*. DOI:10.1016/j.celrep.2014.09.013.
114. Gomez Perdiguero *et al.* (2015). Tissue-resident macrophages originate from yolk-sac-derived erythro-myeloid progenitors. *Nature*. DOI:10.1038/nature13989.
115. Sheng *et al.* (2015). Most Tissue-Resident Macrophages Except Microglia Are Derived from Fetal Hematopoietic Stem Cells. *Immunity*. DOI:10.1016/j.immuni.2015.07.016.
116. Kennedy & Abkowitz (1998). Mature monocytic cells enter tissues and engraft. *Proceedings of the National Academy of Sciences*.
117. Bruno *et al.* (2001). Mouse pre-immunocytes as non-proliferating multipotent precursors of macrophages, interferon-producing cells, CD8 α ⁺ and CD8 α ⁻ dendritic cells. *European Journal of Immunology*. DOI:10.1002/1521-4141(200111)31:11<3403::aid-immu3403>3.0.co;2-t.
118. Geissmann *et al.* (2003). Blood monocytes consist of two principal subsets with distinct migratory properties. *Immunity*. DOI:10.1016/s1074-7613(03)00174-2.
119. Fogg *et al.* (2006). A clonogenic bone marrow progenitor specific for macrophages and dendritic cells. *Science (New York, N.Y.)*. DOI:10.1126/science.1117729.
120. Landsman & Jung (2007). Lung Macrophages Serve as Obligatory Intermediate between Blood Monocytes and Alveolar Macrophages. *The Journal of Immunology*. DOI:10.4049/jimmunol.179.6.3488.
121. Geissmann *et al.* (2010). Development of monocytes, macrophages, and dendritic cells. *Science (New York, N.Y.)*. DOI:10.1126/science.1178331.
122. Laar *et al.* (2016). Yolk Sac Macrophages, Fetal Liver, and Adult Monocytes Can Colonize an Empty Niche and Develop into Functional Tissue-Resident Macrophages. *Immunity*. DOI:10.1016/j.immuni.2016.02.017.
123. Misharin *et al.* (2017). Monocyte-derived alveolar macrophages drive lung fibrosis and persist in the lung over the life span. *The Journal of experimental medicine*. DOI:10.1084/jem.20162152.

124. Asada *et al.* (2004). Antiinflammatory Roles of Peroxisome Proliferator-activated Receptor γ in Human Alveolar Macrophages. *American Journal of Respiratory and Critical Care Medicine*. DOI:10.1164/rccm.200207-740oc.
125. Barletta *et al.* (2012). Leukocyte compartments in the mouse lung: Distinguishing between marginated, interstitial, and alveolar cells in response to injury. *Journal of Immunological Methods*. DOI:10.1016/j.jim.2011.09.013.
126. Patel *et al.* (2015). In vivo compartmental analysis of leukocytes in mouse lungs. *American journal of physiology. Lung cellular and molecular physiology*. DOI:10.1152/ajplung.00140.2015.
127. Fehrenbach *et al.* (2008). Neoalveolarisation contributes to compensatory lung growth following pneumonectomy in mice. *European Respiratory Journal*. DOI:10.1183/09031936.00109407.
128. Knust *et al.* (2009). Stereological Estimates of Alveolar Number and Size and Capillary Length and Surface Area in Mice Lungs. *The Anatomical Record: Advances in Integrative Anatomy and Evolutionary Biology*. DOI:10.1002/ar.20747.
129. Vasilescu *et al.* (2012). Assessment of morphometry of pulmonary acini in mouse lungs by nondestructive imaging using multiscale microcomputed tomography. *Proceedings of the National Academy of Sciences*. DOI:10.1073/pnas.1215112109.
130. Westphalen *et al.* (2014). Sessile alveolar macrophages communicate with alveolar epithelium to modulate immunity. *Nature*. DOI:10.1038/nature12902.
131. Ferin (1982). Pulmonary alveolar pores and alveolar macrophage-mediated particle clearance. *The Anatomical Record*. DOI:10.1002/ar.1092030208.
132. Peão *et al.* (1993). Morphological Evidence for Migration of Particle-Laden Macrophages through the Inter-alveolar Pores of Kohn in the Murine Lung. *Cells Tissues Organs*. DOI:10.1159/000147509.
133. Schneberger *et al.* (2011). Monocyte and macrophage heterogeneity and Toll-like receptors in the lung. *Cell and Tissue Research*. DOI:10.1007/s00441-010-1032-2.
134. Becher *et al.* (2014). High-dimensional analysis of the murine myeloid cell system. *Nature Immunology*. DOI:10.1038/ni.3006.
135. Franke-Ullmann *et al.* (1996). Characterization of murine lung interstitial macrophages in comparison with alveolar macrophages in vitro. *Journal of immunology (Baltimore, Md. : 1950)* 157, 3097–104.
136. Bedoret *et al.* (2009). Lung interstitial macrophages alter dendritic cell functions to prevent airway allergy in mice. *The Journal of clinical investigation*. DOI:10.1172/jci39717.
137. Thepen *et al.* (1991). Regulation of immune response to inhaled antigen by alveolar macrophages: differential effects of in vivo alveolar macrophage elimination on the induction of tolerance vs. immunity. *European Journal of Immunology*. DOI:10.1002/eji.1830211128.
138. Parod & Brain (1986). Immune opsonin-independent phagocytosis by pulmonary macrophages. *Journal of immunology (Baltimore, Md. : 1950)* 136, 2041–7.
139. Li (2012). Eat-me signals: Keys to molecular phagocyte biology and ‘Appetite’ control. *Journal of Cellular Physiology*. DOI:10.1002/jcp.22815.
140. Möller *et al.* (2006). Mucociliary and long-term particle clearance in airways of patients with immotile cilia. *Respiratory Research*. DOI:10.1186/1465-9921-7-10.
141. Taylor *et al.* (2005). MACROPHAGE RECEPTORS AND IMMUNE RECOGNITION. *Annual Review of Immunology*. DOI:10.1146/annurev.immunol.23.021704.115816.
142. Chroneos *et al.* (1996). Purification of a Cell-surface Receptor for Surfactant Protein A. *Journal of Biological Chemistry*. DOI:10.1074/jbc.271.27.16375.
143. Holmskov *et al.* (1997). Isolation and characterization of a new member of the scavenger

- receptor superfamily, glycoprotein-340 (gp-340), as a lung surfactant protein-D binding molecule. *The Journal of biological chemistry*. DOI:10.1074/jbc.272.21.13743.
144. Forbes *et al.* (2007). Alveolar macrophage depletion is associated with increased surfactant pool sizes in adult rats. *Journal of Applied Physiology*. DOI:10.1152/jappphysiol.00995.2006.
 145. Fisher *et al.* (2000). Pulmonary-specific expression of SP-D corrects pulmonary lipid accumulation in *SP-D* gene-targeted mice. *American Journal of Physiology-Lung Cellular and Molecular Physiology*. DOI:10.1152/ajplung.2000.278.2.l365.
 146. Carey & Trapnell (2010). The molecular basis of pulmonary alveolar proteinosis. *Clinical Immunology*. DOI:10.1016/j.clim.2010.02.017.
 147. Varol *et al.* (2007). Monocytes give rise to mucosal, but not splenic, conventional dendritic cells. *Journal of Experimental Medicine*. DOI:10.1084/jem.20061011.
 148. Nayak *et al.* (2016). Long-Term Persistence of Donor Alveolar Macrophages in Human Lung Transplant Recipients That Influences Donor-Specific Immune Responses. *American Journal of Transplantation*. DOI:10.1111/ajt.13819.
 149. Tan & Krasnow (2016). Developmental origin of lung macrophage diversity. *Development*. DOI:10.1242/dev.129122.
 150. Lavin *et al.* (2014). Tissue-Resident Macrophage Enhancer Landscapes Are Shaped by the Local Microenvironment. *Cell*. DOI:10.1016/j.cell.2014.11.018.
 151. Huffman *et al.* (1996). Pulmonary epithelial cell expression of GM-CSF corrects the alveolar proteinosis in GM-CSF-deficient mice. *Journal of Clinical Investigation*. DOI:10.1172/jci118461.
 152. Schneider *et al.* (2014). Induction of the nuclear receptor PPAR- γ by the cytokine GM-CSF is critical for the differentiation of fetal monocytes into alveolar macrophages. *Nature Immunology*. DOI:10.1038/ni.3005.
 153. Todd *et al.* (2016). Alveolar macrophage development in mice requires L-plastin for cellular localization in alveoli. *Blood*. DOI:10.1182/blood-2016-03-705962.
 154. Guthridge *et al.* (2006). Growth factor pleiotropy is controlled by a receptor Tyr/Ser motif that acts as a binary switch. *The EMBO Journal*. DOI:10.1038/sj.emboj.7600948.
 155. Bhattacharya *et al.* (2015). Dual Role of GM-CSF as a Pro-Inflammatory and a Regulatory Cytokine: Implications for Immune Therapy. *Journal of Interferon & Cytokine Research*. DOI:10.1089/jir.2014.0149.
 156. Hamilton (2008). Colony-stimulating factors in inflammation and autoimmunity. *Nature Reviews Immunology*. DOI:10.1038/nri2356.
 157. Cornish *et al.* (2009). G-CSF and GM-CSF as therapeutic targets in rheumatoid arthritis. *Nature Reviews Rheumatology*. DOI:10.1038/nrrheum.2009.178.
 158. Tazawa *et al.* (2019). Inhaled GM-CSF for Pulmonary Alveolar Proteinosis. *New England Journal of Medicine*. DOI:10.1056/nejmoa1816216.
 159. Tontonoz & Spiegelman (2008). Fat and Beyond: The Diverse Biology of PPAR γ . *Annual Review of Biochemistry*. DOI:10.1146/annurev.biochem.77.061307.091829.
 160. Bonfield *et al.* (2003). Peroxisome Proliferator-Activated Receptor- γ Is Deficient in Alveolar Macrophages from Patients with Alveolar Proteinosis. *American Journal of Respiratory Cell and Molecular Biology*. DOI:10.1165/rcmb.2003-0148oc.
 161. Robb *et al.* (1995). Hematopoietic and lung abnormalities in mice with a null mutation of the common beta subunit of the receptors for granulocyte-macrophage colony-stimulating factor and interleukins 3 and 5. *Proceedings of the National Academy of Sciences*. DOI:10.1073/pnas.92.21.9565.
 162. Gibeon *et al.* (2014). Lipid-laden bronchoalveolar macrophages in asthma and chronic cough.

Respiratory Medicine. DOI:10.1016/j.rmed.2013.10.005.

163. Joshi *et al.* (2018). Alveolar Macrophages. *Cellular Immunology*. DOI:10.1016/j.cellimm.2018.01.005.
164. Loering *et al.* (2019). Lung development and emerging roles for type 2 immunity. *The Journal of Pathology*. DOI:10.1002/path.5211.
165. Saluzzo *et al.* (2017). First-Breath-Induced Type 2 Pathways Shape the Lung Immune Environment. *Cell Reports*. DOI:10.1016/j.celrep.2017.01.071.
166. Jetten *et al.* (2014). Anti-inflammatory M2, but not pro-inflammatory M1 macrophages promote angiogenesis in vivo. *Angiogenesis*. DOI:10.1007/s10456-013-9381-6.
167. Stout & Suttles (2004). Functional plasticity of macrophages: reversible adaptation to changing microenvironments. *Journal of leukocyte biology*. DOI:10.1189/jlb.0504272.
168. Martinez *et al.* (2008). Macrophage activation and polarization. *Frontiers in bioscience : a journal and virtual library*. DOI:10.2741/2692.
169. Zanganeh *et al.* (2016). Iron oxide nanoparticles inhibit tumour growth by inducing pro-inflammatory macrophage polarization in tumour tissues. *Nature Nanotechnology*. DOI:10.1038/nnano.2016.168.
170. Gordon & Martinez (2010). Alternative Activation of Macrophages: Mechanism and Functions. *Immunity*. DOI:10.1016/j.immuni.2010.05.007.
171. Barron & Wynn (2011). Macrophage activation governs schistosomiasis-induced inflammation and fibrosis. *European Journal of Immunology*. DOI:10.1002/eji.201141869.
172. Mosser & Edwards (2008). Exploring the full spectrum of macrophage activation. *Nature Reviews Immunology*. DOI:10.1038/nri2448.
173. Geissmann *et al.* (2010). Unravelling mononuclear phagocyte heterogeneity. *Nature reviews. Immunology*. DOI:10.1038/nri2784.
174. Murray *et al.* (2014). Macrophage Activation and Polarization: Nomenclature and Experimental Guidelines. *Immunity*. DOI:10.1016/j.immuni.2014.06.008.
175. Xue *et al.* (2014). Transcriptome-Based Network Analysis Reveals a Spectrum Model of Human Macrophage Activation. *Immunity*. DOI:10.1016/j.immuni.2014.01.006.
176. Jablonski *et al.* (2015). Novel Markers to Delineate Murine M1 and M2 Macrophages. *PLOS ONE*. DOI:10.1371/journal.pone.0145342.
177. Mantovani *et al.* (2002). Macrophage polarization: tumor-associated macrophages as a paradigm for polarized M2 mononuclear phagocytes. *Trends in Immunology*. DOI:10.1016/s1471-4906(02)02302-5.
178. Biswas & Mantovani (2010). Macrophage plasticity and interaction with lymphocyte subsets: cancer as a paradigm. *Nature Immunology*. DOI:10.1038/ni.1937.
179. Bertolini *et al.* (2016). Genetic background affects the expansion of macrophage subsets in the lungs of Mycobacterium tuberculosis -infected hosts. *Immunology*. DOI:10.1111/imm.12591.
180. Rodriguez *et al.* (2017). Arginine Metabolism in Myeloid Cells Shapes Innate and Adaptive Immunity. *Frontiers in Immunology*. DOI:10.3389/fimmu.2017.00093.
181. Gallardo-Soler *et al.* (2008). Arginase I Induction by Modified Lipoproteins in Macrophages: A Peroxisome Proliferator-Activated Receptor- γ/δ -Mediated Effect that Links Lipid Metabolism and Immunity. *Molecular Endocrinology*. DOI:10.1210/me.2007-0525.
182. Xu *et al.* (2003). STAT-1 and c-Fos interaction in nitric oxide synthase-2 gene activation. *American Journal of Physiology-Lung Cellular and Molecular Physiology*. DOI:10.1152/ajplung.00441.2002.
183. Forstermann & Sessa (2012). Nitric oxide synthases: regulation and function. *European Heart Journal*. DOI:10.1093/eurheartj/ehr304.

184. Rath *et al.* (2014). Metabolism via Arginase or Nitric Oxide Synthase: Two Competing Arginine Pathways in Macrophages. *Frontiers in Immunology*. DOI:10.3389/fimmu.2014.00532.
185. Gong *et al.* (2008). Inflammatory macrophage migration requires MMP-9 activation by plasminogen in mice. *Journal of Clinical Investigation*. DOI:10.1172/jci32750.
186. Sun *et al.* (2007). Interleukin-12 Promotes Gamma Interferon-Dependent Neutrophil Recruitment in the Lung and Improves Protection against Respiratory Streptococcus pneumoniae Infection. *Infection and Immunity*. DOI:10.1128/iai.01403-06.
187. Laza-Stanca *et al.* (2006). Rhinovirus Replication in Human Macrophages Induces NF- κ B-Dependent Tumor Necrosis Factor Alpha Production. *Journal of Virology*. DOI:10.1128/jvi.00162-06.
188. Swann *et al.* (2008). Demonstration of inflammation-induced cancer and cancer immunoediting during primary tumorigenesis. *Proceedings of the National Academy of Sciences*. DOI:10.1073/pnas.0708594105.
189. Freire & Van Dyke (2013). Natural resolution of inflammation. *Periodontology 2000*. DOI:10.1111/prd.12034.
190. Murray & Wynn (2011). Protective and pathogenic functions of macrophage subsets. *Nature Reviews Immunology*. DOI:10.1038/nri3073.
191. Tarique *et al.* (2015). Phenotypic, Functional, and Plasticity Features of Classical and Alternatively Activated Human Macrophages. *American Journal of Respiratory Cell and Molecular Biology*. DOI:10.1165/rcmb.2015-0012oc.
192. Stein *et al.* (1992). Interleukin 4 potently enhances murine macrophage mannose receptor activity: a marker of alternative immunologic macrophage activation. *The Journal of Experimental Medicine*. DOI:10.1084/jem.176.1.287.
193. Raes *et al.* (2005). Macrophage galactose-type C-type lectins as novel markers for alternatively activated macrophages elicited by parasitic infections and allergic airway inflammation. *Journal of Leukocyte Biology*. DOI:10.1189/jlb.0304212.
194. Martinez *et al.* (2009). Alternative Activation of Macrophages: An Immunologic Functional Perspective. *Annual Review of Immunology*. DOI:10.1146/annurev.immunol.021908.132532.
195. Nieuwenhuizen *et al.* (2012). Allergic airway disease is unaffected by the absence of IL-4R α -dependent alternatively activated macrophages. *Journal of Allergy and Clinical Immunology*. DOI:10.1016/j.jaci.2012.03.011.
196. Lin *et al.* (2019). Tumor-associated macrophages in tumor metastasis: biological roles and clinical therapeutic applications. *Journal of Hematology & Oncology*. DOI:10.1186/s13045-019-0760-3.
197. Boorsma *et al.* (2013). Macrophage Heterogeneity in Respiratory Diseases. *Mediators of Inflammation*. DOI:10.1155/2013/769214.
198. Byrne *et al.* (2015). Pulmonary macrophages: key players in the innate defence of the airways. *Thorax*. DOI:10.1136/thoraxjnl-2015-207020.
199. Belchamber & Donnelly (Springer, Cham, 2017). Macrophage Dysfunction in Respiratory Disease. in. DOI:10.1007/978-3-319-54090-0_12.
200. Mims (2015). Asthma: definitions and pathophysiology. *International Forum of Allergy & Rhinology*. DOI:10.1002/alr.21609.
201. Girodet *et al.* (2016). Alternative Macrophage Activation Is Increased in Asthma. *American Journal of Respiratory Cell and Molecular Biology*. DOI:10.1165/rcmb.2015-0295oc.
202. Melgert *et al.* (2010). Macrophages. *American Journal of Respiratory Cell and Molecular Biology*. DOI:10.1165/rcmb.2009-0016oc.

203. Moreira *et al.* (2010). Serum amyloid P attenuates M2 macrophage activation and protects against fungal spore-induced allergic airway disease. *Journal of Allergy and Clinical Immunology*. DOI:10.1016/j.jaci.2010.06.010.
204. Abdelaziz *et al.* (2020). Alternatively activated macrophages; a double-edged sword in allergic asthma. *Journal of Translational Medicine*. DOI:10.1186/s12967-020-02251-w.
205. Thomas (2002). Effects of inhaled tumour necrosis factor alpha in subjects with mild asthma. *Thorax*. DOI:10.1136/thorax.57.9.774.
206. Berry *et al.* (2006). Evidence of a Role of Tumor Necrosis Factor α in Refractory Asthma. *New England Journal of Medicine*. DOI:10.1056/nejmoa050580.
207. Hayashi *et al.* (2007). T helper 1 cells stimulated with ovalbumin and IL-18 induce airway hyperresponsiveness and lung fibrosis by IFN- and IL-13 production. *Proceedings of the National Academy of Sciences*. DOI:10.1073/pnas.0706378104.
208. Goleva *et al.* (2008). Corticosteroid-resistant asthma is associated with classical antimicrobial activation of airway macrophages. *Journal of Allergy and Clinical Immunology*. DOI:10.1016/j.jaci.2008.07.007.
209. Hussell & Bell (2014). Alveolar macrophages: plasticity in a tissue-specific context. *Nature Reviews Immunology*. DOI:10.1038/nri3600.
210. Dietert (2014). Macrophages as targets of developmental immunotoxicity. *OA Immunology*.
211. Jones *et al.* (2013). M2 macrophage polarisation is associated with alveolar formation during postnatal lung development. *Respiratory Research*. DOI:10.1186/1465-9921-14-41.
212. Italiani & Boraschi (2014). From Monocytes to M1/M2 Macrophages: Phenotypical vs. Functional Differentiation. *Frontiers in Immunology*. DOI:10.3389/fimmu.2014.00514.
213. Rószler (2015). Understanding the Mysterious M2 Macrophage through Activation Markers and Effector Mechanisms. *Mediators of Inflammation*. DOI:10.1155/2015/816460.
214. Lipscomb *et al.* (1986). Human alveolar macrophages: HLA-DR-positive macrophages that are poor stimulators of a primary mixed leukocyte reaction. *Journal of immunology (Baltimore, Md. : 1950)* 136, 497–504.
215. Blumenthal *et al.* (2001). Human alveolar macrophages induce functional inactivation in antigen-specific CD4 T cells. *Journal of Allergy and Clinical Immunology*. DOI:10.1067/mai.2001.112845.
216. Morris *et al.* (2003). Loss of integrin $\alpha v \beta 6$ -mediated TGF- β activation causes Mmp12-dependent emphysema. *Nature*. DOI:10.1038/nature01413.
217. Misharin *et al.* (2013). Flow Cytometric Analysis of Macrophages and Dendritic Cell Subsets in the Mouse Lung. *American Journal of Respiratory Cell and Molecular Biology*. DOI:10.1165/rcmb.2013-0086ma.
218. Snelgrove *et al.* (2008). A critical function for CD200 in lung immune homeostasis and the severity of influenza infection. *Nature Immunology*. DOI:10.1038/ni.1637.
219. Barclay & Brown (2006). The SIRP family of receptors and immune regulation. *Nature Reviews Immunology*. DOI:10.1038/nri1859.
220. Mahbub *et al.* (2012). Advanced Age Impairs Macrophage Polarization. *Journal of Interferon & Cytokine Research*. DOI:10.1089/jir.2011.0058.
221. Heymsfield & Wadden (2017). Mechanisms, Pathophysiology, and Management of Obesity. *New England Journal of Medicine*. DOI:10.1056/nejmra1514009.
222. Börjeson (1976). The Aetiology Of Obesity In Children. A Study of 101 Twin Pairs. *Acta Paediatrica*. DOI:10.1111/j.1651-2227.1976.tb04887.x.
223. Stunkard *et al.* (1986). A Twin Study of Human Obesity. *JAMA: The Journal of the American Medical Association*. DOI:10.1001/jama.1986.03380010055024.

224. Stunkard *et al.* (1990). The Body-Mass Index of Twins Who Have Been Reared Apart. *New England Journal of Medicine*. DOI:10.1056/nejm199005243222102.
225. Saunders *et al.* (2007). Meta-Analysis of Genome-wide Linkage Studies in BMI and Obesity. *Obesity*. DOI:10.1038/oby.2007.269.
226. Walley *et al.* (2009). The genetic contribution to non-syndromic human obesity. *Nature Reviews Genetics*. DOI:10.1038/nrg2594.
227. Brandkvist *et al.* (2019). Quantifying the impact of genes on body mass index during the obesity epidemic: longitudinal findings from the HUNT Study. *BMJ*. DOI:10.1136/bmj.l4067.
228. Abdelaal *et al.* (2017). Morbidity and mortality associated with obesity. *Annals of Translational Medicine*. DOI:10.21037/atm.2017.03.107.
229. Abarca-Gómez *et al.* (2017). Worldwide trends in body-mass index, underweight, overweight, and obesity from 1975 to 2016: a pooled analysis of 2416 population-based measurement studies in 1289 million children, adolescents, and adults. *The Lancet*. DOI:10.1016/s0140-6736(17)32129-3.
230. Segula (2014). Complications of obesity in adults: a short review of the literature. *Malawi medical journal : the journal of Medical Association of Malawi* 26, 20–4.
231. Meldrum *et al.* (2017). Obesity pandemic: causes, consequences, and solutions-but do we have the will? *Fertility and sterility*. DOI:10.1016/j.fertnstert.2017.02.104.
232. (2019). Body mass index - BMI. <http://www.euro.who.int/en/health-topics/disease-prevention/nutrition/a-healthy-lifestyle/body-mass-index-bmi>.
233. Eknoyan (2007). Adolphe Quetelet (1796 1874) the average man and indices of obesity. *Nephrology Dialysis Transplantation*. DOI:10.1093/ndt/gfm517.
234. Bray & Gray (1988). Obesity. Part I–Pathogenesis. *The Western journal of medicine* 149, 429–41.
235. Prospective Studies Collaboration (2009). Body-mass index and cause-specific mortality in 900 000 adults: collaborative analyses of 57 prospective studies. *The Lancet*. DOI:10.1016/s0140-6736(09)60318-4.
236. Wellens *et al.* (1996). Relationships Between the Body Mass Index and Body Composition. *Obesity Research*. DOI:10.1002/j.1550-8528.1996.tb00510.x.
237. Blundell *et al.* (2014). Beyond BMI–phenotyping the obesities. *Obesity facts*. DOI:10.1159/000368783.
238. Antonopoulos & Tousoulis (2017). The molecular mechanisms of obesity paradox. *Cardiovascular Research*. DOI:10.1093/cvr/cvx106.
239. Tremmel *et al.* (2017). Economic Burden of Obesity: A Systematic Literature Review. *International Journal of Environmental Research and Public Health*. DOI:10.3390/ijerph14040435.
240. Snel *et al.* (2012). Ectopic Fat and Insulin Resistance: Pathophysiology and Effect of Diet and Lifestyle Interventions. *International Journal of Endocrinology*. DOI:10.1155/2012/983814.
241. Ibrahim (2010). Subcutaneous and visceral adipose tissue: structural and functional differences. *Obesity Reviews*. DOI:10.1111/j.1467-789x.2009.00623.x.
242. Shabalina *et al.* (2013). UCP1 in Brite/Beige Adipose Tissue Mitochondria Is Functionally Thermogenic. *Cell Reports*. DOI:10.1016/j.celrep.2013.10.044.
243. Cypess *et al.* (2009). Identification and Importance of Brown Adipose Tissue in Adult Humans. *New England Journal of Medicine*. DOI:10.1056/nejmoa0810780.
244. van Marken Lichtenbelt *et al.* (2009). Cold-Activated Brown Adipose Tissue in Healthy Men. *New England Journal of Medicine*. DOI:10.1056/nejmoa0808718.
245. De Matteis *et al.* (2013). Exercise as a new physiological stimulus for

- brown adipose tissue activity. *Nutrition, Metabolism and Cardiovascular Diseases*. DOI:10.1016/j.numecd.2012.01.013.
246. Spalding *et al.* (2008). Dynamics of fat cell turnover in humans. *Nature*. DOI:10.1038/nature06902.
247. Trayhurn (2007). Adipocyte biology. *Obesity Reviews*. DOI:10.1111/j.1467-789x.2007.00316.x.
248. Zuk *et al.* (2001). Multilineage Cells from Human Adipose Tissue: Implications for Cell-Based Therapies. *Tissue Engineering*. DOI:10.1089/107632701300062859.
249. Tang & Lane (2012). Adipogenesis: From Stem Cell to Adipocyte. *Annual Review of Biochemistry*. DOI:10.1146/annurev-biochem-052110-115718.
250. Letterova *et al.* (2014). PPAR γ and the global map of adipogenesis and beyond. *Trends in endocrinology and metabolism: TEM*. DOI:10.1016/j.tem.2014.04.001.
251. Grant & Dixit (2015). Adipose tissue as an immunological organ. *Obesity*. DOI:10.1002/oby.21003.
252. Stolarczyk (2017). Adipose tissue inflammation in obesity: a metabolic or immune response? *Current Opinion in Pharmacology*. DOI:10.1016/j.coph.2017.08.006.
253. Coelho *et al.* (2013). Biochemistry of adipose tissue: an endocrine organ. *Archives of medical science : AMS*. DOI:10.5114/aoms.2013.33181.
254. Kershaw & Flier (2004). Adipose Tissue as an Endocrine Organ. *The Journal of Clinical Endocrinology & Metabolism*. DOI:10.1210/jc.2004-0395.
255. Ouchi *et al.* (2011). Adipokines in inflammation and metabolic disease. *Nature Reviews Immunology*. DOI:10.1038/nri2921.
256. Lehr *et al.* (2012). Adipokines: A treasure trove for the discovery of biomarkers for metabolic disorders. *PROTEOMICS - Clinical Applications*. DOI:10.1002/prca.201100052.
257. Samaras *et al.* (2010). Subcutaneous and Visceral Adipose Tissue Gene Expression of Serum Adipokines That Predict Type 2 Diabetes. *Obesity*. DOI:10.1038/oby.2009.443.
258. Sell & Eckel (2010). Adipose tissue inflammation: novel insight into the role of macrophages and lymphocytes. *Current opinion in clinical nutrition and metabolic care*. DOI:10.1097/mco.0b013e32833aab7f.
259. Lee *et al.* (2009). Getting the message across: mechanisms of physiological cross talk by adipose tissue. *American Journal of Physiology-Endocrinology and Metabolism*. DOI:10.1152/ajpendo.00015.2009.
260. Jo *et al.* (2009). Hypertrophy and/or Hyperplasia: Dynamics of Adipose Tissue Growth. *PLoS computational biology*. DOI:10.1371/journal.pcbi.1000324.
261. Itoh *et al.* (2011). Adipose Tissue Remodeling as Homeostatic Inflammation. *International Journal of Inflammation*. DOI:10.4061/2011/720926.
262. Weisberg *et al.* (2003). Obesity is associated with macrophage accumulation in adipose tissue. *The Journal of clinical investigation*. DOI:10.1172/jci19246.
263. Zhang *et al.* (2002). Tumor Necrosis Factor- Stimulates Lipolysis in Differentiated Human Adipocytes Through Activation of Extracellular Signal-Related Kinase and Elevation of Intracellular cAMP. *Diabetes*. DOI:10.2337/diabetes.51.10.2929.
264. Nguyen *et al.* (2007). A subpopulation of macrophages infiltrates hypertrophic adipose tissue and is activated by free fatty acids via Toll-like receptors 2 and 4 and JNK-dependent pathways. *The Journal of biological chemistry*. DOI:10.1074/jbc.m706762200.
265. Huang *et al.* (2012). Saturated fatty acids activate TLR-mediated proinflammatory signaling pathways. *Journal of lipid research*. DOI:10.1194/jlr.d029546.
266. Cani *et al.* (2008). Changes in Gut Microbiota Control Metabolic Endotoxemia-Induced Inflammation in High-Fat Diet-Induced Obesity and Diabetes in Mice. *Diabetes*.

DOI:10.2337/db07-1403.

267. Cani *et al.* (2009). Changes in gut microbiota control inflammation in obese mice through a mechanism involving GLP-2-driven improvement of gut permeability. *Gut*. DOI:10.1136/gut.2008.165886.
268. Teixeira *et al.* (2012). Potential mechanisms for the emerging link between obesity and increased intestinal permeability. *Nutrition Research*. DOI:10.1016/j.nutres.2012.07.003.
269. Mariman & Wang (2010). Adipocyte extracellular matrix composition, dynamics and role in obesity. *Cellular and molecular life sciences : CMLS*. DOI:10.1007/s00018-010-0263-4.
270. González-Muniesa *et al.* (2016). Effects of Hyperoxia on Oxygen-Related Inflammation with a Focus on Obesity. *Oxidative Medicine and Cellular Longevity*. DOI:10.1155/2016/8957827.
271. Hara *et al.* (2011). Rho and Rho-Kinase Activity in Adipocytes Contributes to a Vicious Cycle in Obesity That May Involve Mechanical Stretch. *Science Signaling*. DOI:10.1126/scisignal.2001227.
272. Furukawa *et al.* (2004). Increased oxidative stress in obesity and its impact on metabolic syndrome. *The Journal of clinical investigation*. DOI:10.1172/jci21625.
273. Giordano *et al.* (2013). Obese adipocytes show ultrastructural features of stressed cells and die of pyroptosis. *Journal of Lipid Research*. DOI:10.1194/jlr.m038638.
274. Yan *et al.* (2013). Omega-3 Fatty Acids Prevent Inflammation and Metabolic Disorder through Inhibition of NLRP3 Inflammasome Activation. *Immunity*. DOI:10.1016/j.immuni.2013.05.015.
275. Uysal *et al.* (1997). Protection from obesity-induced insulin resistance in mice lacking TNF- α function. *Nature*. DOI:10.1038/39335.
276. Senn *et al.* (2003). Suppressor of Cytokine Signaling-3 (SOCS-3), a Potential Mediator of Interleukin-6-dependent Insulin Resistance in Hepatocytes. *Journal of Biological Chemistry*. DOI:10.1074/jbc.m210689200.
277. Jager *et al.* (2007). Interleukin-1 β -Induced Insulin Resistance in Adipocytes through Down-Regulation of Insulin Receptor Substrate-1 Expression. *Endocrinology*. DOI:10.1210/en.2006-0692.
278. Roth *et al.* (2011). Changes in adipose-derived inflammatory cytokines and chemokines after successful lifestyle intervention in obese children. *Metabolism*. DOI:10.1016/j.metabol.2010.03.023.
279. Phillips & Perry (2013). Does Inflammation Determine Metabolic Health Status in Obese and Nonobese Adults? *The Journal of Clinical Endocrinology & Metabolism*. DOI:10.1210/jc.2013-2038.
280. Yamauchi *et al.* (2001). The fat-derived hormone adiponectin reverses insulin resistance associated with both lipoatrophy and obesity. *Nature Medicine*. DOI:10.1038/90984.
281. Fujisaka *et al.* (2009). Regulatory Mechanisms for Adipose Tissue M1 and M2 Macrophages in Diet-Induced Obese Mice. *Diabetes*. DOI:10.2337/db08-1475.
282. Mafort *et al.* (2016). Obesity: systemic and pulmonary complications, biochemical abnormalities, and impairment of lung function. *Multidisciplinary Respiratory Medicine*. DOI:10.1186/s40248-016-0066-z.
283. Peters *et al.* (2018). Beyond BMI: Obesity and Lung Disease. *Chest*. DOI:10.1016/j.chest.2017.07.010.
284. Sideleva *et al.* (2012). Obesity and Asthma. *American Journal of Respiratory and Critical Care Medicine*. DOI:10.1164/rccm.201203-0573oc.
285. Zhi *et al.* (2016). 'Obesity Paradox' in Acute Respiratory Distress Syndrome: Asystematic Review and Meta-Analysis. *PLOS ONE*. DOI:10.1371/journal.pone.0163677.

286. Pihlilä *et al.* (2017). The Predictors of Obesity Hypoventilation Syndrome in Obstructive Sleep Apnea. *Balkan Medical Journal*. DOI:10.4274/balkanmedj.2015.1797.
287. Friedman & Andrus (2012). Obesity and pulmonary hypertension: A review of pathophysiologic mechanisms. *Journal of Obesity*. DOI:10.1155/2012/505274.
288. Behrens *et al.* (2014). Body size and physical activity in relation to incidence of chronic obstructive pulmonary disease. *CMAJ*. DOI:10.1503/cmaj.140025.
289. Chu *et al.* (2019). Palmitic Acid-Rich High-Fat Diet Exacerbates Experimental Pulmonary Fibrosis by Modulating Endoplasmic Reticulum Stress. *American Journal of Respiratory Cell and Molecular Biology*. DOI:10.1165/rcmb.2018-0324oc.
290. Franssen *et al.* (2008). Obesity and the lung: 5 Obesity and COPD. *Thorax*. DOI:10.1136/thx.2007.086827.
291. Lederer *et al.* (2011). Obesity and Primary Graft Dysfunction after Lung Transplantation. *American Journal of Respiratory and Critical Care Medicine*. DOI:10.1164/rccm.201104-0728oc.
292. Smith *et al.* (2007). Diet-Induced Obese Mice Have Increased Mortality and Altered Immune Responses When Infected with Influenza Virus. *The Journal of Nutrition*. DOI:10.1093/jn/137.5.1236.
293. Jain & Chaves (2011). Obesity and Influenza. *Clinical Infectious Diseases*. DOI:10.1093/cid/cir448.
294. Gries *et al.* (2015). Obese patients with idiopathic pulmonary fibrosis have a higher 90-day mortality risk with bilateral lung transplantation. *The Journal of Heart and Lung Transplantation*. DOI:10.1016/j.healun.2014.09.031.
295. Bartness & Song (2007). Brain-adipose tissue neural crosstalk. *Physiology & behavior*. DOI:10.1016/j.physbeh.2007.04.002.
296. R. Moschen *et al.* (2012). Adiponectin: Key Player in the Adipose Tissue-Liver Crosstalk. *Current Medicinal Chemistry*. DOI:10.2174/092986712803833254.
297. Trayhurn *et al.* (2011). Secreted proteins from adipose tissue and skeletal muscle – adipokines, myokines and adipose/muscle cross-talk. *Archives of Physiology and Biochemistry*. DOI:10.3109/13813455.2010.535835.
298. El-Kadre & Tinoco (2013). Interleukin-6 and obesity. *Current Opinion in Clinical Nutrition and Metabolic Care*. DOI:10.1097/mco.0b013e32836410e6.
299. Mancuso (2010). Obesity and lung inflammation. *Journal of Applied Physiology*. DOI:10.1152/jappphysiol.00781.2009.
300. Hsu *et al.* (2007). Leptin improves pulmonary bacterial clearance and survival in ob/ob mice during pneumococcal pneumonia. *Clinical & Experimental Immunology*. DOI:10.1111/j.1365-2249.2007.03491.x.
301. Sun *et al.* (2009). Ambient Air Pollution Exaggerates Adipose Inflammation and Insulin Resistance in a Mouse Model of Diet-Induced Obesity. *Circulation*. DOI:10.1161/circulationaha.108.799015.
302. Watson *et al.* (2010). Reduction of total lung capacity in obese men: comparison of total intrathoracic and gas volumes. *Journal of Applied Physiology*. DOI:10.1152/jappphysiol.01267.2009.
303. Salome *et al.* (2010). Physiology of obesity and effects on lung function. *Journal of Applied Physiology*. DOI:10.1152/jappphysiol.00694.2009.
304. Brazzale *et al.* (2015). Optimizing respiratory function assessments to elucidate the impact of obesity on respiratory health. *Respirology*. DOI:10.1111/resp.12563.
305. Unterborn (2001). Pulmonary function testing in obesity, pregnancy, and extremes of body habitus. *Clinics in chest medicine* 22, 759–67.

306. Medoff *et al.* (2009). Adiponectin Deficiency Increases Allergic Airway Inflammation and Pulmonary Vascular Remodeling. *American Journal of Respiratory Cell and Molecular Biology*. DOI:10.1165/rcmb.2008-0415oc.
307. Krommidas *et al.* (2010). Plasma leptin and adiponectin in COPD exacerbations: Associations with inflammatory biomarkers. *Respiratory Medicine*. DOI:10.1016/j.rmed.2009.08.012.
308. Lundblad *et al.* (2005). Tumor Necrosis Factor- α Overexpression in Lung Disease. *American Journal of Respiratory and Critical Care Medicine*. DOI:10.1164/rccm.200410-1349oc.
309. Williams *et al.* (2015). Innate and ozone-induced airway hyperresponsiveness in obese mice: role of TNF- α . *American Journal of Physiology-Lung Cellular and Molecular Physiology*. DOI:10.1152/ajplung.00393.2014.
310. Hoffman *et al.* (2017). Developmental origins of health and disease: current knowledge and potential mechanisms. *Nutrition Reviews*. DOI:10.1093/nutrit/nux053.
311. Oken & Gillman (2003). Fetal Origins of Obesity. *Obesity Research*. DOI:10.1038/oby.2003.69.
312. Heerwagen *et al.* (2010). Maternal obesity and fetal metabolic programming: a fertile epigenetic soil. *American Journal of Physiology-Regulatory, Integrative and Comparative Physiology*. DOI:10.1152/ajpregu.00310.2010.
313. Godfrey *et al.* (2017). Influence of maternal obesity on the long-term health of offspring. *The Lancet Diabetes & Endocrinology*. DOI:10.1016/s2213-8587(16)30107-3.
314. Leddy *et al.* (2008). The impact of maternal obesity on maternal and fetal health. *Reviews in obstetrics & gynecology* 1, 170–8.
315. Mamun *et al.* (2011). Associations of maternal pre-pregnancy obesity and excess pregnancy weight gains with adverse pregnancy outcomes and length of hospital stay. *BMC Pregnancy and Childbirth*. DOI:10.1186/1471-2393-11-62.
316. Stothard *et al.* (2009). Maternal Overweight and Obesity and the Risk of Congenital Anomalies. *JAMA*. DOI:10.1001/jama.2009.113.
317. Aune *et al.* (2014). Maternal Body Mass Index and the Risk of Fetal Death, Stillbirth, and Infant Death. *JAMA*. DOI:10.1001/jama.2014.2269.
318. Lopez-Jaramillo *et al.* (2018). Obesity and Preeclampsia: Common Pathophysiological Mechanisms. *Frontiers in Physiology*. DOI:10.3389/fphys.2018.01838.
319. Dietl (2005). Maternal obesity and complications during pregnancy. *Journal of Perinatal Medicine*. DOI:10.1515/jpm.2005.018.
320. Harmon & Hannon (2018). Maternal obesity: a serious pediatric health crisis. *Pediatric Research*. DOI:10.1038/pr.2018.50.
321. Sferruzzi-Perri & Camm (2016). The Programming Power of the Placenta. *Frontiers in Physiology*. DOI:10.3389/fphys.2016.00033.
322. Lewis & Desoye (2017). Placental Lipid and Fatty Acid Transfer in Maternal Overnutrition. *Annals of Nutrition and Metabolism*. DOI:10.1159/000463397.
323. Bugatto *et al.* (2010). Second-Trimester Amniotic Fluid Proinflammatory Cytokine Levels in Normal and Overweight Women. *Obstetrics & Gynecology*. DOI:10.1097/aog.0b013e3181c5367f.
324. Kim *et al.* (2014). Obesity During Pregnancy Disrupts Placental Morphology, Cell Proliferation, and Inflammation in a Sex-Specific Manner Across Gestation in the Mouse¹. *Biology of Reproduction*. DOI:10.1095/biolreprod.113.117259.
325. Song *et al.* (2017). Prenatal high-fat diet alters placental morphology, nutrient transporter expression, and mtorc1 signaling in rat. *Obesity*. DOI:10.1002/oby.21821.
326. Segovia *et al.* (2014). Maternal Obesity, Inflammation, and Developmental Programming.

327. Mayor *et al.* (2015). Maternal high-fat diet is associated with impaired fetal lung development. *American Journal of Physiology-Lung Cellular and Molecular Physiology*. DOI:10.1152/ajplung.00105.2015.
328. Wallace *et al.* (2019). Obesity during pregnancy results in maternal intestinal inflammation, placental hypoxia, and alters fetal glucose metabolism at mid-gestation. *Scientific Reports*. DOI:10.1038/s41598-019-54098-x.
329. Bruce *et al.* (2009). Maternal high-fat feeding primes steatohepatitis in adult mice offspring, involving mitochondrial dysfunction and altered lipogenesis gene expression. *Hepatology*. DOI:10.1002/hep.23205.
330. Mouralidarane *et al.* (2013). Maternal obesity programs offspring nonalcoholic fatty liver disease by innate immune dysfunction in mice. *Hepatology*. DOI:10.1002/hep.26248.
331. Thompson *et al.* (2019). Transgenerational impact of maternal obesogenic diet on offspring bile acid homeostasis and nonalcoholic fatty liver disease. *American Journal of Physiology-Endocrinology and Metabolism*. DOI:10.1152/ajpendo.00474.2018.
332. Yokomizo *et al.* (2014). Maternal high-fat diet induces insulin resistance and deterioration of pancreatic β -cell function in adult offspring with sex differences in mice. *American Journal of Physiology-Endocrinology and Metabolism*. DOI:10.1152/ajpendo.00688.2013.
333. Pileggi *et al.* (2016). Maternal High Fat Diet Alters Skeletal Muscle Mitochondrial Catalytic Activity in Adult Male Rat Offspring. *Frontiers in Physiology*. DOI:10.3389/fphys.2016.00546.
334. Niculescu & Lupu (2009). High fat diet-induced maternal obesity alters fetal hippocampal development. *International Journal of Developmental Neuroscience*. DOI:10.1016/j.ijdevneu.2009.08.005.
335. Mendes-da-Silva *et al.* (2014). Maternal high-fat diet during pregnancy or lactation changes the somatic and neurological development of the offspring. *Arquivos de Neuro-Psiquiatria*. DOI:10.1590/0004-282x20130220.
336. Corder *et al.* (2019). Maternal high-fat diet results in cognitive impairment and hippocampal gene expression changes in rat offspring. *Experimental Neurology*. DOI:10.1016/j.expneurol.2019.04.018.
337. Bilbo & Tsang (2010). Enduring consequences of maternal obesity for brain inflammation and behavior of offspring. *The FASEB Journal*. DOI:10.1096/fj.09-144014.
338. Yan *et al.* (2011). Maternal obesity induces sustained inflammation in both fetal and offspring large intestine of sheep. *Inflammatory Bowel Diseases*. DOI:10.1002/ibd.21539.
339. Fink *et al.* (2014). Pro-Inflammatory macrophages increase in skeletal muscle of high fat-Fed mice and correlate with metabolic risk markers in humans. *Obesity*. DOI:10.1002/oby.20615.
340. Häberg *et al.* (2009). Maternal obesity in pregnancy and respiratory health in early childhood. *Paediatric and Perinatal Epidemiology*. DOI:10.1111/j.1365-3016.2009.01034.x.
341. McIntyre *et al.* (2012). Overweight and obesity in Australian mothers: epidemic or endemic? *Medical Journal of Australia*. DOI:10.5694/mja11.11120.
342. Storme *et al.* (2013). Pathophysiology of persistent pulmonary hypertension of the newborn: Impact of the perinatal environment. *Archives of Cardiovascular Diseases*. DOI:10.1016/j.acvd.2012.12.005.
343. Guerra *et al.* (2013). Maternal Prepregnancy Obesity is an Independent Risk Factor for Frequent Wheezing in Infants by Age 14 Months. *Paediatric and Perinatal Epidemiology*. DOI:10.1111/ppe.12013.
344. Leermakers *et al.* (2013). Maternal weight, gestational weight gain and preschool wheezing: the Generation R Study. *European Respiratory Journal*. DOI:10.1183/09031936.00148212.

345. Forno *et al.* (2014). Maternal Obesity in Pregnancy, Gestational Weight Gain, and Risk of Childhood Asthma. *Pediatrics*. DOI:10.1542/peds.2014-0439.
346. Rusconi & Popovic (2017). Maternal obesity and childhood wheezing and asthma. *Paediatric Respiratory Reviews*. DOI:10.1016/j.prrv.2016.08.009.
347. Griffiths *et al.* (2016). Maternal high-fat hypercaloric diet during pregnancy results in persistent metabolic and respiratory abnormalities in offspring. *Pediatric Research*. DOI:10.1038/pr.2015.226.
348. MacDonald *et al.* (2017). Maternal high-fat diet in mice leads to innate airway hyperresponsiveness in the adult offspring. *Physiological Reports*. DOI:10.14814/phy2.13082.
349. Smoothy *et al.* (2019). Maternal high fat diet compromises survival and modulates lung development of offspring, and impairs lung function of dams (female mice). *Respiratory Research*. DOI:10.1186/s12931-019-0976-3.
350. Grasmann *et al.* (2017). Effects of fetal exposure to high-fat diet or maternal hyperglycemia on L-arginine and nitric oxide metabolism in lung. *Nutrition & Diabetes*. DOI:10.1038/nutd.2016.56.
351. Altaany *et al.* (2013). Crosstalk between hydrogen sulfide and nitric oxide in endothelial cells. *Journal of Cellular and Molecular Medicine*. DOI:10.1111/jcmm.12077.
352. Kramer *et al.* (2009). Prenatal inflammation and lung development. *Seminars in Fetal and Neonatal Medicine*. DOI:10.1016/j.siny.2008.08.011.
353. McEvoy *et al.* (2013). Maternal High-Fat Diet Induced Obesity As A Modifier Of Offspring Lung Development. in *b58. Chronic obstructive pulmonary disease and diet impacts on populations and systems* A3175–A3175.
354. Mayor *et al.* (2013). In Utero Exposure to Maternal High Fat Diet Increases Fetal Lung Inflammation Impairing Lung Development. in *AAP national conference and exhibition* <https://aap.confex.com/aap/2013/webprogram/Paper21997.html>.
355. Song *et al.* (2015). Maternal high-fat diet feeding during pregnancy and lactation augments lung inflammation and remodeling in the offspring. *Respiratory Physiology & Neurobiology*. DOI:10.1016/j.resp.2014.12.003.
356. Ornellas *et al.* (2017). Obese fathers lead to an altered metabolism and obesity in their children in adulthood: review of experimental and human studies. *Journal de Pediatria*. DOI:10.1016/j.jpmed.2017.02.004.
357. Agarwal *et al.* (2018). Maternal obesity, diabetes during pregnancy and epigenetic mechanisms that influence the developmental origins of cardiometabolic disease in the offspring. *Critical Reviews in Clinical Laboratory Sciences*. DOI:10.1080/10408363.2017.1422109.
358. Mørkve Knudsen *et al.* (2018). Transgenerational and intergenerational epigenetic inheritance in allergic diseases. *Journal of Allergy and Clinical Immunology*. DOI:10.1016/j.jaci.2018.07.007.
359. Perez & Lehner (2019). Intergenerational and transgenerational epigenetic inheritance in animals. *Nature Cell Biology*. DOI:10.1038/s41556-018-0242-9.
360. Alhashem *et al.* (2014). Exercise protects against obesity induced semen abnormalities via downregulating stem cell factor, upregulating Ghrelin and normalizing oxidative stress. *EXCLI journal* 13, 551–572.
361. Rato *et al.* (2014). High-energy diets: a threat for male fertility? *Obesity Reviews*. DOI:10.1111/obr.12226.
362. McPherson *et al.* (2013). Improving Metabolic Health in Obese Male Mice via Diet and Exercise Restores Embryo Development and Fetal Growth. *PLoS ONE*. DOI:10.1371/journal.pone.0071459.

363. Ng *et al.* (2010). Chronic high-fat diet in fathers programs β -cell dysfunction in female rat offspring. *Nature*. DOI:10.1038/nature09491.
364. Soubry (2018). POHaD: why we should study future fathers. *Environmental Epigenetics*. DOI:10.1093/eep/dvy007.
365. Brust *et al.* (2015). Lifetime development of behavioural phenotype in the house mouse (*Mus musculus*). *Frontiers in Zoology*. DOI:10.1186/1742-9994-12-s1-s17.
366. Brown *et al.* (1999). A method of endotracheal intubation and pulmonary functional assessment for repeated studies in mice. *Journal of Applied Physiology*. DOI:10.1152/jappl.1999.87.6.2362.
367. Ellis *et al.* (2015). TRAIL + monocytes and monocyte-related cells cause lung damage and thereby increase susceptibility to influenza– *S treptococcus pneumoniae* coinfection. *EMBO reports*. DOI:10.15252/embr.201540473.
368. Yu *et al.* (2016). A Protocol for the Comprehensive Flow Cytometric Analysis of Immune Cells in Normal and Inflamed Murine Non-Lymphoid Tissues. *PLOS ONE*. DOI:10.1371/journal.pone.0150606.
369. Newell *et al.* (2012). Cytometry by Time-of-Flight Shows Combinatorial Cytokine Expression and Virus-Specific Cell Niches within a Continuum of CD8+ T Cell Phenotypes. *Immunity*. DOI:10.1016/j.immuni.2012.01.002.
370. Nettesey *et al.* (2018). OMIP-050: A 28-color/30-parameter Fluorescence Flow Cytometry Panel to Enumerate and Characterize Cells Expressing a Wide Array of Immune Checkpoint Molecules. *Cytometry Part A*. DOI:10.1002/cyto.a.23608.
371. Pachón *et al.* (2012). Subjectivity and flow cytometric variability. *Nature Reviews Immunology*. DOI:10.1038/nri3158-c1.
372. Mair *et al.* (2016). The end of gating? An introduction to automated analysis of high dimensional cytometry data. *European Journal of Immunology*. DOI:10.1002/eji.201545774.
373. Naim *et al.* (2014). SWIFT-scalable clustering for automated identification of rare cell populations in large, high-dimensional flow cytometry datasets, Part 1: Algorithm design. *Cytometry Part A*. DOI:10.1002/cyto.a.22446.
374. Aghaeepour *et al.* (2013). Critical assessment of automated flow cytometry data analysis techniques. *Nature Methods*. DOI:10.1038/nmeth.2365.
375. Saeys *et al.* (2016). Computational flow cytometry: helping to make sense of high-dimensional immunology data. *Nature Reviews Immunology*. DOI:10.1038/nri.2016.56.
376. Nowicka *et al.* (2017). CyTOF workflow: differential discovery in high-throughput high-dimensional cytometry datasets. *F1000Research*. DOI:10.12688/f1000research.11622.2.
377. Jiang *et al.* (2020). CytoML: A GatingML Interface for Cross Platform Cytometry Data Sharing. <https://github.com/RGLab/CytoML>.
378. Finak & Jiang (2019). flowWorkspace: Infrastructure for representing and interacting with gated and ungated cytometry data sets.
379. Van Gassen *et al.* (2019). FlowSOM: Using self-organizing maps for visualization and interpretation of cytometry data.
380. Wilkerson *et al.* (2010). ConsensusClusterPlus: a class discovery tool with confidence assessments and item tracking. *Bioinformatics* 26, 1572–1573.
381. Krijthe (2015). {Rtsne}: T-Distributed Stochastic Neighbor Embedding using Barnes-Hut Implementation. <https://github.com/jkrijthe/Rtsne>.
382. Dutta & Sengupta (2016). Men and mice: Relating their ages. *Life Sciences*.

DOI:10.1016/j.lfs.2015.10.025.

383. Thurlbeck (1967). Internal surface area and other measurements in emphysema. *Thorax*. DOI:10.1136/thx.22.6.483.
384. Feuchtinger *et al.* (2015). Image analysis of immunohistochemistry is superior to visual scoring as shown for patient outcome of esophageal adenocarcinoma. *Histochemistry and Cell Biology*. DOI:10.1007/s00418-014-1258-2.
385. Primer designing tool. <https://www.ncbi.nlm.nih.gov/tools/primer-blast/>.
386. Vandesompele *et al.* (2002). Accurate normalization of real-time quantitative RT-PCR data by geometric averaging of multiple internal control genes. *Genome Biology*. DOI:10.1186/gb-2002-3-7-research0034.
387. Livak & Schmittgen (2001). Analysis of Relative Gene Expression Data Using Real-Time Quantitative PCR and the $2^{-\Delta\Delta CT}$ Method. *Methods*. DOI:10.1006/meth.2001.1262.
388. RStudio Team (2018). RStudio: Integrated Development Environment for R. <http://www.rstudio.com/>.
389. R Core Team (2018). R: A Language and Environment for Statistical Computing. <https://www.r-project.org/>.
390. Robinson & Hayes (2018). broom: Convert Statistical Analysis Objects into Tidy Tibbles. <https://cran.r-project.org/package=broom>.
391. Fox *et al.* (2018). car: Companion to Applied Regression. <https://cran.r-project.org/package=car>.
392. Wilke (2019). cowplot: Streamlined Plot Theme and Plot Annotations for 'ggplot2'. <https://cran.r-project.org/package=cowplot>.
393. Wickham *et al.* (2019). dplyr: A Grammar of Data Manipulation. <https://cran.r-project.org/package=dplyr>.
394. Ellis *et al.* (2019). flowCore: Basic structures for flow cytometry data.
395. Wickham (2019). forcats: Tools for Working with Categorical Variables (Factors). <https://cran.r-project.org/package=forcats>.
396. Wickham *et al.* (2020). ggplot2: Create Elegant Data Visualisations Using the Grammar of Graphics. <https://cran.r-project.org/package=ggplot2>.
397. Wilke (2020). ggridges: Ridgeline Plots in 'ggplot2'. <https://cran.r-project.org/package=ggridges>.
398. Zhu (2019). kableExtra: Construct Complex Table with 'kable' and Pipe Syntax. <https://cran.r-project.org/package=kableExtra>.
399. Xie (2020). knitr: A General-Purpose Package for Dynamic Report Generation in R. <https://cran.r-project.org/package=knitr>.
400. Edwards (2020). lemon: Freshing Up your 'ggplot2' Plots. <https://cran.r-project.org/package=lemon>.
401. Bache & Wickham (2014). magrittr: A Forward-Pipe Operator for R. <https://cran.r-project.org/package=magrittr>.
402. Henry & Wickham (2019). purrr: Functional Programming Tools. <https://cran.r-project.org/package=purrr>.
403. Allaire *et al.* (2020). rmarkdown: Dynamic Documents for R. <https://cran.r-project.org/package=rmarkdown>.
404. Krijthe (2018). Rtsne: T-Distributed Stochastic Neighbor Embedding using a Barnes-Hut Implementation. <https://cran.r-project.org/package=Rtsne>.
405. Wickham (2018). scales: Scale Functions for Visualization. <https://cran.r-project.org/package=scales>.

406. Wickham (2019). stringr: Simple, Consistent Wrappers for Common String Operations. <https://cran.r-project.org/package=stringr>.
407. Wickham & Henry (2019). tidyr: Easily Tidy Data with 'spread()' and 'gather()' Functions. <https://cran.r-project.org/package=tidyr>.
408. Xie (2020). bookdown: Authoring Books and Technical Documents with R Markdown. <https://cran.r-project.org/package=bookdown>.
409. Wickham *et al.* (2018). readr: Read Rectangular Text Data. <https://cran.r-project.org/package=readr>.
410. LaTeX - A document preparation system. <https://www.latex-project.org/>.
411. Wickham (2014). Tidy Data. *Journal of Statistical Software*. DOI:10.18637/jss.v059.i10.
412. Heijden *et al.* (2015). High-fat diet induced obesity primes inflammation in adipose tissue prior to liver in C57BL/6j mice. *Aging*. DOI:10.18632/aging.100738.
413. Greenlee-Wacker (2016). Clearance of apoptotic neutrophils and resolution of inflammation. *Immunological reviews*. DOI:10.1111/imr.12453.
414. Hochreiter-Hufford & Ravichandran (2013). Clearing the dead: apoptotic cell sensing, recognition, engulfment, and digestion. *Cold Spring Harbor perspectives in biology*. DOI:10.1101/cshperspect.a008748.
415. Erwig & Henson (2008). Clearance of apoptotic cells by phagocytes. *Cell Death & Differentiation*. DOI:10.1038/sj.cdd.4402184.
416. Roberts *et al.* (2011). Placental structure and inflammation in pregnancies associated with obesity. *Placenta*. DOI:10.1016/j.placenta.2010.12.023.
417. Dagvadorj *et al.* (2015). Lipopolysaccharide Induces Alveolar Macrophage Necrosis via CD14 and the P2X7 Receptor Leading to Interleukin-1 α Release. *Immunity*. DOI:10.1016/j.immuni.2015.03.007.
418. Surwit *et al.* (1988). Diet-Induced Type II Diabetes in C57BL/6J Mice. *Diabetes*. DOI:10.2337/diab.37.9.1163.
419. Surwit *et al.* (1991). Control of Expression of Insulin Resistance and Hyperglycemia by Different Genetic Factors in Diabetic C57BL/6J Mice. *Diabetes*. DOI:10.2337/diab.40.1.82.
420. Jones *et al.* (2009). High-fat diet before and during pregnancy causes marked up-regulation of placental nutrient transport and fetal overgrowth in C57/BL6 mice. *The FASEB Journal*. DOI:10.1096/fj.08-116889.
421. Fjære *et al.* (2014). Indomethacin Treatment Prevents High Fat Diet-induced Obesity and Insulin Resistance but Not Glucose Intolerance in C57BL/6J Mice. *Journal of Biological Chemistry*. DOI:10.1074/jbc.m113.525220.
422. Collins *et al.* (2004). Genetic vulnerability to diet-induced obesity in the C57BL/6J mouse: Physiological and molecular characteristics. *Physiology and Behavior*. DOI:10.1016/j.physbeh.2004.02.006.
423. Rebuffé-Scrive *et al.* (1993). Regional fat distribution and metabolism in a new mouse model (C57BL/6J) of non-insulin-dependent diabetes mellitus. *Metabolism: clinical and experimental*. DOI:10.1016/0026-0495(93)90190-y.
424. Nishikawa *et al.* (2007). Involvement of sex, strain and age factors in high fat diet-induced obesity in C57BL/6J and BALB/cA mice. *Experimental Animals*. DOI:10.1538/expanim.56.263.
425. Wen *et al.* (2013). Treadmill Exercise Training Modulates Hepatic Cholesterol Metabolism and Circulating PCSK9 Concentration in High-Fat-Fed Mice. *Journal of Lipids*. DOI:10.1155/2013/908048.
426. Luo *et al.* (2020). Metabolic Syndrome Is Reduced in C57BL/6J Mice Fed High-Fat Diets Supplemented with Oak Tannins. *Current Developments in Nutrition*.

DOI:10.1093/cdn/nzaa033.

427. Couvreur *et al.* (2011). Unexpected Long-Term Protection of Adult Offspring Born to High-Fat Fed Dams against Obesity Induced by a Sucrose-Rich Diet. *PLoS ONE*. DOI:10.1371/journal.pone.0018043.
428. Licholai *et al.* (2018). Why Do Mice Overeat High-Fat Diets? How High-Fat Diet Alters the Regulation of Daily Caloric Intake in Mice. *Obesity*. DOI:10.1002/oby.22195.
429. Heindel & Saal (2008). Meeting report: Batch-to-batch variability in estrogenic activity in commercial animal diets - Importance and approaches for Laboratory Animal Research. in *Environmental health perspectives*. DOI:10.1289/ehp.10524.
430. Speakman (2019). Use of high-fat diets to study rodent obesity as a model of human obesity. DOI:10.1038/s41366-019-0363-7.
431. Bortolin *et al.* (2018). A new animal diet based on human Western diet is a robust diet-induced obesity model: Comparison to high-fat and cafeteria diets in term of metabolic and gut microbiota disruption. *International Journal of Obesity*. DOI:10.1038/ijo.2017.225.
432. Hintze *et al.* (2018). Modeling the western diet for preclinical investigations. DOI:10.1093/advances/nmy002.
433. Thomas *et al.* (2011). Inflammatory Phenotyping Identifies CD11d as a Gene Markedly Induced in White Adipose Tissue in Obese Rodents and Women. *The Journal of Nutrition*. DOI:10.3945/jn.110.127068.
434. Platt *et al.* (2014). Adult offspring of high-fat diet-fed dams can have normal glucose tolerance and body composition. *Journal of Developmental Origins of Health and Disease*. DOI:10.1017/s2040174414000154.
435. Lang *et al.* (2019). Effects of different diets used in diet-induced obesity models on insulin resistance and vascular dysfunction in C57BL/6 mice. *Scientific Reports*. DOI:10.1038/s41598-019-55987-x.
436. Buyukdere *et al.* (2019). Cafeteria diet increased adiposity in comparison to high fat diet in young male rats. *PeerJ*. DOI:10.7717/peerj.6656.
437. Lanza *et al.* (2014). Effects of a post-weaning cafeteria diet in young rats: Metabolic syndrome, reduced activity and low anxiety-like behaviour. *PLoS ONE*. DOI:10.1371/journal.pone.0085049.
438. Gomez-Smith *et al.* (2016). A physiological characterization of the Cafeteria diet model of metabolic syndrome in the rat. *Physiology and Behavior*. DOI:10.1016/j.physbeh.2016.09.029.
439. Oliva *et al.* (2017). In rats fed high-energy diets, taste, rather than fat content, is the key factor increasing food intake: A comparison of a cafeteria and a lipid-supplemented standard diet. *PeerJ*. DOI:10.7717/peerj.3697.
440. Götz *et al.* (2011). Comparison of particle-exposure triggered pulmonary and systemic inflammation in mice fed with three different diets. *Particle and Fibre Toxicology*. DOI:10.1186/1743-8977-8-30.
441. Tunglund (Elsevier, 2018). Dysbiosis of the Microbiota: Therapeutic Strategies Utilizing Dietary Modification, Pro- and Prebiotics and Fecal Transplant Therapies in Promoting Normal Balance and Local GI Functions. in *Human microbiota in health and disease*. DOI:10.1016/b978-0-12-814649-1.00009-0.
442. Wang & Liao (2012). A Mouse Model of Diet-Induced Obesity and Insulin Resistance. in *Methods in molecular biology*. DOI:10.1007/978-1-61779-430-8_27.
443. Lee *et al.* (2011). Inflammation Is Necessary for Long-Term but Not Short-Term High-Fat Diet-Induced Insulin Resistance. *Diabetes*. DOI:10.2337/db11-0194.
444. Williams *et al.* (2014). The Development of Diet-Induced Obesity and Glucose Intolerance in C57Bl/6 Mice on a High-Fat Diet Consists of Distinct Phases. *PLoS ONE*.

DOI:10.1371/journal.pone.0106159.

445. Mosser *et al.* (2015). High-fat diet-induced β -cell proliferation occurs prior to insulin resistance in C57Bl/6J male mice. *American Journal of Physiology-Endocrinology and Metabolism*. DOI:10.1152/ajpendo.00460.2014.
446. Kahle *et al.* (2013). Phenotypic comparison of common mouse strains developing high-fat diet-induced hepatosteatosis. *Molecular Metabolism*. DOI:10.1016/j.molmet.2013.07.009.
447. Ozaki *et al.* (2016). Muscle growth across a variety of exercise modalities and intensities: Contributions of mechanical and metabolic stimuli. *Medical Hypotheses*. DOI:10.1016/j.mehy.2015.12.026.
448. Drago *et al.* (1982). Aromatization of Testosterone by Adipose Tissue and Sexual Behavior of Castrated Male Rats. *Biology of Reproduction*. DOI:10.1095/biolreprod27.4.765.
449. Saad & Gooren (2011). The Role of Testosterone in the Etiology and Treatment of Obesity, the Metabolic Syndrome, and Diabetes Mellitus Type 2. *Journal of Obesity*. DOI:10.1155/2011/471584.
450. Koster *et al.* (2011). Does the Amount of Fat Mass Predict Age-Related Loss of Lean Mass, Muscle Strength, and Muscle Quality in Older Adults? *The Journals of Gerontology Series A: Biological Sciences and Medical Sciences*. DOI:10.1093/gerona/glr070.
451. Schaap *et al.* (2006). Inflammatory Markers and Loss of Muscle Mass (Sarcopenia) and Strength. *The American Journal of Medicine*. DOI:10.1016/j.amjmed.2005.10.049.
452. Koza *et al.* (2006). Changes in gene expression foreshadow diet-induced obesity in genetically identical mice. *PLoS Genetics*. DOI:10.1371/journal.pgen.0020081.
453. Yang *et al.* (2014). Variations in body weight, Food Intake and body composition after long-term high-fat diet feeding in C57BL/6J mice. *Obesity*. DOI:10.1002/oby.20811.
454. Mull *et al.* (2014). The Murphy Roths Large (MRL) mouse strain is naturally resistant to high fat diet-induced hyperglycemia. *Metabolism: Clinical and Experimental*. DOI:10.1016/j.metabol.2014.09.007.
455. Roberts *et al.* (2015). Successful metabolic adaptations leading to the prevention of high fat diet-induced murine cardiac remodeling. *Cardiovascular Diabetology*. DOI:10.1186/s12933-015-0286-0.
456. Ornellas *et al.* (2015). Programming of Obesity and Comorbidities in the Progeny: Lessons from a Model of Diet-Induced Obese Parents. *PLOS ONE*. DOI:10.1371/journal.pone.0124737.
457. Russell & Burch (Methuen, 1959). *The principles of humane experimental technique*.
458. Kim *et al.* (2012). High Fat Diet-Induced Gut Microbiota Exacerbates Inflammation and Obesity in Mice via the TLR4 Signaling Pathway. *PLoS ONE*. DOI:10.1371/journal.pone.0047713.
459. Klop *et al.* (2013). Dyslipidemia in Obesity: Mechanisms and Potential Targets. *Nutrients*. DOI:10.3390/nu5041218.
460. Lee *et al.* (2001). Saturated Fatty Acids, but Not Unsaturated Fatty Acids, Induce the Expression of Cyclooxygenase-2 Mediated through Toll-like Receptor 4. *Journal of Biological Chemistry*. DOI:10.1074/jbc.m011695200.
461. Hwang *et al.* (2016). Mechanisms for the activation of Toll-like receptor 2/4 by saturated fatty acids and inhibition by docosahexaenoic acid. *European Journal of Pharmacology*. DOI:10.1016/j.ejphar.2016.04.024.
462. Suganami *et al.* (2007). Role of the Toll-like Receptor 4/NF- κ B Pathway in Saturated Fatty Acid-Induced Inflammatory Changes in the Interaction Between Adipocytes and Macrophages. *Arteriosclerosis, Thrombosis, and Vascular Biology*. DOI:10.1161/01.atv.0000251608.09329.9a.

463. Hotamisligil (2005). Role of Endoplasmic Reticulum Stress and c-Jun NH2-Terminal Kinase Pathways in Inflammation and Origin of Obesity and Diabetes. *Diabetes*. DOI:10.2337/diabetes.54.suppl_2.s73.
464. Inoguchi *et al.* (2000). High glucose level and free fatty acid stimulate reactive oxygen species production through protein kinase C-dependent activation of NAD(P)H oxidase in cultured vascular cells. *Diabetes*. DOI:10.2337/diabetes.49.11.1939.
465. Raetz (1990). Biochemistry of Endotoxins. *Annual Review of Biochemistry*. DOI:10.1146/annurev.bi.59.070190.001021.
466. Munford & Hall (1986). Detoxification of bacterial lipopolysaccharides (endotoxins) by a human neutrophil enzyme. *Science*. DOI:10.1126/science.3529396.
467. Rogero & Calder (2018). Obesity, Inflammation, Toll-Like Receptor 4 and Fatty Acids. *Nutrients*. DOI:10.3390/nu10040432.
468. Kitchens *et al.* (1992). Lipopolysaccharide (LPS) partial structures inhibit responses to LPS in a human macrophage cell line without inhibiting LPS uptake by a CD14-mediated pathway. *The Journal of Experimental Medicine*. DOI:10.1084/jem.176.2.485.
469. Torre *et al.* (1994). Effect of Recombinant IL-1 Beta and Recombinant Gamma Interferon on Septic Acute Lung Injury in Mice. *Chest*. DOI:10.1378/chest.105.4.1241.
470. Severgnini *et al.* (2004). Activation of the STAT pathway in acute lung injury. *American Journal of Physiology-Lung Cellular and Molecular Physiology*. DOI:10.1152/ajplung.00349.2003.
471. Everhart *et al.* (2006). Duration and Intensity of NF- κ B Activity Determine the Severity of Endotoxin-Induced Acute Lung Injury. *The Journal of Immunology*. DOI:10.4049/jimmunol.176.8.4995.
472. Gross *et al.* (2018). LPS-induced Acute Lung Injury Involves NF- κ B-mediated Downregulation of SOX18. *American Journal of Respiratory Cell and Molecular Biology*. DOI:10.1165/rcmb.2016-0390oc.
473. Notter (CRC Press, 2000). *Lung surfactants: basic science and clinical applications*.
474. Fröhlich *et al.* (2016). Measurements of Deposition, Lung Surface Area and Lung Fluid for Simulation of Inhaled Compounds. *Frontiers in Pharmacology*. DOI:10.3389/fphar.2016.00181.
475. Dixon & Peters (2018). The effect of obesity on lung function. *Expert Review of Respiratory Medicine*. DOI:10.1080/17476348.2018.1506331.
476. Centers for Disease Control and Prevention (CDC) (2009). Intensive-care patients with severe novel influenza A (H1N1) virus infection - Michigan, June 2009. *MMWR. Morbidity and mortality weekly report* 58, 749–52.
477. Vaillant *et al.* (2009). Epidemiology of fatal cases associated with pandemic H1N1 influenza 2009. *Eurosurveillance*. DOI:10.2807/ese.14.33.19309-en.
478. Fezeu *et al.* (2011). Obesity is associated with higher risk of intensive care unit admission and death in influenza A (H1N1) patients: a systematic review and meta-analysis. *Obesity Reviews*. DOI:10.1111/j.1467-789x.2011.00864.x.
479. Sheridan *et al.* (2012). Obesity is associated with impaired immune response to influenza vaccination in humans. *International Journal of Obesity*. DOI:10.1038/ijo.2011.208.
480. Petrilli *et al.* (2020). Factors associated with hospital admission and critical illness among 5279 people with coronavirus disease 2019 in New York City: prospective cohort study. *BMJ*. DOI:10.1136/bmj.m1966.
481. Dietz & Santos-Burgoa (2020). Obesity and its Implications for COVID-19 Mortality. *Obesity*. DOI:10.1002/oby.22818.
482. Kassir (2020). Risk of COVID-19 for patients with obesity. *Obesity Reviews*. DOI:10.1111/obr.13034.

483. Karlsson *et al.* (2010). Diet-Induced Obesity Impairs the T Cell Memory Response to Influenza Virus Infection. *The Journal of Immunology*. DOI:10.4049/jimmunol.0903220.
484. Easterbrook *et al.* (2011). Obese mice have increased morbidity and mortality compared to non-obese mice during infection with the 2009 pandemic H1N1 influenza virus. *Influenza and Other Respiratory Viruses*. DOI:10.1111/j.1750-2659.2011.00254.x.
485. Hoffmann *et al.* (2016). Viral and bacterial co-infection in severe pneumonia triggers innate immune responses and specifically enhances IP-10: a translational study. *Scientific Reports*. DOI:10.1038/srep38532.
486. Alfaraj *et al.* (2019). Middle East Respiratory Syndrome Coronavirus (MERS-CoV) infection during pregnancy: Report of two cases & review of the literature. *Journal of Microbiology, Immunology and Infection*. DOI:10.1016/j.jmii.2018.04.005.
487. Wong *et al.* (2004). Pregnancy and perinatal outcomes of women with severe acute respiratory syndrome. *American Journal of Obstetrics and Gynecology*. DOI:10.1016/j.ajog.2003.11.019.
488. Tranchot-Diallo *et al.* (1997). Modulations of Cytokine Expression in Pregnant Women. *American Journal of Reproductive Immunology*. DOI:10.1111/j.1600-0897.1997.tb00218.x.
489. Dealtry *et al.* (2000). The Th2 Cytokine Environment of the Placenta. *International Archives of Allergy and Immunology*. DOI:10.1159/000024441.
490. Sykes *et al.* (2012). The Th1:Th2 Dichotomy of Pregnancy and Preterm Labour. *Mediators of Inflammation*. DOI:10.1155/2012/967629.
491. Dashraath *et al.* (2020). Coronavirus disease 2019 (COVID-19) pandemic and pregnancy. *American Journal of Obstetrics and Gynecology*. DOI:10.1016/j.ajog.2020.03.021.
492. Singh & Perfect (2007). Immune Reconstitution Syndrome and Exacerbation of Infections after Pregnancy. *Clinical Infectious Diseases*. DOI:10.1086/522182.
493. Rothman (1990). No adjustments are needed for multiple comparisons. *Epidemiology (Cambridge, Mass.)* 1, 43–6.
494. Software GraphPad Inc. (2017). When it makes sense to not correct for multiple comparisons. https://www.graphpad.com/guides/prism/7/statistics/index.htm?stat%7B/_%7Dwhen%7B/_%7Dto%7B/_%7Dnot%7B/_%7Dcorrect%7B/_%7Dfor%7B/_%7D2.htm.
495. Allard *et al.* (2018). Alveolar Macrophages in the Resolution of Inflammation, Tissue Repair, and Tolerance to Infection. *Frontiers in Immunology*. DOI:10.3389/fimmu.2018.01777.
496. Chen *et al.* (2016). Immunoproteasome dysfunction augments alternative polarization of alveolar macrophages. *Cell Death & Differentiation*. DOI:10.1038/cdd.2016.3.
497. Xie *et al.* (2016). Effects of IRF1 and IFN- β interaction on the M1 polarization of macrophages and its antitumor function. *International Journal of Molecular Medicine*. DOI:10.3892/ijmm.2016.2583.
498. Cui *et al.* (2018). Distinct Migratory Properties of M1, M2, and Resident Macrophages Are Regulated by α D β 2 and α M β 2 Integrin-Mediated Adhesion. *Frontiers in Immunology*. DOI:10.3389/fimmu.2018.02650.
499. Zhu *et al.* (2016). Connexin 43 Mediates White Adipose Tissue Beiging by Facilitating the Propagation of Sympathetic Neuronal Signals. *Cell Metabolism*. DOI:10.1016/j.cmet.2016.08.005.
500. Recabal *et al.* (2018). Connexin-43 Gap Junctions Are Responsible for the Hypothalamic Tanycyte-Coupled Network. *Frontiers in Cellular Neuroscience*. DOI:10.3389/fncel.2018.00406.
501. Henson (2005). Dampening inflammation. *Nature Immunology*. DOI:10.1038/ni1205-1179.
502. Wherry & Kurachi (2015). Molecular and cellular insights into T cell exhaustion. *Nature*

Reviews Immunology. DOI:10.1038/nri3862.

503. Zent & Elliott (2017). Maxed out macs: physiologic cell clearance as a function of macrophage phagocytic capacity. *The FEBS Journal*. DOI:10.1111/febs.13961.
504. Pinney *et al.* (2020). Macrophage hypophagia as a mechanism of innate immune exhaustion in mAb-induced cell clearance. *Blood*. DOI:10.1182/blood.2020005571.
505. Gahring & Daynes (1986). Desensitization of animals to the inflammatory effects of ultraviolet radiation is mediated through mechanisms which are distinct from those responsible for endotoxin tolerance. *The Journal of Immunology*.
506. Xiong & Medvedev (2011). Induction of endotoxin tolerance in vivo inhibits activation of IRAK4 and increases negative regulators IRAK-M, SHIP-1, and A20. *Journal of Leukocyte Biology*. DOI:10.1189/jlb.0611273.
507. Biswas & Lopez-Collazo (2009). Endotoxin tolerance: new mechanisms, molecules and clinical significance. *Trends in Immunology*. DOI:10.1016/j.it.2009.07.009.
508. Cani *et al.* (2007). Metabolic Endotoxemia Initiates Obesity and Insulin Resistance. *Diabetes*. DOI:10.2337/db06-1491.
509. Nagpal *et al.* (2018). Obesity-Linked Gut Microbiome Dysbiosis Associated with Derangements in Gut Permeability and Intestinal Cellular Homeostasis Independent of Diet. *Journal of Diabetes Research*. DOI:10.1155/2018/3462092.
510. Takemura *et al.* (2007). Adiponectin modulates inflammatory reactions via calreticulin receptor-dependent clearance of early apoptotic bodies. *Journal of Clinical Investigation*. DOI:10.1172/jci29709.
511. Bullen *et al.* (2007). Regulation of adiponectin and its receptors in response to development of diet-induced obesity in mice. *American Journal of Physiology-Endocrinology and Metabolism*. DOI:10.1152/ajpendo.00245.2006.
512. Claycombe *et al.* (2008). A role for leptin in sustaining lymphopoiesis and myelopoiesis. *Proceedings of the National Academy of Sciences*. DOI:10.1073/pnas.0712053105.
513. Frasca & McElhaney (2019). Influence of Obesity on Pneumococcus Infection Risk in the Elderly. *Frontiers in Endocrinology*. DOI:10.3389/fendo.2019.00071.
514. Vernooy *et al.* (2013). Leptin as regulator of pulmonary immune responses: Involvement in respiratory diseases. *Pulmonary Pharmacology & Therapeutics*. DOI:10.1016/j.pupt.2013.03.016.
515. Mancuso *et al.* (2018). Ablation of the leptin receptor in myeloid cells impairs pulmonary clearance of *Streptococcus pneumoniae* and alveolar macrophage bactericidal function. *American Journal of Physiology-Lung Cellular and Molecular Physiology*. DOI:10.1152/ajplung.00447.2017.
516. Lin *et al.* (2000). Development of high fat diet-induced obesity and leptin resistance in C57Bl/6J mice. *International Journal of Obesity*. DOI:10.1038/sj.ijo.0801209.
517. Wilding Crawford *et al.* (2010). Histology atlas of the developing mouse hepatobiliary system with emphasis on embryonic days 9.5-18.5. *Toxicologic Pathology*. DOI:10.1177/0192623310374329.
518. Lephart *et al.* (2004). Dietary isoflavones alter regulatory behaviors, metabolic hormones and neuroendocrine function in Long-Evans male rats. *Nutrition and Metabolism*. DOI:10.1186/1743-7075-1-16.
519. Baker (1995). Endocrine Activity of Plant-Derived Compounds: An Evolutionary Perspective. *Experimental Biology and Medicine*. DOI:10.3181/00379727-208-43845.
520. Adlercreutz (1998). Evolution, Nutrition, Intestinal Microflora, and Prevention of Cancer: A Hypothesis. *Experimental Biology and Medicine*. DOI:10.3181/00379727-217-44228.
521. Rizzetto *et al.* (2018). Connecting the immune system, systemic chronic

- inflammation and the gut microbiome: The role of sex. *Journal of Autoimmunity*. DOI:10.1016/j.jaut.2018.05.008.
522. Kelmenson There is no such thing as a C57BL/6 mouse! <https://www.jax.org/news-and-insights/jax-blog/2016/june/there-is-no-such-thing-as-a-b6-mouse>.
523. Sans-Fons *et al.* (2013). Arginine Transport Is Impaired in C57Bl/6 Mouse Macrophages as a Result of a Deletion in the Promoter of Slc7a2 (CAT2), and Susceptibility to Leishmania Infection Is Reduced. *The Journal of Infectious Diseases*. DOI:10.1093/infdis/jit084.
524. Duleu *et al.* (2004). Mouse Strain Susceptibility to Trypanosome Infection: An Arginase-Dependent Effect. *The Journal of Immunology*. DOI:10.4049/jimmunol.172.10.6298.
525. Oliveira *et al.* (2014). A Defective TLR4 Signaling for IFN- β Expression Is Responsible for the Innately Lower Ability of BALB/c Macrophages to Produce NO in Response to LPS as Compared to C57BL/6. *PLoS ONE*. DOI:10.1371/journal.pone.0098913.
526. Nadeau-Vallée *et al.* (2016). Sterile inflammation and pregnancy complications: a review. *Reproduction*. DOI:10.1530/rep-16-0453.
527. Nicholson *et al.* (2010). Diet-induced Obesity in Two C57BL/6 Substrains With Intact or Mutant Nicotinamide Nucleotide Transhydrogenase (Nnt) Gene. *Obesity*. DOI:10.1038/oby.2009.477.
528. Bourdi *et al.* (2011). Mispairing C57BL/6 Substrains of Genetically Engineered Mice and Wild-Type Controls Can Lead to Confounding Results as It Did in Studies of JNK2 in Acetaminophen and Concanavalin A Liver Injury. *Chemical Research in Toxicology*. DOI:10.1021/tx200143x.
529. Mattapallil *et al.* (2012). The Rd8 Mutation of the Crb1 Gene Is Present in Vendor Lines of C57BL/6N Mice and Embryonic Stem Cells, and Confounds Ocular Induced Mutant Phenotypes. *Investigative Ophthalmology & Visual Science*. DOI:10.1167/iovs.12-9662.
530. Siddika *et al.* (2016). Prenatal ambient air pollution exposure and the risk of stillbirth: systematic review and meta-analysis of the empirical evidence. *Occupational and Environmental Medicine*. DOI:10.1136/oemed-2015-103086.
531. (Elsevier, 1998). *Handbook of Developmental Neurotoxicology*. DOI:10.1016/b978-0-12-648860-9.x5000-6.
532. Vogelgesang *et al.* (2014). Cigarette Smoke Exposure during Pregnancy Alters Fetomaternal Cell Trafficking Leading to Retention of Microchimeric Cells in the Maternal Lung. *PLoS ONE*. DOI:10.1371/journal.pone.0088285.
533. Redline *et al.* (2010). Murine Fetoplacental Infection Models. *Infection and Immunity*. DOI:10.1128/iai.00641-10.
534. Samsioe *et al.* (2008). Fetal death persists through recurrent pregnancies in mice following Ljungan virus infection. *Birth Defects Research Part B: Developmental and Reproductive Toxicology*. DOI:10.1002/bdrb.20169.
535. Ma *et al.* (2018). Gold nanoparticles cause size-dependent inhibition of embryonic development during murine pregnancy. *Nano Research*. DOI:10.1007/s12274-018-1969-0.
536. Bronson & Bale (2016). The Placenta as a Mediator of Stress Effects on Neurodevelopmental Reprogramming. *Neuropsychopharmacology*. DOI:10.1038/npp.2015.231.
537. Salihu (2011). Maternal Obesity and Stillbirth. *Seminars in Perinatology*. DOI:10.1053/j.semperi.2011.05.019.
538. Tessier *et al.* (2013). Role of leptin in pregnancy: Consequences of maternal obesity. *Placenta*. DOI:10.1016/j.placenta.2012.11.035.
539. Hayes *et al.* (2012). Adverse Fetal and Neonatal Outcomes Associated with a Life-Long High Fat Diet: Role of Altered Development of the Placental Vasculature. *PLoS ONE*.

DOI:10.1371/journal.pone.0033370.

540. Reynolds *et al.* (2014). High fat and/or high salt intake during pregnancy alters maternal meta-inflammation and offspring growth and metabolic profiles. *Physiological Reports*. DOI:10.14814/phy2.12110.
541. Baack *et al.* (2016). Consequences of a Maternal High-Fat Diet and Late Gestation Diabetes on the Developing Rat Lung. *PLOS ONE*. DOI:10.1371/journal.pone.0160818.
542. Luzzo *et al.* (2012). High Fat Diet Induced Developmental Defects in the Mouse: Oocyte Meiotic Aneuploidy and Fetal Growth Retardation/Brain Defects. *PLoS ONE*. DOI:10.1371/journal.pone.0049217.
543. King *et al.* (2013). The effects of an obesogenic diet during pregnancy on fetal growth and placental gene expression are gestation dependent. *Placenta*. DOI:10.1016/j.placenta.2013.09.006.
544. Edlow *et al.* (2016). Males are from Mars, and females are from Venus: Sex-specific fetal brain gene expression signatures in a mouse model of maternal diet-induced obesity. *American Journal of Obstetrics and Gynecology*. DOI:10.1016/j.ajog.2016.02.054.
545. Christians *et al.* (2019). Effects of high-fat diets on fetal growth in rodents: A systematic review. DOI:10.1186/s12958-019-0482-y.
546. Wallace *et al.* (2004). Nutritionally Mediated Placental Growth Restriction in the Growing Adolescent: Consequences for the Fetus1. *Biology of Reproduction*. DOI:10.1095/biolreprod.104.030965.
547. Jawerbaum & White (2017). Review on intrauterine programming: Consequences in rodent models of mild diabetes and mild fat overfeeding are not mild. *Placenta*. DOI:10.1016/j.placenta.2017.02.009.
548. Nam *et al.* (2017). Choline prevents fetal overgrowth and normalizes placental fatty acid and glucose metabolism in a mouse model of maternal obesity. *Journal of Nutritional Biochemistry*. DOI:10.1016/j.jnutbio.2017.08.004.
549. Heyob *et al.* (2019). Maternal high-fat diet alters lung development and function in the offspring. *American Journal of Physiology-Lung Cellular and Molecular Physiology*. DOI:10.1152/ajplung.00331.2018.
550. Liang *et al.* (2009). Gestational high saturated fat diet alters C57BL/6 mouse perinatal skeletal formation. *Birth Defects Research Part B: Developmental and Reproductive Toxicology*. DOI:10.1002/bdrb.20204.
551. Murabayashi *et al.* (2013). Maternal high-fat diets cause insulin resistance through inflammatory changes in fetal adipose tissue. *European Journal of Obstetrics and Gynecology and Reproductive Biology*. DOI:10.1016/j.ejogrb.2013.02.003.
552. Takahashi *et al.* (1999). Effect of the fat/carbohydrate ratio in the diet on obesity and oral glucose tolerance in C57BL/6J mice. *Journal of Nutritional Science and Vitaminology*. DOI:10.3177/jnsv.45.583.
553. Hu *et al.* (2018). Dietary Fat, but Not Protein or Carbohydrate, Regulates Energy Intake and Causes Adiposity in Mice. *Cell Metabolism*. DOI:10.1016/j.cmet.2018.06.010.
554. Showalter *et al.* (2018). Obesogenic diets alter metabolism in mice. *PLoS ONE*. DOI:10.1371/journal.pone.0190632.
555. El Akoum *et al.* (2011). Nature of fatty acids in high fat diets differentially delineates obesity-linked metabolic syndrome components in male and female C57BL/6J mice. *Diabetology and Metabolic Syndrome*. DOI:10.1186/1758-5996-3-34.
556. Nakatani *et al.* (2003). A low fish oil inhibits SREBP-1 proteolytic cascade, while a high-fish-oil feeding decreases SREBP-1 mRNA in mice liver: Relationship to anti-obesity. *Journal of Lipid Research*. DOI:10.1194/jlr.m200289-jlr200.
557. Buettner *et al.* (2006). Defining high-fat-diet rat models: Metabolic and molecular effects of

- different fat types. *Journal of Molecular Endocrinology*. DOI:10.1677/jme.1.01909.
558. Gallou-Kabani *et al.* (2007). C57BL/6J and A/J mice fed a high-fat diet delineate components of metabolic syndrome. *Obesity*. DOI:10.1038/oby.2007.238.
559. Arnold *et al.* (2014). High fat diet produces brain insulin resistance, synaptodendritic abnormalities and altered behavior in mice. *Neurobiology of Disease*. DOI:10.1016/j.nbd.2014.03.011.
560. Ornellas *et al.* (2013). Sexual dimorphism in fat distribution and metabolic profile in mice offspring from diet-induced obese mothers. *Life Sciences*. DOI:10.1016/j.lfs.2013.08.005.
561. Dahlhoff *et al.* (2014). Peri-conceptual obesogenic exposure induces sex-specific programming of disease susceptibilities in adult mouse offspring. *Biochimica et Biophysica Acta (BBA) - Molecular Basis of Disease*. DOI:10.1016/j.bbadis.2013.11.021.
562. Cardenas-Perez *et al.* (2018). Maternal overnutrition by hypercaloric diets programs hypothalamic mitochondrial fusion and metabolic dysfunction in rat male offspring. *Nutrition and Metabolism*. DOI:10.1186/s12986-018-0279-6.
563. Bry *et al.* (2007). IL-1 β Disrupts Postnatal Lung Morphogenesis in the Mouse. *American Journal of Respiratory Cell and Molecular Biology*. DOI:10.1165/rcmb.2006-0116oc.
564. Hogmalm *et al.* (2014). IL-1 β expression in the distal lung epithelium disrupts lung morphogenesis and epithelial cell differentiation in fetal mice. *American Journal of Physiology - Lung Cellular and Molecular Physiology*. DOI:10.1152/ajplung.00154.2013.
565. Simon *et al.* (2006). Epithelial cell PPAR γ contributes to normal lung maturation. *The FASEB Journal*. DOI:10.1096/fj.05-5410fje.
566. Huang *et al.* (2019). Targeting Peroxisome Proliferator-Activated Receptor-Gamma Decreases Host Mortality After Influenza Infection in Obese Mice. *Viral Immunology*. DOI:10.1089/vim.2019.0016.
567. Chawla (2010). Control of Macrophage Activation and Function by PPARs. *Circulation Research*. DOI:10.1161/circresaha.110.216523.
568. Ricote *et al.* (1998). The peroxisome proliferator-activated receptor- γ is a negative regulator of macrophage activation. *Nature*. DOI:10.1038/34178.
569. Daynes & Jones (2002). Emerging roles of PPARs in inflammation and immunity. *Nature Reviews Immunology*. DOI:10.1038/nri912.
570. Sun *et al.* (2012). Maternal High-Fat Diet During Gestation or Suckling Differentially Affects Offspring Leptin Sensitivity and Obesity. *Diabetes*. DOI:10.2337/db11-0957.
571. Purcell *et al.* (2011). Maternal stress and high-fat diet effect on maternal behavior, milk composition, and pup ingestive behavior. *Physiology & Behavior*. DOI:10.1016/j.physbeh.2011.05.012.
572. Chen *et al.* (2017). Effect of high-fat diet on secreted milk transcriptome in midlactation mice. *Physiological Genomics*. DOI:10.1152/physiolgenomics.00080.2017.
573. Schittny (2017). Development of the lung. *Cell and Tissue Research*. DOI:10.1007/s00441-016-2545-0.
574. Knudsen *et al.* (2010). Assessment of air space size characteristics by intercept (chord) measurement: An accurate and efficient stereological approach. *Journal of Applied Physiology*. DOI:10.1152/jappphysiol.01100.2009.
575. Voswinckel (2004). Characterisation of post-pneumonectomy lung growth in adult mice. *European Respiratory Journal*. DOI:10.1183/09031936.04.10004904.
576. Upadhyay *et al.* (2019). Time-restricted feeding reduces high-fat diet associated placental inflammation and limits adverse effects on fetal organ development. *Biochemical and Biophysical Research Communications*. DOI:10.1016/j.bbrc.2019.04.154.
577. Domingo-Gonzalez *et al.* (2020). Diverse homeostatic and immunomodulatory

- roles of immune cells in the developing mouse lung at single cell resolution. *eLife*. DOI:10.7554/elife.56890.
578. Mubarak *et al.* (IntechOpen, 2019). Eosinophilic Asthma. in *Asthma - biological evidences*. DOI:10.5772/intechopen.84297.
579. Yu *et al.* (2014). Innate lymphoid cells and asthma. *Journal of Allergy and Clinical Immunology*. DOI:10.1016/j.jaci.2014.02.015.
580. Moreland *et al.* (2001). TNF- α and IL-1 β are not essential to the inflammatory response in LPS-induced airway disease. *American Journal of Physiology-Lung Cellular and Molecular Physiology*. DOI:10.1152/ajplung.2001.280.1.1173.
581. Kobayashi (2006). Neutrophil Infiltration and Chemokines. *Critical Reviews™ in Immunology*. DOI:10.1615/critrevimmunol.v26.i4.20.
582. Jeyaseelan *et al.* (2005). Induction of CXCL5 During Inflammation in the Rodent Lung Involves Activation of Alveolar Epithelium. *American Journal of Respiratory Cell and Molecular Biology*. DOI:10.1165/rcmb.2005-0063oc.
583. Bozic *et al.* (1995). Expression and biologic characterization of the murine chemokine KC. *The Journal of Immunology* 154, 6048 LP–6057.
584. Driscoll *et al.* (1995). Cloning, expression, and functional characterization of rat MIP-2: a neutrophil chemoattractant and epithelial cell mitogen. *Journal of Leukocyte Biology*. DOI:10.1002/jlb.58.3.359.
585. Balamayooran *et al.* (2010). Mechanisms of Neutrophil Accumulation in the Lungs Against Bacteria. *American Journal of Respiratory Cell and Molecular Biology*. DOI:10.1165/rcmb.2009-0047tr.
586. Schyns *et al.* (2018). Lung Interstitial Macrophages: Past, Present, and Future. *Journal of Immunology Research*. DOI:10.1155/2018/5160794.
587. Osterholzer *et al.* (2005). CCR2 and CCR6, but Not Endothelial Selectins, Mediate the Accumulation of Immature Dendritic Cells within the Lungs of Mice in Response to Particulate Antigen. *The Journal of Immunology*. DOI:10.4049/jimmunol.175.2.874.
588. GeurtsvanKessel *et al.* (2009). Dendritic cells are crucial for maintenance of tertiary lymphoid structures in the lung of influenza virus-infected mice. *The Journal of Experimental Medicine*. DOI:10.1084/jem.20090410.
589. Lukens *et al.* (2009). Respiratory Syncytial Virus-Induced Activation and Migration of Respiratory Dendritic Cells and Subsequent Antigen Presentation in the Lung-Draining Lymph Node. *Journal of Virology*. DOI:10.1128/jvi.00452-09.
590. Serbina *et al.* (2003). TNF/iNOS-Producing Dendritic Cells Mediate Innate Immune Defense against Bacterial Infection. *Immunity*. DOI:10.1016/s1074-7613(03)00171-7.
591. Montante & Brinkman (2019). Flow cytometry data analysis: Recent tools and algorithms. *International Journal of Laboratory Hematology*. DOI:10.1111/ijlh.13016.
592. Li *et al.* (2019). Deep Cytometry: Deep learning with Real-time Inference in Cell Sorting and Flow Cytometry. *Scientific Reports*. DOI:10.1038/s41598-019-47193-6.
593. Hastie *et al.* (Springer New York, 2009). *The Elements of Statistical Learning*. DOI:10.1007/978-0-387-84858-7.
594. Dietert (2014). Developmental Immunotoxicity, Perinatal Programming, and Noncommunicable Diseases: Focus on Human Studies. *Advances in Medicine*. DOI:10.1155/2014/867805.
595. Murphy *et al.* (2008). The Prolonged Life-Span of Alveolar Macrophages. *American Journal of Respiratory Cell and Molecular Biology*. DOI:10.1165/rcmb.2007-0224rc.

Eidesstattliche Versicherung

Ich, Ernesto Elorduy Vergara, geboren am 21. Juni 1989 in Puebla, Mexiko, erkläre hiermit an Eides statt, dass ich die vorliegende Dissertation mit dem Titel

The role of parental obesity in lung development and alveolar macrophage priming

selbständig verfasst, mich außer der angegebenen keiner weiteren Hilfsmittel bedient und alle Erkenntnisse, die aus dem Schrifttum ganz oder annähernd übernommen sind, als solche kenntlich gemacht und nach ihrer Herkunft unter Bezeichnung der Fundstelle einzeln nachgewiesen habe.

Ich erkläre des Weiteren, dass die hier vorgelegte Dissertation nicht in gleicher oder in ähnlicher Form bei einer anderen Stelle zur Erlangung eines akademischen Grades eingereicht wurde.

Oberschleißheim, 06.09.2021

Ernesto Elorduy Vergara